

School of Pharmacy and Biomedical Sciences

**Pharmaceutical and Biological Evaluation of
Nano Photosensitizers for Cancer Therapy**

Behin Sundara Raj

**This thesis is presented for the Degree of
Doctor of Philosophy
of
Curtin University**

March 2018

Declaration

I declare that to the best of my knowledge and belief this thesis is my own account of my research and contains no material previously published by any other person except where due acknowledgement has been made. This thesis contains no material which has been accepted for the award of any other degree or diploma in any university.

Signature: ... S. Behin

Date: ... 29/03/2018

Acknowledgement

Foremost, I would like to express my sincere gratitude to my supervisor, Dr. Yan Chen for her advice, guidance, support, encouragement and patience throughout the course of study leading to this thesis. I am thankful to my co-supervisor Professor Xia Lou for the timely guidance, support and providing nanoparticles throughout the study. It would be impossible to complete this thesis without their expertise and immense knowledge in the subject.

I express my sincere gratitude to Curtin University for providing me with International Postgraduate Research Scholarship (IPRS) for undertaking the Doctor of Philosophy. I am grateful to Professor Dr Kevin Batty, Head of School, School of Pharmacy, Professor Dr Lynne Emmerton, Deputy Head and Director of Research and Graduate Studies, School of Pharmacy, and Professor Dr John Mamo, Director, CHIRI-Biosciences, for their efforts on developing a better academic atmosphere and creating an excellent research environment.

I would like to thank Giuseppe Luna and Jorge Martinez for their evergreen support throughout the work. I would like to express my appreciation to Dr Rob Steuart for providing facility to carry out the UV chamber experiments, Dr Connie Jackaman for her training and support in confocal microscopy, Dr Joanna Kelly for her support in tissue culture facility and Jeanne Lemasurier for her support throughout flow cytometry experiments.

I would like to thank Dr Andrew Crowe and Dr Simon Fox for providing the Caco-2 and 3T3 cell lines for the study, Dr Crispin Dass for demonstrating few animal experiments and Dr Beng Chua for providing the required support required during the animal study. Special thanks to Kunal Patel, Department of Chemical Engineering for synthesizing nanoparticles and supporting in ICP-OES experiments.

My deep sense of gratitude to my fellow PhD students for their support: Yan Jing for teaching me the animal study experiments and working together in flow cytometry, cell culture and confocal experiments. Bhawna Gauri for her support and standing beside me even at late hours of animal study. Naz Hasan Huda for assisting in confocal

experiment and cell culture experiments. Fatima Naushin Jahan for providing the digital vernier caliper. Omar Elaskalani for providing the caspase-3 reagent. Sangeetha Mathavan for assisting in Graphpad Prism. Thiru Sabapathy and Revathy for providing valuable support throughout the cell culture works.

I extend my thoughtful gratitude to Pastor Rajimon Oonnooni and Perth Tabernacle Church members for their support and prayers during my tenure of work. I would also like to express my gratitude to Pastor Sunil Jacob, Pastor Valsala Kumar and Dr Thankamony for their support and prayers.

My deep and sincere thanks to my wife, Punitha Isaac Samraj and my beloved son Alden Haniel, for their love and understanding throughout this journey. They have sacrificed their time and sleep to ease my stressful days. I would like to thank my parents Mr Sundara Raj & Mrs Reeni Hemalatha and my brother Mr Ruban who support me throughout my life even though they are far away.

Dedication

I dedicate this thesis to my beloved parents Mr Sundara Raj and Mrs Reeni Hemalatha for their inseparable love, support and prayers.

Table of Contents

Declaration	ii
Acknowledgement	iii
Dedication.....	v
Table of contents.....	vi
List of Figures.....	xi
List of Tables.....	xiv
Abbreviations.....	xv
Abstract.....	xxi
Chapter 1	General Introduction
1.1	Cancer and cancer treatment.....2
1.1.1	Chemotherapy.....2
1.1.2	Radiotherapy.....3
1.2	PDT.....3
1.2.1	History of PDT.....3
1.2.2	Mechanism of PDT.....4
1.2.3	Light wavelength in PDT.....7
1.3	Photosensitizers for PDT8
1.3.1	First generation PSs.....8
1.3.2	Second generation PSs.....8
1.3.3	New development of PSs.....9
1.4	Nanomaterials as PSs.....10
1.4.1	Metal oxide-based NPs.....10
1.4.2	ZnO NPs.....12
1.4.3	Hybrid NPs.....15
1.4.4	Silica NPs.....16
1.5	Cell killing mechanisms in PDT.....17
1.5.1	PDT and Apoptosis.....17
1.5.2	PDT and Necrosis.....18
1.5.3	PDT and Autophagy.....18
1.6	PDT in skin cancer treatment.....19
1.7	Overall objectives.....21

Chapter 2	Materials and Methods	
1.0	Materials.....	23
1.1	Chemicals used in <i>In vitro</i> studies	23
1.2	Chemicals used in <i>in vivo</i> studies.....	24
1.3	Hybrid NPs used in <i>in vitro</i> and <i>in vivo</i> studies.....	24
2.0	Methods.....	25
	<i>In vitro</i> studies.....	25
2.1	Cell culture.....	25
2.2	UV chamber optimization.....	26
2.3	Pharmaceutical evaluation of hybrid NPs.....	26
2.4	Evaluation of cytotoxicity.....	26
2.5	Evaluation of hybrid NPs in PDT.....	28
2.6	Evaluation of PDT of hybrid NPs with multiple UV-A Irradiations.....	29
2.7	Morphology change of cells after hybrid NPs and UV-A treatment.....	29
2.8	Singlet oxygen detection.....	29
2.9	ROS detection by DCFH-DA.....	30
2.10	ROS quenching by NAC.....	32
2.11	NAC treated cytotoxicity assay.....	32
2.12	Evaluation of cellular uptake of hybrid NPs.....	33
	(a) Quantitative analysis.....	34
	(b) Qualitative analysis.....	35
2.13	Apoptosis assay by flow cytometry.....	37
2.14	Total cell associated zinc and iron measurement by ICP.....	38
2.15	Caspase 3/7 assay.....	39
	<i>In vivo study</i>	40
2.16	Preparation of B16-F10 mouse melanoma tumour cells.....	40
2.17	Animals and tumour inoculation.....	40
2.18	Preparation studies for UV-A irradiation.....	41
2.19	Experimental design for <i>in vivo</i> studies.....	43
2.20	Administration of hybrid NPs and assessment of tumour growth.....	44
2.21	Collection of biological samples.....	45

2.22	Statistical analysis.....	46
Chapter 3	Results and discussion	
3.1	Cell cultures.....	48
3.2	UV CHAMBER optimization.....	48
3.3	Characterisation of hybrid NPs as nano-PSs.....	50
3.4	Stability of hybrid NPs in different medium.....	52
3.5	Evaluation of cytotoxicity.....	54
	(i) Cytotoxicity of hybrid NPs in B16-F10 cells.....	54
	(ii) Cytotoxicity of hybrid NPs in Caco-2 cells.....	56
	(iii) Cytotoxicity of hybrid NPs in 3T3 cells.....	58
3.6	Phototoxic effect of hybrid NPs.....	60
	(i) Phototoxic effect of hybrid NPs in B16-F10 cells.....	61
	(ii) Phototoxic effect of hybrid NPs in Caco-2 cells.....	63
3.7	Phototoxic effect of hybrid NPs in B16-F10 cells after multiple irradiations.....	66
3.8	Singlet oxygen generation by hybrid NPs in PDT.....	67
3.9	Intracellular ROS production by hybrid NPs in PDT.....	68
	(i) Intracellular ROS production in B16-F10 cells.....	69
	(ii) Intracellular ROS production in Caco-2 cells.....	72
	(iii) Confirmation of ROS production in cells.....	76
3.10	Cytotoxicity of hybrid NPs after ROS quenching.....	78
3.11	Morphological changes of cells after treatment with hybrid NPs and UV-A light.....	79
3.12	Quantitative investigation of cellular uptake of hybrid NPs in PDT.....	80
3.13	Qualitative investigation of cellular uptake of hybrid NPs.....	83
3.14	Total cell associated zinc and iron in PDT.....	90
3.15	Apoptosis study and caspase 3/7 activity in PDT.....	92
3.16	Selection of melanoma animal model for <i>in-vivo</i> studies.....	102
3.17	UV LED SMART optimization.....	103
3.18	Antitumour activity of hybrid NPs alone and in combination with UV-A.....	104
	(i) Tumour growth pattern during the whole study.....	105
	(ii) Tumour growth pattern up to day 16 post treatment.....	107

	(iii) Tumour weight reduction by hybrid NPs.....	109
	(iv) The impact of treatments on animal survival and life prolongation rate.....	112
	(v) Impact of treatments on the health of animal.....	114
3.19	General discussion.....	121
Chapter 4	Summary, future research scope and conclusions	
4.1	General summary.....	126
4.2	Limitations of the study and future work.....	129
4.3	Conclusion.....	130
References	131
Appendices		
Appendix 1:	Structure, TGA curve & XRD analysis of the hybrid NPs.....	154
Appendix 2:	Sample preparation for Mycoplasma Testing.....	155
Appendix 3:	Calibration curve of B16-F10, Caco-2 and 3T3 cells.....	157
Appendix 4:	Cryopreservation and thawing of cells.....	158
Appendix 5:	UV CHAMBER BS02 Radiation officer approval.....	159
Appendix 6:	MTT solution preparation and storage.....	160
Appendix 7:	10X Binding buffer preparation for apoptosis assay.....	160
Appendix 8:	Animal ethics approval.....	161
Appendix 9:	Animal health monitoring score card.....	162
Appendix 10:	Radiation safety approval for UV LED SMART.....	163
Appendix 11:	BS02 UV CHAMBER-sensor, UV-MAT & UV LED SMART company manuals.....	164
Appendix 12:	Dose response curves of hybrid NPs at 24 h dark and 24 h UV- A treated in B16-F10 cells.....	175
Appendix 13:	Dose response curves of hybrid NPs at 24 h dark and 24 h UV- A treated in Caco-2 cells.....	177
Appendix 14:	ROS generation in B16-F10 cells by hybrid NPs and in	

	combination with UV-A irradiation.....	179
Appendix 15:	ROS generation in DMEM medium treated with NPs (no cells).....	180
Appendix 16:	ROS generation in Caco-2 cells by hybrid NPs and in combination with UV-A irradiation.....	181
Appendix 17:	ROS generation in DMEM medium treated with NPs (no cells).....	182
Appendix 18:	Morphology of B16-F10 cells after hybrid NPs treatment.....	183
Appendix 19:	Morphology of Caco-2 cells after hybrid NPs treatment.....	187
Appendix 20:	Morphology of 3T3 cells after hybrid NPs treatment.....	192
Appendix 21:	Calibration curve of FZSiFA50 and FZSi-FITC NPs in RIPA buffer.....	195
Appendix 22:	Morphology of B16-F10 cells after NPs treatment (Caspase).....	196
Appendix 23:	Tumour growth pattern of individual treatment groups up to day 16 post-treatment.....	198
Appendix 24:	Images of melanoma tumour in different treatment groups....	201
Appendix 25:	Tumour growth delay and inhibition by the hybrid NPs and UV-A.....	204
Appendix 26:	Copyright clearance.....	207
Appendix 27:	Publications and presentations.....	214

List of Figures

Figure 1.1	Mechanism of PDT.....	5
Figure 1.2	Different modifications with NPs.....	10
Figure 1.3	ZnO nano-PS in PDT.....	15
Figure 1.4	Design of the hybrid NPs.....	21
Figure 2.1	Schematic representation of the animal treatment.....	40
Figure 2.2	Image showing the UV LED SMART and break out box.....	42
Figure 2.3	Experimental design used in optimising the UV LED SMART..	43
Figure 2.4	The schematic treatment plan and end point for <i>in vivo</i> studies..	43
Figure 3.1	UV irradiation BS02 chamber and UV MAT.....	48
Figure 3.2	The inner set up of UV irradiation chamber BS02 during experiment.....	49
Figure 3.3	Particle size distribution (DLS spectra) of unmodified (FZ NPs) and modified NPs (FZS-FA100 NPs).....	51
Figure 3.4	TEM images of A: FZ, B: FZSi, C: FZSiFA25 and D: FZSiFA50 NPs.....	52
Figure 3.5	UV-visible diffuse reflectance spectroscopy of ZnO and hybrid NPs.....	52
Figure 3.6	The viability of B16-F10 cells upon exposure to hybrid NPs for (A) 6 h and (B) 24 h at different concentrations.....	56
Figure 3.7	The viability of Caco-2 cells upon exposure to hybrid NPs for (A) 6 h and (B) 24 h at different concentrations.....	58
Figure 3.8	The viability of 3T3 cells upon exposure to hybrid NPs for (A) 6 h and (B) 24 h at different concentrations.....	60
Figure 3.9	Phototoxicity in (A) B16-F10 and (B) Caco-2 cells upon exposure to hybrid NPs for 24 h.....	62
Figure 3.10	Cell viability of B16-F10 cells after multiple UV-A irradiation...	67
Figure 3.11	Absorbance of DPBF exposed to hybrid NPs and UV-A.....	68
Figure 3.12	ROS generation in B16-F10 cells in dark upon exposure to hybrid NPs.....	71
Figure 3.13	ROS generation in B16-F10 cells after UV-A irradiation upon exposure to hybrid NPs.....	72

Figure 3.14	ROS generation in Caco-2 cells in the dark upon exposure to hybrid NPs.....	74
Figure 3.15	ROS generation in Caco-2 cells after UV-A irradiation upon exposure to hybrid NPs.....	75
Figure 3.16	ROS production in B16-F10 cells after treatment with 5 mM NAC and hybrid NPs.....	77
Figure 3.17	ROS production in Caco-2 cells after treatment with 5 mM NAC and hybrid NPs.....	77
Figure 3.18	Cell viability of B16-F10 cells after 5 mM and 15 mM NAC pre-treatment.....	78
Figure 3.19	Morphology changes of B16-F10 cells before and after treatment with UV, FZNPs and both.....	80
Figure 3.20	Cellular uptake of FZSiFA50 and FZSi-FITC NPs in B16-F10 cells (both dark and UV).....	82
Figure 3.21	Cellular uptake of FZSiFA50 and FZSi-FITC NPs in Caco-2 cells (both dark and UV).....	82
Figure 3.22	CLSM images of B16-F10 cells after 6 h treatment with FZSiFA50 (blue coloured) and FZSi-FITC (green coloured) NPs.....	84
Figure 3.23	Z stack images of B16-F10 cells after FZSiFA50 NPs treatment (dark).....	85
Figure 3.24	Z stack images of B16-F10 cells after FZSi-FITC NPs treatment (dark).....	86
Figure 3.25	CLSM images of B16-F10 cells after 6 h treatment with FZSiFA50 (blue coloured) and FZSi-FITC (green coloured) followed by UV-A irradiation.....	87
Figure 3.26	Z stack images of B16-F10 cells after FZSiFA50 NPs and UV-A treatment.....	88
Figure 3.27	Z stack images of B16-F10 cells after FZSi-FITC NPs and UV-A treatment.....	89
Figure 3.28	B16-F10 cells after NPs treatment with 12.5 µg/mL concentration (Flow cytometry).....	95

Figure 3.29	B16-F10 cells after NPs treatment with 12.5 µg/mL concentration+ UV-A irradiation (Flow cytometry).....	96
Figure 3.30	B16-F10 cells after NPs treatment with 100 µg/mL concentration (Flow cytometry).....	97
Figure 3.31	B16-F10 cells after NPs treatment with 100 µg/mL concentration+ UV-A irradiation (Flow cytometry).....	98
Figure 3.32	Compilation of apoptosis levels in B16-F10 cells.....	99
Figure 3.33	Caspase 3/7 activity in B16-F10 cells treated with FZSi and FZSiFA50 NPs.....	101
Figure 3.34	Cell morphology changes in B16-F10 cells during caspase 3/7 assay.....	102
Figure 3.35	Image showing the UV LED SMART and a mouse irradiated with the UV LED SMART.....	104
Figure 3.36	The tumour growth pattern of individual treatment groups over the whole study period.....	106
Figure 3.37	The compilation of tumour growth of different treatment groups up to day 16 post tumour cell inoculation.....	107
Figure 3.38	The comparative weight of tumour in each treated group at the end point.....	111
Figure 3.39	The image shows the tumour size of different treated groups after sacrifice.....	112
Figure 3.40	Change in body weight of mice bearing B16-F10 melanoma tumour after cell inoculation.....	116
Figure 3.41	Images are showing the organ profile (spleen, kidney, lungs, liver) (top-bottom) of different treatment groups after sacrifice...	120
Figure 3.42	The image is showing the growth of B16-F10 melanoma tumour in C57BL/6 mice.....	121

List of Tables

Table 1.1	Different metal oxide-based NPs in PDT.....	11
Table 1.2	ZnO NPs in PDT.....	14
Table 2.1	The B16-F10, 3T3 and Caco-2 cell culture details.....	25
Table 2.2	Animal study experimental design of different treatment groups.....	44
Table 3.1	UV CHAMBER BS02: Operation conditions.....	49
Table 3.2	Information about the hybrid NPs.....	51
Table 3.3	Stability study of hybrid NPs in different medium at 37 °C.....	53
Table 3.4	Stability study of hybrid NPs in different medium (zeta potential).....	53
Table 3.5	Synergistic effect of hybrid NPs & UV-A irradiation in photokilling of B16-F10 cells.....	63
Table 3.6	Synergistic effect of hybrid NPs & UV-A irradiation in photokilling of Caco-2 cells.....	64
Table 3.7	ED ₅₀ and PI calculation in B16-F10 and Caco-2 cells.....	65
Table 3.8	Singlet oxygen quantum yield of hybrid NPs.....	68
Table 3.9	Total intracellular metal content in B16-F10 and Caco-2 cells...	91
Table 3.10	UV LED SMART optimization.....	104
Table 3.11	Summary of tumour volume and tumour volume inhibitory effect on day 16 of the study.....	109
Table 3.12	Survival time and life prolongation of different treatment groups over the whole period.....	113
Table 3.13	Body weight and organs weight of different treatment groups...	119
Table 3.14	Comparison of our hybrid NPs with the other reported NPs in melanoma tumour model.....	124

Abbreviations

$^1\text{O}_2$	Singlet oxygen
4HNE	aldehyde-4-hydroxy-2-nonenal
3T3	Mouse embryo fibroblasts
A375	Human skin malignant melanoma
A549	Human lung carcinoma
ABS	Australian bureau of statistics
Ac-DEVD-AFC	Caspase-3 substrate
AFC	7-amino-4-trifluoromethyl coumarin
ALA	5-Aminolevulinic acid
ALA-PDT	5-Aminolevulinic acid-photodynamic therapy
APH	Acid phosphatase assay
Au-ZnO	Gold-Zinc oxide
B16-F10	Mouse melanoma
BCC	Basal cell carcinoma
BD	Bowen's disease
BODIPY	Boron-dipyrromethene
BSA	Bovine serum albumin
Caco-2	Colorectal adenocarcinoma
CAL27	Human tongue squamous cell carcinoma
CAT	Catalase
CLSM	Confocal laser scanning microscopy
CR	Complete response
CT	Computed tomography
Cyt-c	Cytochrome-c
DCC	Dicyclohexyl carbodiimide
DCFH-DA	2,7-Dichlorofluorescein diacetate
DCF	2,7-Dichlorofluorescein
DLS	Dynamic light scattering
DMEM	Dulbecco's modified eagle's medium
DMSO	Dimethyl sulfoxide
DNA	Deoxyribose nucleic acid
DNR	Daunorubicin

DOX	Doxorubicin
DPBF	1,3-diphenyl isobenzofuran
ECT	Electro chemotherapy
EDTA	Ethylenediamine tetraacetate
ED ₅₀	Median effective dose
EPR	Enhanced permeability and retention
ERK1/2	Extracellular signal-regulated kinases
FA	Folic acid
FBS	Foetal bovine serum
FDA	Food and Drug Administration
FITC	Fluorescein isothiocyanate
FZ	Zinc oxide-Iron oxide nanoparticles
FZSi	Zinc oxide- Iron oxide nanoparticles coated with silica
FZSiFA25	Zinc oxide-Iron oxide nanoparticles coated with silica and folic acid
FZSiFA50	Zinc oxide-Iron oxide nanoparticles coated with silica and a high level of folic acid
GEMMs	Genetically engineered mouse models
GR	Glutathione reductase
GSH	Glutathione
GSHPx	Glutathione peroxidase
GST	glutathione-S-transferases
h	Hour
HaCaT	Mouse choriocarcinoma
HBSS	Hanks balanced salt solution
HCT-116	Human colon colorectal carcinoma
HeLa	Human cervix adenocarcinoma
HepG2	Human liver cancer cell
HELF	Human embryo lung fibroblasts
HLaC 78	Human larynx squamous cell carcinoma
HMME	Hematoporphyrin monomethyl ether
HNSCC	Head and neck squamous cell carcinoma
HP	Hematoporphyrin
HpD	Hematoporphyrin derivative

HPPH	(2-[1-hexyloxyethyl]-2-devinyl pyropheophorbide-a)
hs NPs	Hollow silica nanoparticles
hs (215)	Hollow silica nanoparticles 215 nm size
hs (430)	Hollow silica nanoparticles 430 nm size
hsFA (215)	Hollow silica nanoparticles with folic acid 215 nm size
hsFA (430)	Hollow silica nanoparticles with folic acid 430 nm size
ICP-MS	Inductively coupled plasma mass spectrometry
ICP-OES	Inductively coupled plasma optical emission spectroscopy
IR	Infra-red
i.t	Intra tumour
IV	Intravenous
J/cm ²	Joules per centimetre square
JNK	Jun N-terminal kinases
KB	Human papilloma carcinoma
L929	Mouse fibroblast cells
LED	Light emitting diode
LET	Linear energy transfer
LoVo	Human metastatic colorectal adenocarcinoma
MAL	Methyl aminolevulinate
MAPK	mitogen -activated protein kinases
MCF7	Human breast adenocarcinoma
mL	Millilitre
MM	Malignant melanomas
MMP	Mitochondrial membrane potential
MRI	Magnetic resonance imaging
m-THPC	5,10,15,20-meta-tetra(hydroxyphenyl)chlorin
MTT	Methyl thiazolyldiphenyl-tetrazolium bromide
MTD	Maximum tolerated dose
NAC	N-acetyl cysteine
NaOH	Sodium hydroxide
NIR	Near Infra-red
NF-Kb	Nuclear factor kappa-light-chain-enhancer of activated B cells
NMSC	Non-melanoma skin cancer
NPs	Nanoparticles

NPSs	Nano photosensitizers
ns	Nano second
P38MAPK	p38 mitogen-activated protein kinases
PARP	Poly (ADP-ribose) polymerase
PBS	Phosphate buffered saline
PC2	Physical containment level 2
Pc4	Phthalocyanine
PCR	Polymerase chain reaction
PDI	Poly dispersity index
PDT	Photo dynamic therapy
PET	Positron emitted tomography
PEI	Polyethylenimine
PEG	Polyethylene glycol
PFA	Paraformaldehyde
P-gp	P-glycoproteins
PI	Phototoxic index
p-NPP	Para nitrophenyl phosphate
PpIX	Protoporphyrin
P/S	Penicillin-streptomycin
PS	Photosensitizer
PSs	Photosensitizers
PVP	Polyvinyl pyrolidone
QBC939	Human cholangiocarcinoma
QD	Quantum dots
RES	Reticuloendothelial system
RIPA	Radio immuno precipitation assay
RNS	Reactive nitrogen species
ROI	Reactive oxygen intermediates
ROS	Reactive oxygen species
RT	Room temperature
rpm	Revolutions per minute
SBCC	Superficial basal cell cancer
SCC	Squamous cell carcinoma
SD	Standard deviation

SMMC-7721	Human hepatocellular carcinoma
SOD	Superoxide dismutase
SOP	Standard operating procedure
SPIONS	Superparamagnetic iron oxide nanoparticles
TEM	Transmission electron microscope
TEOS	Tetraethyl orthosilicate
TGA	Thermo gravimetric analysis
TNF- α	Tumour necrosis factor
TNFR	Tumour necrosis factor receptor
TVI	Tumour volume inhibitory rate
UV	Ultra violet radiation
UV-A	Ultra violet-A radiation with a wavelength of 365 nm
UVD0	UV-A radiation treated on day zero, same day as NPs treatment
UVD3	UV-A radiation treated on day three
WHO	World Health Organisation

Abstract

Photodynamic therapy (PDT) offers an alternative or adjuvant treatment option to other cancer therapies due to its known ability to provide targeted therapy to the organ and its related tissues with minimal invasiveness. PDT involves a photosensitizer (PS), a light source to activate the PS within the diseased tissue in the presence of oxygen. In recent years, nanoparticles of semiconductor metal oxides that have appealing photophysical properties have been increasingly studied as a new class nano photosensitizer (nano-PS) in PDT. Most studies have been limited to the materials design and *in vitro* assessment of the suitability of such materials as PSs. The aim of this project was to evaluate the pharmaceutical and biological properties of a novel class of semiconductor-based nano-PS consisting of a hybrid zinc oxide (ZnO) and iron oxide (Fe_3O_4) nanocore that was surface coated with silica and conjugated with folic acid (FA), and to determine how they can be effectively utilised to produce cancer-killing effects upon exposure to UV-A irradiation, both *in vitro* and *in vivo*.

On characterization of the hybrid NPs, Fe_3O_4 -ZnO (FZ), silica-coated FZ (FZSi) and folic acid modified FZSi (FZSiFA25 and FZSiFA50) NPs were found to be 13-19 nm in size determined by dynamic light scattering (DLS); while, silanization and folate modification led to some change in morphology, size and zeta potential. Stability of those NPs in the culture medium, Dulbecco's modified Eagle's medium (DMEM), was reasonable and none exceeded 50 nm of particle size in 24 hours, indicating that the results of our experimental work were unlikely affected by the stability of NPs.

Cellular responses of the hybrid NPs were studied in mouse melanoma cells (B16-F10), Caco-2 and 3T3 cells. The results indicated a dose and time-dependent toxicity of the hybrid NPs. UV-A irradiation of the hybrid NPs resulted in a drastic reduction in B16-F10 and Caco-2 cell viability, demonstrating a synergistic effect between the NPs and UV-A irradiation. FA conjugation enhanced the photo-induced toxicity in melanoma cells at low NPs dose, indicating greater NPs-cell interactions facilitated by the targeting ligand. Singlet oxygen quantum yield determined by the chemical trapping method confirmed the production of singlet oxygen by hybrid NPs which is expected to be one of the main cell killing mechanisms of hybrid NPs. Furthermore, the production of reactive oxygen species (ROS) by the hybrid NPs were detected in

cells (both in the dark and in PDT), likely contributed to the cell-killing ability of nano-PSs. Such ROS induced cell-killing effect of hybrid NPs was confirmed by the observation of enhanced cell viability associated with the pre-treatment of N-acetyl cysteine (NAC), an antioxidant commonly used for ROS study, which led to a significant decrease in ROS production. Results also showed that double and triple irradiation conditions produced better, and more drastic cell-killing compared to single radiation, confirming repeatability of the photo-killing of nano-PSs in PDT.

Cellular uptake study confirmed the time-dependent uptake of NPs in the cancer cells and the FA; modified hybrid NPs exhibited better cellular uptake compared to those without FA. NPs localisation in cells was qualitatively confirmed by the confocal microscopy images after NPs treatment. The detection of the elevated level of total cell-associated zinc and iron further confirmed the cellular uptake of FZSiFA50 NPs and the enhancement of cell-associated metal levels might be a significant contributing factor towards the cellular toxicity. Cell metal content study also revealed that FZSi NPs appeared to undergo faster decomposition than FZSi FA50 NPs, under the UV-A irradiation, in B16-F10 cells. Flow cytometry study revealed that apoptosis process led to the dose and time-based cell death by hybrid NPs. The morphological changes of the cells on treatment with hybrid NPs further confirmed the cell death involved apoptosis. The caspase-dependent apoptosis pattern of cell death was evident in B16-F10 cells following treatment with the hybrid NPs and UV-A irradiation. FZSi and FZSiFA50 NPs showed different apoptotic and necrotic pattern. These *in vitro* findings warranted the selection of FZSi and FZSiFA50 NPs for the further *in vivo* study.

The antitumour effects of PDT with hybrid NPs were assessed using a melanoma mouse model (B16-F10) in C57BL/6 male mice. A dose of 2 mg/kg NPs was administered to the mice intratumorally. The UV-A radiation was given immediately to UVD0 groups and after 3 days interval for UVD3 groups following NPs treatment. The results indicate that up to day 16 the FZSiFA50 NPs with UVD3 group had the strongest antitumour effect with 95% tumour volume inhibitory rate as compared to the UV-A alone (65%) and FZSiFA50 NPs alone (58%) groups, suggesting FA surface modification of hybrid NPs may have enhanced its tumour cell uptake, together with the photoreactivity of hybrid NPs, which led to strong tumour inhibition. Over the

whole period of study, however, both FZSi and FZSiFA50 NPs with UVD3 showed strong antitumour effects with life prolongation rate of 44.5% and 31.2% respectively, which are significantly greater than the rest (UV alone 21.3%, FZSi & FZSiFA50 NPs alone 0 & 15.6%, FZSi & FZSiFA50 NPs with UVD0 15.6% & 5.8%). Our animal study demonstrated that the interval between the UV-A irradiation and NPs treatment is playing a pivotal role in augmenting the antitumour effect of PDT with hybrid NPs.

Overall, we concluded that the developed novel hybrid NPs had fulfilled the criteria to be effective PSs for PDT with UV-A against cancer cells *in vitro* and *in vivo*. They are promising candidates to be developed into a clinically applicable PS for cancer PDT. The studies of these hybrid NPs in this PhD project provide us a better understanding in designing the semiconductor metal oxides-based nano-PS for PDT.

CHAPTER 1

GENERAL INTRODUCTION

1.1 Cancer and cancer treatment

Cancer is a devastating disease affecting the world, and the cancer cases are increasing at an alarming rate globally. Cancer as the global health challenge refers to more than 277 different types of the disease. It causes the second most extensive mortality in the world. This tissue level disease presents challenges in accurate diagnosis and effective treatments (Hassanpour *et al.*, 2017, Parvanian *et al.*, 2017). Cancer caused 8.8 million deaths in 2015 and 1 in 6 deaths worldwide (WHO, 2017). In Australia, 134,174 cases have been diagnosed with cancer so far in 2017. According to statistics skin cancer such as melanoma had caused 1839 deaths in 2017, which counts for 10.4% of total cancer cases (Cancer Australia, 2017). Although there is a broad understanding of cancer, there is an unmet need for research.

Extensive research in cancer has led to the fast development of treatment modalities in areas such as chemotherapy, radiotherapy, gene therapy and immunotherapy (Cancer Council Australia, 2017). Many conventional cancer therapies are suffering from limitations such as poor drug solubility, fast deactivation of the drug, unfavourable biodistribution, pharmacokinetics and being toxic to healthy cells which all contribute to many unwanted side effects. Photodynamic therapy (PDT), delivered by nanotechnology, is a promising alternative solution and can be used in combination with the existing treatment to overcome the limitations facing cancer therapy (Arruebo *et al.*, 2011).

1.1.1 Chemotherapy

Chemotherapy has offered increased survival rate to patients with distinct types of cancer, though it causes severe side effects and declines in cognitive functions (Vitali *et al.*, 2017). They are provided to patients at the maximum tolerated dose (MTD) (Wu *et al.*, 2017; Chen *et al.*, 2017; Lambert *et al.*, 2017). Systemic side effects include acute and delayed nausea, mouth ulcerations and cognitive impairments and long-term side effects can lead to developing other type cancers (Wang *et al.*, 2016). Also, chemotherapy has reported relapse and developed resistance with 90% of the drugs, especially in metastatic cancers (Wu *et al.*, 2017; Chen *et al.*, 2017). Targeting tumour vascular cells rather than tumour cells can reduce the relapse, drug resistance and barriers that prevent anti-cancer effects. This provides the basis for metronomic chemotherapeutic treatment, targeting tumour vascular cells with low doses of

chemotherapeutic agents for a prolonged time (Abu Lila & Ishida, 2017), a concept which potentially can be used in combination therapy of PDT with chemotherapy.

1.1.2 Radiotherapy

In radiotherapy, high-energy X-rays are delivered in fractions to a local region. The fractions are delivered in brief time points within 10-15 min. Sometimes chemotherapy is given along radiotherapy called chemo-radiation (Smith & Prewett, 2017). Almost 50% cancer patients receive radiotherapy as part of their treatment, and 40% receive towards curative treatment (Baskar *et al.*, 2012). It is an excellent treatment option for patients with significant risk disease and those who cannot tolerate surgery. The biggest advantage of radiotherapy is the provision of local treatment, although may not be selective enough. The major limitation is it cannot be used for the treatment of disseminated disease as irradiation of the whole body with appropriate doses is not possible (Chummun & Mc Lean, 2017; Craythome & Al-Niami, 2017). Radiotherapy can be delivered in two ways, externally through high-energy radiation source to the site of action and internally through radioactive sources sealed in catheters called brachytherapy (Song *et al.*, 2017). Radiotherapy mechanism of action is the destruction of deoxyribonucleic acid (DNA) permanently, which leads the cells to apoptosis. Radiotherapy may damage the healthy cells at or near the treatment area of ionizing radiation, causing detrimental effects including fatigue and skin problems, which is often suffered by patients (Mazonakis *et al.*, 2017; Baskar *et al.*, 2012). Biological effects of radiation depend on linear energy transfer (LET), dose, dose fractionation and sensitivity of the treated tissues or organ (Baskar *et al.*, 2012). Side effects of radiation therapy may include skin toxicity, mucositis, diarrhoea and dry mouth (Wang *et al.*, 2016). High dose of radiation could lead to the risk of developing secondary cancer during the radiation therapy (Ng & Suryak, 2015). These consequences of conventional cancer treatments led to the extensive development of PDT as an alternative treatment strategy against many types of cancer.

1.2 PDT

1.2.1 History of PDT

In 1907, Von Tappeiner and Jodlbauer defined PDT, and Lipson is largely responsible for initiating the modern era of PDT (Dougherty, 1993). In the 1960s Lipson and his colleagues have studied the PS, hematoporphyrin derivative (HpD) (Dougherty, 1993;

Triesscheijn *et al.*, 2006; Moan & Peng, 2003). He has looked for a diagnostic agent towards tumour detection. Dougherty and his colleagues, (1989) developed PDT further in 1975, by treating experimental animal tumours (Dougherty, 1989). In 1978, Dougherty first demonstrated the clinical effectiveness of PDT by performing treatments on patients with cutaneous or subcutaneous tumours and observed partial or complete recovery in the majority of the patients (Dougherty *et al.*, 1978). Photofrin (HpD), was the first PS in PDT used for bladder cancer in Canada introduced in 1993. Since then there have been more than 200 PDT clinical trial studies involving other types of PSs, and PDT is continually gaining clinical acceptance (Agostinis *et al.*, 2011).

1.2.2 Mechanism of PDT

Unlike radiation therapy which uses high energy of the radiation, PDT uses a lower energy radiation and can be repeated at the same site several times if required (American cancer society, 2017). The clinical PDT involves a combination of light and PSs as drugs to achieve selective damage to diseased/target cells and tissues (Allison *et al.*, 2008). There are three phases involved in PDT: excitation of the photosensitizer (PS) by a given dose of light of a suitable wavelength, generation of toxic oxygen species and cell death (Paszko *et al.*, 2011). The presence of adequate molecular oxygen in tissues is a requirement for a successful PDT. Because of the use of localised light and photosensitizers (PSs), PDT can provide a better-targeted treatment than chemotherapy or radiation therapy with fewer side effects. However, the localised effect of PDT, on the other hand, also leads to its limitation in treating large tumours due to the limited penetration of light and it cannot treat a tumour that has metastasized already. Regarding cancer treatment, PDT is most suitable for skin-related cancers such as Bowen's disease, basal cell cancers and actinic keratosis, head and neck cancer and, oesophageal and non-small cell lung cancer (Oniszczyk *et al.*, 2016; Yang *et al.*, 2017).

In PDT, the light source is chosen to coincide with the maximum absorption wavelength of the PS. The PS works by transferring the absorbed photon energy to oxygen molecules to generate reactive oxygen species (ROS) including singlet oxygen ($^1\text{O}_2$), which leads to apoptosis and necrosis in the photosensitized cells (Lim *et al.*, 2013; Shibu *et al.*, 2013). The ROS are highly reactive, and hence they react with the

biomolecules inside tumour tissues, leading to their destruction (Shibu *et al.*, 2013). Some PSs may selectively accumulate in tumour tissues, possibly due to the leaky vasculature, poor lymphatic drainage and abnormal stromal composition of tumour tissues (Brown *et al.*, 2004).

PS is a critical component of PDT; its chemical and physical nature can significantly influence the effectiveness as well as the application of PDT. For instance, soluble PS and particulate PS could have entirely different biodistribution, resulting in the different regional therapy (Abrahamse & Hamblin, 2016). It was suggested that PS delivered via appropriate receptor-mediated carrier systems, could bind to the receptors up-regulated in the disease tissues. They could be used for PDT in treating conditions like atherosclerosis, autoimmune diseases, parasitic and bacterial infections and age-related macular degeneration (Sharman, 2004). Figure 1.1 illustrates the working mechanisms of PDT.

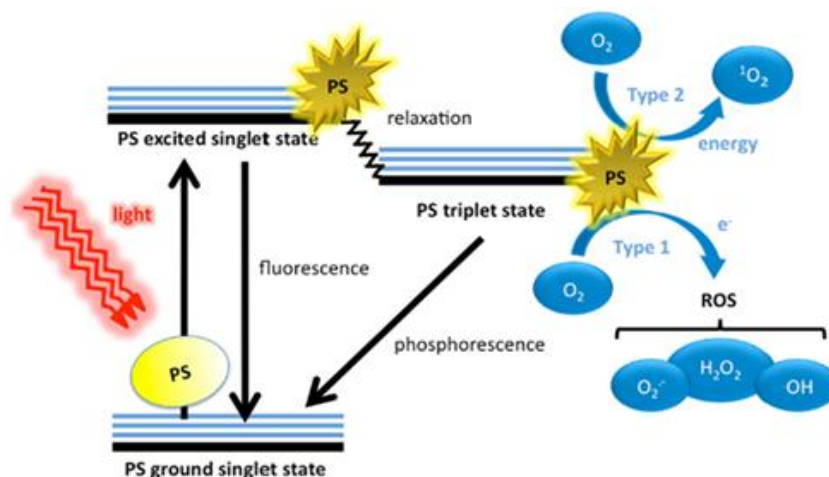


Figure 1.1 Mechanism of PDT (Dai *et al.*, 2012)

The PS when exposed to the light of adequate wavelength gets excited from ground singlet state to excited singlet state. Intersystem crossover leads to the conversion of excited singlet state to an excited triplet state, which lasts a longer time. The PS at excited triplet state can undergo two types of reactions with the surrounding molecules. The type 1 reaction occurs through a hydrogen or electron transfer, leading to the production of free radicals like hydroxyl, hydrogen peroxide (H_2O_2) and superoxide. The type 2 reaction occurs due to the energy transfer to the oxygen molecule leading to the formation of (1O_2). The 1O_2 is extremely active and has a very short lifetime (<40 ns) and can diffuse only $0.02 \mu m$ in cells before getting deactivated. The 1O_2 and

free radicals formed are collectively called ROS (Nonell & Flors, 2016). The ROS damages its site of generation and other intracellular components along with proteins, lipids and DNA and plays vital roles in PDT assisted cancer cell killing (Zhao & He, 2010; Allison & Moghissi, 2013).

PDT offers many advantages over conventional cancer therapies (American Cancer Society, 2017). These include:

- It is a highly localized therapy and used for specific tumour treatments
- Repetition of PDT therapy without cumulative toxicity is possible
- PDT is often an outpatient therapy which means the patient spends less time in the hospital.
- PSs can be modified to have multiple functions with the possibility of carrying drugs or diagnostic agents at the same time, providing metronomic chemotherapy or diagnosis.
- PDT can induce immunity, thus contributing to long-term tumour control, sparing extracellular tissue matrix that allows post-PDT regeneration of healthy tissue.
- PDT therapy provides cost-effectiveness compared to the conventional therapies.
- PDT is used as a single treatment modality and as an adjuvant treatment at various stages in cancer patient management.

The major limitations of PDT include (Paszko *et al.*, 2011):

- PDT has a limitation in treating deep-seated tumours and solid tumours due to inaccessibility of light
- It is restricted by the localisation and distribution of PSs *in vivo*
- It is not possible to treat metastasized cancers with PDT
- Photosensitivity of skin over a prolonged period of exposure to a light source can affect the patient health post-treatment

The major factor that determines the efficacy of PDT is the selectivity and effectiveness of delivering PS to the target site and the production of ROS by the PS under the light. Many factors contribute to the generation of ROS which includes nature and chemistry of the PS used, light source intensity and wavelength, the

distance between light source and PS and oxygen concentration in the tissues (Zhu *et al.*, 2007).

1.2.3 Light wavelength in PDT

The primary requirement for treatment with PDT is to make sure the light is delivered to the target tissue and can activate PS. Each PS has an optimal wavelength and intensity of light activation (Wan & Lin, 2014). The choice of the light source in PDT is based on the nature of PS. The efficacy of PDT is dependent on dosimetry, which includes total light dose, light exposure time and delivery mode of light (single or multiple irradiations). The effects of the light source can affect the therapeutic effects of PDT (Henderson *et al.*, 2006). The currently approved PSs absorb in the spectral regions between 600-800 nm, where light penetration into the skin is few millimetres, limiting PDT to treating skin lesions alone. Most tissue chromophores, including oxyhemoglobin, deoxyhemoglobin, melanin and fat, absorb weakly in the near-infrared (NIR) spectral range (700-1100 nm), the wavelengths where the deepest penetration of light is achieved, but most PSs have absorption bands at wavelengths shorter than 800 nm (Chatterjee *et al.*, 2008).

Nowadays, lasers are widely explored as a PDT light source. Modern diode lasers are portable and do not require separate electric supply, providing excellent stable power output for more extended time (Mang, 2004). Diode lasers are approved for use in human oesophageal (630 nm, Photofrin) and lung cancer (652 nm, Foscan) (Yoon *et al.*, 2013). Alternatives for lasers include light emitting diodes (LED) where light is produced by electroluminescence. LEDs are compact, lightweight and require less energy than lasers. LEDs are manufactured with different wavelength output (630 nm, 670 nm, 690 nm) that can be used in PDT for irradiation (Yoon *et al.*, 2013). However, such powerful light sources require specially designed PS in PDT (Allison & Moghissi, 2013).

Light delivery for a large surface, such as skin surface was reportedly by using broad-spectrum fluorescent lamps. The higher irradiance from sunlight was used in conventional phototherapy (See *et al.*, 2016). Phototherapy also uses middle wave ultraviolet rays (UV) (UVB, 290-315 nm) and long wave UV (UVA, 315-400 nm) (Krutmann & Morita, 1999). Many metal oxides semiconductors, including ZnO NPs,

are responsive to the lights within this range of wavelengths. UV-A radiation has certain advantages such as 1) many PSs absorb UV-A radiation better than UV-B; 2) sunlight naturally contains more UV-A than UV-B; 3) it has better penetration across dermis layer of skin than UV-B (Maddodi *et al.*, 2012). UV-A is also used in the treatment of skin lymphoma, in combination with psoralen, known as PUVA (American cancer society, 2017). However, the limited penetration depth of UV-A radiation is a major limitation (Smith *et al.*, 2012) and hence deep-seated solid tumours cannot be reached. However, such limitation may be compensated to a certain extent when an effective and powerful PS is employed. Once the light source is selected, the ultimate success of PDT then relied on the delivery and property of PS. In the following sections, the focus will be on PS.

1.3 Photosensitizers for PDT

1.3.1 First generation PSs

The first-generation PSs are Hp and its related derivatives isolated from haemoglobin. Later, porphyrin dimers and oligomers isolated from HpD were introduced as photofrin (Zhang *et al.*, 2017). Even though photofrin is used in treating different cancers it suffered severe limitations due to the lack of chemical purity as it is a mixture containing more than 60 molecules. The long half-life of photofrin and occurrence of strong skin accumulation led to skin photosensitization even for 2 to 3 months after photofrin treatment. An effective skin penetration with the first generation PSs is not obtained due to the short wavelength activation (Allison *et al.*, 2008; Shibhu *et al.*, 2013).

1.3.2 Second generation PSs

The second-generation PSs are derived from Hp but with less toxicity and unwanted tissue accumulation due to their high purity. They include phthalocyanines, naphthalocyanine and chlorines. They are effective in the generation of $^1\text{O}_2$ and has a strong absorption wavelength range of 650-800 nm. They also exhibited selectivity towards diseased tissues and fast elimination from body reducing their side effects (Allison *et al.*, 2008). The second-generation PSs acquired clinically are aminolevulinic acid, porphycenes, and phthalocyanines (Shibhu *et al.*, 2013). The drawbacks of the currently available second-generation PSs (Allison *et al.*, 2008) are:

- Difficulty in synthesizing and manufacturing a stable product

- The poor photoactivity of the PSs hence, activation energy required prolonged illumination times
- Inappropriate tissue half-lives causing difficulty in optimizing illumination schedule
- Tissue retention causing problems in post-therapy for patients
- Hydrophobicity of PS

1.3.3 New development of PSs

More recent research in PDT focuses on developing next-generation PSs that can be activated with light of longer wavelength, higher ROS production and have better tumour specificity. To achieve this, many approaches have been reported, including 1) modifying the already existing PSs with bioconjugates like peptides, antibody or antisense; 2) encapsulation of PS in carriers or chemical conjugation of PS to carriers that can transport the PSs effectively to the target site (Lucky *et al.*, 2015; Zhang *et al.*, 2017). Some of the recently developed anti-cancer PSs include chlorin, phthalocyanine and distyryl boron dipyrromethene (BODIPY) derivatives (Zhang *et al.*, 2017). Different nano strategies have been studied for PDT and being assessed both *in vitro* and *in vivo*. The different nano delivery systems include micelles, liposomes, quantum dots, metal-based NPs, polymer NPs, dendrimer NPs, carbon nanotubes, silica NPs and hybrid NPs (Shibhu *et al.*, 2013). Multifunctional nature of NPs may open options for personalized diagnosis and treatment of cancer, including via PDT. Major areas where NPs can provide significant breakthroughs include (Parvanian *et al.*, 2017; Ramirez-Garcia *et al.*, 2017):

- As carriers of specific biomarkers for cancer detection
- As contrast agents for tumour imaging
- As PSs for PDT
- As adjuvants for vaccine delivery
- As delivery systems and acting as therapeutic agents to target cells
- As molecular imaging agents for monitoring of treatment

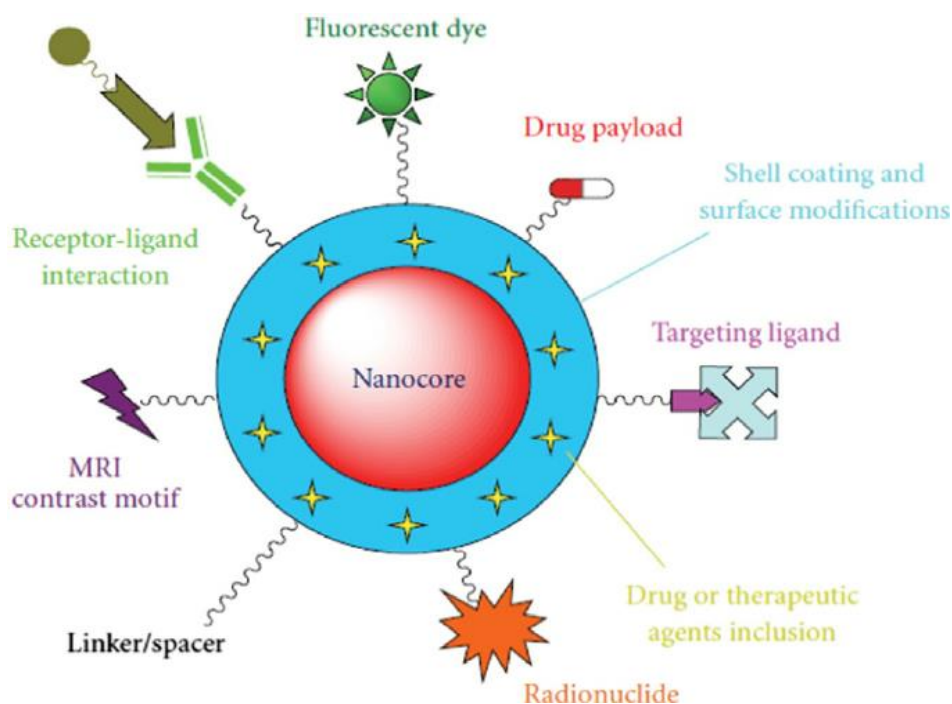


Figure 1.2 Different modifications with NPs (Chatterjee *et al.*, 2014)

1.4 Nanomaterials as PSs

NPs hold promising strategies in PDT which include 1) large surface area that can be modified for biochemical features; 2) enhanced cellular uptake due to the smaller size and large distribution volumes; 3) accumulation of nano-PSs in tumour site due to enhanced permeability and retention (EPR) effect (Li, 2013). The NPs used in PDT serve as either active or passive NPs. The active NPs themselves function as a PS while the passive NPs function as a carrier for the PSs which can be either soluble and insoluble (Thakor & Gambhir, 2013; Shibhu *et al.*, 2013). The active NPs for PDT are further sub-classified as PS NPs, upconversion NPs and self-lighting NPs (Li, 2013). As a drug carrier, nanomaterials can be used for soluble and even insoluble PS (Shibhu *et al.*, 2013). Details are discussed in the following section.

1.4.1 Metal oxide-based NPs

Semiconductor metal oxide NPs based PS is another upcoming approach in PDT. The widely studied semiconductor nano-PS includes titanium oxide (TiO₂), ZnO and graphene oxide (GO) (Smith *et al.*, 2012; Kalluru *et al.*, 2016). The nanosize of the metal oxides helps them in cell penetration and ROS production on irradiation (Zheng *et al.*, 2016). Metal oxide NPs can act as photosensitizing agents in place of PS molecules and kill tumour cells *in vitro* and *in vivo*. They can be directed to the tumour

site via attached tumour-targeting ligands. Compared to other type of materials, metal oxides are more efficient in producing photosensitization due to their better photocatalytic property (wide band gap), on illumination with light source leads to production of large amounts of ROS, ultimately leading to cell apoptosis (Vinardell & Mitjans, 2015). Graphene oxide-(polyethylene glycol-folic acid) PEG-FA mediated PDT upon NIR light (980 nm) resulted in a reduction of cell viability in B16-F10 tumour model (Kalluru *et al.*, 2016). ZnO NPs modified with metal ions like iron (Fe), Ag, lead (Pb) and cobalt (Co) has proved to induce an anti-proliferative effect on HepG2 cells irradiated with UV rays (320-400 nm). A significant increase in H₂O₂, nitric oxide (NO) and superoxide dismutase (SOD) levels and a significant reduction in catalase (CAT), glutathione peroxidase (GSH-Px) levels are reported with the metals modified ZnO NPs and attributed for their anti-proliferative effects (Ismail *et al.*, 2014). Table 1.1 illustrates the different types of metal oxide-based NPs used in PDT and their implications.

Table 1.1 Different metal oxide-based NPs in PDT

Type of metal oxide-based nano-PS	PDT	Effects reported	Reference
Graphene oxide coated with PEG-FA (~100 nm)	808 nm, NIR lasers, 288 J/cm ² . 980 nm, NIR laser, 345.6 J/cm ²	In B16-F10 cells. No cellular death in the dark. PDT at 808 nm: 35 % viability at 75 µg/mL. 980 nm: 85% cell death at 75 µg/mL	Kalluru <i>et al.</i> , 2016
Titanium oxide NPs	Germicidal UV lamp, 3 min	In SMMC-7721 cells. 10% cell death with TiO ₂ NPs alone (25 µg/mL, 48 h). TiO ₂ with UV radiation at similar condition 35% cell death	Zhang <i>et al.</i> , 2014
Iron oxide modified pyropheophorbide (74 nm)	675 nm laser, 9 J/cm ²	In human ovarian cancer cells (SKOV-3). At 32 µg/mL 15% cell death in dark. With PDT 65% cell death observed	Tan <i>et al.</i> , 2016
FA-GO-ZnO	Visible light radiation	In HeLa cells >90% cell viability in the dark (100 µg/mL). After light exposure 19.6% cell viability.	Hu <i>et al.</i> , 2013
Ag-ZnO Fe-ZnO Pb-ZnO	UV light	In HepG2 cells, IC ₅₀ 42.6 (Fe-ZnO), 37.2 (Ag-ZnO), 72.2 (Pb-ZnO).	Ismail <i>et al.</i> , 2014
Au-ZnO	UV light	In HeLa cells at dark (100 µg/mL) >80% cell viability. After light exposure 28% cell viability	Kang <i>et al.</i> , 2015

1.4.2 ZnO NPs

ZnO is an inorganic metal oxide classified as a semiconductor in group II-VI, with covalence in the boundary between ionic and covalent semiconductors. A broad energy band (3.37 eV), high bond energy (60 meV) and high thermal and mechanical stability at room temperature make it attractive for potential use in electronics, optoelectronics and laser technology (Mirzaei & Darroudi, 2017). The piezo and pyroelectric properties of ZnO makes it suitable as a sensor, energy generator and photocatalyst in hydrogen production (Radzimska *et al.*, 2014). ZnO has broad applications in cosmetics and sunscreens, food industry, paints, optoelectronic, electronic devices and biomedical industries.

Physicochemical properties of ZnO NPs such as size and charge have a strong influence on its stability, targeting ability, biodistribution and elimination. For instance, the dissolution rate of ZnO NPs is size dependent, where smaller size NPs exhibited better dissolution rate in artificial gastric fluid (Wang *et al.*, 2007). Furthermore, it is critical for cell internalisation. It is reported that the entry of ZnO NPs into cells was based on size with small sized 20 nm, positively charged NPs entering the cells better than 70 nm NPs (Yu *et al.*, 2011). The size played a crucial role in their elimination. 20 nm sized ZnO particles were eliminated faster than 70 nm NPs (Paek *et al.*, 2013). Also, the harmful effect of ZnO NPs to healthy body cells was related to its size, with size range, 4-20 nm caused more harm (Hong *et al.*, 2013). Yuan *et al.* (2010) reported that cytotoxicity against HELF cells was independent of the size of the ZnO NPs in size range 20-40 nm. In another study, Baek *et al.* (2012) demonstrated that the ZnO NPs mainly accumulated in liver, lungs and kidney and size of the NPs (20 nm & 70 nm) did not play a significant role in its distribution characters, even at high dosage.

Naturally, ZnO NPs are stable in the aqueous state due to the high density of electric charge (Akhtar *et al.*, 2012). ZnO NPs with a negative surface charge is better absorbed into systemic circulation compared to positive charged NPs although the tissue distribution is not based on the charge. The faecal excretion of positive charged ZnO NPs is higher than the negative charged ZnO NPs (Paek *et al.*, 2013). A detailed report about ZnO NPs as an experimental therapeutic agent can be found in the recent review by Zheng *et al.* (2016).

ZnO NPs in PDT

ZnO is cheap, stable and has photoluminescence. It absorbs UV-A and UV-B radiation, and facilitates the production of ROS, acting as a PS (Gupta *et al.*, 2013). Zhang *et al.* (2014) reported ZnO NPs as a new class of PS. ZnO with its photocatalytic property is induced by a light source to produce cancer cell destruction in PDT. There are substantial amounts of data indicating ZnO alone or in combination with UV light can produce anticancer effects (Kalluru *et al.*, 2016; Guo *et al.*, 2008; Vijayaraghavan *et al.*, 2015; Hariharan *et al.*, 2013).

Table 1.2 shows the compilation involving ZnO as a PS in PDT and its effects. Yang and Ma, (2014) demonstrated that the cytotoxicity of ZnO NPs is dose, time and irradiation wavelength dependent. The irradiation enhanced cytotoxicity within first 8 to 16 h, with photocatalytic reactions being the dominant factor during the early stage of cell destruction (Yang & Ma, 2014). The light excited PS resulted in ROS generation which was responsible for cellular and molecular events leading to selective tumour destruction (Yang & Ma, 2014; Li *et al.*, 2010). It is suggested that the irradiation treatment assisted ZnO NPs to gain better dispersion conditions that may promote the uptake of NPs into cells and elicit a higher cell death rate. ZnO suspension generated a more significant number of oxyradicals when irradiated with visible light at 400-500 nm compared to ZnO alone (Yang & Ma, 2014).

A study examining the combination of UV-A mediated photocatalytic therapy and chemotherapy with paclitaxel or cisplatin showed elimination of tumour cells at low concentration levels of ZnO was possible. The cell lines did not show a reduction in cell viability following UV-A treatment alone or when exposed to ZnO NPs without UV-A irradiation (Hackenberg *et al.*, 2012). Another study by Guo *et al.* (2008) using photoexcited ZnO NPs and daunorubicin demonstrated the synergistic effect on leukaemia cell lines. Even though ZnO NPs inhibited cancer growth, UV irradiation enhanced this effect.

Table 1.2 ZnO NPs in PDT

Cell lines used	PDT	Effects reported	References
HLaC 78 laryngeal squamous cell carcinoma	4 KW UV lamp of light intensity 20 mW/cm ² used. UVA radiation for 15 min, filtered to wavelength between 340 -440 nm	ZnO (0.2 µg/mL) +UV-A, IC50 1.2 µg/mL in HLAC 78 cell line	(Hackenberg <i>et al.</i> , 2012)
Cal-27 human tongue squamous cell carcinoma		ZnO (0.2 µg/mL) +UV-A, IC50 1.6 µg/mL in Cal-27 cell line	
A549 human bronchoalveolar carcinoma	UVGL-58 UVA, 366 nm UVGL-25 UVC, 254 nm	Cells irradiated with UVA (53.5% viable cells), UVC (49.1% viable cells) had higher cytotoxicity under equivalent dose (25 µg/mL) and time conditions (3 h) compared to dark control group (85.9% viable cells).	(Yang & Ma, 2014)
HeLa cells	150W mercury vapour lamp and tungsten halogen lamp (spectral window 300-700 nm)	ZnO/PVP nanorod at 50 µg/mL, viable cells more than 80% ZnO/PVP nanocomposite with daunorubicin loaded at 50 µg/mL, viable cells less than 30%. Free daunorubicin at same concentration was above 40%	(Hariharan <i>et al.</i> , 2013)
SMMC-7721 cancer cells	Germicidal lamp (UVC=254 nm). 0.1 mW/cm ²	ZnO (20 nm), only ZnO NPs at 25 µg/mL, cell viability above 60%, with ZnO NPs+UV less than 40% viable cells. ZnO (60 nm), only ZnO NPs at 25 µg/mL, viable cells close to 60%, with ZnO NPs+UV less than 40 % viable cells. ZnO (100 nm), only ZnO NPs at 25 µg/mL, viable cells 50%, with ZnO NPs+UV less than 30% viable cells.	(Li <i>et al.</i> , 2010)
SMMC-7721 hepatocarcinoma cells	Germicidal UV lamp (0.1 mW/cm ² , for 3 min)	ZnO at 100 µg/mL had no impact on cell viability (more than 90% viable cells). ZnO+UV at 100 µg/mL cell viability reduced to nearly 50%.	(Zhang <i>et al.</i> , 2014)

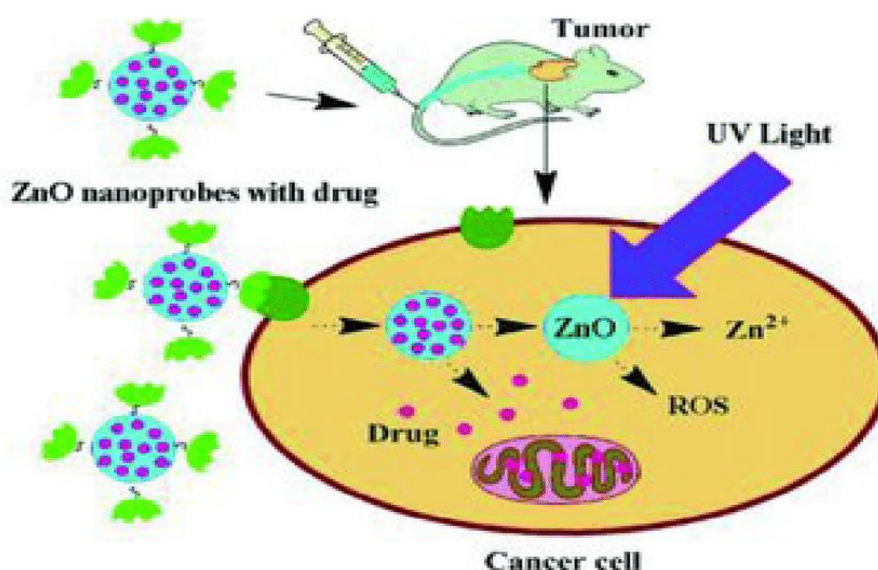


Figure 1.3 ZnO nano-PS in PDT (Bhat *et al.*, 2017).

1.4.3 Hybrid NPs

Hybrid NPs are nanostructures whose biological effects are better than the individual components. When individual components are used in the treatment of cancer, they have limited use and multiple systems like hybrid NPs may serve the purpose better (Sailor & Park, 2012). The advantages of hybrid NPs are: 1) multiple components can be integrated into a mono system; 2) monitoring the progress and efficacy of therapy throughout the entire treatment course is possible (Sailor & Park, 2012). Feng *et al.* (from Professor Xia Lou's group) reported TiO₂-SiO₂ core-shell structures that suppress human nasopharyngeal epidermoid cancer cells (KB) *in vitro*. These NPs are non-toxic in dark conditions in KB and L929 cells and exerted toxicity only when irradiated with UV light; due to the super photo optic properties of the core materials of TiO₂. Later, they developed Fe₃O₄-ZnO hybrid NPs and reported that it has significantly improved photophysical properties of ZnO, which provided the strong basis for using such hybrid NPs as a PS in PDT (Feng *et al.*, 2014). The hybrid ZnO NPs are developed to decrease recombination rate of photogenerated electron-hole pairs and segregating the charge carriers for ROS formation. Enhanced ROS formation leads to better photo-killing against cancer cells (Zheng *et al.*, 2016). Further studies on the cytotoxic activity of Fe₃O₄-ZnO hybrid NPs against Caco-2 exhibited cell death of more than 85% 24 h post-NPs treatment (50 μg/mL) with UV-A irradiation (10 J/cm²) (Patel *et al.*, 2017). These results demonstrated that the hybrid semiconductor

nanomaterials could serve as a potential PS against cancer, although further study needs to be conducted using different cancer cell lines. Also, a combination of NPs and its incorporated therapeutic agents, have been reported to show synergistic effect with the potential to address drug resistance and tumour heterogeneity (He *et al.*, 2015).

Studies on hybrid semiconductor NPs include the work by Gao *et al.* (2017) who developed a special type of oxygen generating hybrid NPs to improve PDT efficiency, with manganese dioxide NPs in indocyanine green modified hyaluronic acid NPs and tested it against SCC7 tumour model. When irradiated with a laser, 808 nm, 300 J/cm² more than 86.83% cells were killed. Work by Karbalaee *et al.* (2016) demonstrated that graphene oxide-TiO₂ hybrid NPs could serve as a PS against A375 melanoma cells. Even at a low dose of 1 µg/mL the hybrid, PS exhibited 25% cell death at UV light dose for 10 min. Kang *et al.* (2015) reported that nanorods made of Au-ZnO hybrid were able to reduce the HeLa cell viability to 28%, after 2 min UV light irradiation.

1.4.4 Silica NPs

Silica NPs has attracted a lot of attention in the biomedical field due to its hydrophilicity and versatility which renders it with biocompatibility, good chemical stability and easier surface modification (Wang *et al.*, 2008). It has been used as a drug carrier, for gene delivery (Csogor *et al.*, 2003) and as fluorescent probe. Silica NPs are transparent and do not function as a PS, however, encapsulating PS in silica NPs is a common approach for PS delivery (Shibhu *et al.*, 2013). For instance, silica has been used for better delivery of complex organic PS drugs such as phthalocyanine (Pc4), 5,10,15,20-meta-tetra(hydroxyphenyl)chlorin (m-THPC), protoporphyrin IX (PpIX) and (2-[1-hexyloxyethyl]-2-devinyl pyropheophorbide-a) (HPPH) (Roy *et al.*, 2003; Simon *et al.*, 2010). Deng *et al.* (2013) also reported the beneficial effect of loading PS polyhematoporphyrin (C₃₄H₃₈N₄NaO₅, Photosan-II, PS) in hollow silica (hs) NPs against human cholangiocarcinoma QBC939 cells in PDT (630 nm laser as light source, dose 10 J/cm²). There is a significant difference in the cell killing with PS loaded hs NPs killed 95.3% cells whereas free PS could kill only 55.7% cells. Despite its use as carrier for various purposes, in the design of hybrid NPs used in this study, SiO₂ was used to improve the dispersion and biocompatibility of the hybrid NPs

(Wang *et al.*, 2008; Han *et al.*, 2008), and as a precursor for the further conjugation of the targeting ligand FA.

1.5 Cell killing mechanisms in PDT

The cell death post PDT treatment involves multiple pathways. The different cell death mechanisms activated by PDT are discussed below. The different processes that destroy tumours by PDT are direct cellular damage, indirect vascular shutdown and activation of immune responses against tumour cells (Dougherty *et al.*, 1998; Dolmans *et al.*, 2003). The three major processes controlling the cell death are apoptosis, necrosis and autophagy. Apoptosis and necrosis are classified according to cellular, morphological and biochemical characters. Necrosis involves extensive cell lysis and cell death associated with membrane damage, leakage of cellular components to extracellular space and cell swelling at the endpoint (Majno & Joris, 1995). Apoptosis is a more regulated form of cell death, associated with mitochondrial dysfunction, loss of mitochondrial membrane potential and respiratory chain inhibition, cellular shrinkage, DNA fragmentation and membrane blebbing (Majno & Joris, 1995). Apoptosis or necrosis can occur in response to treatment in a dose-dependent fashion. The cells that fail to undergo cell death through apoptosis undergo autophagy, where the cells are recycled (Kessel & Oleinick, 2018).

1.5.1 PDT and apoptosis

Apoptosis is initiated by death receptors activation or mitochondrial release of cytochrome c. These events ultimately activate the executioner caspases (caspase-3, -6 and -7). The caspases on activation cleave the cellular substrates, leading to morphological and biochemical changes observed in dying cells (Mroz *et al.*, 2011). Bcl-2 and other members of the family inhibit apoptosis and PDT is believed to photodamage Bcl-2 and other anti-apoptotic proteins and activate pro-apoptotic proteins (Kessel & Oleinick, 2018). After PDT, the opening of the mitochondrial membrane permeability pores occurs and results in dissolution of mitochondrial membrane potential, which is expected to be the main reason behind cytochrome c release (Mroz *et al.*, 2011). Death receptors belong to tumour necrosis factor receptor (TNFR) family, and TNFR signalling is believed to be an important factor in immune response, inducing apoptosis (Mroz *et al.*, 2011). Studies have revealed ultrastructural

and biochemical features of apoptosis following PDT. PDT of tumour cells resulted in immediate or early apoptosis, within 30-60 min of initial treatment (Luo *et al.*, 1996).

Protein kinase pathways in PDT induced apoptosis

Activation of mitogen-activated protein kinase (MAPK) pathways is a character of oxidant-induced apoptosis. H₂O₂ treatment resulted in sustained activation of all three major MAPK pathways (extracellular signal-regulated kinases (ERK 1/2), JNK and p38 MAPK) in HeLa cells (Purdom & Chen, 2005). H₂O₂ induced JNK activation, may involve the participation of death receptors, receptor tyrosine kinases and redox-related molecules (Shen & Liu, 2006). ROS signalling interacts with other physiological signalling pathways by acting on different protein phosphatases (Rhee *et al.*, 2005).

1.5.2 PDT and Necrosis

Although the factors that lead the cells to PDT mediated necrosis is not clear, it is believed either high concentration of PS or high light dose or a combination of both is believed to cause necrotic cell death. High dose of PDT may inactivate the enzymes responsible for inducing caspase and related events, ultimately inhibiting apoptosis and the cells undergo necrosis (Morz *et al.*, 2011). Direct photodamage of the plasma membrane also leads to necrotic cell death. Many PDT protocols do not rely on necrotic cell death mechanism as it can be a nonspecific effect, leading to adverse effects on healthy cells (Kessel & Oleinick, 2018).

1.5.3 PDT and Autophagy

Autophagy has a two-sided effect where it can defend against ROS damage clearing the cell of damaged organelles or induce autophagic cell death. Many PSs target autophagy-related organelles lysosomes and endosomes (Morz *et al.*, 2011). Autophagy can offer partial protection against mitochondrial damage after PDT but not when lysosomes are the PDT target. Thus, targeting lysosomes may result in lethal photodamage (Kessel & Oleinick, 2018).

PDT and ROS

ROS generated in mitochondria or elsewhere in cells, can induce damage to cellular components including nucleic acids, phospholipids and proteins (Orrenius *et al.*,

2011). ROS produced by a PS upon radiation consists of a list of oxidative species which includes superoxide anion, hydroxyl radical, H₂O₂, hypochlorous acid and ¹O₂. The major factors behind NP induced ROS may vary from one type to another. For the semiconductor metal oxides, it includes the nature of the core NPs, the NP-cell interactions, and the coating (shell) component. The coating has a negative impact on the ROS generation by the core NP, as reported by Feng *et al.* 2015a, it also affects the NP-cell interaction, mostly in a positive way especially when a targeting ligand is present. NPs due to their smaller size, therefore, high surface to volume ratio, have been reported to generate a higher level of ROS, than the same material in powder form (Wilson *et al.*, 2002). Upon light activation, the PSs undergo photochemical reaction to generate ROS under aerobic condition, dominated by ¹O₂. The photochemical ROS generation leads to direct cell killing at the site of PS activation. The main therapeutic value of PDT is targeted cell killing, controlled by site-specific generation of ROS (Gomer *et al.*, 1989).

The complete mechanism of PS in PDT *in vivo* is yet to be elucidated, although tumour cellular events, vascular inflammation and systemic immune effects have been proposed (Allison & Moghissi, 2013). However, it is known that inflammatory and immune responses together could maximise the tumour damage with PDT (Brown *et al.*, 2004).

1.6 PDT in skin cancer treatment

Skin cancer occurs when skin is damaged or excessively exposed to UV radiation. Skin cancer is of three types: basal cell carcinoma (BCC), squamous cell carcinoma (SCC) and melanoma, the most dreadful one. The BCC and SCC are classified as non-melanoma skin cancers (Chummun & Mc Lean, 2017). 80% of new cancers diagnosed in Australia are skin cancers, and Australia has the highest occurrence rate of skin cancers globally (Cancer Council, Australia). The exact sequence of events that transform melanocytes to malignant melanoma is unknown, though it is believed to have genetic mutations which alter cell growth, differentiation and death and enhance its susceptibility to UV radiation (Chummun & Mc Lean, 2017; Craythome & Al-Niami, 2017). Surgery is the only curative option for melanoma currently. Electrochemotherapy (ECT) is effective in treating melanomas which involves short

electrical pulse, which destabilizes the cell membrane and enhances the cell permeability of cytotoxic drugs (Chummun & Mc Lean, 2017).

To avoid prolonged photo sensitivity on systemic administration, topically applied PSs have been developed for skin cancer therapy. The commercially available PSs for skin cancer include ALA and methyl ester methyl 5-aminolevulinate (MAL) (Zhao & He, 2010). ALA-PDT is mainly used to treat dermatological cancers in human beings (Morton *et al.*, 2013; Wan & Lin, 2014). ALA-PDT in the treatment of human Bowen's disease (SCC in situ) has been successful with response rates between 82-100% in 1 to 2 years (Salim *et al.*, 2003). PDT is used for the treatment of BCC as a single agent or as an adjuvant (Berroeta *et al.*, 2007).

Skin cancer treatment can obviously be benefited from PDT as the cancer tissues are easily accessible to the light, plus, currently, there is an urgent need for better treatment in skin cancer like melanoma. In a recent study, the hybrid NPs in combination with UV light has shown a better anticancer effect against A375 melanoma cells. For instance, graphene oxide-TiO₂ hybrid NPs (1 & 100 µg/mL, 24 h) in combination with UV light (10 min) exhibited 20% and 50% cell growth inhibition, whereas, only hybrid NPs exhibited 10% and 25% cell growth inhibition (Karbalaie *et al.*, 2016). This PhD project will investigate the potential application of the new class hybrid Fe₃O₄-ZnO NPs as an effective nano-PS against melanoma cells and other cancer cells.

1.7 OVERALL OBJECTIVES

The principle aim of the research is to study systemically, both *in vitro* and *in vivo*, the pharmaceutical and biological properties of a new class nano-PSs that are composed of Fe₃O₄ and ZnO and further conjugated with a targeting ligand FA through a silica precursor. As shown in Figure 1.4, the hybrid NPs contain Fe₃O₄ and ZnO in a mass ratio of (1:4) with a silica shell thickness of 4-5 nm (Feng *et al.*, 2015a). The research was firstly focused on the *in vitro* characterisation of the hybrid Fe₃O₄-ZnO NPs, to understand their pharmaceutical and biological properties, and how they could be utilised efficiently to produce cancer-killing effects in cells. The study was then extended to an animal cancer model via intra-tumour administration of the selected NPs for further investigation of the PDT effect on melanoma tumours.

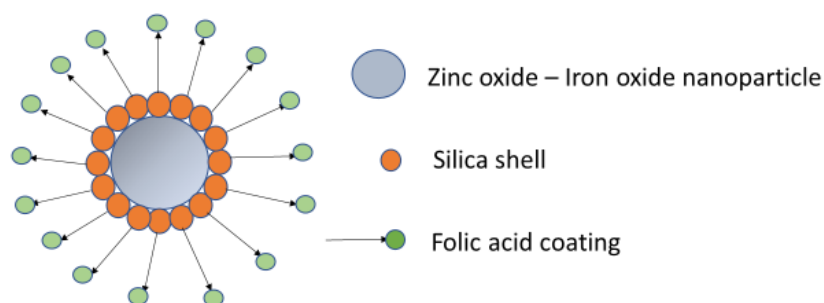


Figure 1.4: A schematic illustration of the nano-PS: Fe₃O₄-ZnO hybrid NPs

The project was designed to answer the following questions:

- How effective can the new class nano-PS be as an anticancer drug attenuated by UV irradiation under designated wavelength?
- How does the nature of nano-PS influence its cytotoxicity?
- Does targeting ligand FA enhance cancer cells killing of nano-PS?
- What is the major mechanism of cell killing effects of new class nano-PS and how it affects its cellular uptake?
- To what extent the surface modification of the nano-PS has an impact on cytotoxicity and its *in vivo* anticancer activity?
- What are the therapeutic effects of PDT with the new class hybrid nano-PS in an animal model?
- How does the time interval between treatment of nano-PS and UV-A irradiation affect the therapeutic outcome of PDT?

CHAPTER 2

MATERIALS AND METHODS

1. Materials

1.1 Chemicals used in *In vitro* studies

The following materials were used in *in vitro* studies. Those chemicals were purchased from Sigma-Aldrich (Castle Hill, Australia): 2,7-Dichlorofluorescein diacetate (DCFH-DA, D6883, 50 MG, $\geq 97\%$), 1,3-Diphenylisobenzofuran (DPBF, 105481-1 G), N-Acetyl-L-Cysteine (NAC $\geq 99\%$, A7250, 5G), Propidium iodide (PI, P4170, 10MG), 3-(4,5-dimethylthiazol-2-yl)-5-(3-cyboxymethoxyphenyl)-2-(4-sulfohenyl)-2H-tetrazolium (MTT, $\geq 97.5\%$, M2128), Dulbecco's modified eagle's medium-high glucose (DMEM, D5671), Phosphate buffered saline (PBS, 806552, 1L), Hank's Balanced salt solution (HBSS, H6648), Penicillin-Streptomycin (P4333), Fluorescein isothiocyanate (F7250, 50 MG), L-Glutamine (G7513-100 mL), Trypan blue (T6146), Triton X-100 (T8787), Bovine serum albumin (BSA, A2153, $> 96\%$), radio-immune precipitation assay buffer (RIPA buffer, R0278), Paraformaldehyde (PFA, P6148, $\geq 94.0\%$), Tetraethyl orthosilicate (131903,-1L, 98%) and Trypsin-EDTA (T4299, 100 mL). Ethanol, methanol and DMSO were sourced from VWR, Australia. Foetal bovine serum (FBS, FBS-001-AU) was obtained from SerANA (WA) Pty Ltd (Bunbury, Australia). Distilled water was purified from tap water by Hydro-Check Systems (Model no.414R, Hydro-Check Systems, Inc., Carlsbad, USA) and further sterilised by autoclave at 121°C for 1 h.

Vectashield antifade mounting medium (H-1000) was purchased from Vector Laboratories, Inc. (Burlingame, USA). Tryple express enzyme (12604-021) was obtained from Life Technologies Australia Pty Ltd (Scoresby, Australia). HyClone PBS (SH30256.02) was procured from GE Healthcare Australia Pty Ltd. (Parramatta, Australia). FITC Annexin V (556419, 200 tests) was purchased from BD Biosciences, Australia. Nitric acid (70% w/w) was acquired from Ajax chemicals, Australia. The Caspase 3/7 reagent (Ac-DEVD-AFC, ALX-260-032-M005, 5 mg) was purchased from Cayman Chemicals (14459), Australia. Confocal microscopy glass slides and coverslips (22 mm), Ibidi micro-dish (35 mm) were procured from Ibidi, Germany. The Corning T25, T75 and T175 tissue culture plates, 96 and 24 well plates, 96 well black plates (used for ROS assay) were purchased from Sigma-Aldrich (Castle Hill, Australia).

1.2 Chemicals used in *in vivo* studies

B16-F10 melanoma mouse tumour cell line (ATCC CRL 6475) was purchased from ATCC, US through In Vitro Technologies, Australia. DMEM high glucose (D5671, Sigma), Penicillin-Streptomycin (P4333, Sigma), L-Glutamine (G7513, Sigma) were purchased from Sigma Aldrich, Australia. Tryple Express Enzyme (catalogue no 12604013, Thermo Fisher) was purchased from Life Technologies, Australia. Fetal bovine serum (FBS, FBS-001-AU) was obtained from SerANA (WA) Pty Ltd (Bunbury, Australia). T75, T175 flasks, sterile pipettes (5 ml) were purchased from Interpath, Australia. UV LED SMART, 365 nm with breakout box was purchased from Opsytec Dr Grobel, Germany. I.R. Thermometer was purchased from Thermo Fisher (Catalog no.15-077-968, Australia). Digital vernier calliper was acquired from Kincome (part. No. K11100, Australia).

Dissecting scissors, 115 mm, straight (Catalog no. T104-2, ProSciTech) was purchased from ProSciTech, Australia. R & D systems Cultrex PathClear Basement membrane extract with phenol red (Matrigel) (Catalog no. RDS343200501P, In Vitro Technologies) was purchased from In vitro Technologies, Australia. Sterile scalpel blades no. 20 (Catalog no. 16827, BD Biosciences) and ultra-fine needle insulin syringe (Catalog no. 16296, BD Biosciences) were purchased from BD Biosciences, Australia. All other chemicals used in the experiments were of molecular biology grade and used as received unless otherwise specified.

Male C57BL/6 mice aged four weeks were purchased from Animal Resource Centre, Perth, Australia. All the animal purchase and studies were duly reviewed and approved by Animal Ethics Committee of Curtin University before the start of the animal study (Approval number AEC 2016-41). The animal ethics approval letter is attached in Appendix 8.

1.3 Hybrid NPs used in *in vitro* and *in vivo* studies

The novel hybrid NPs studied in this thesis work were provided by Professor Xia Lou of the Department of Chemical Engineering, Curtin University. Details of the synthesis and characterisation methods can be found in previous publications (Feng *et al.*, 2015b, Patel *et al.*, 2017).

2. Methods

In vitro studies

2.1 Cell culture

B16-F10, 3T3 and Caco-2 cell lines were procured from the ATCC. The culture details for the three cell lines are presented in Table 2.1. Cell growth, morphology and confluency were regularly monitored with a Nikon inverted microscope (Eclipse TS100, Nikon Instruments Inc., Tokyo, Japan) and images were captured with the attached Nikon digital sight camera (DS-Fi2) and controller (DS-L3). Mycoplasma was routinely tested for in the facility by genomic PCR using cells cultured in an antibiotic-free medium. Sample preparation for the mycoplasma testing is explained in Appendix 2.

Table 2.1. The B16-F10, 3T3 and Caco-2 cell culture details

	B16-F10	3T3	Caco-2
Cell type	Mouse skin Melanoma	Mouse Embryo Fibroblasts	Human epithelial colorectal adenocarcinoma cells
Origin	ATCC	ATCC	ATCC
Passage number	1-10	20-30	81-91
Culturing flasks (medium volume)		Corning T25 (5-6 mL) Corning T75 (8-10 mL) Corning T175 (20 mL)	
Frequency of medium change		Every 2 to 3 days	
Cytotoxicity (96 well)	✓	✓	✓
Uptake studies (24 well)	✓	-	✓
ROS detection (96 well black)	✓	-	✓
Confocal Microscopy	Performed only in B16-F10 cells	-	-
Culture medium	DMEM-high glucose	DMEM-high glucose	DMEM-high glucose
Serum	10% (v/v) FBS	10% (v/v) FBS	10% (v/v) FBS
Supplements	1% (v/v) P/S 1% (v/v) glutamine	1% (v/v) P/S 1% (v/v) glutamine	1% (v/v) P/S 1% (v/v) glutamine

After reaching 70-80% confluency, the B16-F10, 3T3 and Caco-2 cells were trypsinized, centrifuged (Allegra X-12 Centrifuge, Beckman Coulter, Inc., Brea, USA) and cultured by seeding into appropriate plates for experiments. The specific culture medium and culture conditions are summarised in Table 2.1. The culture was carried

out at 37°C with, 5% CO₂ and 95% humidified air in an incubator (Lab friend, C170, Australia). Cryopreservation and thawing of cells are described in Appendix 4.

2.2 UV chamber optimization

A UV chamber (UV BS02 chamber from UV Groebel, Germany) with controllable dose setting was used in the study. It was supplied with UV-A lamps (365 nm, 8x15W output) to our requirement. The UV chamber employed in the experiment was approved by the radiation safety officer, Curtin University (Appendix 5). The time taken to reach the fixed dose of 10 J/cm² was investigated under different conditions: variable distance between light source and cell culture plates, temperature change in the culture well due to the heat generated from the light source and time of UV-A exposure. The temperature of the medium in cell culture plates was measured using an IR thermometer (4470CC, Infrared traceable thermometer gun, ThermoFisher, Australia) before and after light exposure.

2.3 Pharmaceutical evaluation of hybrid NPs

Stability of NPs in different medium

The stability of NPs is highly critical as it may impact on NPs uptake by cells, their toxicity and availability of NPs at the cellular level. The stability of NPs was analysed in two different medium PBS and DMEM high glucose. The DMEM was supplemented with 10% FBS and 1% L-Glutamine. The NP suspensions were stored at 37°C in stability chamber (Challenge 700, Angelantoni Industrie spa, Italy) for various time periods (0 h, 6 h, and 24 h). The hydrodynamic particle size was assessed via dynamic light scattering (DLS) using a Zetasizer Nano ZS (Malvern Instruments, UK). Zeta potential measurement was carried out using the same instrument. The size and zeta-potential experiments were conducted with a concentration of 100 µg/mL NPs suspension. Samples were dispersed in the medium using an ultrasonic bath (Unisonics, Australia) for 5 min before measurement.

2.4 Evaluation of cytotoxicity

Cytotoxicity of NPs under investigation was assessed by 3-(4,5-dimethylthiazol-2-yl)-5-(3-cayboxymethoxyphenyl)-2-(4-sulfophenyl)-2H-tetrazolium (MTT) assay as described by Mosmann (Mosmann *et al.*, 1983; Hackenberg *et al.*, 2012), with some

modifications. NPs at 12.5 – 100 µg/mL were tested in three cell lines and at two-time points (6 h and 24 h). The test procedure followed is described below:

1. MTT was dissolved in PBS (pH 7.4) to obtain a stock concentration of 1 mg/mL in a sterile container and wrapped in aluminium foil for protection against the light (refer Appendix 6 for the detailed procedure of MTT stock solution preparation).
2. Corning 96-well plates were used for cell seeding and the assessment. The seeding density of various cells is specified in the next section.
3. After 70-80% cell growth in the 96 well plates, the cell medium was replaced with 100 µL of medium containing different concentrations of the NPs.
4. At predetermined time points (6 h and 24 h) after NPs treatment, 100 µL of MTT solution was added to the cells in the culture, attaining a final MTT concentration of 0.5 mg/mL, and further incubated for 3 h.
5. After 3 h, the medium in each well was aspirated, and cells were washed twice with PBS (100 µL per well each time) and replaced with 100 µL DMSO and left for 10 min at the incubator to completely dissolve the MTT formazan crystals.
6. The quantity of formed formazan crystal is directly proportional to the number of viable cells and measured by recording absorbance at 570 nm using the Enspire ® 2300 multimode plate reader (Perkin Elmer Corporation, Wellesley, USA).
7. Simultaneously, wells containing NPs in medium without cells were used as the NPs blank. The blank data was subtracted from each corresponding NPs sample data to obtain the net absorbance data.
8. The cells treated with medium served as the control and medium alone served as the blank.
9. Cell viability was calculated following Equation 2.1:

$$\text{Cell Viability (\%)} = \frac{A_{\text{test}} - A_{\text{NP blank}}}{A_{\text{control}} - A_{\text{medium blank}}} \times 100 \quad (\text{Equation 2.1})$$

Where A_{test} is the absorbance of the formazan produced by cells incubated with NPs in medium, $A_{\text{NP blank}}$ is the absorbance associated with just NPs in medium without cells, A_{control} is the absorbance of just cells in medium and $A_{\text{medium blank}}$ corresponded

to the absorbance of the DMEM medium. The results were reported as an average of four replicates with STD.

(i) Cytotoxicity in B16-F10 cells

5×10^3 cells per well were seeded in 96-well plates and incubated for 48 h. After 70-80 % confluency, the cell medium was completely removed and replaced with fresh medium containing hybrid NPs (FZ, FZSi, FZSiFA25 and FZSiFA50 NPs at concentrations of 12.5, 25, 50 and 100 $\mu\text{g}/\text{mL}$) and treated for 6 h and 24 h. After NPs treatment, MTT solution 100 μL (1 mg/mL) was added per well and incubated for 3 h at 37°C. The resulting formazan product was dissolved in DMSO (100 μL per well). The absorbance was quantified at 570 nm using a microplate reader (Perkin Elmer, US). The entire experimental set up was replicated, and unpaired t-test was performed using the two sets of quadruplicate results. If the first two data sets were statistically different ($P < 0.05$), then another replicate was carried out.

(ii) Cytotoxicity in Caco-2 and 3T3 cells

The same procedure was carried out in both Caco-2 and 3T3 cells. The initial cell density was 5000 cells per well and 2000 cells per well for Caco-2 and 3T3 respectively. Other conditions were same as above.

2.5 Evaluation of hybrid NPs in PDT

The toxicity of photoactivated NPs was assessed using MTT procedure following the UV-A radiation. The study was carried out in B16-F10 and Caco-2 cells at 24 h post treatment only. For both cell lines, 5×10^3 cells per well were seeded and allowed to grow for 48 h. The cell culture medium was replaced with fresh medium containing FZ, FZSi, FZSiFA25 and FZSiFA50 NPs at concentrations of 12.5, 25, 50 and 100 $\mu\text{g}/\text{mL}$. After the exposure of the cells with NPs for 24 h, the plates were treated with UV-A radiation (365 nm) at a dose of 10 J/cm^2 in a BS-02 UV chamber (8 x 15 W lamps at 120 W total power output) for 9.18 min (at 10 cm distance from the UV-A lights). Chamber temperature was monitored using an IR thermometer (4470CC, Infrared traceable thermometer gun, ThermoFisher, Australia) and maintained via circulating fan within the chamber. The cells were cultured further for 24 h, and cell viability was assessed via the MTT assay described in Section 2.4.

2.6 Evaluation of PDT of hybrid NPs with multiple UV-A irradiations

One of the advantages of using hybrid NPs in PDT is that the administration of a single dose of NPs or PS permits repeated application of multiple doses of PDT. This is achieved simply by repeated irradiation of light source, resulting in continuous anticancer effects. Hence the impact of multiple irradiations on the hybrid NPs was studied in this experiment. Double radiation was given with a 2 h interval, and triple radiation was given 2 h post second radiation. The irradiation dose and conditions were followed as per the phototoxicity protocol used for single irradiation (Section 2.5). This study was carried out only at the lowest concentration (12.5 $\mu\text{g/mL}$) in B16-F10 cells, where the percentage of viable cells remained higher compared to the other doses. Cell viability was calculated according to equation 2.1 with A_{test} corresponded to the cells incubated with NPs in a medium that is exposed to multiple UV-A radiations. The cells treated with multiple irradiations alone served as an additional control.

2.7 Morphology change of cells after hybrid NPs and UV-A treatment

To study morphology, change of cells, after treatment with hybrid NPs, B16-F10/Caco-2 cells were seeded (5×10^3), (3T3 cells, 2×10^3) in DMEM high glucose complete medium. NPs treatment and conditions were maintained similar to cytotoxicity in B16-F10 cells described in section 2.4. Cells were observed immediately after the treatment of NPs using (20X magnification) phase contrast microscopy (Eclipse TS100, Nikon Instruments Inc., Tokyo, Japan). Morphology changes concerning a different dose of NPs and different conditions (dark 6 h & 24h, UV-A light) were recorded.

2.8 Singlet oxygen detection

Singlet oxygen is believed to be one of the main reasons behind cellular toxicity of NPs and the singlet oxygen production ability of the investigated NPs outside cells was analysed using the chemical trapping method, known as the 1,3-diphenyl isobenzofuran (DPBF) method. The singlet oxygen generating ability of a PS was measured by its quantum yield as reported in the literature (De Rosa, & Crutchley, 2002; Nadhman *et al.*, 2014).

Singlet oxygen quantification was carried out as per the method described by Xiao (Xiao *et al.*, 2011; Nadhman *et al.*, 2014), with some modifications. DPBF solution was prepared by dissolving 0.15 mM DPBF in ethanol. Hybrid NPs (12.5 µg/ mL, 100 µL) was dispersed in 200 µL of DPBF solution. The mixture was placed in a sealed quartz cuvette and exposed to UV-A light source (BS02 UV chamber, 365 nm). After every 30-s exposure to UV-A, the absorbance of the mixture was measured at 410 nm, for up to 180 s, by a UV 3000 spectrophotometer (ORI, Germany). The UV-A lamp cuts off when the chamber door is opened at any particular time point, and this provision was used for the short time points between 30 s and 180 s. The absorbance of NPs in the dark was deducted from the absorbance of photo-irradiated NPs. The decrease in absorbance caused by photobleaching of DPBF was measured in the hybrid NPs. The natural logarithm values of absorption of DPBF were plotted against the irradiation time and fit by a first order linear least-squares model to obtain the decay rate of the photosensitized process (Nadhman *et al.*, 2014). Rose Bengal was used as the standard at the same concentration as the NPs, exposed to UV-A light and absorbance was measured at 410 nm for the degradation of DPBF.

$$\Phi\Delta N = \Phi\Delta_{\text{standard}} \times (k_N/k_{\text{standard}}) \quad (\text{Equation 2.2})$$

$\Phi\Delta N$ is the singlet oxygen quantum yield of NPs

$\Phi\Delta_{\text{standard}}$ is the singlet oxygen quantum yield of Rose Bengal (0.86)

K_{standard} is the slope of standard (Rose Bengal)

k_N is the slope of NPs

k_{standard} and k_N were determined from the slopes of the time-dependent decrease of DPBF plots, expressed as the decrease of absorbance at 410 nm.

2.9 ROS detection by DCFH-DA

2',7'-dichlorofluorescein diacetate (DCFH-DA) is a fluorogenic dye that measures hydroxyl radical, peroxy radical and hydrogen peroxide activity within the cell (Gomes *et al.*, 2005). Generation of ROS species was measured following oxidation of 2',7'-dichlorofluorescein (DCFH) and its diacetate form (DCFH-DA) inside cells (Yang & Ma, 2014). The DCFH-DA is cell permeable and hydrolysed by cellular esterase to DCFH, a compound which is unable to cross the cellular membrane. This

non- fluorescent DCFH, oxidized by intracellular ROS converts to a highly fluorescent compound, 2',7'-dichlorofluorescein (DCF).

A DCFH-DA stock solution in methanol of 10 mM was diluted 500-fold in HBSS without any other additive to yield a 20 μ M working solution. Cells were washed twice with HBSS and then incubated with DCFH-DA working solution for 1 h in an incubator under dark environment (37°C). The extracellular DCFH-DA was removed by washing with HBSS and followed by treatment with hybrid NPs dissolved in cell culture medium. The NPs were treated with different doses 12.5, 25 and 50 μ g/mL for various time periods of 0 h, 2 h, 6 h and 24 h. After NPs treatment, free NPs were removed by HBSS washing and fluorescence was measured at 485 nm excitation and 520 nm emission using a microplate reader. Cells with no NPs treatment at each time point was used as the control and medium was used as the blank. Serum in medium has been reported capable of producing fluorescence in DCF assay without presence of cells (Tetz *et al.*, 2013). Chemical activation of DCFH-DA to DCF is also possible. Hence cell free controls are important when using DCF assay. 0 h represents 5 min time point of NPs treatment. ROS generation was measured in the dark and under UV-A light-exposed conditions in B16-F10 and Caco-2 cells. UV-A radiation was given immediately following NPs treatment. Black 96 well plates with clear bottom were used for fluorescence detection.

$$\text{DCF fluorescence intensity (\%)} = \frac{F_{\text{test}} - F_{\text{NP blank}}}{F_{\text{control}} - F_{\text{medium blank}}} \times 100 \quad (\text{Equation 2.3})$$

Where F_{test} is the DCF fluorescence intensity produced in cells treated with NPs in medium, $F_{\text{NP blank}}$ is the DCF fluorescence associated with just NPs in medium without cells, F_{control} is the DCF fluorescence of just cells in medium and $F_{\text{medium blank}}$ corresponded to the DCF fluorescence of the DMEM medium.

With UV-A treated samples: F_{test} is the DCF fluorescence intensity produced in cells treated with NPs+UV-A irradiation in medium, F_{control} is the DCF fluorescence of just cells in the medium. DCF fluorescence of the cells in DMEM medium exposed to UV-A irradiation served as an additional control.

2.10 ROS quenching by NAC

This study was designed for the confirmation of NPs ability to generate ROS. N-acetyl-L-cysteine (NAC) can interact directly with ROS and RNS because it is a quencher of oxygen free radicals (Ostrovsky *et al.*, 2009; Heim *et al.*, 2015). NAC stock solution 5 mM was prepared in DMEM medium. After 48 h of cell growth, 100 μ L NAC was added to each well and left for 24 h in the incubator. NAC solution was removed, and cells were washed twice with HBSS and then incubated with DCFH-DA working solution for 1 h in an incubator under dark environment (37°C). The extracellular DCFH-DA was removed by washing with HBSS and followed by treatment with hybrid NPs dissolved in cell culture medium. The NPs were treated with different doses 12.5, 25 and 50 μ g/mL for various time periods of 0 h, 2 h, 6 h and 24 h. After NPs treatment, free NPs were removed by HBSS washing and fluorescence was measured at 485 nm excitation and 520 nm emission using a microplate reader. ROS generation after pre-treatment with NAC (ROS quencher) was measured in the dark and under UV-A, given immediately following NPs treatment) light-exposed conditions in B16-F10 and Caco-2 cells. The ROS quenching by NAC was assessed with unmodified (FZ NPs) and surface modified (FZSi NPs). Cells with no NPs treatment served as the control and medium served as the blank. The cells irradiated with UV-A radiation served as an additional control for UV treated samples. The DCF fluorescence intensity was calculated according to the equation 2.3. Black 96 well plates with clear bottom were used for the experiment.

2.11 NAC treated cytotoxicity assay

A separate cytotoxicity study involving pre-treatment of cells with ROS quencher NAC was performed to confirm the impact of ROS on cell cytotoxicity. The NPs concentration 100 μ g/mL that exhibited a maximum reduction in cell viability was used for the study. Briefly, B16-F10 cells after 48 h of cell growth were replaced with NAC (100 μ L, 5 mM & 15 mM dissolved in DMEM medium). The NAC treated wells were incubated for 24 h followed by washing with PBS and replaced with fresh medium containing NPs (at the concentration of 100 μ g/mL). The B16-F10 cells treated with NAC served as the control and B16-F10 cells treated with 100 μ L NPs (no NAC) served as an additional control. The cell viability MTT assay (described in section 3.2.2(iv)) after NAC pre-treatment was carried out in B16-F10 cells (dark only).

$$\text{Cell Viability (\%)} = \frac{A_{\text{test}} - A_{\text{NP blank}}}{A_{\text{control}} - A_{\text{medium blank}}} \times 100 \quad (\text{Equation 2.4})$$

Where A_{test} is the absorbance of the formazan produced by cells pre-treated with NAC and incubated with NPs in medium, $A_{\text{NP blank}}$ is the NAC pre-treated absorbance associated with just NPs in medium without cells, A_{control} is the absorbance of cells pre-treated with NAC in medium and $A_{\text{medium blank}}$ corresponding to the NAC pre-treated absorbance of the DMEM medium alone.

2.12 Evaluation of cellular uptake of hybrid NPs

Two types of study were conducted to assess the effect of NP ligands and incubation time on the cellular uptake of the NPs. They are a) quantitative assay involving fluorescence measurement of the NPs uptaken by the cells using a plate reader spectrophotometer and b) the qualitative assay, using confocal laser scanning microscopy (CLSM) for visual confirmation of the NP internalisation and cellular localisation. Both quantitative and qualitative study was performed in B16-F10 melanoma cells.

Fluorescein isothiocyanate (FITC) attached FZSi NPs (FZSi-FITC) and FZSiFA50 NPs were used for the cellular uptake experiments, as they contain FITC and FA, as the respective fluorescent moieties. FZSi-FITC NPs were prepared by chemically attaching the fluorophore molecules within the silica shell. In brief, 0.1500 g of FZSi NPs were dispersed in 40 mL of milli-q water to which 1.65 mL of ammonium hydroxide solution (25% wt) was added. 1.5 mg of FITC was dissolved in 20 mL ethanol and added to the NP dispersion, and the resulting solution was stirred mechanically for 15 min. 35 μL of TEOS was mixed with 20 mL of ethanol, and the solution was added dropwise over a 10 min period to the NP dispersion containing the FITC. The reaction was allowed to proceed for 3 h in the dark with continual mechanical stirring. Finally, the FITC- labelled NPs were washed to remove non-bound FITC and air dried. The FZSi-FITC labelling was carried out in the Department of Chemical Engineering.

a) Quantitative analysis

The quantitative assay was conducted by determining the amount of NPs uptake per mg of cell protein using the procedure below (Kooijmans *et al.*, 2012):

1. The cells were seeded onto a nunc-24 well plate at a density of 5,000 cells/well with DMEM high glucose medium with appropriate supplements (Table 2.1).
2. The medium was replaced every third day, and cells were maintained at 37°C, 5% CO₂ and 95% humidified air until they become nearly 70-80% confluent (2-3 days).
3. The medium was removed, and cells were rinsed twice with 500 µL of pre-warmed HBSS. The cells were incubated for 30 min in HBSS at 37°C for equilibration.
4. After 30 min, the HBSS was replaced with 500 µL of HBSS containing NPs at a concentration of 100 µg/mL.
5. After 2 and 6 h incubation time (UV-A irradiation was given immediately following NPs treatment), the medium was aspirated, and cells were washed quickly three times with cold PBS to remove excess NPs.
6. 200 µL RIPA buffer was added to each well and shaken on platform mixer (Ratek platform mixer, OM6, Ratek Instruments Pty Ltd, Boronia, Australia) for 10 min to solubilize the cells (Eigenmann *et al.*, 2013).
7. The plate was centrifuged for 5 min at 3200 g, and the supernatant was used for analysis of cell protein and NPs content.

Protein analysis: 10 µL supernatant was placed in a 96-well plate and 150 µL Pierce™ 660 nm protein assay reagent was added. The plate was incubated for 5 min at RT and absorbance was determined at 660 nm using the plate reader. BSA standards were placed on the same plate and analysed similarly to obtain a calibration curve. The cell protein quantity in each well was determined using the constructed calibration curve.

NP analysis: 50 µL supernatant was placed in a black 96-well microplate, and the fluorescence intensity was measured at excitation/emission wavelength of 283/451 nm for FZSiFA50 NPs (Patel *et al.*, 2017) and 492/518 nm for FZSi-FITC NPs (Baird *et al.*, 2012) using the plate reader. Known concentrations of NPs (10 to 300 µg/mL in RIPA buffer) were prepared and analysed similarly to the samples to generate a calibration curve. The NPs uptake in each well was determined using the constructed

calibration curve. The cells in culture medium without NPs treatment were used as the control. For each type of NPs at each time point, the microgram of NPs uptake per mg of cell protein was calculated.

Cell uptake study design for hybrid NPs with different time points, NPs and conditions are described below:

- Incubation temperature : 37°C
- Time points : 2 h and 6 h
- NP1 : (FZSi-FITC) no targeting ligand
- NP2 : (FZSiFA50) FA was the targeting ligand.
- NPs concentration used : 100 µg/mL
- Experiment condition : Dark and UV-A irradiated conditions
- Cell lines : B16-F10 and Caco-2 cells

b) Qualitative analysis

This study was performed to assess the internalisation and localisation of two fluorescent labelled NPs (FZSi-FITC and FZSiFA50), which exerted relatively better cytotoxic activity in B16-F10 cells. The cell nucleus was stained with a propidium iodide solution (50 µg/mL), and the NPs with fluorescent ligands FA and FITC were used in this study. The solution preparation procedures are briefly described below:

Propidium iodide working solution

The propidium iodide stock solution was prepared with deionized water at a concentration of 1mg/mL. The solution was protected from light wrapped in aluminium foil and stored at 4°C. Saline sodium citrate buffer (0.3 M NaCl, 0.03 M sodium citrate, pH 7.0) was prepared separately and used for the dilution of propidium iodide to produce a working concentration of 50 µg/mL.

Hybrid NPs preparation

FZSiFITC and FZSiFA50 NPs were dispersed in DMEM medium free of FBS, to prevent any serum interaction with the staining reagents. The hybrid NPs were used at a concentration of 100 µg/mL and dispersed in a sonic bath for 15 min before cells treatment.

(i) Immunostaining procedure for cells grown on coverslip

1. B16-F10 cells (5000 cells/well) were seeded on the ethanol-sterilized glass coverslips (ProSciTech, Cat.G408, Dia-22 mm) placed in a 6-well plate. The experiment commenced when the cells reached 70-80% confluency.
2. The medium was removed, and cells were rinsed twice and equilibrated with PBS (1mL) for 30 min at 37°C.
3. After the removal of PBS solution, 1 mL of NPs in DMEM serum free medium (100 µg/mL) was replaced in each well (UV-A treated) and incubated for 6 h.
4. The medium was removed, and cells were rinsed twice with 2 mL of cold PBS quickly. The quick washes ensured that the cells retained their original morphology and did not deform/shrink due to the absence of essential nutrients and ions.
5. 2 mL of warm (37°C) methanol: glacial acetic acid (3:1) was added to the cells for fixation (fixation dehydrates cells/tissues, causing proteins to denature and precipitate in situ) and permeabilization and incubated for 15 min at RT in the dark and washed twice with 2 mL water each time.
6. 2 mL of cold (4°C) 0.1% Triton X-100/PBS was added and incubated for exactly 3 min to permeabilize the cells. Longer treatment could cause the propidium iodide to stain all the cellular components.
7. Cells were rinsed twice with 2 mL PBS; the coverslip was removed carefully and placed in a new dry well. Precaution was taken to keep the slides always wet.
8. Propidium iodide working solution (20 µL) was added and incubated for 5 min and rinsed with 2 mL PBS.
9. 8 µL of mounting medium (Vectashield, Vector Laboratories, US) was placed on a clean microscope slide.
10. The coverslip containing cells was removed from the well and mounted on the slide with mounting medium with cells face upside down so that the cells touch the mounting medium avoiding any air bubble.
11. The slide was left in the open (but in the dark) to evaporate the excess moisture for 4-5 h and then clear nail polish was used to seal the coverslip to avoid further moisture loss entirely.
12. After the nail polish was completely dried, the prepared slides were stored at 4°C to prevent the complete loss of moisture from the slide. The image was

taken with a Nikon A1 Confocal Laser Microscope (Nikon Instruments Inc., Tokyo, Japan).

(ii) Immunostaining procedure for cells grown in Ibidi micro-dish

1. In 35 mm Ibidi, micro-dish cells were seeded at 5000 cells per micro-dish. The experiment commenced when the cells reached 70-80% confluency.
2. Steps 2-8 (described in immunostaining procedure for cells grown on coverslip) were followed.
3. Images were taken with the Nikon A1 Confocal Laser Microscope.

2.13 Apoptosis assay by Flow cytometry

Annexin V-FITC/PI assay was performed for the detection and discrimination of apoptotic and dead cells. Apoptotic cells are otherwise undetectable by staining with propidium iodide.

1. B16-F10 cells (2×10^5 /well) were seeded in a 6-well plate. After reaching 70-80% cell confluency, 1 mL medium was replaced with equal volume of medium containing hybrid NPs (FZSi & FZSiFA50 NPs, 12.5 & 100 $\mu\text{g/mL}$, incubated 6 h & 24 h). Separate 6-well plates were used for NPs treated in the dark and NPs activated with UV-A irradiation. Cells were incubated further for 6 h and 24 h after UV-A treatment.
2. The cell supernatant was collected, followed by addition of Tryple-X (~1 mL per well) to detach any attached cells at the bottom of the plates, followed by the addition of DMEM medium.
3. The cell suspension was transferred to 15 mL centrifuge tubes and centrifuged at 3750 g for 5 min.
4. The supernatant was removed, and the cell pellet was washed by addition of PBS (1 mL each time) twice.
5. The pellet was resuspended in 100 μL of 1 X binding buffer (refer Appendix 7 for preparation of 10 X binding buffer) and maintained in cold condition.
6. 5 μL of FITC Annexin V was added to each sample, followed by the addition of 10 μL of propidium iodide (50 $\mu\text{g/mL}$).
7. The samples were maintained in the dark for 15 min at RT.

8. Finally, 400 μL of 1X binding buffer was added to each tube and sample was analysed using CANTO-II cell analyser (BD FACSCanto II, Australia) within 1 h.
9. The apoptosis assay was carried out in B16-F10 cells, and the cells with no hybrid NPs treatment served as the control.

2.14 Total cell associated zinc and iron measurement by ICP

The total elemental zinc and iron content within the cells after NPs treatment was measured by ICP-OES (Perkin Elmer Optima 8300 spectrometer, US). The analysis was performed at the wavelengths of 238.2 and 206.2 nm for iron and zinc, respectively. The cellular uptake of the hybrid NPs and the impact of UV-A radiation on the uptake was analysed.

1. The cells (B16-F10 and Caco-2) were seeded onto a nunc-24 well plate at a density of 5000 cells per well with DMEM high glucose medium and appropriate supplements (Table 2.1).
2. The medium was replaced every three days, and cells were maintained at 37°C, 5% CO₂ and 95% humidified air until 70% to 80% confluency (2-3 days).
3. The medium was removed, and cells were rinsed twice with 500 μL of pre-warmed HBSS. The cells were incubated for 30 min in HBSS at 37°C for equilibration.
4. After 30 min, the HBSS was replaced with 500 μL of HBSS containing NPs at a concentration of 100 $\mu\text{g}/\text{mL}$.
5. After a predetermined incubation time (2 h and 6 h), (UV-A irradiation given immediately after NPs treatment), the medium was aspirated, and cells were washed quickly three times with cold PBS to remove excess NPs.
6. 1000 μL RIPA buffer was added to each well and shaken on platform mixer for 10 min to solubilize the cells (Eigenmann *et al.*, 2013).
7. Concentrated nitric acid (70% w/w, 2 mL) was added to the samples to dissolve the zinc and iron metals and heated at 60°C for 2 h until a clear solution was formed and further diluted as required with milli-Q water before analysis
8. The ICP-OES analysis was conducted in the Department of Chemical Engineering, Curtin University using ICP-OES (Perkin Elmer Optima 8300 spectrometer, US). Zinc and iron standards were analysed in the concentration range between 50 ppb to 300 ppb.

9. B16-F10 and Caco-2 cells with no hybrid NPs treatment served as the control.

2.15 Caspase 3/7 assay

The caspase 3/7 assay is used for the apoptosis analysis in NPs treated cells. It is a luminescent assay used to measure caspase-3 activity in purified enzyme preparations or cultures of adherent or suspension cells. The assay kit provided a proluminescent caspase-3/7 substrate, which contained the tetrapeptide sequence DEVD.

1. B16-F10 cells were seeded in 6 well plates (5000 cells per well), after reaching 80% confluency the DMEM high glucose medium was replaced with medium containing hybrid NPs (FZSi & FZSiFA50, in two different concentrations 12.5 & 100 $\mu\text{g/mL}$) and incubated for 1 h and 2 h respectively. Cells were incubated further for 1 h and 2 h after UV-A treatment.
2. Change in morphology of the cells after NPs treatment was captured through Nikon inverted microscope and images were captured with attached Nikon digital sight camera (DS-Fi2).
3. The supernatant was removed, and RIPA buffer containing protease inhibitor (100 $\mu\text{g/mL}$) was added (200 μL per well), and the plate was maintained on ice for 5 min.
4. Any cells at the bottom of the plate were scraped with a cell scraper.
5. Cell lysate and cells were centrifuged at 12,000 g for 10 min at 4°C.
6. The supernatant or cell lysate was collected for cell protein analysis.
7. A small aliquot of the supernatant (10 μL) was taken for protein concentration analysis using Pierce protein assay reagent, left at RT for 5 min and absorbance measured at 660 nm. The standard calibration curve was plotted using BSA dissolved in RIPA buffer.
8. Then, the samples were diluted with RIPA buffer to make sure the protein levels are the same in all the wells.
9. 25 μL caspase reagent Ac-DEVD-AFC (50 μM , final concentration) dissolved in a reagent buffer (20 mM HEPES, 10% glycerol, 2 mM DTT, pH 7.5) was added to 96- well plate (black side, clear bottom), followed by addition of 50 μL cell lysate and incubated at 37°C for 1 h.
10. The AFC fluorescence was measured using a plate reader (Perkin Elmer, UK) with 400/ 505 nm excitation/emission wavelength. Ac-DEVD-AFC reagent

with buffer was used as the blank. The cells with no NPs treatment were used as the control.

11. The experiment was carried out in the same manner for both dark and UV irradiated samples.

***In vivo* study**

2.16 Preparation of B16-F10 mouse melanoma tumour cells

B16-F10 melanoma tumour cells, originally derived from mice were grown using DMEM high glucose medium containing 1% PEN-STREP, 1% glutamine and 10 % bovine serum (Overwijk *et al.*, 2001). The medium was changed every third day. On 80% confluency, the cells were trypsinized using Tryple-X (~3 min). Double volume of complete medium (ie for 1 mL Tryple-X, 2 mL complete medium was added for neutralisation) was added, and centrifuged at 3,200 g for 5 min. The generated cell pellet was washed twice with HBSS. The cell pellet was redispersed in HBSS to produce cell density of 2×10^7 cells/mL. The 1mL volume of cell suspension was mixed with equal volume of Matrigel and transferred to the icebox for inoculation on mice. The Matrigel permits high local concentration of tumour cells to produce a more solid tumour mass.

2.17 Animals and tumour inoculation

C57BL/6 male mice (4 weeks old) were obtained from the Animal Resource Centre, Perth, Australia. Animals were acclimatized, monitored and housed according to the standard operating husbandry procedures in the animal house at Curtin University and weighed before implanting tumour cells with an electronic balance. The experiments were performed according to the Australian Code of Practice for the care and use of animals for scientific purposes. Health monitoring scorecards were used to ensure consistency in monitoring procedures (Appendix 9). Animals were monitored at least three times a week, every day or every second day after treatments. A schematic diagram of the mice treatment since they arrived at the animal facility in Curtin University is given in Figure 2.1:

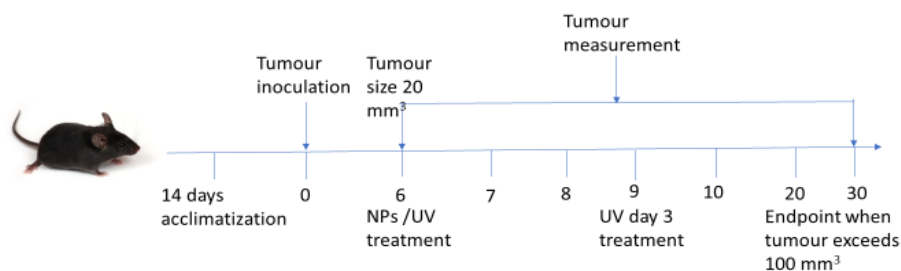


Figure 2.1. Schematic representation of the animal treatment

Anaesthesia

According to the standard operating procedure (SOP) (Research facility manual, Curtin University, 2014), animals were placed carefully in the anaesthetic chamber, and a mixture of oxygen (1.5-3L/min) and isoflurane (4%) was pumped into the chamber from the vaporiser. Once the animal was anaesthetised, the animal was removed from the chamber and anaesthesia was maintained using a nose mask (vaporiser) with a mixture of isoflurane (1-2.5%) and oxygen (0.5-1L/min). Reflexes of the animal were tested before starting the procedure. After tumour inoculation, treatment and tumour measurement the animal was immediately removed from nose mask and allowed to recover freely in the cage and monitored. The animal was observed until full recovery for any residual effect from the anaesthesia and procedure.

Tumour inoculation in mice

Each mouse was anaesthetized, the dorsal mid-back region of mice was shaved and wiped with ethanol and then injected subcutaneously 5×10^5 of murine B16-F10 cells suspended in 50 μ L (50% Matrigel/ HBSS) on the dorsal mid-back region (Fahmy *et al.*, 2003; Yu *et al.*, 2014). After inoculation tumours were monitored visually according to the SOP TEC-05, Curtin University. Tumour growth was measured every second-day using a digital calliper and calculated using the Equation 2.5 (Yu *et al.*, 2014).

Tumour volume (V) = $L * W * H * \pi/6$ (Equation 2.5)

Where L is the length of the tumour; W is the width of the tumour; H is the depth of tumour and π value is 3.14.

Upon subcutaneous administration of tumour cells, bleb appeared on the spot of injection (Overwijk *et al.*, 2001). The animal with no bleb was excluded from the study. The intratumor treatment started once a tumour reached an average size of 20

mm³ (day 6). The tumour size, tumour appearance, the body weight, activity was also monitored every alternate day during the study.

2.18 Preparation studies for UV-A irradiation

The UV-A radiation source (UV LED SMART) employed in the experiment had been approved by the radiation safety officer, Curtin University, before the study (Appendix 10). To easily deliver the UV dose to mice, we used a handheld UV-A irradiation device UV LED SMART (Figure 2.2) and developed a specific protocol for its delivery of UV-A irradiation, which can be applied to a clinical setting in the future.



Figure 2.2. Image showing the UV LED SMART which was used as the UV-A radiation light source for animal study. Break out box helps to use the UV LED SMART without the need for a computer during irradiation.

The use of UV LED SMART was optimised with C57BL/6 male mice skin (with and without hair) first before the animal study. The mice skin was provided by a researcher of our group who worked with B16-F10 melanoma tumour in the same strain of mice. The skin tissue was collected from a tumour grown region (after removal of a tumour beneath). The skin was ~ 1mm thick and used for study immediately on the day it was collected. The skin samples collected from three different animals with tumour burden on the same day immediately after mice were sacrificed, were tested for UV-A penetration through the mice skin.

The time taken to reach the fixed dose of 10 J/cm² on the base of the skin was investigated using both mouse skin with and without hair. The impact of distance between UV-A light source and mouse skin at the time to reach the dose was studied. In all setup experiments the tumour skin was mounted on the sensor of the UV BS02 chamber (UV irradiation chamber, Opsytec, BS02) (UV chamber used for the *in vitro*

study, Appendix 11) to permit the measurement of the irradiated dose. The UV LED SMART was mounted at 1 cm distance to prevent any direct heating effect. The experimental set up used in the study is described below in Figure 2.3. The parameters of distance between light source and mouse skin, heat generated from the light source, duration of light exposure and the diameter of the light beam on the skin were taken into consideration to optimise the study. The temperature of the light beam on the mouse skin was measured using an I.R Thermometer (Thermo Fisher, Australia) before and after light exposure.

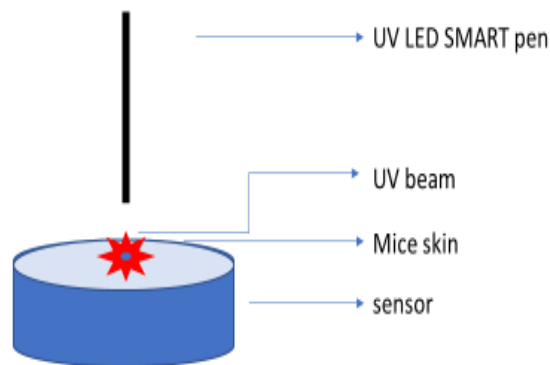


Figure 2.3. The experimental design used in optimising the UV LED SMART system. The sensor was connected to UV Chamber BS02, which displays the UV dose and time taken to reach the dose.

The UV-A light dose used for the animal study was 10 J/cm^2 mimicking exactly the light dose used in *in vitro* studies. From the pilot study, the dose of 10 J/cm^2 was reached at a time of 3 min 42 seconds. The temperature of the skin was measured before and after UV-A radiation treatment, to assess if hyperthermia was produced and if there was any temperature rise which could cause any discomfort to the animal.

2.19 Experimental design for *in vivo* studies

Tumour-bearing male mice C57 BL/6 were divided into nine groups, six each with body weight ranging 20-25 mg ($n=6$). The mice in control and UV treatment groups were administered saline to mimic the experimental procedures in the other groups. Mice were sacrificed according to the guidelines of research facility manual, Curtin University when any mice with a tumour greater than 100 mm^3 in size or the body weight of mice reduced by more than 10%, or more than 50% tumour turned necrotic. Therefore, the termination time (i.e. endpoint) of mice might be different in a group, depending on conditions of a tumour and animal welfare.

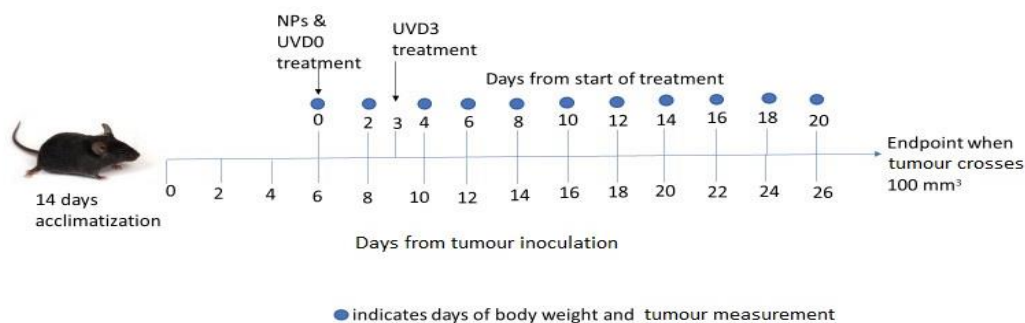


Figure 2.4. The schematic treatment plan and the end point for *in vivo* studies

2.20 Administration of hybrid NPs and assessment of tumour growth

The NPs dose used in the study was 2 mg/kg. The hybrid NPs were dispersed in PBS (5 mg/mL) and subjected to sonication in a bath sonicator for 15 min, before use. According to the body weight, the hybrid NPs were injected into each animal using a 0.3 mL insulin syringe and the maximum volume injected was 10 μ L. The intratumor administration of hybrid NPs started on the 6th day at an average, when a tumour reached 20 mm³ size. The NPs were injected approximately in the middle of a tumour, and UV-A irradiation for the respective treatment groups was given immediately or three days later. The tumour size was measured every alternate day using a digital calliper. The tumour volume was determined using the formula stated in section 2.17. The tumour region was shaved and maintained in a wet condition with 70% ethanol during the measurement using a calliper to facilitate better detection of a tumour (Overwijk *et al.*, 2001). Injection and irradiation of UV-A light were carried out with mice under anaesthesia by isoflurane vaporiser to reduce the stress caused by the procedure.

Table 2.2. Animal experimental design of different treatment groups

Treatment Group	Treatment Received (intratumor administration)
Control (Saline)	Saline was given on treatment day 0
Saline+UVD0	Saline+UV-A radiation was given on treatment day 0
FZSiNPs D0	FZSi NPs were given on treatment day 0
FZSiFA50NPs D0	FZSiFA50 NPs were given on treatment day 0
FZSiNPs + UVD0	FZSiNPs and UV-A radiation was given on treatment day 0
FZSiFA50NPs + UVD0	FZSiFA50NPs and UV-A radiation was given on treatment day 0
SalineD0+UVD3	Saline was given on treatment day 0, and UV-A radiation was given on treatment day 3
FZSiNPsD0 + UVD3	FZSiNPs were given on treatment day 0, and UV-A radiation was given on treatment day 3
FZSiFA50NPsD0 + UVD3	FZSiFA50NPs were given on treatment day 0, and UV-A radiation was given on treatment day 3

The treatment day 0 corresponds to day 6 post tumour inoculation in mice. Treatment day 3 corresponds to day 9 post tumour inoculation in mice. The terms D0 and D3 will be used in the text from now on.

The animals were sacrificed at the endpoint which varies from one mice to another because of reasons stated previously. Therefore, results were analysed in different ways to allow comparison as below:

- Tumour growth pattern during the whole study (26 days)
- Tumour growth pattern up to day 16 post tumour cell inoculation
- Tumour growth delay and inhibition
- Animal survival and life prolongation rate
- Body weight changes and organs weight

Tumour growth and antitumour effect of treatments were assessed using various approaches including tumour growth plot, tumour weight at the sacrificed time, tumour volume inhibitory rate (TVI%) and life prolongation rate (%).

Tumour volume inhibitory rate (TVI %) = $(1 - T_{vt}/T_{vc}) \times 100$ (Equation 2.6)

(Li *et al.*, 2017)

T_{vt} = Tumour volume average of treatment group at time t

T_{vc} = Tumour volume average of control at time t

Life prolongation rate (%) = $(C_{treated}/C_{control} - 1) \times 100$ (Equation 2.7)

(Li *et al.*, 2017)

$C_{treated}$ = Average survival days of treated mice

$C_{control}$ = Average survival days of control mice

2.21 Collection of biological samples

After the animals were sacrificed, the organs were collected for future biodistribution studies. Briefly, the animal was anaesthetized and tested for reflexes. Once the animal was confirmed anaesthetized, blood was collected from the heart from the left lateral thoracic wall near the point of the flexed elbow using a suitable gauge needle and syringe (23-25G and 1-3 ml syringe for mice). A V-cut through the skin and abdominal wall was made, and a volume of saline was slowly injected into the heart to flush out the remaining blood from the circulation. After flushing out all the blood, various organs (lungs, kidney and liver) and tumour (in mice) were harvested, wiped

with filter paper, weighed and stored in labelled glass vials at -80°C until further analysis. Blood was collected in tubes containing, ethylenediamine tetraacetate (EDTA) (10% w/v) and centrifuged at 3,000 x g for 10 min, and the serum was separated and stored at -80 °C. Due to the limitation of resources, time, further analysis of the blood and organ samples were planned in the future studies.

2.22 Statistical analysis

In vitro data were analysed using two-way-ANOVA, via Tukey's multiple comparisons test (GraphPad Prism V 7.03). Statistical significance was considered at $p < 0.05$. The animal group results were statistically compared with one-way ANOVA followed by a Tuckey's multiple comparisons test, using GraphPad Prism statistical software (v 7.03, GraphPad Inc., CA, USA).

CHAPTER 3

RESULTS AND DISCUSSION

3.1 Cell cultures

The cell culture experiments were conducted in a physical containment level 2 (PC2) cell culture laboratory with the highest possible quality of the media, cell-line, cell culture consumables and personal hygiene. The mycoplasma testing was conducted regularly to ensure the cells were free of any microbial contamination and the results were reliable.

3.2 UV CHAMBER optimization

UV irradiation chamber BS02 (UV-A, 365 nm) was purchased from UV Grobel, Germany. The key features and advantages of UV BS02 chamber are summarised below:

- The irradiation chamber BS-02 is small and robust equipment and can function with time- or dose-controlled irradiation of samples with UV light.
- The chamber operates at about 25°C, and the chamber contains a circulating fan which minimizes thermal damage to the samples.
- The optional feature UV -MAT can be connected externally to the chamber and be used for precise dose and time measurement. It maintains a constant dose independent of lamp ageing, temperature, and pollution.
- The chamber has inbuilt calibrated radiometer sensors for dose measurement, and it is designed with an excellent safety feature; the UV lamps cut off if the door is opened during the study.



Figure 3.1 UV Irradiation BS02 chamber and UV MAT

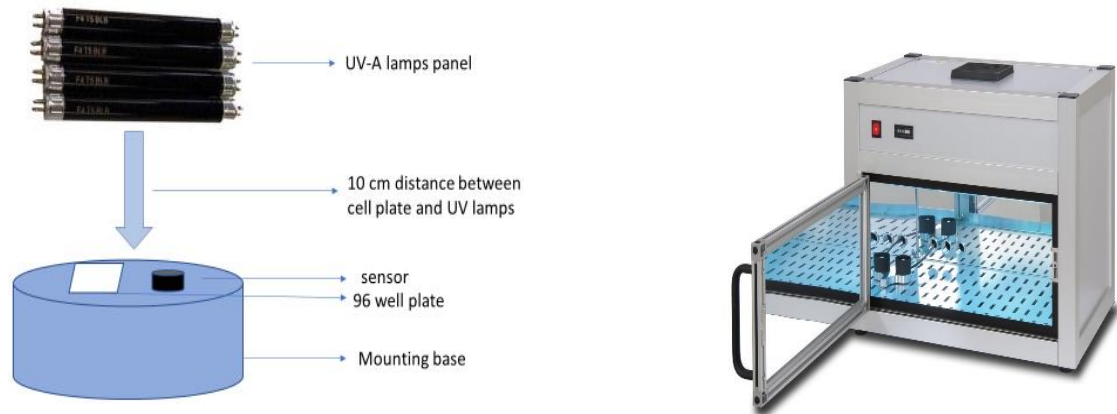


Figure 3.2 The set-up of UV irradiation chamber BS02 during the experiment.

The complete set up was enclosed inside the UV chamber. The mounting base was made using cardboard boxes wrapped in aluminium foil to achieve the 10-cm distance required for the experiment.

Table 3.1. UV CHAMBER BS02: Operation conditions

Distance	Irradiance (mW/cm ²)	Time (min)	Dose produced (J/cm ²)
5 cm	24.47	1.34	2
	25.57	3.23	5
	25.74	6.34	10
10 cm	18.39	1.51	2
	18.46	4.34	5
	18.48	9.18	10
15 cm	14.28	2.25	2
	14.42	5.54	5
	14.43	11.37	10
20 cm	11.89	2.51	2
	11.95	7.02	5
	11.99	14.12	10

UV irradiance is the radiant power of UV arriving at the sample surface per unit area. It is photon flux, expressed in mW/cm². The UV dose known as energy density is calculated by multiplying irradiance and time of exposure (in seconds) (Bolton & Lindon, 2003). As shown in Figure 3.2 the sensor and the cell culture plates were maintained at the same level during the experiment, to monitor the UV dose accurately. The temperature was recorded before and after irradiation in the cell culture plates during the experiment. Our trial study had recorded only negligible increase (1-2°C) in the temperature after UV irradiation treatment. However, the temperature was monitored for PDT experiments.

The radiation dose was directly affected by both time and distance. When the dose was fixed at 10 J/cm^2 and the distance was varied: 5 cm distance took 6.34 min, 10 cm distance took 9.18 min, 15 cm distance took 11.37 min, and 20 cm distance took 14.12 min. It took 2.84 min more to reach the dose when distance was increased from 5 to 10 cm. The time increased nearly 2-fold when distance increased from 5 to 20 cm (Table 3.1). We decided to use 10 cm distance between the UV-A lamps and cell culture plates for all experiments as it had a minimum increase of time to reach 10 J/cm^2 UV-A dose and negligible rise in temperature. We selected this dose to enhance the effect of nano-PS with UV-A irradiation while ensuring the UV dose alone does not kill the cells insignificant amount (at 10 J/cm^2 UV dose, the B16-F10 and Caco-2 cells maintained 96.79% and 95.32% cell viability, described in section 3.6). The instrument setting ensured that the UV irradiation chamber consistently offered reproducible UV doses during the study.

3.3 Characterisation of hybrid NPs as nano-PSs

Physical properties and morphology

The physical properties of hybrid NPs were examined before the cellular studies. The morphology was studied using TEM, and hydrodynamic particle size and size distribution were determined via dynamic light scattering (DLS) using Zetasizer Nano-ZS (Malvern Instruments, UK). FA content was analysed by Thermogravimetric analysis (TGA) curve (Appendix 1), and optical properties of the NPs were studied by UV-vis diffuse reflectance spectroscopy in the department of Chemical Engineering (Table 3.2). The structure of the hybrid NPs and the XRD analysis highlighting the distribution of Fe and Zn are shown in Appendix 1.

TEM images (Figure 3.4) showed electron photomicrographs of hybrid NPs used in this study. The presence of silica layer had increased the particle size of silica modified FZ NPs (Table 3.2). Pure ZnO exhibits absorbance at 400 nm with band gap energy 3.1 eV. Fe_3O_4 exhibits absorbance between 350 and 650 nm region. The hybrid NPs used in the study had absorbance related to both ZnO and Fe_3O_4 (Figure 3.5, 430 nm, 2.9 eV band gap energy) (Patel *et al.*, 2017) confirming their potential to be used as PSs.

Table 3.2 Information about the hybrid NPs

Nanoparticle	Particle size (nm) ^a	Zeta potential(mV)	Optical property (nm) ^b	Folate content ^c
FZ NPs	13.0 ± 1.1	-0.91	430	none
FZSi NPs	17.6 ± 2.0	-16.5	430	none
FZSiFA25 NPs	18.7 ± 2.2	-17.2	430	0.059 mmol/g
FZSiFA50 NPs	18.9 ± 1.3	-20.6	430	0.085 mmol/g

a particle size was measured by DLS; **b** optical property was measured by UV-Visible diffuse reflectance spectroscopy; **c** folate content was measured by thermogravimetric analysis curve;

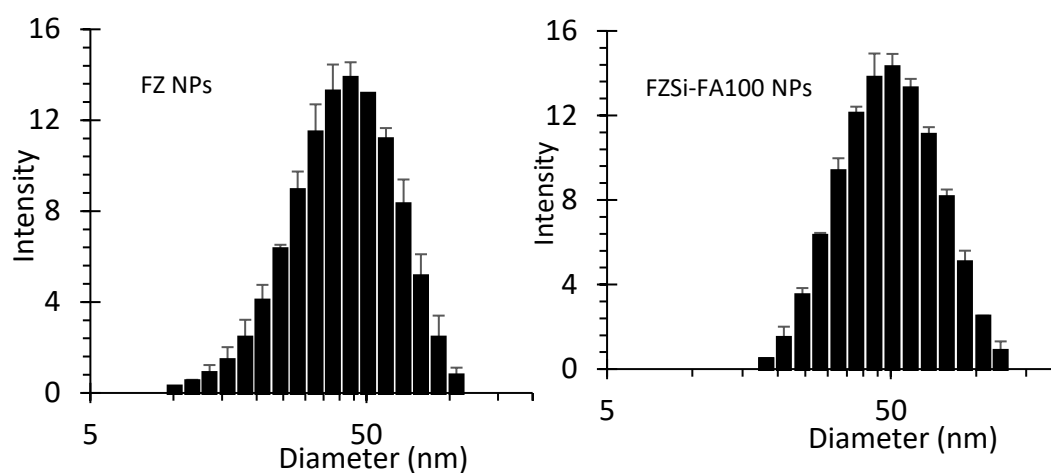
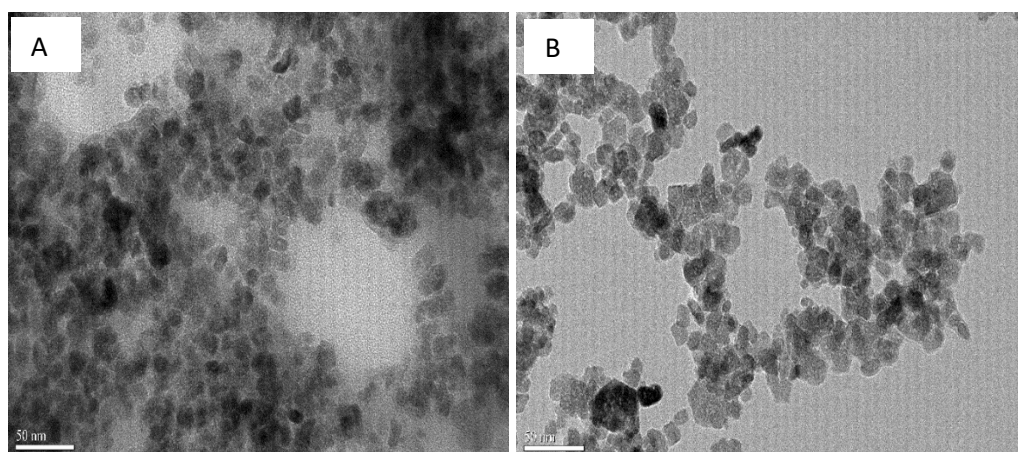


Figure 3.3 Particle size distribution (DLS spectra) of FZNPs and silica coated FZSi-FA100 NPs.



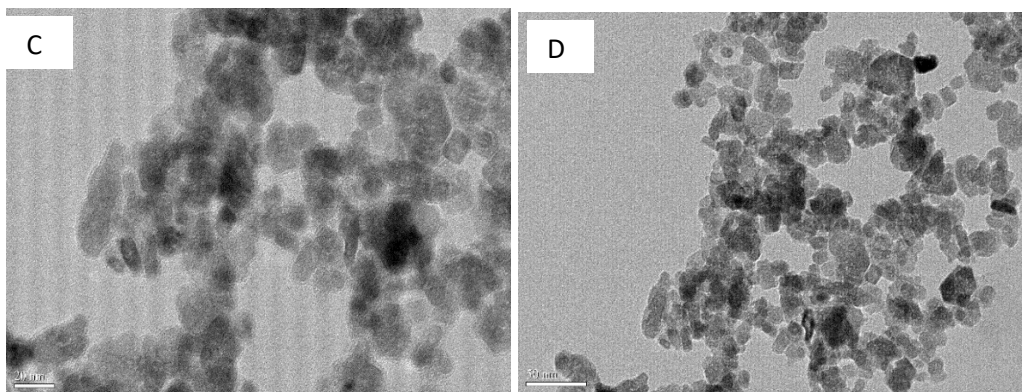


Figure 3.4 TEM images of A: FZ, B: FZSi, C: FZSiFA25 and D: FZSiFA50 NPs (Patel *et al.*, 2017)

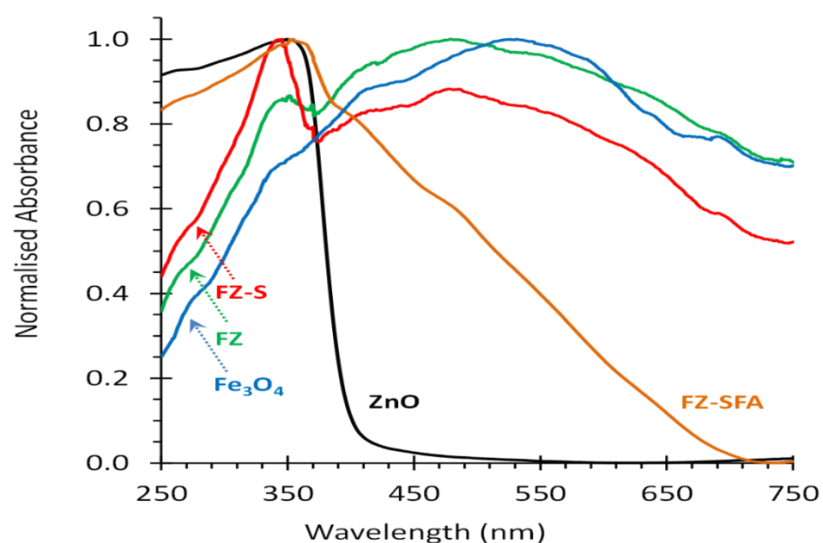


Figure 3.5 UV-visible diffuse reflectance spectroscopy spectra of ZnO (Patel *et al.*, 2017)

3.4 Stability of hybrid NPs in different medium

DMEM high glucose medium was used in the cell culture studies, and the stability of hybrid NPs in this cell culture medium was compared with that in PBS (Table 3.3 & 3.4). The pH of both the medium was measured as ~ 7.2 and 7.6. The particle size of the FZSi, FZSiFA25 and FZSiFA50 NPs increased due to silica and FA coating compared to uncoated FZNPs (Table 3.3), consistent with the earlier reported work (Feng *et al.*, 2015b).

Table 3.3 Stability study of hybrid NPs in different medium at 37 °C

NP formulation	Diameter of the particles (nm) \pm SD					
	PBS			DMEM		
	0 h	6 h	24 h	0 h	6 h	24 h
FZ	13.0 \pm 1.3	33.7 \pm 2.3	56.6 \pm 11.1	15.4 \pm 1.1	28.1 \pm 2.3	35.0 \pm 10.1
FZSi	17.6 \pm 2.1	28.4 \pm 1.4	29.3 \pm 1.0	17.8 \pm 1.3	26.4 \pm 1.4	32.7 \pm 1.0
FZSiFA25	18.7 \pm 2.5	24.6 \pm 1.5	28.7 \pm 9.2	19.1 \pm 4.2	19.8 \pm 6.6	26.7 \pm 3.3
FZSiFA50	18.9 \pm 1.4	25.3 \pm 6.2	25.9 \pm 2.1	19.9 \pm 2.4	25.4 \pm 3.7	27.0 \pm 2.4

All data are mean \pm SD of three individual experiments. The measurements were undertaken at room temperature using DLS.

The NPs which exerted higher negative zeta potential values showed better stability in DMEM containing FBS compared to PBS across all types of NPs and time points (Table 3.4). BSA, the primary component of fetal bovine serum (FBS), exerts negative charge at higher pH values (>5.1). Hence negative charge on the NPs surface could indicate adsorption of FBS components.

Table 3.4 Stability study of hybrid NPs in different medium (Zeta potential)

NP	Surface charge \pm SD(mV)					
	PBS			DMEM		
	0 h	6 h	24 h	0 h	6 h	24 h
FZ	-0.91 \pm 0.1	-0.83 \pm 0.2	-0.76 \pm 0.1	-0.9 \pm 0.1	-0.92 \pm 0.2	-0.97 \pm 0.2
FZSi	-16.5 \pm 2.2	-16.4 \pm 1.0	-16.0 \pm 0.8	-16.3 \pm 1.6	-16.4 \pm 3.2	-17.7 \pm 1.3
FZSiFA25	-17.2 \pm 2.1	-16.7 \pm 1.3	-16.4 \pm 3.2	-17.1 \pm 4.1	-17.8 \pm 2.6	-18.5 \pm 3.2
FZSiFA50	-20.6 \pm 4.3	-20.4 \pm 3.2	-20.1 \pm 2.1	-20.8 \pm 2.7	-22.4 \pm 3.2	-23.7 \pm 1.2

All data are mean \pm SD of three individual experiments. The measurements were undertaken at room temperature by DLS.

The adsorption of BSA onto NPs could also provide protective colloid effect (Dominguez-Medina *et al.*, 2013), further stabilizing NPs via steric stabilization. Similar observations were reported by other research groups (Anders *et al.*, 2015; Chia *et al.*, 2016a; Pandey *et al.*, 2016; Chia *et al.*, 2016b), where serum proteins were also used. As expected, the increase in folate content from FA25 to FA50 increased the negative charge of the NPs. Greater the magnitude of zeta potential, higher electrostatic repulsion and better stability of the NPs was observed. It was not surprising to see that significant aggregation of NPs at 24 h in PBS with uncoated FZ NPs, due to the less negative charge on the surface compared to the silica modified

NPs. A stabilizing agent or a capping agent like PEG may enhance the stability of hybrid NPs.

The physical dimensions of the aggregates formed can affect the reactive surface area, reactivity, bioavailability and toxicity of the NPs (Gatoo *et al.*, 2014). In this study, all NPs stayed below 60 nm during the 24 h study. For FZSi and FZSiFA NPs, their particle size had remained below 35 nm during 24 h. Therefore, it could be concluded these hybrid NPs were reasonably stable in culture medium over 24 h. As we expected the cell uptake of NPs would be completed by 24 h, it may suggest that the cellular response of hybrid NPs would not be affected by NPs stability in the culture medium.

3.5 Evaluation of cytotoxicity

The cellular toxicity level of hybrid NPs was assessed in B16-F10, Caco-2 and 3T3 cell lines using an MTT based cell viability assay. Cell viability was assessed after incubation in the presence of FZ, FZSi, FZSiFA25 and FZSiFA50 NPs for 6 h and 24 h at various concentrations.

(i) Cytotoxicity of hybrid NPs in B16-F10 cells

As shown in Figure 3.6 the hybrid NPs exhibited time and concentration-dependent cytotoxicity towards B16-F10 melanoma cells. Higher the concentration of hybrid NPs greater was their cell killing ability.

Median effective dose (ED_{50}) values were determined for the NPs by plotting the dose-response curve (cell viability against concentration of NPs) and using line of best fit to calculate the NP dose which killed 50% of cell population in both the conditions (dark, NPs with UV-A irradiation) (Appendix 12). The ED_{50} value for FZ NPs was 45.00 $\mu\text{g/mL}$ and 49.34 $\mu\text{g/mL}$ for FZSi NPs. The ED_{50} values for FZSiFA25 and FZSiFA50NPs were 36.28 $\mu\text{g/mL}$ and 21.44 $\mu\text{g/mL}$ at 6 h respectively. Noteworthy, the FZSiFA50 NPs ED_{50} was nearly half the ED_{50} value compared to FZ NPs (21.44 $\mu\text{g/mL}$ & 45.00 $\mu\text{g/mL}$), which showed the impact of FA attached hybrid NPs in melanoma cells.

Increasing the exposure time from 6 h to 24 h (Figure. 3.6B) attenuated the cell viability across all NPs concentrations. As the hybrid NPs were in contact with the

cells for a longer time and more of NPs would have been taken up by cancer cells. As a result, the ED₅₀ values were decreased to 17.99 µg/mL and 17.15 µg/mL respectively for FZ and FZSiFA25 NPs. Stronger cytotoxicity was observed at 24 h with FZSi, and FZSiFA50 NPs and their ED₅₀ values were 13.76 and 15.18 µg/mL respectively. Although at 24 h, 25, 50 and 100 µg/mL concentrations, FZ NPs exhibited a slightly better cell killing effect than FZSiFA50 NPs, the difference was not statistically significant. More importantly, as the test was conducted in the cell culture, the effect of targeting ligands would be expected to be shown in the early hours. In addition, folic acid is a known molecule promoting cell growth, which may have attributed more to the cell viability at 24 h than that at 6 h, resulting in less difference between FA-coated and non FA-coated NPs. At high dose 100 µg/mL the cell viability reduced to less than 10% across all the hybrid NPs. However, the difference was observed significantly even with the low dose 12.5 µg/mL. For instance, FZ NPs cell viability was 79.08% at 12.5 µg/mL dose, and FZSiFA50 NPs reduced cell viability to 61.61% with 12.5 µg/mL dose. It requires careful selection of dose as the hybrid NPs can exert cytotoxic effect even at the low dose against melanoma cells.

Our results agree with Alarifi *et al.* (2013) who reported 41.40% cell viability when A375 melanoma cells were treated with 20 µg/mL ZnO NPs. Our study reports 35.28% cell viability in B16 melanoma cells when treated with 25 µg/mL FZ NPs. Cloudman S91 melanoma cells treated with 25, 50 and 100 µg/mL ZnO NPs for 24 h reported 50%, 20% and almost 10% cell viability respectively (Wahab *et al.*, 2013). Our results indicate 38.84%, 14.90% and 9.35% cell viability at the similar conditions treated with FZSiFA50 NPs against B16-F10 melanoma cells.

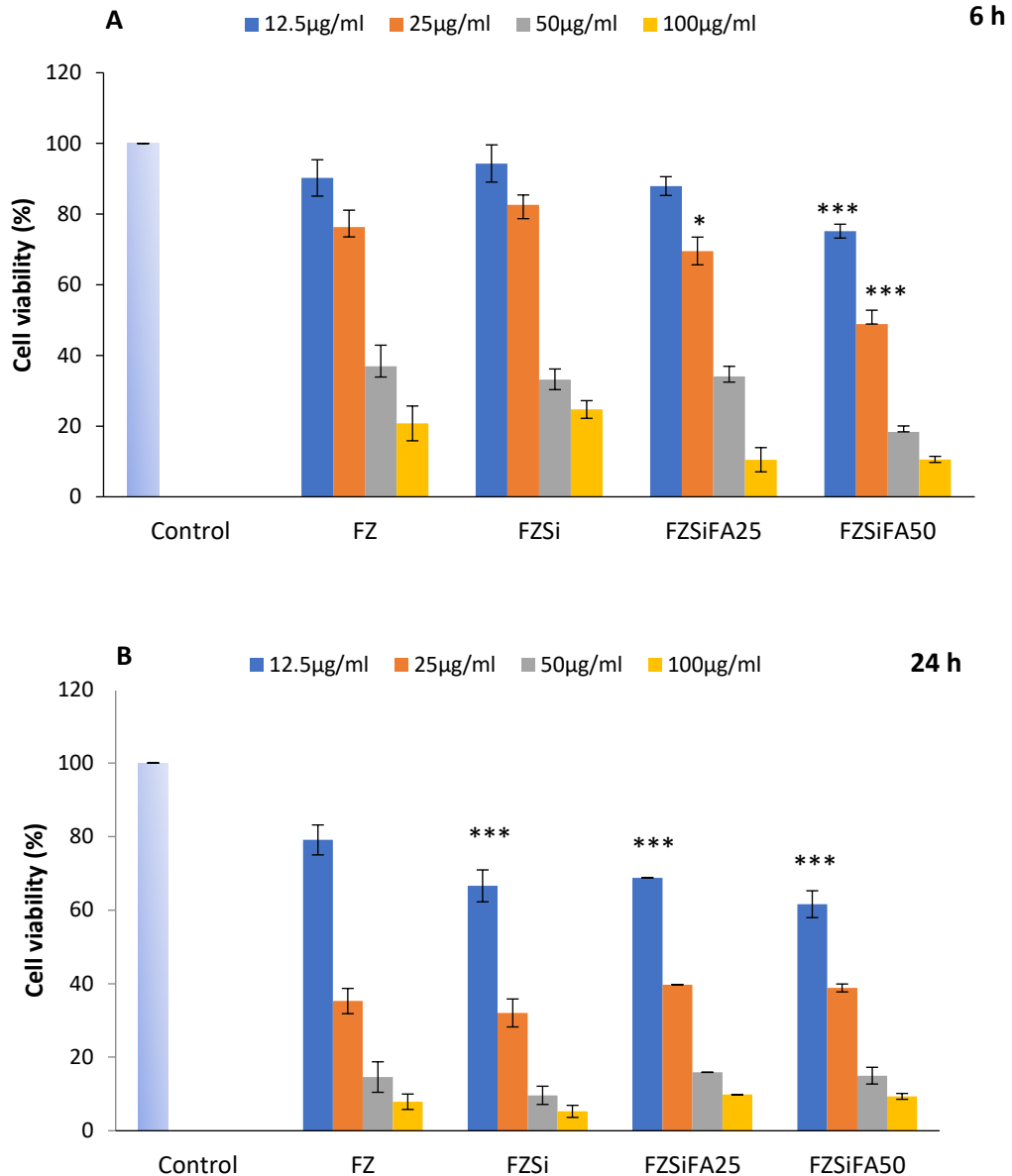


Figure 3.6 The viability of B16-F10 cells upon exposure to various NPs for 6 h (A) and 24 h (B) at different concentrations. Data are represented as mean \pm SD (n=4). Compared to untreated control group all four NPs were significant at all concentrations. * indicates $p < 0.05$; *** indicates $p < 0.001$ when FZ NPs 6 h & 24 h (12.5 & 25 $\mu\text{g/mL}$) groups were compared to other three NPs groups 6 h & 24 h (12.5 & 25 $\mu\text{g/mL}$) cell viability.

The results of this study support modification of hybrid FZ NPs with silica and FA as modified NPs showed enhanced anti-cancer activity against B16-F10 melanoma cells at 12.5 $\mu\text{g/mL}$ dose (Figure 3.6).

(ii) Cytotoxicity of hybrid NPs in Caco-2 cells

Again, the hybrid NPs exhibited time and concentration-dependent cytotoxicity in Caco-2. However, the cytotoxic effect of hybrid NPs towards Caco-2 cells was less

compared to B16-F10 melanoma cells, and the dose-response curves were flatter (Appendix 13).

Increasing the exposure time to 24 h (Figure. 3.7B) attenuated cell viability for all the NPs, across all concentrations, compared to the 6 h treated group ($p < 0.05$). For instance, at 100 $\mu\text{g/mL}$ dose and 6 h, FZ NPs had 63.53% cell viability, which reduced to 3.38% at 24 h (21-fold drop in viable cells). A huge change (up to 50%) in the reduction of cell viability was seen when the NPs concentration increased from 25 to 50 $\mu\text{g/mL}$ at 24 h. For instance, FZ NPs which produced 86.40% cell viability at 25 $\mu\text{g/mL}$ treatment reduced the cell viability to 29.99% with the dose doubled at 50 $\mu\text{g/mL}$. Interestingly, such a change was absent at 6 h. This implies 24 h may be needed to produce the strong cell killing effects against Caco-2 for hybrid NPs.

According to Kang *et al.* (2013), the 30 nm ZnO NPs at 12.5, 25, 50 and 100 $\mu\text{g/mL}$ doses against Caco-2 cells recorded above 60%, less than 40%, less than 10% and less than 1% cell viability. In the present investigation, the FZSiNPs less than 20 nm size in similar concentrations had 83.38%, 71.84%, 24.10% and 0.91% cell viability. Song *et al.* (2014) treated Caco-2 cells with 90 nm ZnO NPs (50 & 100 $\mu\text{g/mL}$) and reported cell viability of 18.21% and 17.87% after 24 h. In our work, FZ NPs produced 29.99% and 3.38% cell viability under similar conditions, indicating severe and greater cytotoxicity at high dose by the hybrid NPs. Also, it was interesting to note that in this study silica and FA modified hybrid NPs were significantly more potent than FZ NPs against Caco-2 cells at 25 $\mu\text{g/mL}$.

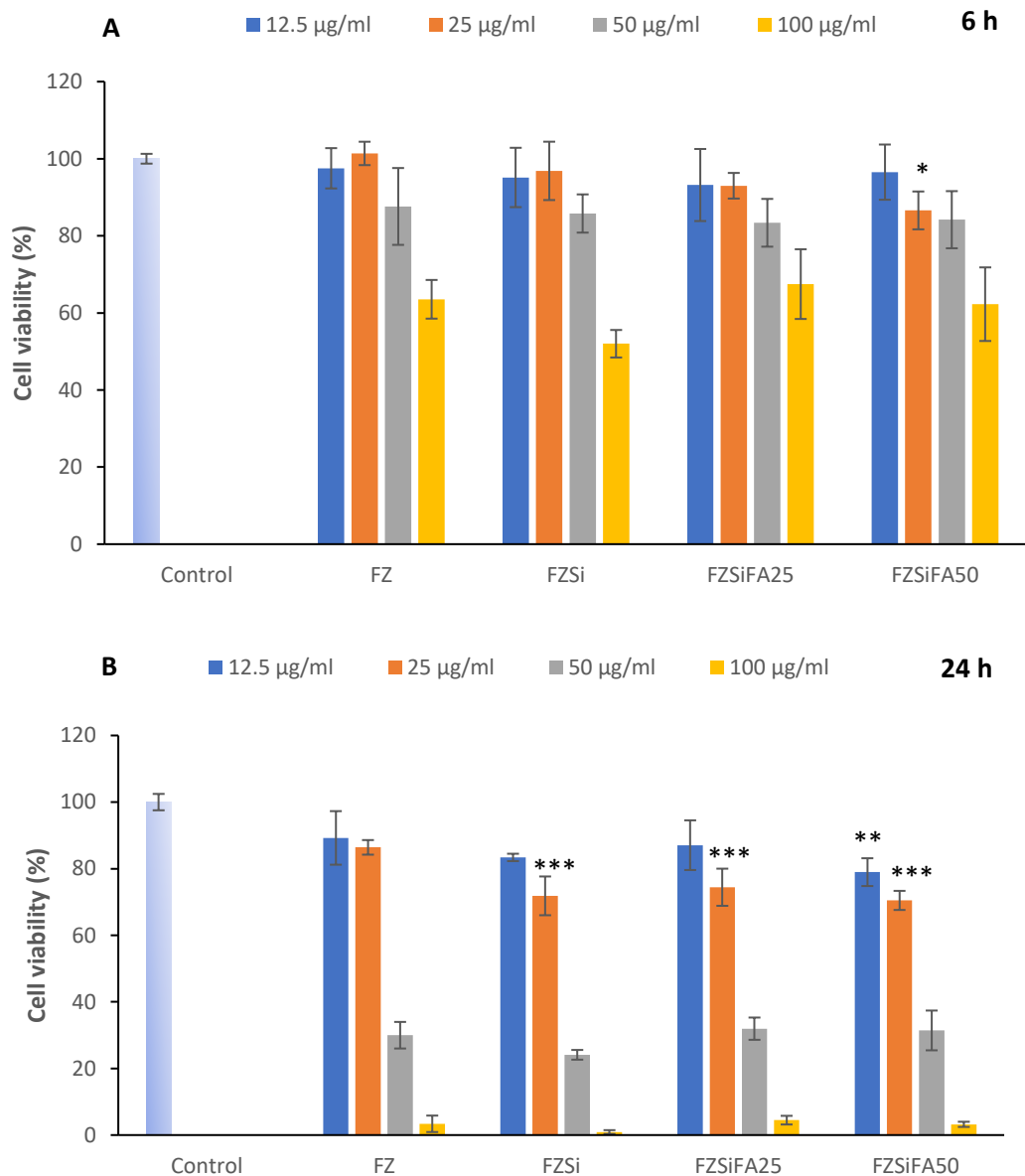


Figure 3.7 The viability of Caco-2 cells upon exposure to various NPs for 6 h (A) and 24 h (B) at different concentrations. Data are represented as mean \pm SD (n=4). Compared to untreated control group all four NPs were significant at all concentrations at 24 h and only at higher doses at 6 h (50 & 100 μ g/mL). * indicates $p < 0.05$, ** indicates $p < 0.01$, *** indicates $p < 0.001$ when FZ NPs 6 h & 24 h (12.5 & 25 μ g/mL) groups were compared to other three NPs groups 6 h & 24 h (12.5 & 25 μ g/mL) cell viability.

(iii) Cytotoxicity of hybrid NPs in 3T3 cells

A strong reduction in cell viability of 3T3 cells was observed across all NPs and concentrations at 6 h and 24 h compared to the control ($p < 0.001$). The nature of the cell line played a prominent role as such a cytotoxic effect was not observed with B16-

F10 and Caco-2 cells when treated with the hybrid NPs. Such cytotoxic effects were reflected by the ED₅₀ values: 15.21 µg/mL and 15.75 µg/mL for FZ and FZSiFA50 NPs respectively after 6 h treatment; 20.85 µg/mL and 25.11 µg/mL for FZSi and FZSiFA25 NPs.

Post 24 h treatment, the cell viability attenuated to 20 - 30% for the NPs at the low dose of 12.5 µg/mL. However, a drastic reduction in cell viability occurred when the NP concentrations were >25 µg/mL (Figure.3.8). No statistically significant difference was detected between the NPs at all concentrations.

Many groups of researchers have reported *in vitro* toxicity of silica-based NPs in 3T3 cells. Stepnik *et al.* (2012) reported toxicity (35%-60% reduction in cell viability) in 3T3 cells with silica NPs between concentrations 10 – 40 µg/mL. Kim *et al.* (2015) reported strong toxicity of silica NPs on 3T3 cells: 4.5% cell viability in 3T3 cells after 24 h treatment of silica NPs at 50 µg/mL concentration and 60 nm particle size. Pandurangan *et al.* (2015) reported changed cell morphology, and almost all cells were dead when 3T3 cells were treated with ZnO NPs at concentration above 30 µg/mL. The toxicity of ZnO NPs against 3T3 cells at 12.8 µg/mL concentration (36 h) was reported by Chandrasekaran & Pandurangan, (2016) where more than 50% cells were inhibited. Our results indicate nearly 70% cell death after 24 h treatment with 12.5 µg/mL FZ hybrid NPs which is not surprising considering the 80% component of hybrid NPs is ZnO. The toxicity of ZnO NPs towards 3T3 may be attributed to the disruption of zinc-dependent enzymes and transcription factors when ZnO dissolves intracellularly (Pandurangan & Kim, 2015). Also, the cell toxicity may arise from soluble metal ions like Zn and Fe (Lu *et al.*, 2015; Malvindi *et al.*, 2014).

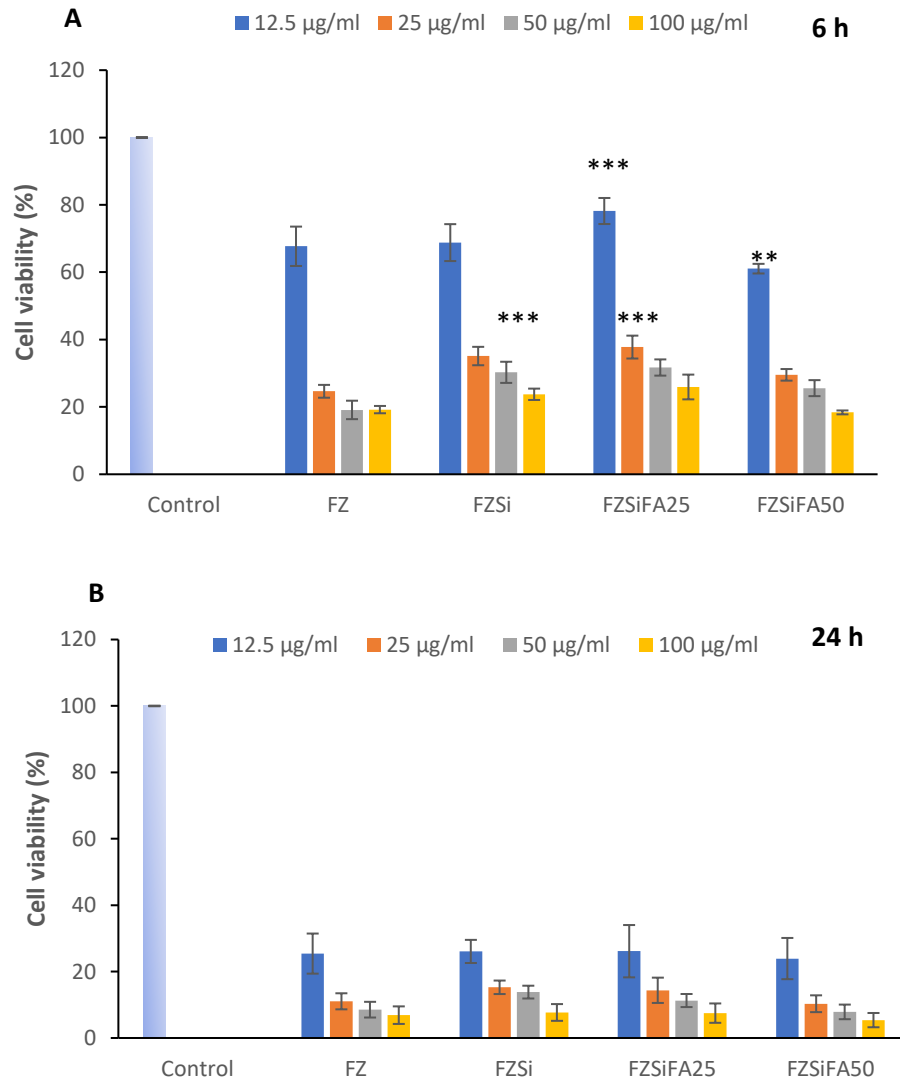


Figure 3.8 The viability of 3T3 cells upon exposure to various NPs for 6 h (A) and 24 h (B) at different concentrations. Data are represented as mean \pm SD (n=4). Compared to untreated control group all four NPs were significant (***) $p < 0.001$ at all concentrations. ** indicates $p < 0.01$, *** indicates $p < 0.001$ when FZ NPs 6 h (12.5 & 25 $\mu\text{g/mL}$) groups were compared to other three NPs groups 6 h (12.5 & 25 $\mu\text{g/mL}$) cell viability.

3.6 Phototoxic effect of hybrid NPs

The impact of UV-A irradiation on the cytotoxic effect of hybrid NPs in cells was analysed by the phototoxicity study. This study would confirm the ability of the hybrid NPs to be used in PDT against cancer as a PS. Given the stronger reduction in cell viability was seen with longer treatment time (24 h) of hybrid NPs (Figure 3.6, 3.7, 3.8 B), 24 h was chosen for phototoxicity studies. Figure 3.9 A & B highlights the photoinduced cell viability reduction by hybrid NPs compared to the only UV treated cells and control (no hybrid NPs treatment) in B16-F10 and Caco-2 cells. The photo-killing effect was concentration dependent as expected.

To compare the photodynamic action of the hybrid NPs, phototoxic index (PI) was calculated by the ratio of ED₅₀ in the dark over ED₅₀ in the light and has been used for the evaluation of PS (Mion *et al.*, 2015). Appendices 12 and 13 show the dose response curve of the respective NPs used to calculate the ED₅₀. Use of this approach requires at least two assay concentration responses be above 50% of the control (ie 50% cell viability) and two below 50% (Sebaugh, 2011). However, our data does not always fulfil such criteria. Therefore, we could only use the estimated PI for comparison and exercise caution in its interpretation.

(i) Phototoxic effect of hybrid NPs in B16-F10 cells

The phototoxic effect of hybrid NPs was highly significant ($p < 0.001$) across all concentrations when compared to the UV treated B16-F10 cells.

At 12.5 µg/mL dose, FZ NPs cell viability was 73.23%. When doubling the dose to 25 µg/mL, there was a remarkable decrease in cell viability in FZ NPs (from 73.23% to 15.28%). The PI values for FZ and FZSi NPs were 1.5 and 1.4, and for FZSiFA25 and FZSiFA50 NPs were 1.2 and 2.0. Based on the PI values, FZSiFA50 NPs exhibited the best phototoxic effect in B16-F10 cells which is also consistent with its strong cell killing effect shown at the lowest dose tested. Such photokilling effect of FZSiFA50 could be attributed to FA coating which may have facilitated the interaction of NPs with cells and consequent cellular uptake.

To be an effective nano-PS, concomitant treatment of hybrid NPs with UV-A irradiation should produce a synergistic therapeutic effect that is more than just the sum of effects from hybrid NP and UV-A. The synergistic effect of hybrid NPs+UV-A irradiation is demonstrated (Table 3.5) by calculation of the ratio of phototoxicity measured over the sum of cytotoxicity of NPs treatment alone with that of UV-A treatment alone. This ratio produces the fold of cell killing by PDT using hybrid NPs as nano-PSs. Only UV-A radiation killing in B16-F10 cells was 3.21%. The fold increase represents the synergistic effect between hybrid NPs and UV-A radiation compared to combined cell killing by NPs alone+ UV-A. No increase indicates the combined cell killing by NPs alone + UV-A radiation better than cell killing by hybrid NPs+UV-A (Table 3.5).

The stronger synergistic effect was observed at low doses 12.5 and 25 $\mu\text{g/mL}$. For instance, 1.47 and 1.2 folds of cell killing were achieved with PDT using FZSiFA50 at NPs dose of 12.5 and 25 $\mu\text{g/mL}$ respectively, while only 1.0 and 1.02 folds of cell killing were seen with 50 and 100 $\mu\text{g/mL}$ dose respectively. PDT intends to use the low dose of PS. Therefore, we can conclude the two most effective PSs at 12.5 $\mu\text{g/mL}$ were FZSi and FZSiFA50 NPs as they produced not only strongest synergistic effect but also strongest actual photokilling effects, while both with high PIs.

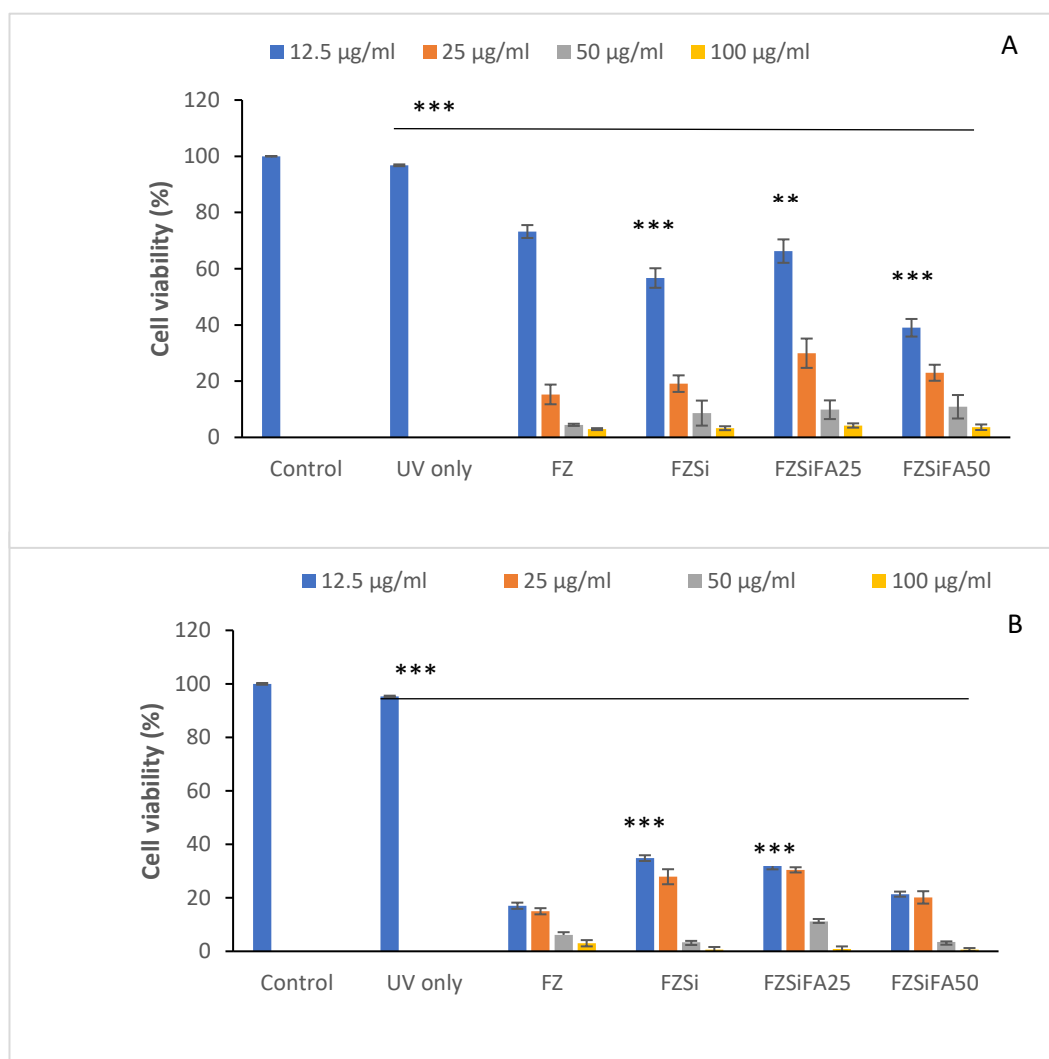


Figure.3.9 Photoinduced reduction in viability of (A) B16-F10 and (B) Caco-2 cells after 24 h upon exposure to hybrid NPs and UV-A irradiation at the dose of 10J/cm². ** indicates p<0.01 and *** indicates p<0.001 compared to the control and only UV treated group with the four NPs at all concentrations and FZ NPs treated group (12.5 $\mu\text{g/mL}$) compared with other three NPs (12.5 $\mu\text{g/mL}$) cell viability.

Table 3.5 Synergistic effect of hybrid NPs & UV-A irradiation in photokilling of B16-F10 cells

Nanoparticle	Concentration (µg/mL)	^a Cell killing by hybrid NPs alone (%)	^b Combined cell killing by hybrid NPs + UV-A (%)	^c Cell killing by UV-A activated hybrid NPs (%)	^d Fold increase in cell killing
FZ	12.5	20.92	24.13	26.77	01.11
	25	64.72	67.93	84.72	01.25
	50	85.40	88.61	95.53	01.08
	100	92.11	95.32	97.06	01.02
FZSi	12.5	33.41	36.62	43.31	01.18
	25	67.97	71.18	80.88	01.14
	50	90.37	93.58	91.36	no increase
	100	94.73	97.94	96.73	no increase
FZSiFA25	12.5	31.20	34.41	33.70	no increase
	25	60.30	63.51	70.10	01.10
	50	84.10	87.31	90.20	01.03
	100	90.20	93.41	95.80	01.02
FZSiFA50	12.5	38.39	41.60	61.00	01.47
	25	61.16	64.37	77.01	01.20
	50	85.01	88.22	89.10	01.00
	100	90.65	93.96	96.38	01.02

a represents the percentage of cell death by hybrid NPs alone

b represents the combined percentage of cell death by hybrid NPs & UV-A (i.e cell death by hybrid NPs alone+ cell death by UV-A alone)

c represents the photokilling of cells by UV-A activated hybrid NPs

d represents the fold increase in cell killing. It was calculated as $d = c/b$

(ii) Phototoxic effect of hybrid NPs in Caco-2 cells

Figure 3.9B highlights the synergistic photoinduced cell killing effects of NPs in PDT with UV-A (calculation explained in Table 3.6). Only UV-A radiation killing in Caco-2 cells was 4.68%. The fold increase represents the synergistic effect between hybrid NPs and UV-A radiation compared to combined cell killing by NPs alone+ UV-A. NA represents the combined cell killing by NPs alone + UV-A radiation better than cell killing by hybrid NPs+UV-A (Table 3.6).

For instance, 15.4% cells were killed by combining the dead cell data of FZ NPs alone (12.5 µg/mL) and UV-A alone. However, 83% cells were killed when 12.5 µg/mL FZ NPs was irradiated with UV-A radiation. The strongest synergistic effect against Caco-2 cell was seen at the lowest NP dose with FZ NPs (5.37 folds), followed by FZSiFA25 (3.86 folds), FZSi & FZSiFA50 (both 3.06 folds) (Table 3.6). The PI index was high for FZ NPs with 12.8, followed by FZSiFA50 NPs with 7.9. FZSi and FZSiFA25 NPs had 4.5 and 4.9 PI values respectively (Table 3.7). Even though the synergistic effect of FZSiFA50 was not the strongest, its actual photokilling effect was greater than FZSi and FZSiFA25 (Figure 3.9B). This suggests FA coating may have increased NPs uptake by cells via folate receptor-mediated endocytosis.

Table 3.6 Synergistic effect of hybrid NPs & UV-A irradiation in photokilling of Caco-2 cells

Nanoparticle	Concentration (µg/mL)	^a Cell killing by hybrid NPs alone (%)	^b Combined cell killing by hybrid NPs+ UV-A (%)	^c Cell killing by UV-A activated hybrid NPs (%)	^d Fold increase in cell killing
FZ	12.5	10.76	15.44	82.96	05.37
	25	13.60	18.28	85.02	04.65
	50	70.01	74.69	93.90	01.26
	100	96.62	100.00	96.98	no increase
FZSi	12.5	16.62	21.30	65.15	03.06
	25	28.16	32.84	72.11	02.19
	50	75.90	80.58	96.59	01.20
	100	99.09	100.00	99.41	no increase
FZSiFA25	12.5	12.94	17.62	68.01	03.86
	25	25.57	30.25	69.54	02.30
	50	68.05	72.73	88.89	01.22
	100	95.52	100.00	99.13	no increase
FZSiFA50	12.5	21.04	25.72	78.62	03.06
	25	29.53	34.21	79.84	02.33
	50	68.58	73.26	96.55	01.32
	100	96.78	100.00	99.37	no increase

a represents the percentage of cell death by hybrid NPs alone

b represents the combined percentage of cell death by hybrid NPs & UV-A (i.e cell death by hybrid NPs alone+ cell death by UV-A alone)

c represents the photokilling of cells by UV-A activated hybrid NPs

d represents the fold increase in cell killing. It was calculated as $d = c/b$

Comparing the photokilling effects of hybrid NPs in Caco-2 with that in B16-F10, it is evident that Caco-2 cells are more sensitive or responsive to PDT with our hybrid

NPs than B16-F10 melanoma cells, especially at the lowest dose tested (12.5 $\mu\text{g/mL}$). This again highlights the complexity of cancer cells, and their sensitivity and response to PS alone and PS in PDT could be vastly different. Such phenomena had been reported in the literature before (Mion *et al.*, 2015).

Table 3.7 ED₅₀ and PI calculation in B16-F10 and Caco-2 cells

Nanoparticle	ED ₅₀ in dark 6h ($\mu\text{g/mL}$)	ED ₅₀ in dark 24 h ($\mu\text{g/mL}$)	ED ₅₀ in UV-A treated 24 h ($\mu\text{g/mL}$)	PI
In B16-F10 cells				
FZ	45.00	17.99	11.48	1.57
FZSi	49.34	13.76	9.65	1.42
FZSiFA25	36.28	17.16	13.27	1.29
FZSiFA50	21.44	15.19	7.41*	2.05
In Caco-2 cells				
FZ	248.40 [#]	39.25	3.06*	12.83
FZSi	172.30 [#]	29.83	6.63*	4.50
FZSiFA25	226.40 [#]	35.23	7.06*	4.99
FZSiFA50	191.30 [#]	31.00	3.88*	7.99

PI represents phototoxic index calculated by (ED₅₀ in dark)/(ED₅₀ in light).

ED₅₀ represents the median effective dose that produces effect in 50 % of population.

ED₅₀ dark was calculated from the cell viability of hybrid NPs in dark Vs the concentration of NPs (dose response curve and line of best fit in GraphPad).

ED₅₀ light was calculated from the cell viability of hybrid NPs after UV-A Irradiation Vs the concentration of NPs (dose response curve and line of best fit in GraphPad).

*** indicates the groups where less than two values were above 50% cell viability when calculating ED₅₀.**

indicates the groups where all the values were above 50 % cell viability when calculating ED₅₀.

The phototoxicity study confirmed the significant synergistic effect existing between the NPs and UV-A irradiation was at the low dose (12.5 $\mu\text{g/mL}$) of NPs and 10 J/cm² UV-A dose. The best PI value was observed with FZ NPs in Caco-2 cells. However, the exact molecular mechanisms behind the synergistic action (NPs+ UV-A irradiation) remains to be determined. Better cytotoxicity under the UV-A light (PDT) compared to dark is considered the best feature of PSs. The developed hybrid NPs (nano-PSs) seems to serve the purpose efficiently in both the cell lines studied. To study the mechanism of cellular deaths mediated by NPs upon UV-A irradiation, the intracellular ROS were monitored which is the topic of later section.

3.7 Phototoxic effect of hybrid NPs in B16-F10 cells after multiple irradiations

To compare the effects of multiple irradiations, the low concentration of NPs 12.5 $\mu\text{g/mL}$ (24 h treatment) was selected, the radiation source and conditions were

followed as per single radiation used in photo killing study. The cell viability reduced as the PDT sessions (double and triple condition) increased in a pattern similar to that increased dose of NPs. The biggest reduction in cell viability (more than 50%) was observed when cells received hybrid NPs with double irradiation treatment. The 3rd UV-A irradiation produced a much smaller further reduction of cell viability, suggesting cells may develop PDT resistance. Again, it was noticed that FZSiFA50 showed a relatively stronger photokilling effect with repeat UV irradiation. The cell viability changes had statistical significance ($p < 0.001$) when multiple irradiated NPs were compared to dark and single radiation. Our results agree with the finding of Chang *et al.* (2014) who also reported better phototoxicity with HP-NPs under double irradiation conditions in HepG2 cells.

From the above cytotoxicity and phototoxicity experiments, we could conclude that the developed hybrid NPs have fulfilled the criteria to be effective PSs for PDT with UV-A against cancer cells. The nature of nano-PS influenced not only its own cytotoxicity but also its PDT effect significantly. The repeat UV-A irradiation produced further cell killing effect in a pattern similar to the increase of NP's dose. Cell viability studies also demonstrated that high level of FA (0.085mmol/g NPs) enhanced the cell killing effect with the strongest effect at a low dose of PS.

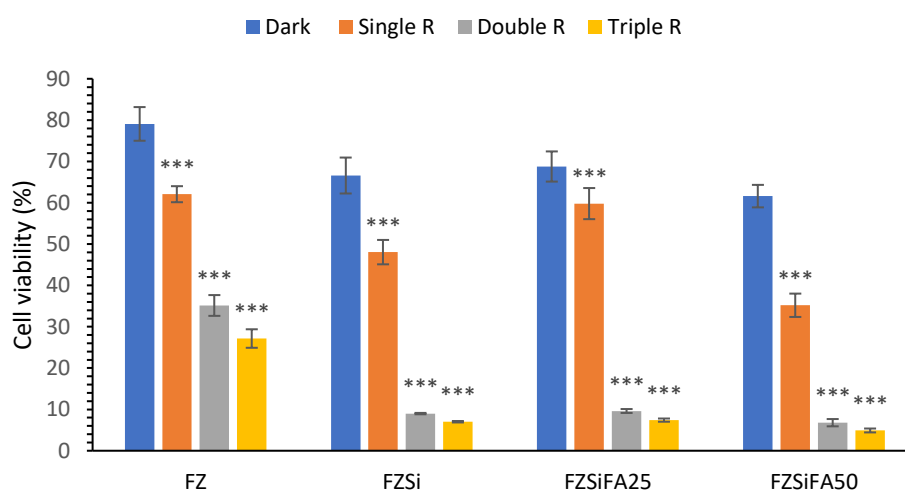


Figure 3.10 Cell viability of B16-F10 cells after multiple UV-A irradiations upon exposure to 12.5 µg/mL NPs for 24 h. Data are represented as mean \pm SD (n=4). *** $p < 0.001$ compared to NPs in the dark.

3.8 Singlet oxygen generation by hybrid NPs in PDT

To elucidate the mechanisms of hybrid NPs in PDT, studies were conducted to detect singlet oxygen and ROS in treated cells. DPBF is commonly used as singlet oxygen and hydroxyl radical trapping reagent, as it can scavenge both $^1\text{O}_2$ and $\text{OH}\cdot$ (Okada *et al.*, 1998; Nadhman *et al.*, 2014). On excitation with UV-A light, the hybrid NPs are photo enhanced into a singlet energy state and went through the inter-system, crossing to the triplet state, and this energy from the excited PS is transferred to the triplet oxygen state and is converted to $^1\text{O}_2$. The released singlet oxygen molecules react with the DPBF and initiate its degradation (Xiao *et al.*, 2011). The production of singlet oxygen is normally quantified using quantum yield, which is the number of singlet oxygen produced per absorbed photon (Huarac *et al.*, 2010). In this study, Rose Bengal was used as a standard as its quantum yield (0.86) is well characterised (Xiao *et al.*, 2011).

The singlet oxygen production depends on the nature of the PS used and concentration of PS (De Rosa & Crutchley, 2002). By employing Rose Bengal as the standard, it was possible to validate the method for quantification of the singlet oxygen quantum yields. Table 3.8 displays the singlet oxygen quantum yield of hybrid NPs. FZ NPs produced 0.85, while the surface modified FZSi produced 0.29. It appears that the silica coating and FA modification had an impact on the generation of singlet oxygen. The further modification of hybrid NPs with FA increased a little of singlet oxygen yield from 0.29 to 0.40 and 0.46 for FZSiFA50 and FZSiFA25 NPs respectively, which may be attributed to the presence of FA in NPs. Although, FA was reported to undergo photodegradation and change its fluorescent property upon UV-A irradiation (Vorobei & Vorobei, 2011), the photodegradation of FA does not appear to have much impact on the UV absorbance at 410 nm (Off *et al.*, 2005), the wavelength which was used in determination of singlet oxygen quantum yield using DPBF method.

Singlet oxygen quantum yield of 0.13 is reported by Nadhman and his colleagues (2014), when 10 $\mu\text{g/mL}$ of ZnO is dissolved in 2 mL DPBF, detected by chemical trapping method. Luengas *et al.* (2014) reported 0.71 singlet oxygen quantum yield for 15 $\mu\text{g/mL}$ of ZnO, detected by fluorimetry analysis. In our study, the FZ hybrid NPs (0.85) had 6.5-fold better yield and 5-fold better yield compared to ZnO NPs (0.13) (Nadhman *et al.*, 2014) and porous silica NPs (0.17) (Xiao *et al.*, 2010). The singlet

oxygen yield of 0.28 by Fe₃O₄/ZnO NPs was reported by Huarac and his group (2010), much lower than quantum yield of 0.85 by the FZ NPs studied in this work. The results confirmed the ability of the hybrid NPs to generate singlet oxygen and therefore, the production of singlet oxygen could contribute to their cytotoxicity.

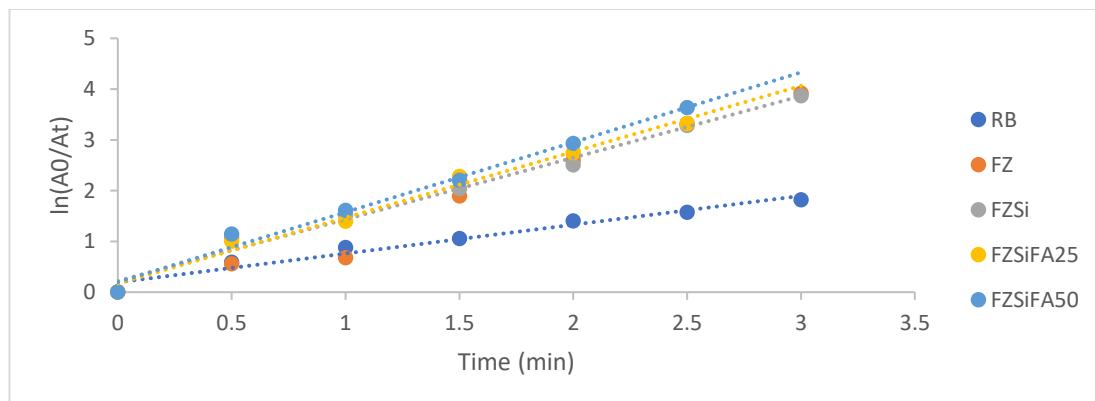


Figure 3.11 Absorbance of DPBF exposed to hybrid NPs and UV-A irradiation

Table 3.8. Singlet oxygen quantum yield of hybrid NPs

No	Nanoparticle	Singlet oxygen quantum yield	Reference
1.	FZ	0.85	Present work
2.	FZSi	0.29	Present work
3.	FZSiFA25	0.46	Present work
4.	FZSiFA50	0.40	Present work

3.9 Intracellular ROS production by hybrid NPs in PDT

ROS plays a vital role in influencing biochemical functions in cells. DCF assay is highly sensitive, linear and specific for measuring oxidative stress in irradiated cells. The responses of cells to oxidative stress varies depending on the magnitude of the stress and could either be upregulated or downregulated. Thus, the level of oxidative stress or ROS determines whether cells likely undergo proliferation, differentiation, senescence or cell death (Mellier & Pervaiz, 2012). Numerous agents that induce apoptosis stimulate intracellular production of ROS, most frequently leading to an accumulation of H₂O₂ (Indran *et al.*, 2011).

The DCFH-DA was used to assess the intracellular ROS generation after cells were exposed to FZ, FZSi, FZSiFA25 and FZSiFA50 NPs at 12.5, 25 and 50 µg/mL concentrations under dark and UV-A irradiation conditions in both B16-F10 and Caco-2 cell lines. Although the starting time point in the study was 0 h, in practice, it should be considered as 5 min time point. The ROS generated by the hybrid NPs in medium (without cells) (both dark and UV-A treated) in comparison to ROS generated by B16-

F10 and Caco-2 cells is described in Appendix 15 and 17 respectively. Comparing to the ROS generated by cells alone (100%), hybrid NPs showed relatively low and consistently level about 15-30% in the dark over 24 h; and increased to about 40-70% with UV-A irradiation in the first 6 h, then reduced to 5-17% at 24 h. There was no correlation with NPs dose.

(i) Intracellular ROS production in B16-F10 cells

Compared to the control (cells), ROS level, as shown by DCF intensity, in hybrid NP treated melanoma cells was enhanced, though not significant, over time in the first 6 h (Figure 3.12) A significant drop of DCF intensity (down to <12%) was seen at 24 h, implying that NPs may neutralise ROS generated by cells at 24 h. No significant differences were observed with coated and uncoated hybrid NPs or different doses.

Upon UV-A irradiation, a different trend emerged. Although UV alone didn't change ROS level, cells received treatment of hybrid NPs, and UV-A showed elevated ROS with the increase of dose and time (up to 6 h) as indicated by high DCF intensity (Figure 3.13). The DCF intensity of cells treated with NPs was maintained close to that of control even at 24 h in most cases.

Overall, the UV-A irradiated hybrid NPs generated better ROS compared to hybrid NPs in the dark at all concentrations, which was significant. After UV-A irradiation, dose and time-dependent ROS generation were demonstrated strongly in FZSiFA25 and FZSiFA50 NPs until 6 h, but not in FZ and FZSi NPs. FZSiFA50 NPs recorded 108%, 118%, 123% ROS at dark and increased to 149%, 211%, and 246% (1.49, 2.11 and 2.45-fold increase in ROS generation) after UV-A exposure (10 J/cm²) (Figure 3.13, D).

A synergistic effect was not observed in ROS generation by photoactivated hybrid NPs compared to the ROS generated by NPs in the dark plus that generated by UV-A alone. There appears to be an inverse correlation between the decrease in cell viability and increase in ROS production until 6 h, but the relationship reversed at 24 h. For instance, FZSiFA50 NPs cell viability at 6 h (50 µg/mL) was 18.37 %, and the ROS yield in the similar condition was 123%. However, at 24 h (50 µg/mL) cell viability was 14.99 %, and the ROS yield was 10.3%. This could be because the effect of ROS may take time to be transferred into the cell viability. The FA surface attachment may have enhanced

the cell interaction with NPs, therefore, resulting more uptake of NPs by cells which led to higher level of ROS production with NPs modified with FA. However, one cannot completely exclude the possibility that the high DCF intensity seen with FA modified NPs was partially a result of FA's photo degradation. A process known to potentially produce strong fluorescence (Vorobei & Vorobei, 2011). The photo degradation products of FA are 6-formylpterin and pterin-6-carboxylic acid which absorb UV-A radiation, and exhibit fluorescence at 445 nm (Vorobei & Vorobei, 2011). In comparison, the ROS detection was performed at 485 nm excitation and 520 nm emission.

Pal *et al.* (2016) reported a decrease in ROS production after 3 h when primary mouse keratinocytes were treated with ZnO NPs and UV-B radiation. Aranda *et al.* (2013) reported masking effect on fluorescence quantification after significant TiO₂, Fe₃O₄ NPs internalization. Further, Fe₃O₄ and Au NPs had been reported that their aggregated particles quenched the fluorescence of DCFH-DA (Aranda *et al.*, 2013).

The accumulation of NPs in melanoma cells may be a reason triggering the production of ROS. Melanoma cells were suggested to be more sensitive to ROS-induced cell death than melanocytes, a vulnerability that can be exploited for the development of new anti-melanoma chemotherapeutics (Liu *et al.*, 2012; Yamaura *et al.*, 2009).

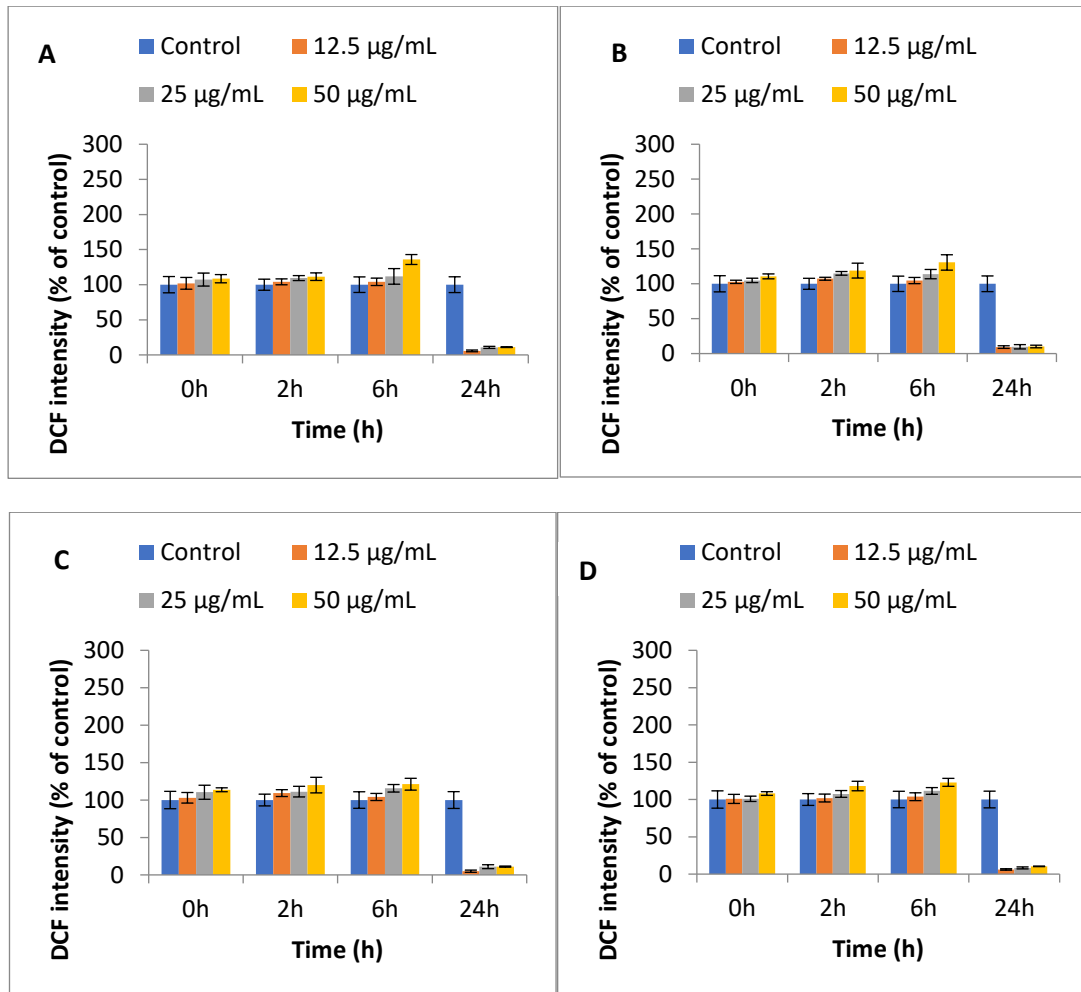


Figure 3.12 ROS generation in B16-F10 cells (dark) upon exposure to various NPs (A) FZ NPs (B) FZSi NPs (C) FZSiFA25 NPs (D) FZSiFA50 NPs for 0, 2, 6 and 24 h at various concentrations. Data are represented as mean \pm SD (n=4). Highly significant difference was observed only at 24 h.

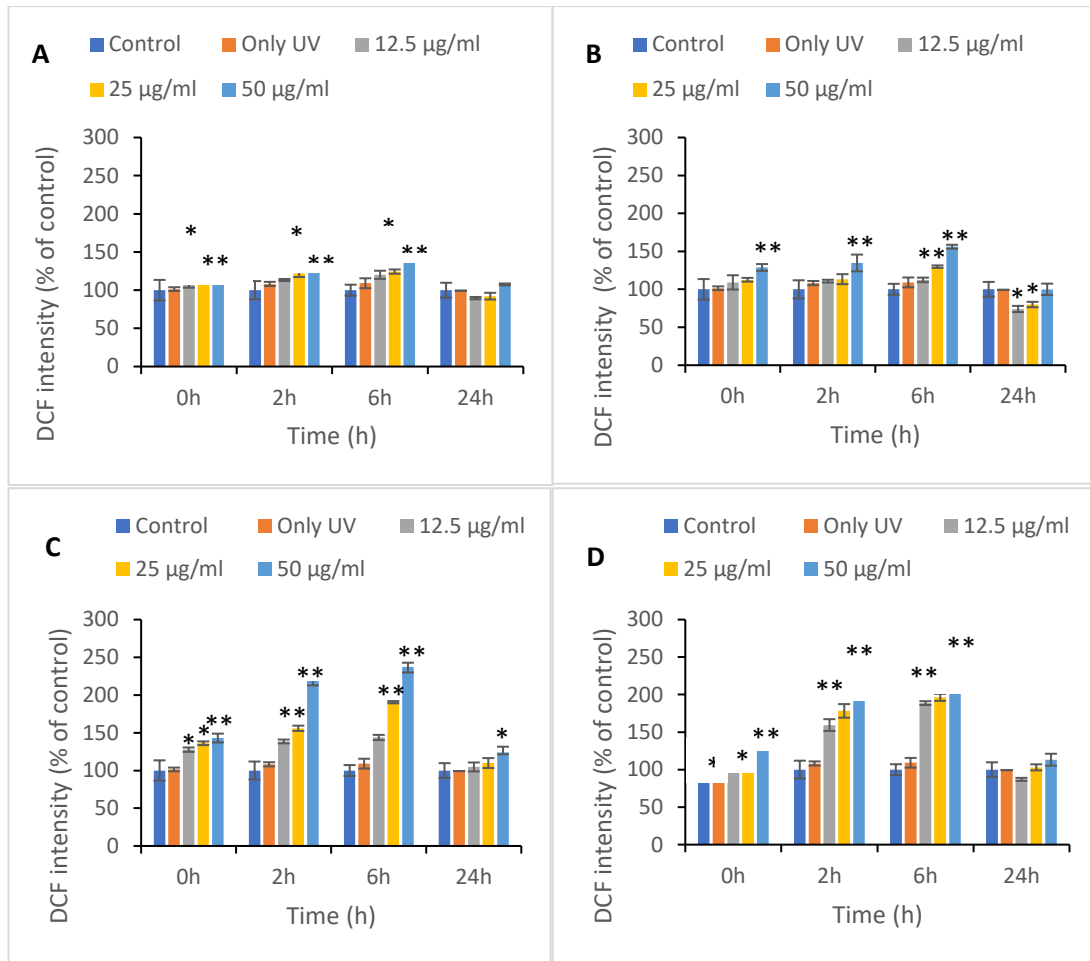


Figure 3.13 ROS generation in B16-F10 cells after treatment with UV-A irradiation activated NPs (A) FZ NPs (B) FZSi NPs (C) FZSiFA25 NPs (D) FZSiFA50 NPs for 0, 2, 6 and 24 h at various concentrations. Data are represented as mean \pm SD (n=4). *p<0.05 and ** p<0.01 compared to the untreated (control) group.

(ii) Intracellular ROS production in Caco-2 cells

Like that seen with B16-F10 cells, DCF intensity in Caco-2 cells was also increased with time and NPs dose up to 6 h (Figure 3.14 & 3.15, Appendix 14). Compared to control, DCF fluorescent intensities increased to 123%, 138%, and 144% at 0, 2 and 6 h for FZ NPs at 50 µg/mL concentration (Figure 3.14 A). However, the ROS yield reduced to 84% at 24 h. A similar reduction in ROS (between 100 µg/mL and 200 µg/mL ZnO) when treating Caco-2 cells was reported by Song and his colleagues (2014). They reported the severe cytotoxicity and more dead cells after 200 µg/mL treatment and hence an adequate number of viable cells are not available to generate ROS. We do speculate a similar reason behind the drop of ROS at 24 h as the cell viability in FZ, FZSi, FZSiFA25 and FZSiFA50 NPs at 100 µg/mL (dark) were 3.38%, 0.91%, 4.48% and 3.22% respectively.

ROS can be generated in three ways:

- 1) Radiation alone: ROS was generated following radiation exposure (Yang & Ma, 2014).
- 2) Cells: ROS generated from cells naturally (Liou & Storz, 2010) are affected by cell viability and decreases with time as cell viability reduces by time on treatment with NPs.
- 3) NPs: ROS are generated by NPs themselves (Yang & Ma, 2014) and as NPs are constantly producing ROS, so this type of ROS appears to be long lasting compared to the other two factors.

Possible reasons behind the reduction of ROS levels are listed below:

- Data in Table 3.9 showed intracellular zinc and iron content in B16-F10 and Caco-2 cells upon the exposure to UV-A. We observed a drop in intracellular level of zinc level at 6 h in Caco-2 cells. The partial dissolution of NPs (if the reduction of intracellular zinc level could be attributed to its dissolution) may have contributed, to a certain extent to the reduction of ROS production in Caco-2 cells at 24 h.
- Aggregation of NPs by time may lead to reduced ROS production.
- The ROS yield is short lived, and the maximum ROS yield may have been missed between the 6 h and 24 h time points.

After UV-A irradiation the DCF fluorescent intensities of FZ NPs increased to 125%, 154%, 147% at 0, 2 and 6 h at 50 $\mu\text{g/mL}$ concentration (Figure 3.15 A).

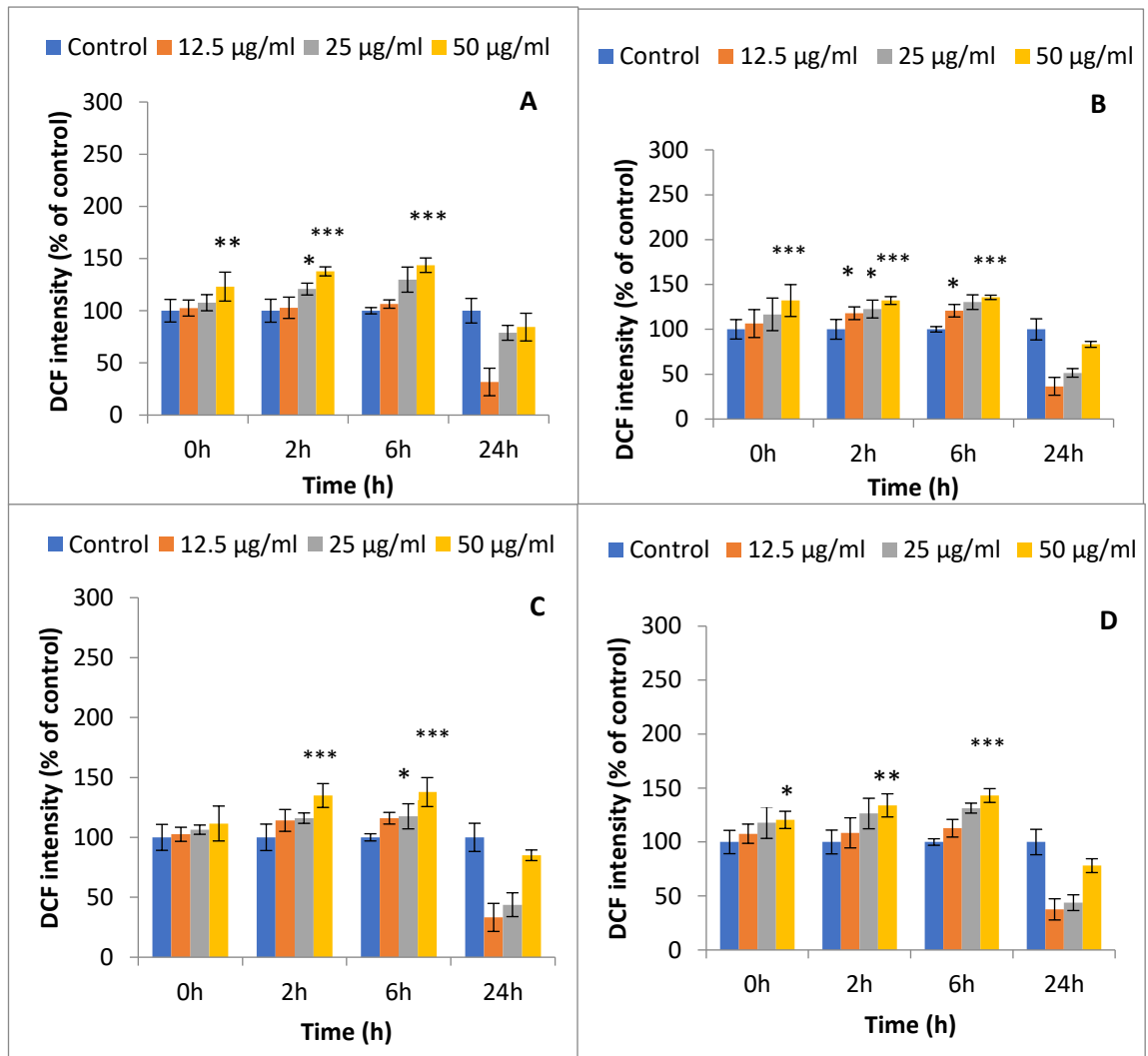


Figure 3.14 ROS generation in Caco-2 cells (dark) upon exposure to various NPs (A) FZ NPs (B) FZSi NPs (C) FZSiFA25 NPs (D) FZSiFA50 NPs for 0, 2, 6 and 24 h at various concentrations. Data are represented as mean \pm SD (n=4). * indicates $p < 0.05$, ** indicates $p < 0.01$ and *** indicates $p < 0.001$ compared to the untreated (control) group. At 24 h all the samples were significant compared to control.

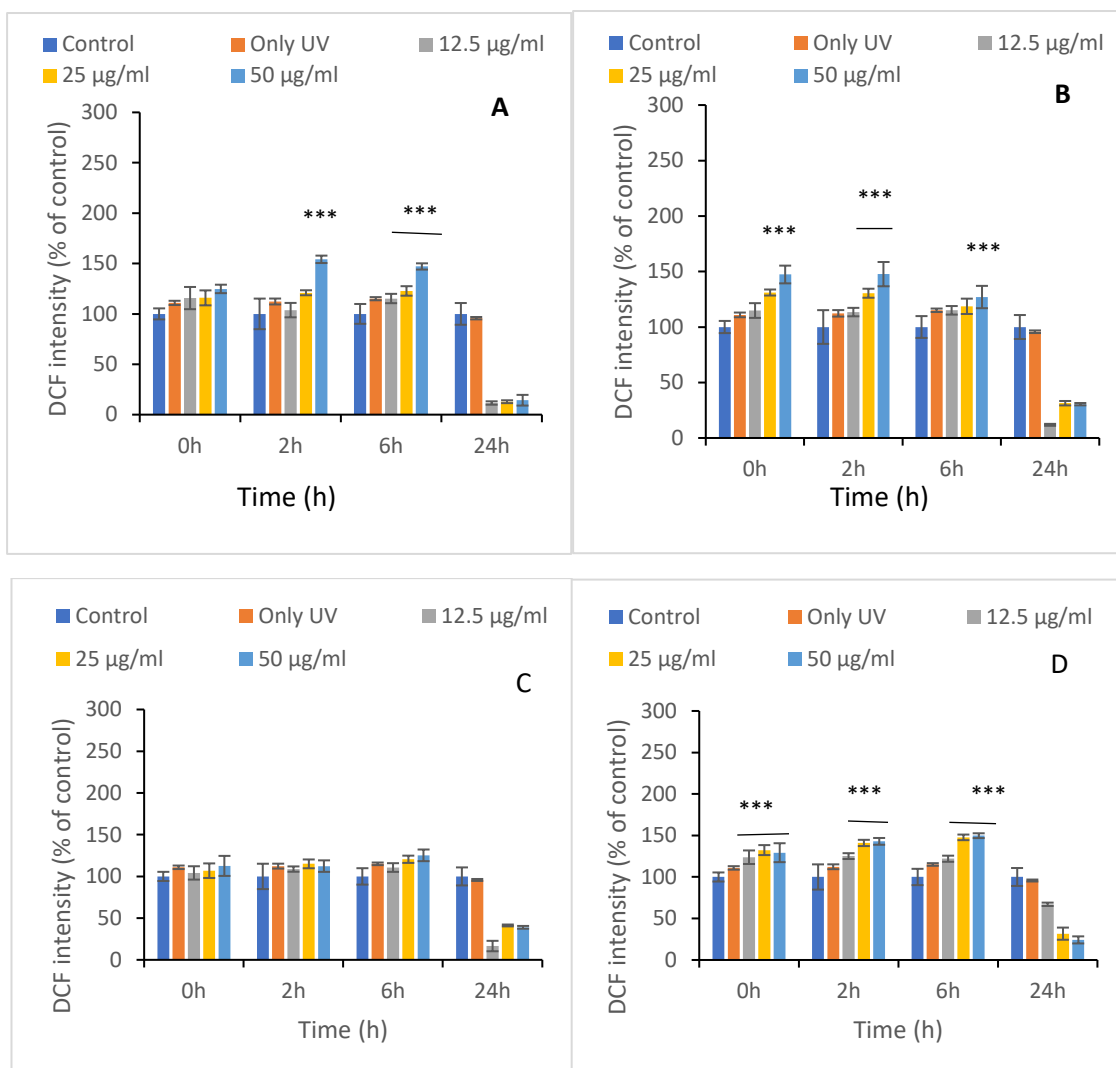


Figure 3.15 ROS generation in Caco-2 cells after treatment with UV-A irradiation activated NPs (A) FZ NPs (B) FZSi NPs (C) FZSiFA25 NPs (D) FZSiFA50 NPs for 0, 2, 6 and 24 h at various concentrations. Data are represented as mean \pm SD (n=4). *** indicates $p < 0.001$ compared to the untreated (control) group.

Synergistic effect of photoactivated hybrid NPs was not observed. Oxidative stress plays a crucial role in NPs-induced cytotoxicity, which leads to an imbalance between ROS generation and antioxidant system (Yang & Ma, 2014; Akhtar *et al.*, 2012). Our results demonstrated that ROS was generated in B16-F10 and Caco-2 cells by hybrid NPs which may have contributed to decreased cell proliferation or even cell death possibly via apoptotic or necrotic pathways. Based on the nature of the cells the ROS generation differs. The ROS generation will result in damage to cellular organelles and cellular membrane which will eventually cause cell death (Ai *et al.*, 2017).

ZnO are direct bandgap semiconductors, which under UV irradiation produces a hole (h⁺) in the valence band and an electron (e⁻) in the conduction band, namely electron/hole pairs. These electron/hole pairs induce a series of photochemical reactions in an aqueous suspension of NPs, generating ROS (Zhang *et al.*, 2014; Akhtar *et al.*, 2012; Zhang *et al.*, 2016). De Berardis and colleagues (2010) had reported significant oxidative stress instigated by ZnO NPs, apparently due to direct interaction of NPs with some components on the cell surface altering mitochondria and endoplasmic reticulum functions and produced intracellular signals activation. Thus, ZnO, the major component of the hybrid NPs, could have assisted in making the hybrid NPs a promising PS for PDT against cancer.

The singlet oxygen quantum yield by the hybrid NPs and the ROS production by the hybrid NPs suggests the possibility of both the type-I and type-II reactions occurring during the energy transfer from excited PS. The detailed mechanism by which the hybrid NPs generate ROS and the role played by each specific free radicals and singlet oxygen inside cells needs further investigation.

(iii) Confirmation of ROS production in cells

To confirm the ROS dependent cell death after NPs exposure, NAC an antioxidant was pretreated in each well (5 mM, 24 h), followed by DCFH-DA and NPs treatment (6 h) (Figure 3.16 & 3.17). Only FZ and FZSi NPs were used in the study. Based on our data (Figure 3.12 & 3.13 for B16-F10 and Figure 3.14 & 3.15 for Caco-2) the time point which produced the highest level of ROS production, 6 h, was chosen for the study. The ROS production (measured by DCF intensity) reduced nearly 50% in both the NPs and across all concentrations in both the cell lines when pre-treated with NAC (Figure 3.16 & Figure 3.17). For instance, in FZ NPs+UV-A treated B16-F10 cells, at 6 h (50 µg/mL) the ROS was 152%, which reduced to 81% on NAC pre-treatment while the control cells which were pre-treated with NAC only exhibited < 16% drop in DCF intensity or ROS level. A similar effect of NAC in reducing the ROS production was observed in Caco-2 cells. For instance, FZSi NPs + UV-A (6 h, 25 µg/mL) recorded 162% ROS which reduced significantly to 53% on NAC pre-treatment while the control cell reduced <16%. These results confirmed that significant level of ROS was generated by the hybrid NPs, a process which may have played a vital role in inducing cytotoxicity in B16-F10 and Caco-2 cells. ROS generation may

be one of the pathways through which hybrid NPs trigger cell death in both the cell lines.

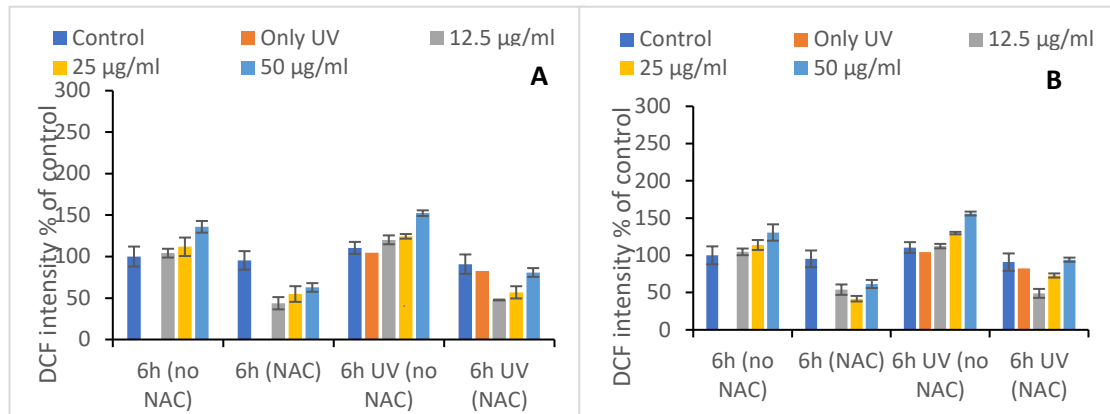


Figure 3.16 ROS detection in B16-F10 cells after 5 mM NAC pre-treatment and different concentration of A) FZ and B) FZSi NPs (6 h) treatment. Data are represented as mean \pm SD (n=3). A significant difference was observed when 6 h (no NAC) group was compared to 6 h (with NAC) group. Control represents B16-F10 cells with cell culture medium and no NPs. Both the dark and UV treated groups are together represented in the graphs.

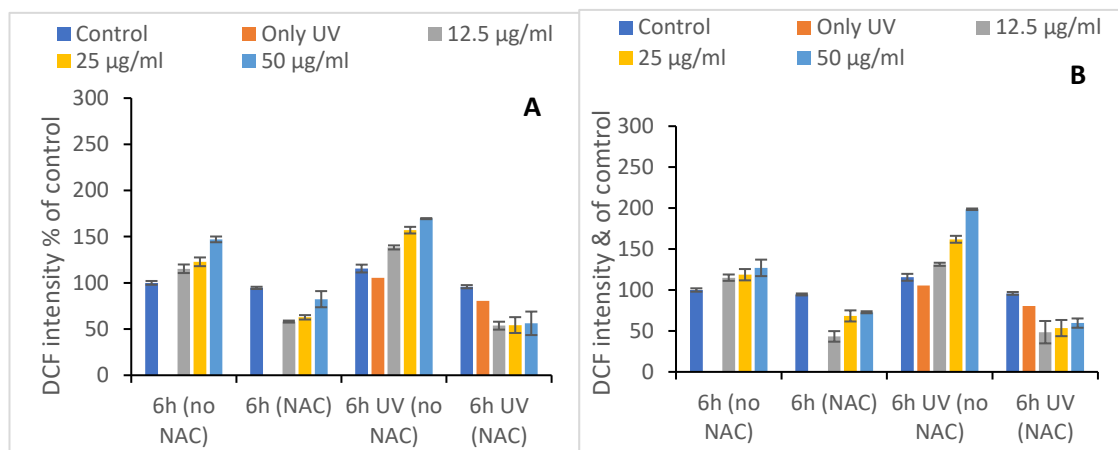


Figure 3.17 ROS detection in Caco-2 cells after 5 mM NAC pre-treatment and different concentration of A) FZ and B) FZSi NPs (6 h) treatment. Data are represented as mean \pm SD n=3). Control represents Caco-2 cells with cell culture medium and no NPs. Both the dark and UV treated groups are together represented in the graphs.

Similar studies using cells pre-treated with NAC were also reported with ZnO NPs to confirm the generation of ROS by ZnO NPs in astrocytes and human T cells. (Wang *et al.*, 2014; Hanley *et al.*, 2008). Heim *et al.* (2015) reported a significant reduction in ROS production across all time points (from 140% to 100% at 6 h) in A549 alveolar cell line pre-treated with NAC then treated with ZnO NPs (100 µg/mL). The ROS production in cells is successfully countered by elevated GSH levels on NAC pre-treatment (Sivalingappa *et al.*, 2012).

3.10 Cytotoxicity of hybrid NPs after ROS quenching

Remediation effects of the antioxidant NAC were further studied in a cell viability recovery test (Yang & Ma, 2014). As the previous study showed that the maximum reduction in cell viability was observed at 24 h with 100 $\mu\text{g}/\text{mL}$ of NPs, hence 100 $\mu\text{g}/\text{mL}$ dose of NPs was chosen, and the cytotoxicity study was carried out for 24 h.

The cell viability of all the NPs increased when pre-treated with antioxidant NAC (5 mM and 15 mM) followed by treatment with NPs at 100 $\mu\text{g}/\text{mL}$ (Figure 3.18). The cell viability enhanced when cells pre-treated with NAC in different concentrations, which was statistically significant ($P < 0.001$) in comparison with only NPs treated group. Cell viability increased nearly 3-4-fold (from 10% increased to 40%) when pre-treated with 5 mM NAC; whereas 5-6-fold (from 10% increased to 60%), when pre-treated with 15 mM NAC.

Our result is consistent with that reported by Wang *et al.* (2014) who reported an increase in cell viability in astrocytes pre-treated with NAC (5 mM) then treated with ZnO NPs. Fukui *et al.* (2012) reported a similar reduction in cell death when pre-treated with 2 mM NAC in A549 lung carcinoma cells. Literature suggested that reduction in glutathione (GSH) levels lead to ROS production and apoptotic cell death can be blocked by NAC (Sivalingappa *et al.*, 2012). As a result, the ROS generation in cells was reduced on pre-treatment with NAC, enhancing the cell viability. Our data support the hypothesis that the production of ROS is a major mechanism of cytotoxicity of PDT generated by hybrid NPs under UV-A irradiation.

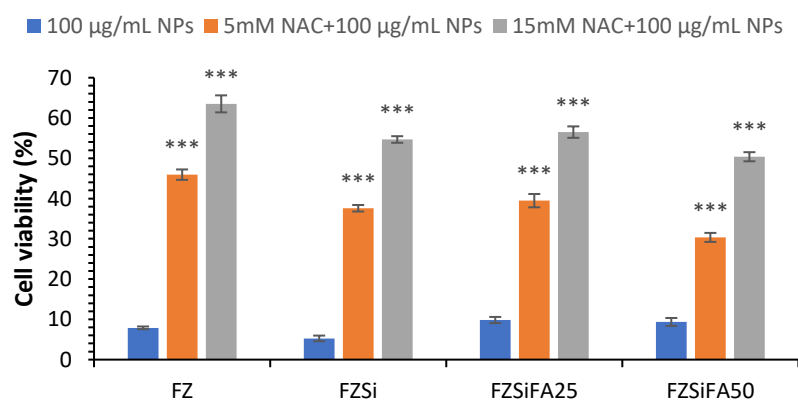


Figure 3.18 Cell viability of B16-F10 cells after 5 mM NAC, 15 mM NAC and 100 $\mu\text{g}/\text{mL}$ NPs treated and only NPs treated for 24 h. Data are represented as mean \pm SD ($n=4$). *** $p < 0.001$ compared to the group without NAC treatment.

3.11 Morphological changes of cells after treatment with hybrid NPs and UV-A light

Morphology changes in cells are the first sign of the impact of NPs treatment, highlighting any cytotoxicity in the cells. Time and concentration-based morphology changes were visible across the three cell lines after 6 h and 24 h NPs treatment. The control cells were of high density and with distinct morphology characters (Figure 3.19 A-C, Appendix 18-20). Cells displayed a circular shape upon exposure to NPs (Figure 3.19 D-I). Once the cells were exposed to UV-A radiation (10 J/cm^2), even at low concentration of NPs, cells appeared to change morphology and detached from the substrate, in a large amount, indicating destruction of the cells (Figure 3.19 J-L). Morphological changes were observed in stages, starting with the rounded and swollen appearance of cells (mainly on 6 h NPs treatment), followed by cells detachment from culture plates (24 h NPs treatment), ultimately resulting in few cells in the plates (UV-A irradiated). Our observation of morphology changes was in complete agreement with Alarifi *et al.* (2013) who noticed notable morphological changes in A375 melanoma cells after treatment with ZnO NPs at $5 \mu\text{g/mL}$ after 24 h. Further exposure to high concentration ZnO ($10 \mu\text{g/mL}$) after 48 h changed the shape of cells and detached them from the surface.

It is accepted that morphological changes are evidence of NPs induced toxicity in B16-F10 cells (Shrikhande *et al.*, 2015). Dark spots were visible inside the cells which correspond to the NPs, that may have aggregated by time. Our stability data of NPs in DMEM medium suggests the minor tendency of NPs to aggregate over time without the presence of cells. (Table 3.3). Ivankovic *et al.* (2006) spotted the similar appearance of vanadium oxide NPs as aggregates accumulated inside the B16-F10 cells. Similar changes in morphology of the three cell lines treated with FZSi, FZSiFA25, and FZSiFA50 NPs can be seen in Appendix 18-20. The reduction in cell viability over time and dose of NPs correlated well with the morphology changes of three cell lines studied.

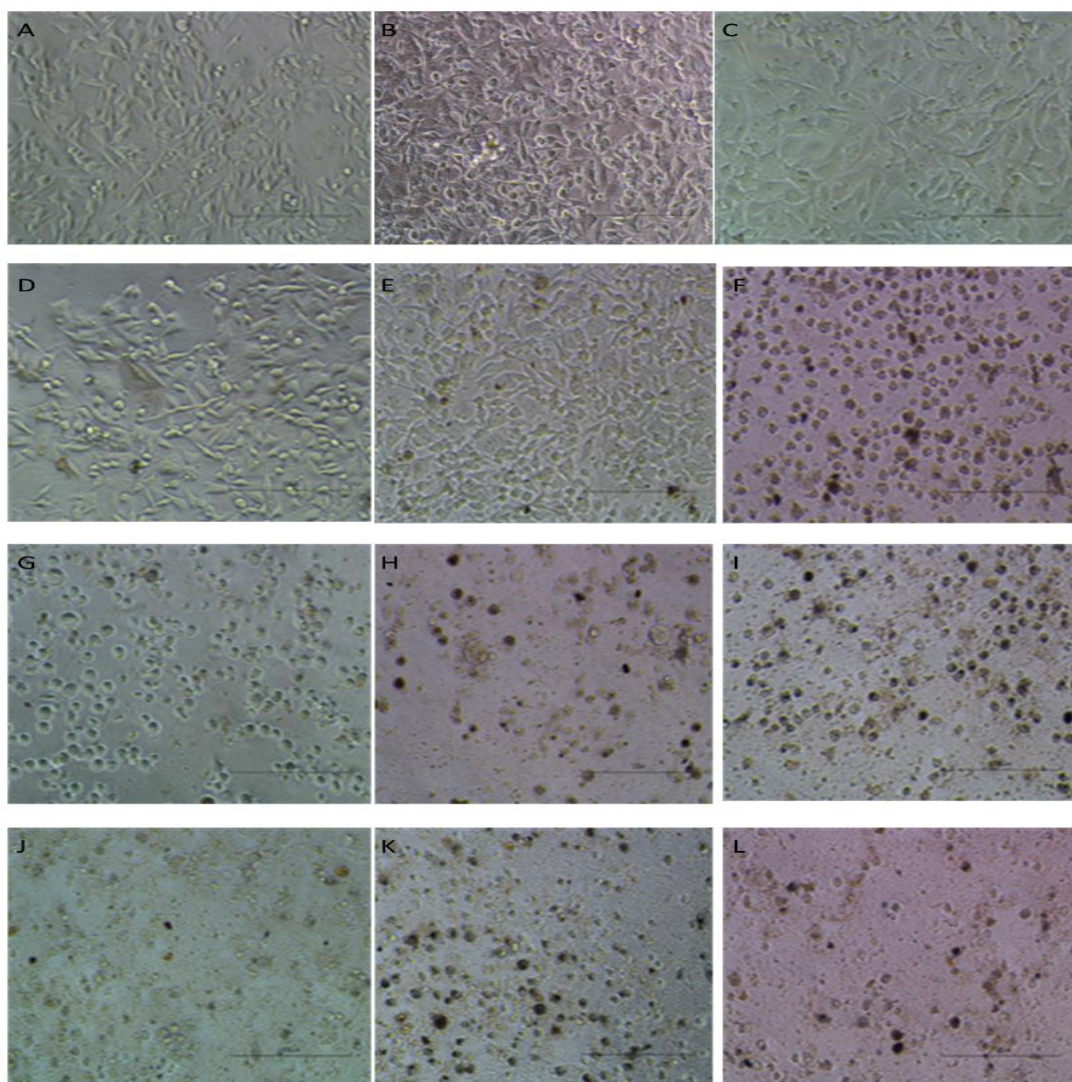


Figure 3.19 Morphology changes of B16-F10 cells before and after treatment with UV, FZNPs and both: (A-C) Control at 6h, 24h and 24h after UV-A radiation exposure (10 J/cm^2). (D-F) FZ NPs 25, 50, 100 $\mu\text{g/mL}$ after 6h treatment. (G-I) FZ NPs 25, 50, 100 $\mu\text{g/mL}$ after 24h treatment. (J-L) FZ NPs 25, 50, 100 $\mu\text{g/mL}$ after 24 h treatment and UV-A radiation exposure.

3.12 Quantitative investigation of cellular uptake of hybrid NPs in PDT

The cellular uptake of hybrid NPs will be one of the prime factor influencing their cytotoxicity on cell lines. This study was conducted to examine the effect of targeting ligand, FA, on cellular uptake of Hybrid NPs at 2 h and 6 h and if such effect was influenced by UV-A irradiation. The study was carried with B16-F10 and Caco-2 cells and two NPs (FZSiFA50, FZSi-FITC) and two separate conditions (NPs alone, NPs+ UV-A irradiation). The NPs FZSiFA50 have FA as the targeting ligand, and fluorescent property of FA and FITC were used for the quantification of the NPs in the cellular uptake study. The FA and FITC quantification were carried out by measuring the fluorescence intensity of the samples and concentrations of NPs were calculated from the calibration curve (Appendix 21).

(i) Effects of targeting ligand and time on cell uptake of NPs

The FZSi-FITC NPs without any targeting ligand were expected to be taken up by cells via endocytosis, which can be used as passive targeting for tumours via the enhanced permeability and retention (EPR) effect, consequently, increase accumulation in tumour cells. Surface modification of NPs with site-specific targeting ligands like FA have demonstrated enhanced cellular uptake (Chen *et al.*, 2011). In our study with B16-F10 cells, at 6 h, FZSi NPs with FA targeting ligand demonstrated enhanced cell uptake, which was about 53% greater than NPs without any targeting ligand (Figure 3.20) whereas at 2 h there was no significant difference. The cellular uptake was almost same in both the NPs at 2 h (Figure 3.20). This suggested that the initial phase of cellular uptake of NPs, i.e. interaction between NPs and cells which takes time. Later, the effect of targeting ligand took place and resulted in better cellular uptake compared to the NPs without a targeting ligand. This indicates the ligand-mediated cell uptake is time-dependent. Because the further increase of uptake was found to be associated with UV-A irradiation, it was thought UV irradiation might have enhanced the cell membrane permeability (Yang & Ma, 2014) or provide energy for endocytosis.

It appears that both time exposure and UV-A irradiation had an impact on hybrid NPs cellular uptake. Longer exposure time, higher NPs uptake. Application of UV-A also increased cellular uptake of NPs, the largest increase was seen at 6 h. In Caco-2 cells, the FZSiFA50 NPs in the dark had greater cellular uptake only at 6 h (25% better compared to FZSi-FITC NPs) and less cellular uptake at 2 h (Figure 3.21). When FZSiFA50 NPs 6 h treatment was compared to that of 2 h, there was a 3.5-fold better uptake and further enhanced by FZSiFA50 NPs plus UV-A irradiation (10 J/cm²) treatment with a 5.9-fold better uptake (Figure 3.21). When FZSi-FITC NPs, after 6 h treatment was compared to that of 2 h, there was a 1.8-fold increase in uptake in the dark and 2-fold in UV-A irradiation conditions (Figure 3.21).

Our results agree with Hu *et al.* (2013) who reported a remarkable improvement in tumour targeting using FA-conjugated graphene oxide-ZnO hybrid NPs in PDT. Ma (2015) reported FA-conjugated ZnO quantum dots provided successful targeting of cancer in the MCF-7 cancer cell. It is well-known that folate receptors are highly expressed in many cancer cells, therefore, can serve as an active target for cancer

treatment (Daiana & Koiti, 2015; Zwickie *et al.*, 2012). Khaing Oo *et al.* (2012) reported better cellular uptake (Gold NPs conjugated with PpIX) ultimately lead to the better generation of singlet oxygen and ROS at the cellular level, destructing the human breast cancer cells. Our data supports this point, with high ROS production being recorded at 6 h at the cellular level in both the tested cell lines in our study. Inverted phase contrast microscopy images after treatment (6 h) with hybrid NPs proved more cellular swelling and damage to cell membranes which confirmed the intracellular presence of NPs.

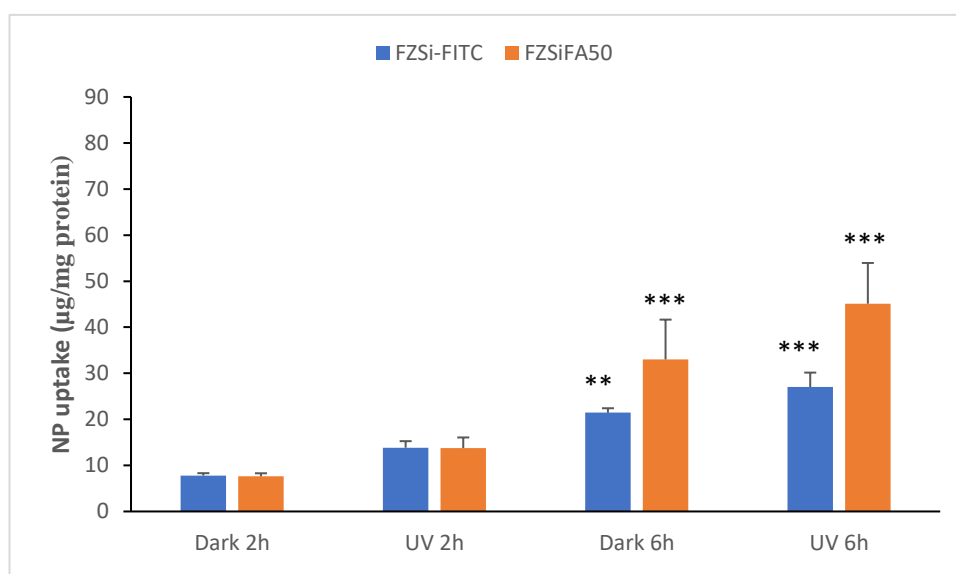


Figure 3.20 Cellular uptake of FZSiFA50 & FZSi-FITC NPs at different time points in B16-F10 cells (both dark and UV). Data are represented as mean \pm SD (n=3). ** p< 0.01 and *p<0.001 compared to FZSiFA50 2 h (dark) and FZSi-FITC 2 h (dark).**

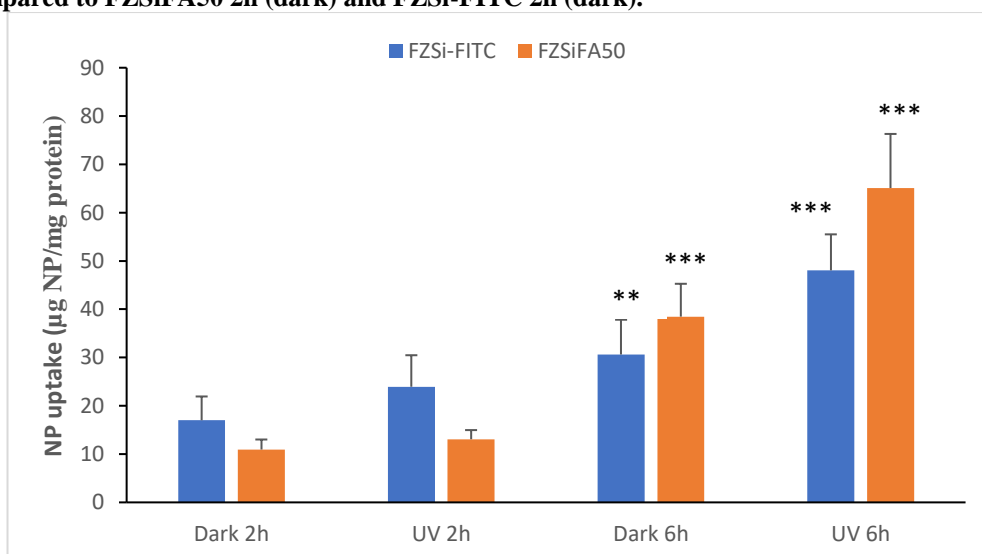


Figure 3.21 Cellular uptake of FZSiFA50 & FZSi-FITC NPs at different time points in Caco-2 cells (both dark and UV). Data are represented as mean \pm SD (n=3). ** p< 0.01 and *p<0.001 compared to FZSiFA50 2 h (dark) and FZSi-FITC 2 h (dark).**

The cellular uptake study was conducted for 6 h because the assay medium (DMEM-high glucose) lacked serum and other growth factors vital for the long-term cell viability. From this study, we concluded

- a) The NPs with the targeting ligand FA had a greater cellular uptake compared to the NPs without a targeting ligand in both cell lines.
- b) The UV-A irradiation had enhanced cellular uptake in both cell lines.
- c) The cellular uptake of NPs was time dependent.

3.13 Qualitative investigation of cellular uptake of hybrid NPs

The cellular uptake of FA50 and FITC attached FZSi NPs were further confirmed by qualitative analysis by confocal microscopy. Confocal laser scanning microscopy (CLSM) is a powerful technique that allows capturing in-depth cross-section image of cells and provides valuable information on the particle localisation in the cells. It can provide selective optical sectioning, high resolution and in-depth imaging of cellular microstructures without the need to physically sectioning the sample. Labelling the nuclei with propidium iodide (red) and the NPs with FA (blue) and FITC (green), the localisation of NPs were visualised. The CLSM study demonstrated that the FA and FITC attached NPs were internalised rather than attached to the cell surface (Figure 3.22 - 3.27). The cellular uptake images were captured after 6 h of treatment with hybrid NPs in DMEM medium, resembling our treatment time with NPs in cell viability study. The cells were viewed using 60 x oil immersion lens. Cells grown on Ibidi micro dish were treated with FZSiFA50 NPs and cells grown on cover slip were treated with FZSi-FITC NPs.

The fluorescence emission intensity of FZSiFA50 NPs was higher than FZ and FZSi NPs, due to the combined fluorescence emission from FA and ZnO, which had been reported earlier (Patel *et al.*, 2017). When the NPs were tagged with fluorescent component (FA and FITC), a high fluorescence was observed in the B16-F10 cells indicating the NPs have penetrated the melanoma cells. The cellular uptake of NPs had increased by time. As expected, fluorescence was detected with FZSi-FITC NPs, due to the presence of FITC. The small size of the NPs (~20 nm) had well supported the cellular uptake of the NPs. The Z stack images of FZSiFA50 NPs alone and UV-A irradiated in B16-F10 cells can be seen in Figure 3.23 & 3.26. The Z stack pictures of FZSi-FITC NPs alone and UV-A irradiated in B16-F10 cells can be seen in Figure

3.24 & 3.27. These images confirmed the localisation of NPs inside the cells by cellular uptake.

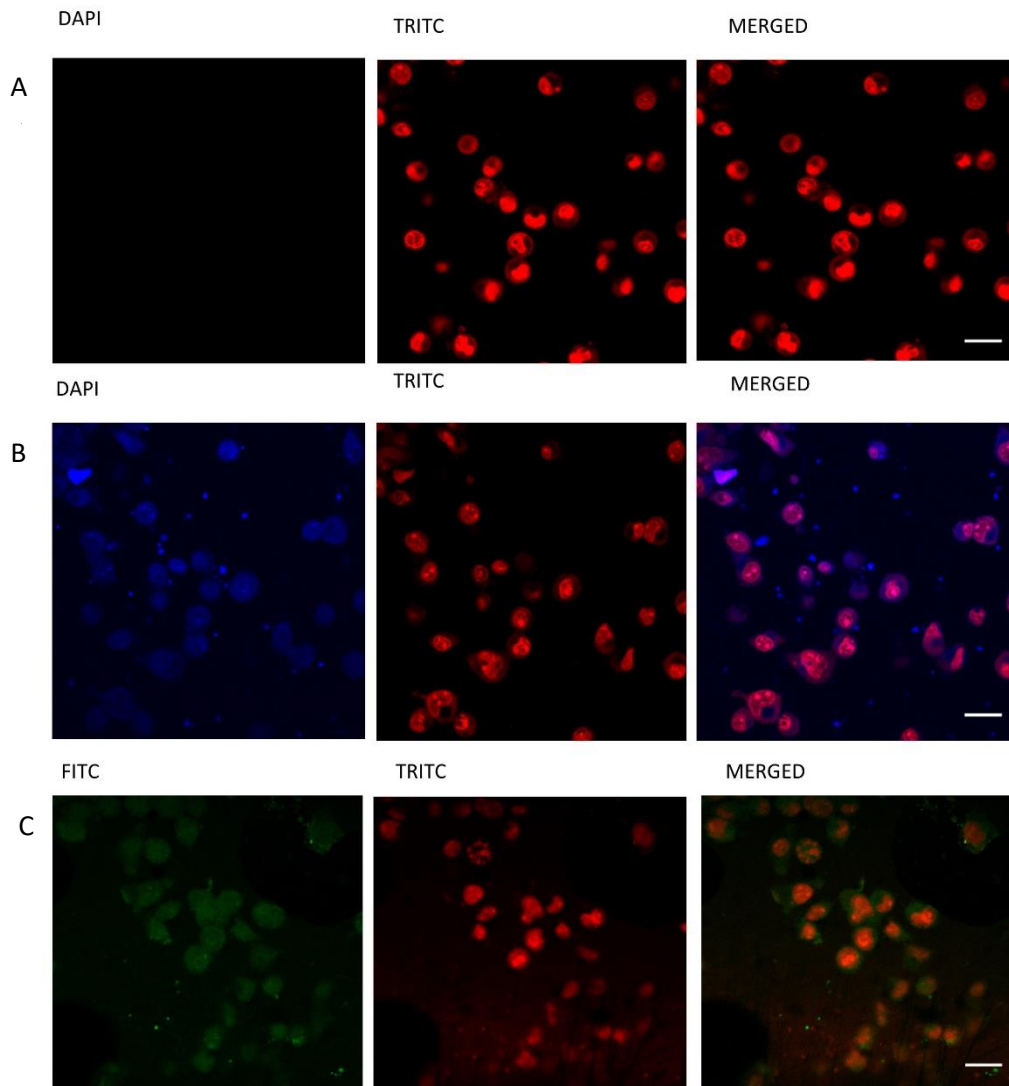


Figure 3.22 CLSM images of B16-F10 cells after 6 h treatment with FZSiFA50 (blue coloured) and FZSi-FITC (green coloured) NPs. (A) Only nucleus stained (control), (B) merged image of FZSiFA50 NPs treated B16-F10 cells, (C) Merged image of FZSi-FITC NPs treated B16-F10 cells. The scale bars correspond to 20 μm . Images in A & B were captured from cells grown in ibidi micro-dish and C was captured from cells grown in the cover slip.

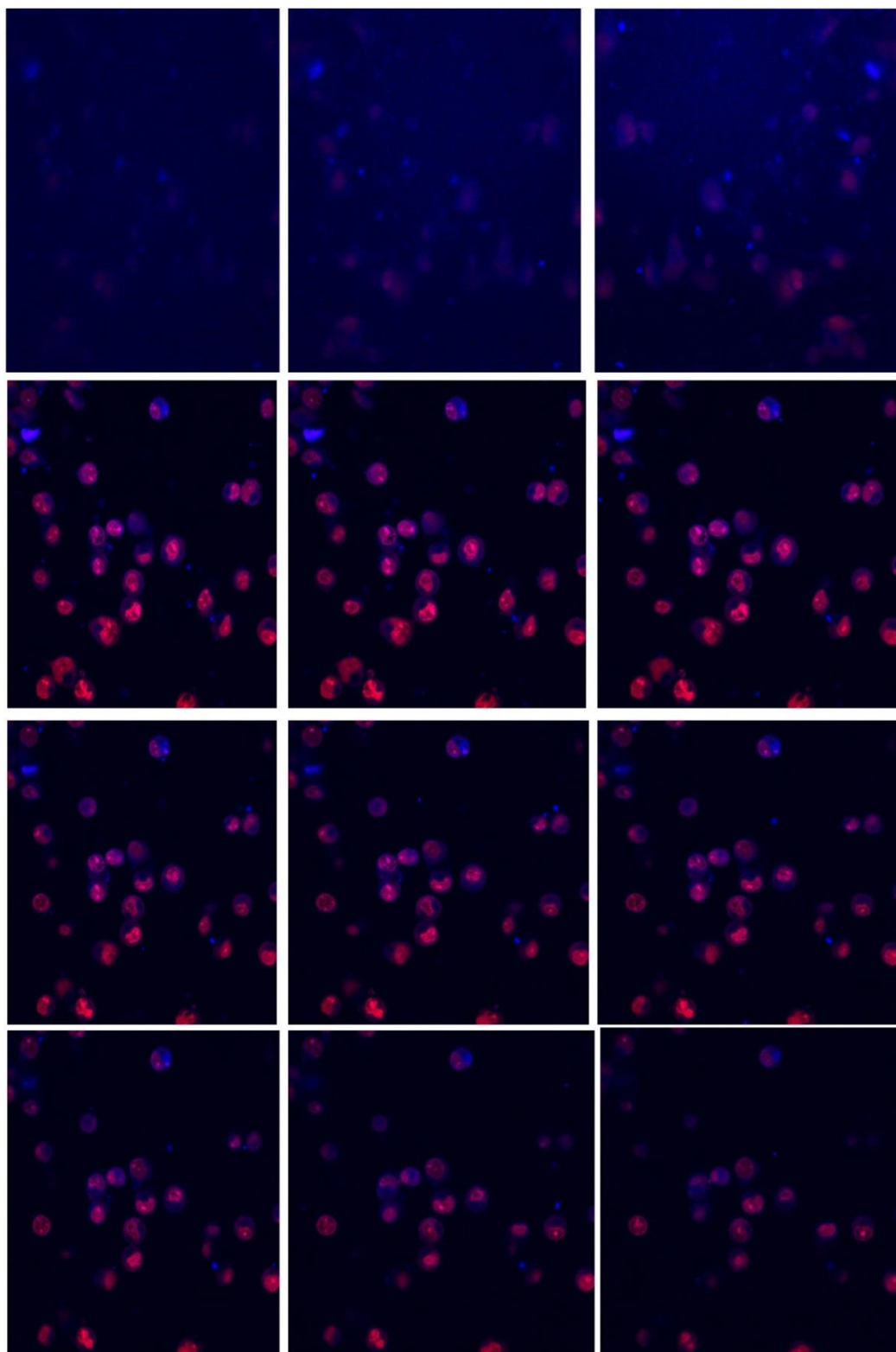


Figure 3.23 Z-stack images of B16-F10 cells treated with FZSiFA50 NPs in the dark. Intracellular distribution of FZSiFA50 NPs in B16-F10 cells after incubation for 6 h at 37°C as observed by CLSM. Blue colour indicates the localisation of NPs inside the cells. Twelve superimposed images of optical sections taken in the vertical axis at intervals of 0.6 μm from the apical surface (left to right; top to bottom, depths 0, 0.6, 1.2, 1.8, 2.4, 3, 3.6, 4.2, 4.8, 5.4, 6 and 6.6 μm from apical surface) confirming the internalisation of blue particles. The nucleus is stained with PI (red). Magnification = 200X. Images were captured from cells grown in ibidi micro-dish.

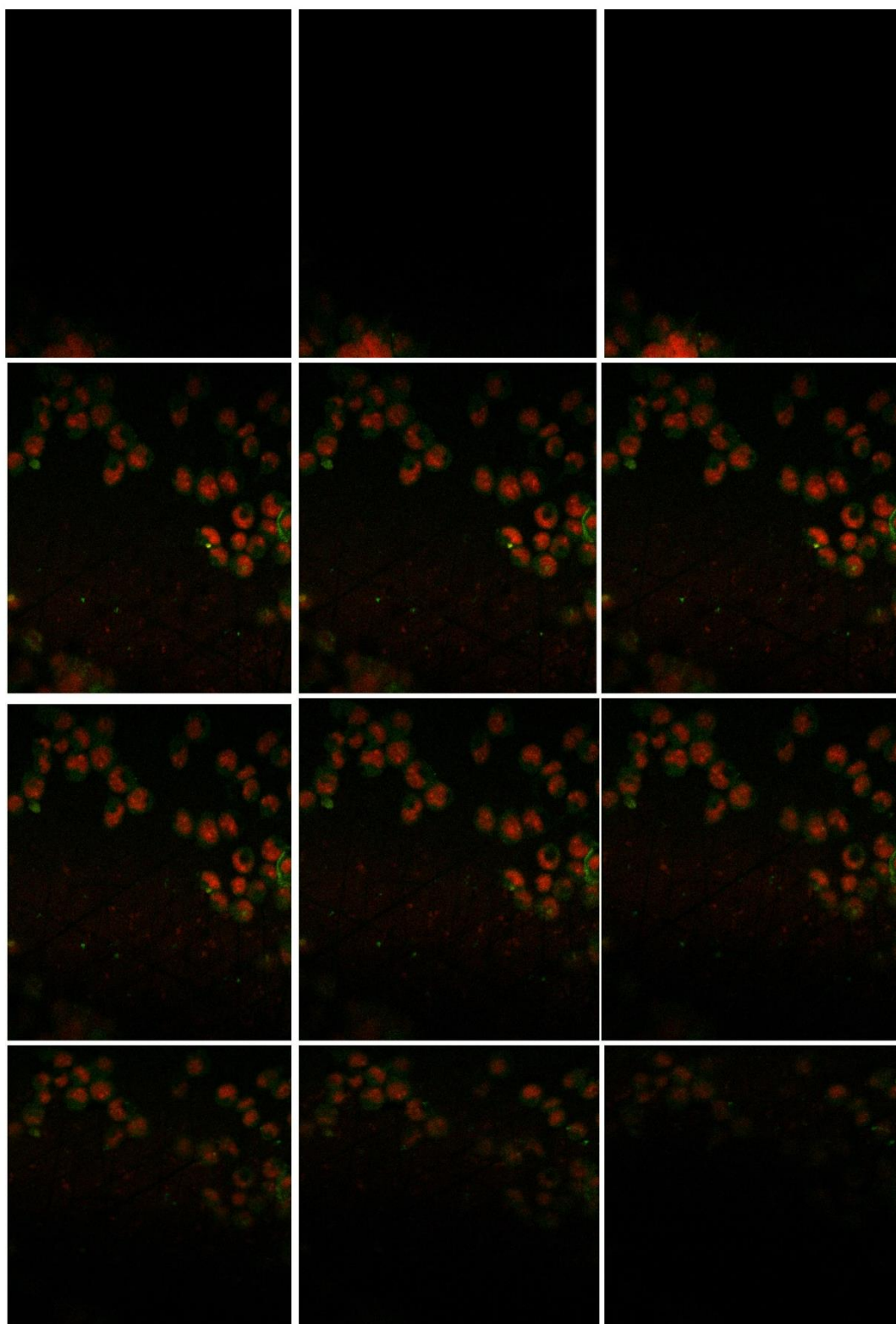


Figure 3.24 Z-stack images of B16-F10 cells treated with FZSi-FITC NPs in the dark. Intracellular distribution of FZSi-FITC NPs in B16-F10 cells after incubation for 6 h at 37°C as observed by CLSM. Green colour indicates the localisation of NPs inside the cells. Twelve superimposed images of optical sections taken in the vertical axis at intervals of 0.6 μm from the apical surface (left to right; top to bottom, depths 0, 0.6, 1.2, 1.8, 2.4, 3, 3.6, 4.2, 4.8, 5.4, 6 and 6.6 μm from apical surface) confirming the internalisation of green particles. The nucleus is stained with PI (red). Magnification = 200X. Images were captured from cells grown in the cover slip.

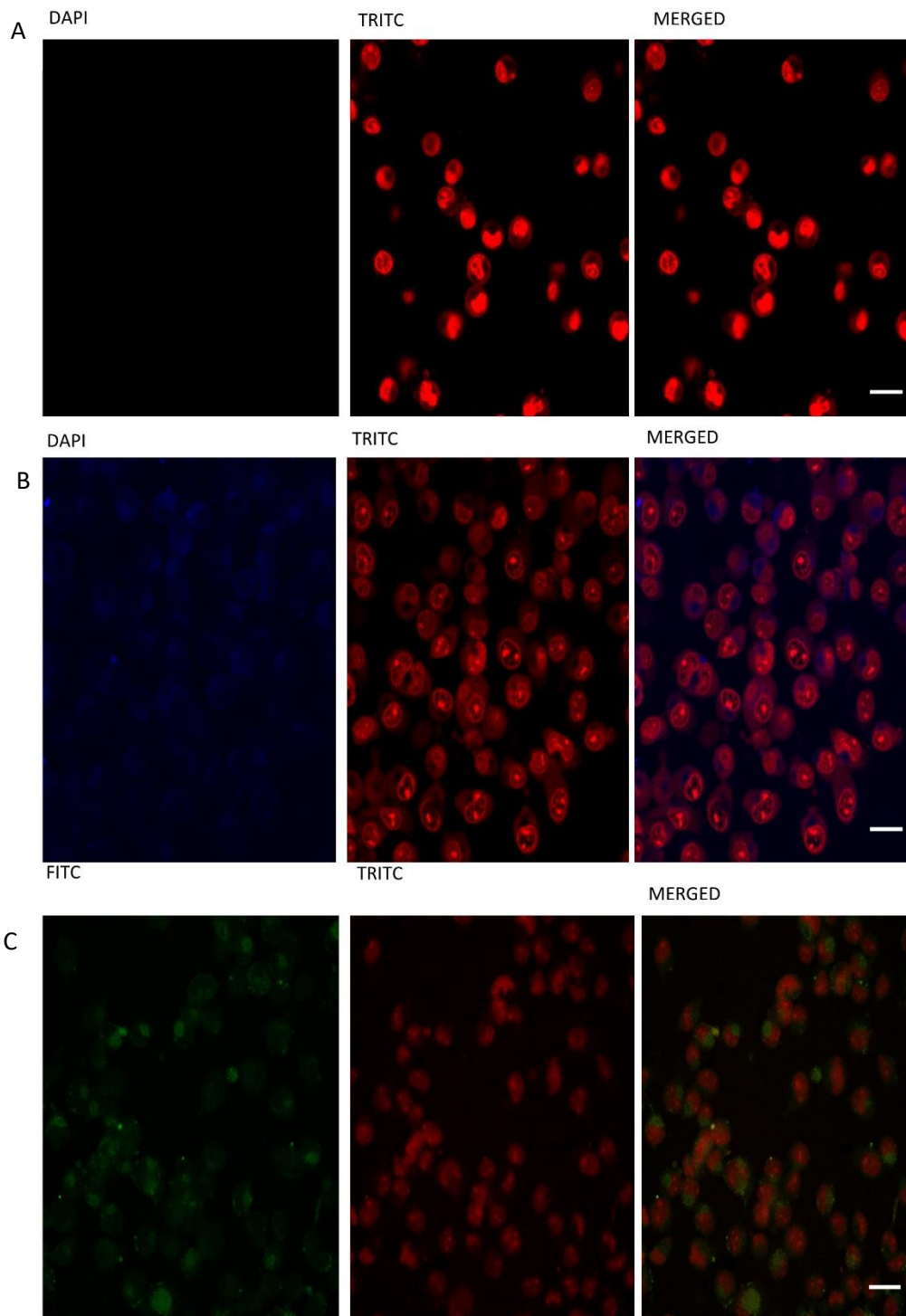


Figure 3.25 CLSM images of B16-F10 cells after 6 h treatment with FZSiFA50 (blue coloured) and FZSi-FITC (green coloured) NPs+UV-A irradiation. (A) Only nucleus stained, (B) merged image of FZSiFA50 NPs treated B16-F10 cells, (C) Merged image of FZSi-FITC NPs treated B16-F10 cells. The scale bars correspond to 20 μm . Images in A & B were captured from cells grown in ibidi micro-dish and C was captured from cells grown in the cover slip.

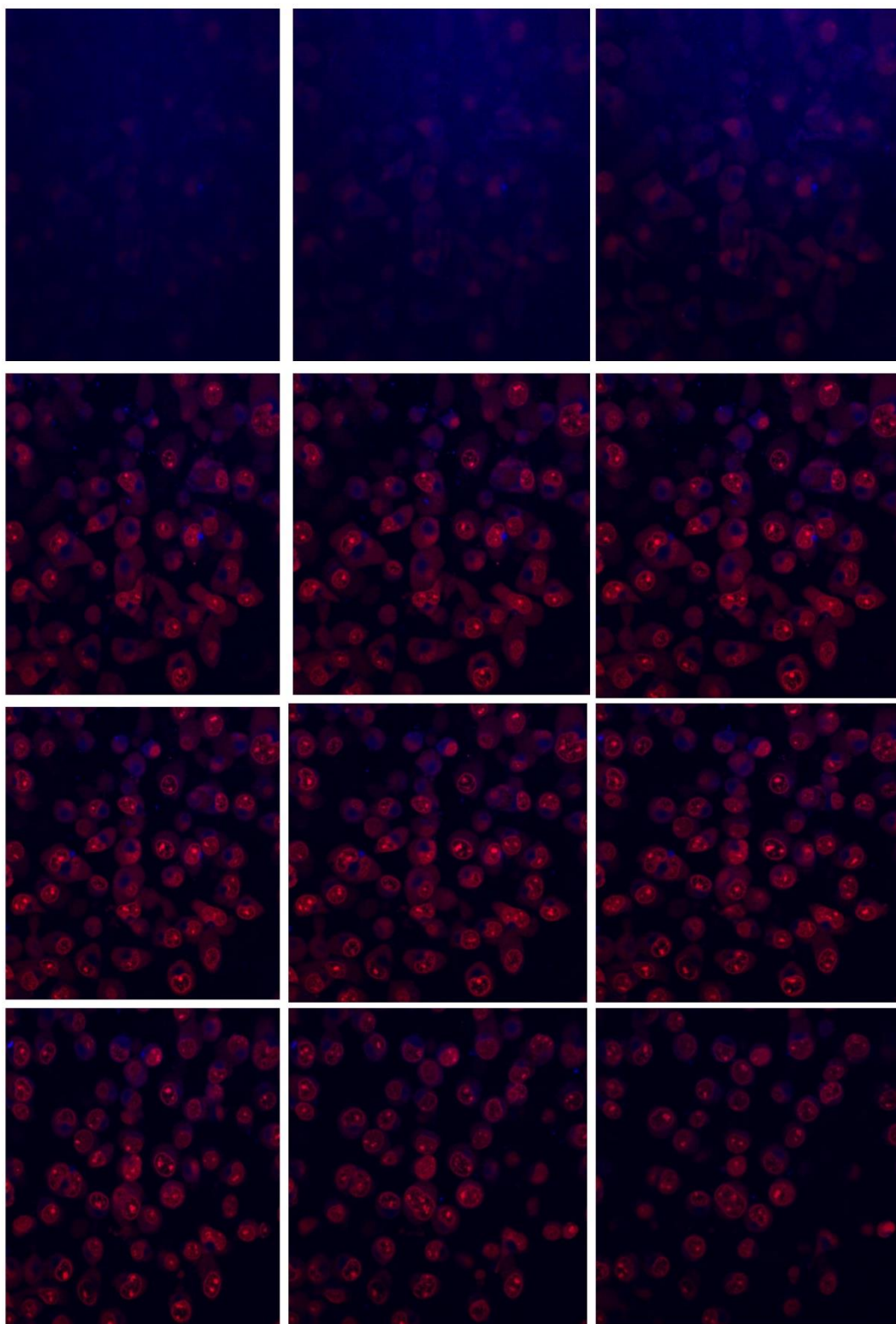


Figure 3.26 Z-stack images of B16-F10 cells treated with FZSiFA50 NPs under UV-A. Intracellular distribution of FZSiFA50 NPs in B16-F10 cells after incubation for 6 h at 37°C as observed by CLSM. Blue colour indicates the localisation of NPs inside the cells. Twelve superimposed images of optical sections taken in the vertical axis at intervals of 0.6 μm from the apical surface (left to right; top to bottom, depths 0, 0.6, 1.2, 1.8, 2.4, 3, 3.6, 4.2, 4.8, 5.4, 6 and 6.6 μm from apical surface) confirming the internalisation of blue particles. The nucleus was stained with PI (red). Magnification = 200X. Images were captured from cells grown in ibidi micro-dish.

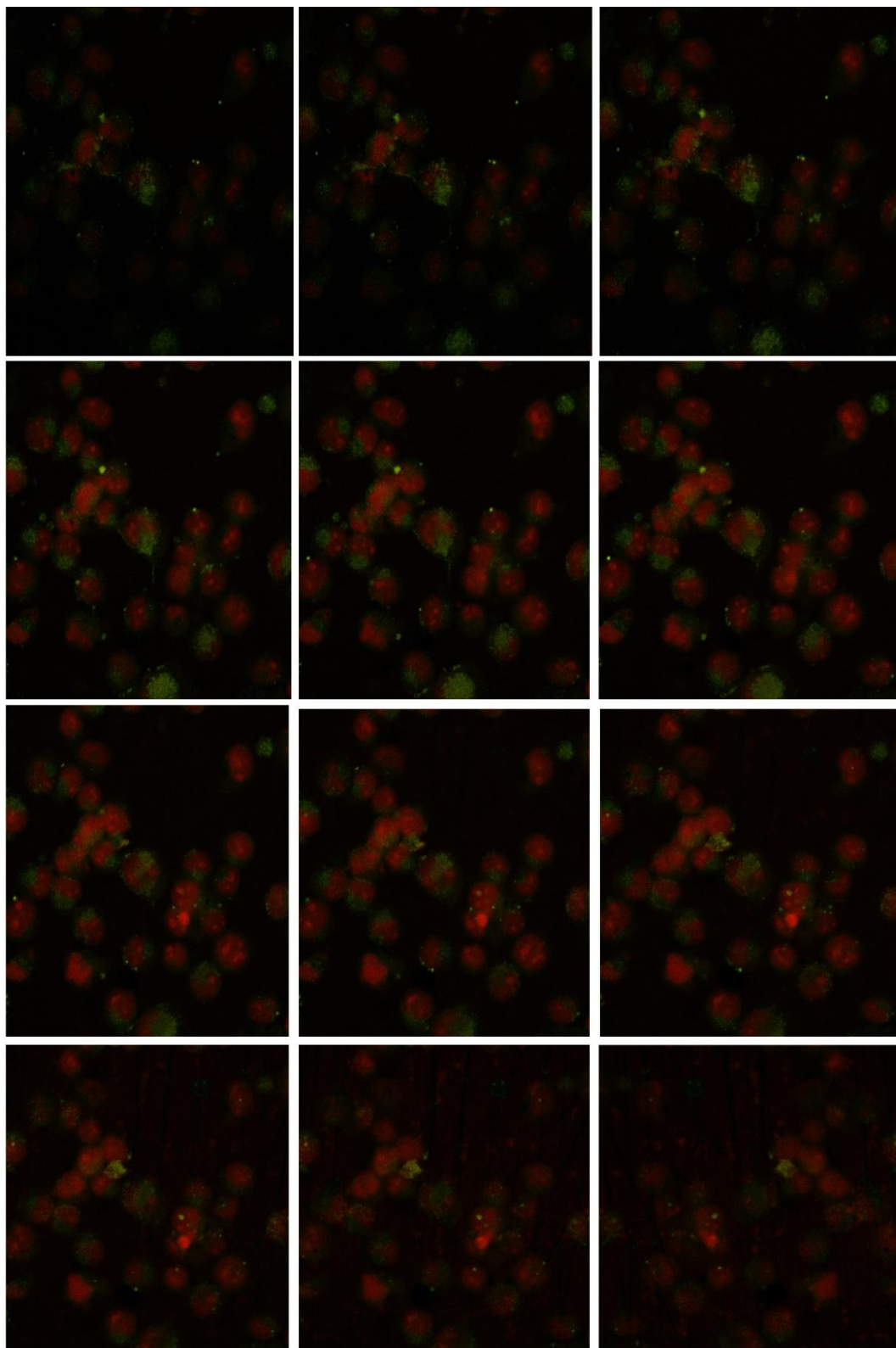


Figure 3.27 Z-stack images of B16-F10 cells treated with FZSi-FITC NPs in UV. Intracellular distribution of FZSi-FITC NPs in B16-F10 cells after incubation for 6 h at 37°C as observed by CLSM. Green colour indicates the localisation of NPs inside the cells. Twelve superimposed images of optical sections taken in the vertical axis at intervals of 0.6 μm from the apical surface (left to right; top to bottom, depths 0, 0.6, 1.2, 1.8, 2.4, 3, 3.6, 4.2, 4.8, 5.4, 6 and 6.6 μm from apical surface) confirming the internalisation of green particles. The nucleus was stained with PI (red). Magnification = 200X. Images were captured from cells grown in the cover slip.

3.14 Total cell associated zinc and iron in PDT

ICP-OES is an analytical technique used for detection of trace metals. It uses emission spectra to identify and quantify the elements present in the sample. The results discussed here is based on the radial detector values, which measures concentrations of elements in samples (Trevizan & Nubrega, 2007). To make sure that we detect metal element derived from NPs at the intracellular level we did study with the high NPs concentration (100 µg/mL) in both cell lines and at two-time points (2 h & 6 h). The ICP-OES results also provide us with information on the cellular uptake of NPs and the impact of treatment time.

Different trends were seen in two cell lines. In B16-F10 cells received treatment of FZSi-FTIC and FZSiFA50 NPs, higher Zn content was detected at 6 h when cells were treated with NPs alone. However, upon UV-A irradiation, the higher level of Zn was recorded at 2 h not 6 h. The photodegradation of Zn may be the possible reason for this reduction. In comparison, the iron levels increased from 0.09 mg/L at 2 h to 0.12 mg/L at 6 h. NPs with UV-A irradiation treatment enhanced the iron levels from 0.10 mg/L at 2 h to 0.25 mg/L at 6 h. The cell-associated iron content data supports the cellular uptake study presented in Figure 3.20. For instance, FZSiFA50 NPs in the dark had 7.63% cellular uptake at 2 h which enhanced to 33.01% after 6 h, providing close to 4-fold enhanced cellular uptake.

Table 3.9 Total intracellular metal content in B16-F10 and Caco-2 cells following NP treatment

Cell line	Metal	Metal content (mg/L)								
		Control*	FZSiFITC (dark)		FZSiFITC (UV)		FZSiFA50 (dark)		FZSiFA50 (UV)	
			2h	6h	2h	6h	2h	6h	2h	6h
B16-F10	Iron	0.043±0.01	0.099±0.00	0.143±0.02	0.353±0.05	0.108±0.02	0.093±0.00	0.122±0.02	0.096±0.01	0.247±0.03
	Zinc	0.033±0.01	0.241±0.05	0.305±0.07	0.286±0.04	0.191±0.03	0.163±0.05	0.301±0.04	0.206±0.02	0.201±0.04
Caco-2	Iron	0.074±0.02	0.098±0.01	0.219±0.02	0.165±0.02	0.078±0.00	0.091±0.03	0.151±0.02	0.128±0.03	0.211±0.02
	Zinc	0.010±0.00	0.263±0.06	0.173±0.01	0.190±0.06	0.127±0.02	0.233±0.06	0.104±0.01	0.055±0.01	0.052±0.01

*Control represents cells without NPs treatment

In Caco-2 cells after 2 h of FZSiFA50 NPs treatment, there was a 23-fold increase in zinc level compared to untreated sample, i.e. cell, (0.01 mg/L to 0.23 mg/L). However, 2 h NPs with UV-A treatment recorded drastic drop in the Zn levels compared to 2 h NPs treatment. A similar trend with drop-in Zn levels was also observed with, 6 h NPs treatment and 6 h NPs+ UV-A treatment (0.1 mg/L, 0.05 mg/L Zn levels respectively) compared to 2 h of NPs treatment. The drop in intracellular levels of Zn was not directly reflected in the cellular uptake study. However, the possible reasons behind this reduction in Zn levels other than photodegradation of Zn may be related to:

- 1) The photodegradation of hybrid NPs was enhanced with the presence of a Fe_3O_4 component, due to the suppressed recombination of the photoinduced electron-hole pairs by the dissolved iron (Feng *et al.*, 2014; Patel *et al.*, 2017).
- 2) In the intracellular environment, endosomal pH ranges at 6 to 4 in lysosomes. ZnO NPs is expected to be highly unstable in such low pH conditions. Literature has reported at such low pH levels NPs were dissolved entirely (Luo *et al.*, 2014; Shen *et al.*, 2013).

The above two processes may have produced soluble Zn which may have effluxed from cells (Eide, 2006). In turn, the Zn level dropped.

The increase in Zn levels from both the NPs at 2 h confirmed the cellular uptake of the NPs. It is interesting to note that the trend of iron levels was different from that of Zn. In FZSiFA50 NPs there was no reduction in the iron levels at 6 h. They enhanced by time (0.09 mg/L at 2 h to 0.15 mg/L at 6 h) and with UV-A irradiation (0.13 mg/L at 2 h UV-A to 0.21 mg/L at 6 h UV-A),

The trend was similar with FZSi-FITC NPs, except the dropped iron levels after UV-A radiation at 6 h. The different levels of Zn and iron metals detected in the two cell lines confirmed the cellular uptake is dependent on the nature of the cell line under study.

3.15. Apoptosis study and caspase 3/7 activity in PDT

The annexin V- PI assay was carried out using the flow cytometry to quantitatively analyse apoptotic and necrotic cells after hybrid NPs treatment alone and in combination with UV-A irradiation. The apoptosis potential of FZSi and FZSiFA50 NPs was investigated by Annexin-V/FITC and PI staining.

Annexin-V/PI plots were divided into four quadrants to distinguish living cells (annexin-V⁻/PI⁻, low left quadrant, Q4), early apoptotic cells (annexin-V⁺/PI⁻, low right quadrant, Q3), late apoptotic (annexin-v⁺/PI⁺, upper right quadrant, Q2) and necrotic cells (Q1). Two different NPs concentration (12.5 and 100 µg/mL) and two different experimental conditions (dark and UV-A irradiated) were applied. For the discussion, the apoptotic cell percentage was calculated as a sum of both the early apoptotic and late apoptotic cells percentage.

As seen in Figure 3.28, no significant apoptosis (3.5%) was observed in untreated control cells, and 96.2% cells were present in the viable chamber. The FZSiNPs treated cells, however, showed increased apoptosis of B16-F10 cells over time (Figure 3.28), the dose of NPs and on exposure to UV-A radiation (Figure 3.29). At 6 h of 12.5 µg/mL, NPs dose treatment 6.5% apoptotic cells were present, which nearly doubled to 12.1% after 24 h. On treatment with FZSi NPs +UV-A radiation (24 h) 10.9%, apoptotic cells were present, along with a considerable amount of 16.5% cells reaching the necrotic chamber. FZSi NPs after, 6 h of 100 µg/mL dose treatment 15.6% cells were present in the apoptotic chamber which enhanced to 88.1% after 24 h and further raised to 94% on exposure to UV-A irradiation after 24 h. The ameliorated apoptotic and necrotic levels were significant in both NPs treated groups compared to untreated control and UV exposed control ($p < 0.001$) at 6 h and 24 h.

FZSiFA50NPs at 12.5 µg/mL showed 8.82% apoptotic cells at 6 h, which increased to 12.7% apoptotic cells after 24 h (Figure 3.28). On treatment with FZSiFA50 NPs 100 µg/mL dose for 6 h, 24.5% apoptotic cells were present (Figure 3.29), (a 3-fold increase compared to 12.5 µg/mL treatment) and at 24 h 24.7% apoptotic cells (a single fold increase compared to 12.5 µg/mL) were present, with a significant 69.8% cells in the necrotic chamber (Figure 3.30). Upon UV-A irradiation of the same dose of NPs, 17.9% apoptotic cells were present at 6 h, which enhanced to 28.9% apoptotic cells and 68% cells in the necrotic chamber at 24 h (Figure 3.31).

Wang *et al.* (2014) reported a rise in apoptotic cell population from 5.8% to 72.8% when ZnO NPs concentration was increased from 4 to 12 µg/mL in astrocytes.

Hackenberg *et al.* (2010) observed a significant increase in necrotic cells from 11.7% without ZnO NPs to 30.2% for ZnO NPs at 2 $\mu\text{g}/\text{mL}$ in the human neck and head squamous carcinoma cells.

On 24 h exposure to 100 $\mu\text{g}/\text{mL}$, NPs (both in dark and UV-A irradiated) the pattern of cell death differed depending on the type of NPs. The FZSi NPs produced apoptotic cell death as the dominant mechanism, and FZSiFA50 NPs produced necrotic cell death (10 fold more compared to FZSi at dark and 16-fold more compared to FZSi after UV-A treatment) as the dominant mechanism (Figure 3.30). The high proportion of positive necrotic cells for FA-attached FZSiNPs (at 24 h and 100 $\mu\text{g}/\text{mL}$) was mainly attributed to the higher intracellular uptake of the NPs that might increase the intracellular level of metal NPs and thereby higher cytotoxic effect. Moreover, the presence of folate as a targeting ligand which led to high level of cellular uptake may be a reason behind the different pattern of death produced by the two NPs on high concentration and UV-A exposure.

As shown in Figure 3.19, the morphological analysis of B16-F10 cells exhibited typical characteristic apoptotic changes, such as the fragmented nucleus, apoptotic bodies, and cells detached from the bottom of the plate after both NPs and NPs with UV-A irradiation treatment. Literature provides evidence that singlet oxygen and ROS are essential for initiation of apoptosis in cancer cells (Simon *et al.*, 2000; Cadenas & Davies, 2000). ROS generated by hybrid NPs and with UV-A irradiation in B16-F10 cells has been described earlier in Figure 3.12 and 3.13. Hence, we can speculate the role of singlet oxygen and ROS generated by hybrid NPs and with UV-A irradiation in fostering apoptosis in melanoma cells.

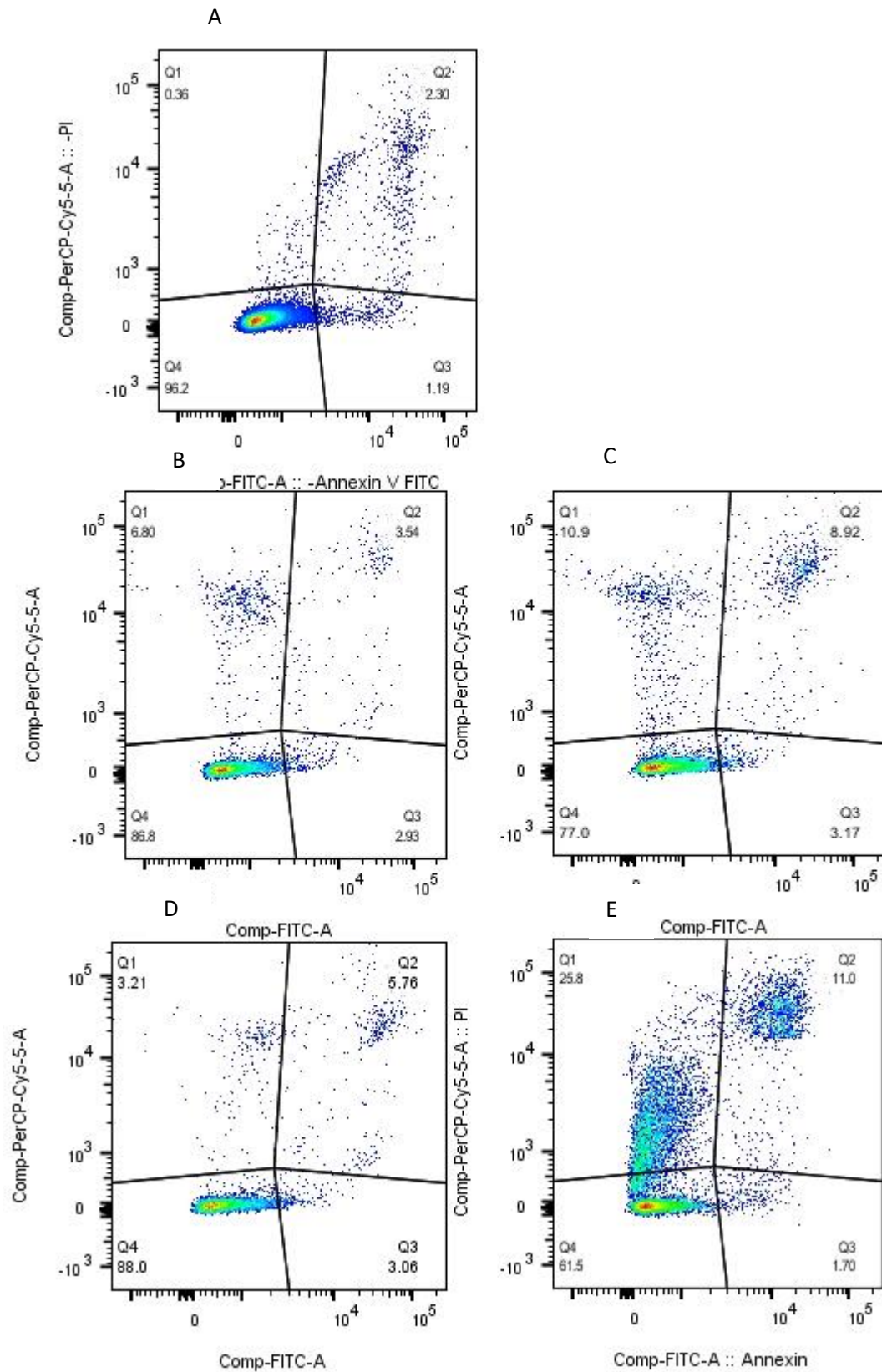


Figure 3.28 B16-F10 cells after nanoparticles treatment with 12.5 µg/mL concentration **A:** Control, **B & C:** FZSi NPs treated 6 h and 24 h. **D & E:** FZSiFA50 NPs treated 6 h and 24 h.

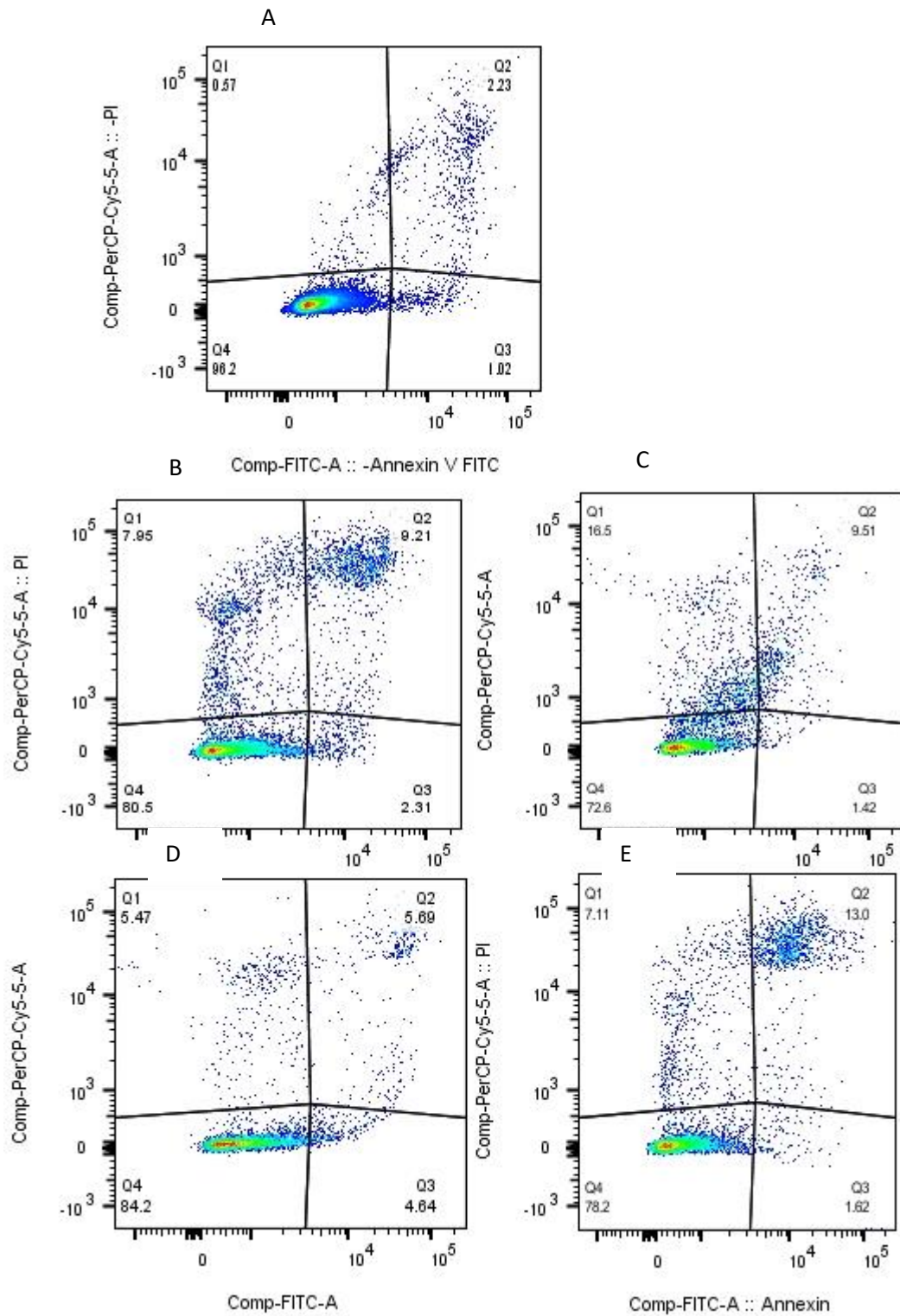


Figure 3.29 B16-F10 cells after nanoparticles treatment with 12.5 $\mu\text{g}/\text{mL}$ concentration and UV-A irradiation. **A:** Control, **B & C:** FZSi NPs treated 6 h and 24 h. **D & E:** FZSiFA50 NPs treated 6 h and 24 h.

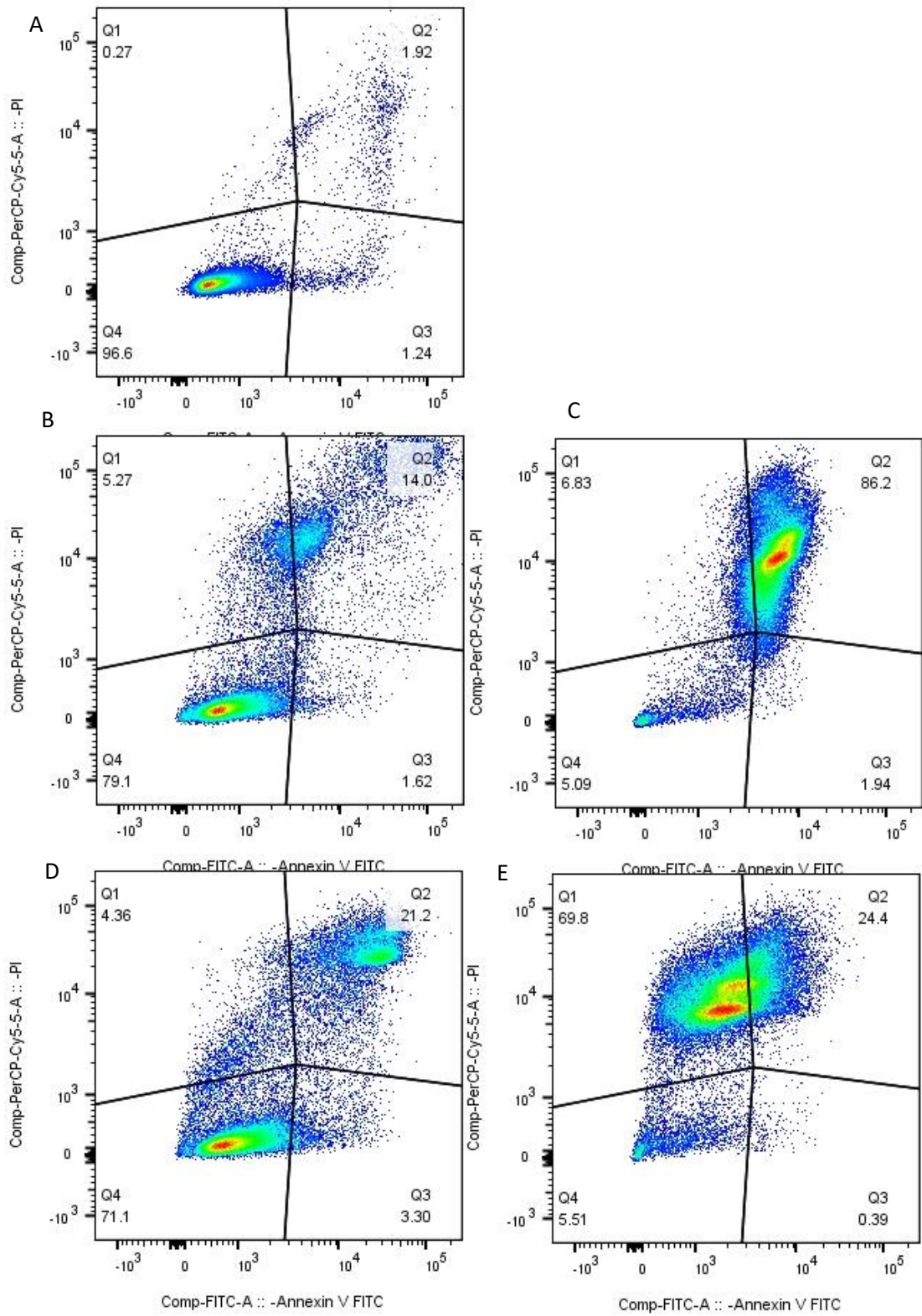


Figure 3.30 B16-F10 cells after nanoparticles treatment with 100 $\mu\text{g}/\text{mL}$ concentration. **A:** Control, **B & C:** FZSi NPs treated 6 h and 24 h. **D & E:** FZSiFA50 NPs treated 6 h and 24 h.

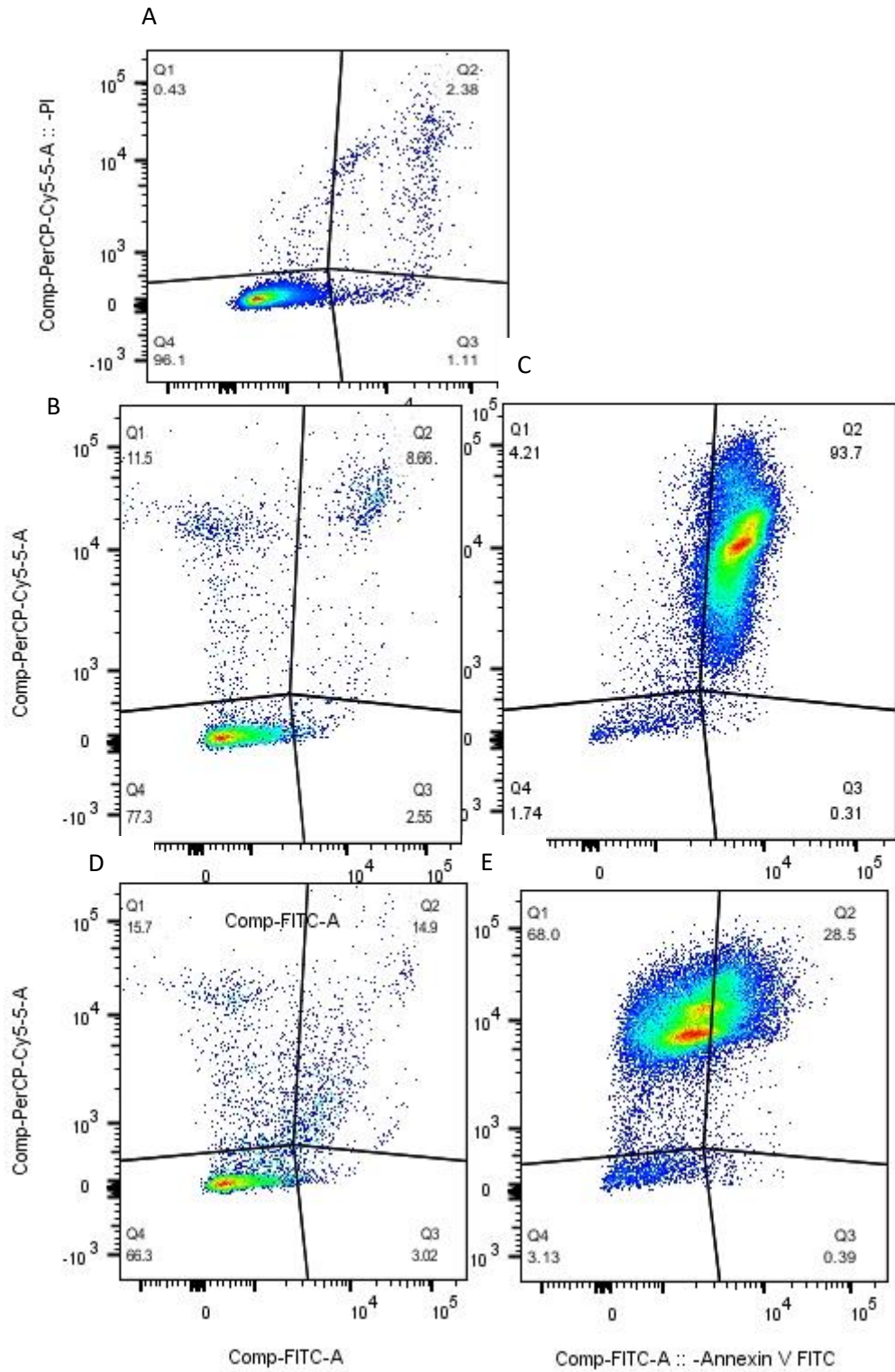
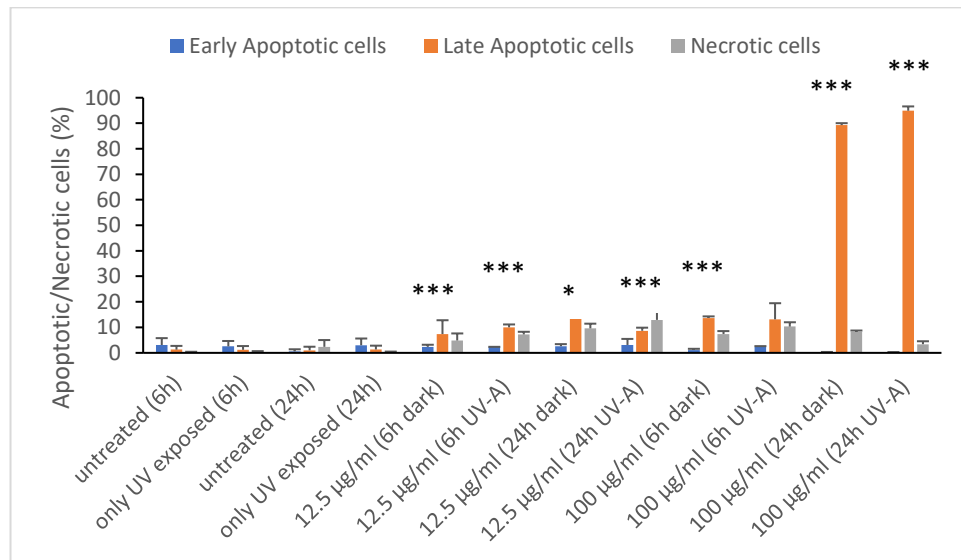


Figure 3.31 B16-F10 cells after nanoparticles treatment with 100 $\mu\text{g}/\text{mL}$ concentration and UV-A irradiation. A: Control, B & C: FZSi NPs treated 6 h and 24 h. D & E: FZSiFA50 NPs treated 6 h and 24 h.

A



B

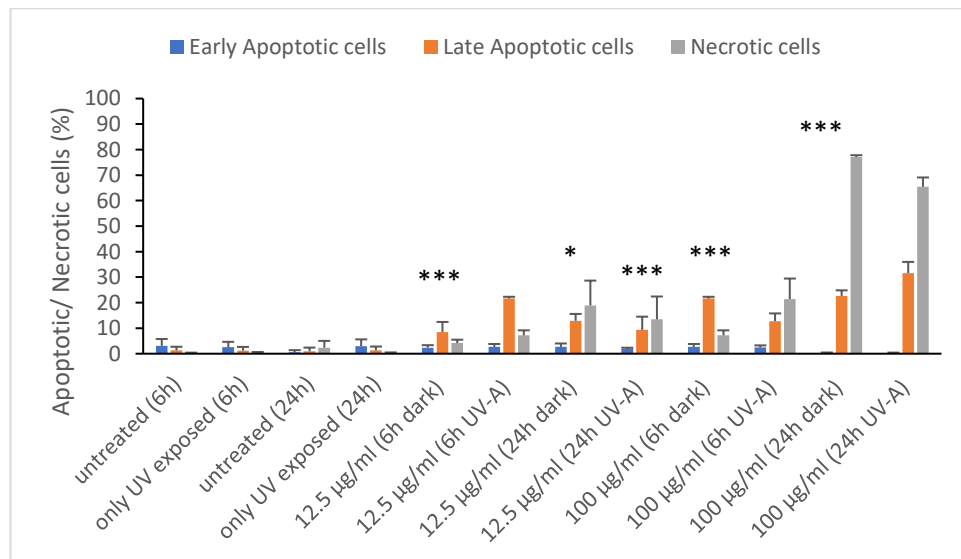


Figure 3.32 Compilation of apoptosis levels in B16-F10 cells after treatment with **A: FZSi NPs** and **B: FZSiFA50 NPs** (12.5 and 100 µg/mL) at 6 h and 24 h (dark, UV irradiation condition 10J/cm²). Data are represented as mean ±SD (n=3). * indicates p<0.05, *** indicates p<0.001 when untreated (6 h) and the only UV exposed (6 h) late apoptotic cells (%) were compared with all the other treatment groups late apoptotic cells (%).

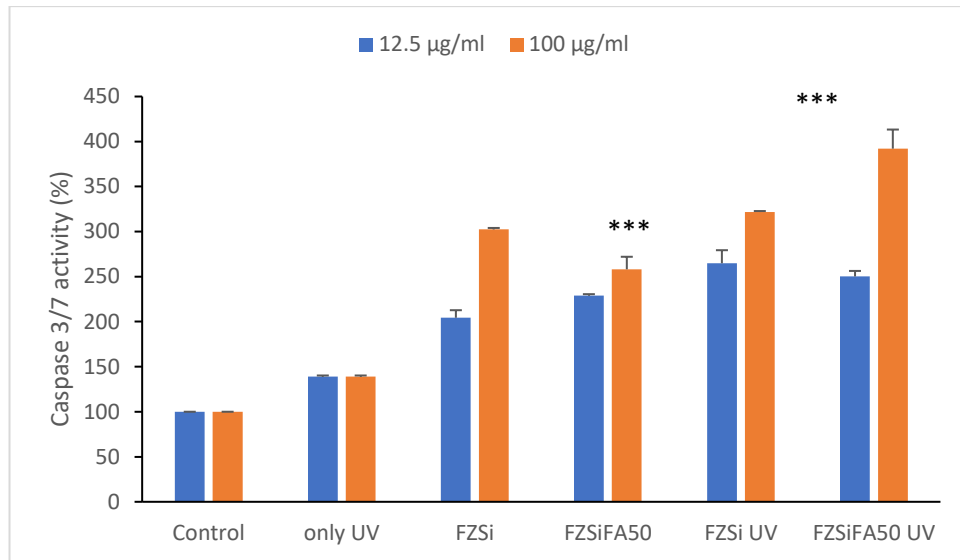
Caspase 3/7 activity

Caspase 3/7 activity is a fluorescent assay that detects the activity of caspase 3/7 in cell lysates. Caspases, a family of aspartic acid specific proteases, are the significant effectors of apoptosis (Ai *et al.*, 2017; Yang *et al.*, 2015). Caspase 3 is execution caspase involved in cleaving substrates, leading to alteration changes linked with apoptosis and ultimately cell death (Anbu *et al.*, 2016). Caspase 3 which plays a crucial

role in apoptotic pathway (Zhang *et al.*, 2014; Yang *et al.*, 2015), was induced following treatment with hybrid NPs (Figure 3.33). Caspase-3/7 activated apoptosis was observed in the B16-F10 cells after hybrid NPs treatment, during Annexin-V/PI staining. The movement of cells in all the three stages (viable cells – early apoptosis – late apoptosis/dead) further confirmed apoptosis. With the treatment of hybrid NPs and UV-A irradiation, the caspase -3/7 activity was enhanced further and statistically significant compared to control group ($p < 0.001$) (Figure 3.33 A and B). When cells were treated with 12.5 and 100 $\mu\text{g/mL}$ FZSi and FZSiFA50 NPs for 1 and 2 h, the activity of caspase-3/7 increased in a concentration-dependent and time-dependent manner. Compared to control FZSi NPs after 1 h, showed a 2-fold increase in caspase-3/7 activity at 12.5 $\mu\text{g/mL}$ and a 3-fold increase at 100 $\mu\text{g/mL}$; after 2 h, the increase was 2.1-fold for 12.5 $\mu\text{g/mL}$ and 3.2-fold for 100 $\mu\text{g/mL}$.

The detection of enhanced caspase -3/7 activities in B16-F10 cells following hybrid NPs treatment, with or without UV-A, supports apoptosis finding by the flow cytometry study discussed early. The cell death seen in cytotoxicity study could be caused by the apoptotic process. The cell morphology changes after NPs treatment, featuring swollen rounded cells (Figure 3.31, Appendix 22) further confirms the apoptotic pathway of cell death. Similar Caspase-3 activity was also reported in A375 human melanoma cells by Alarifi *et al.* (2013), who observed time and concentration-dependent rise in Caspase-3 activity following ZnO NPs treatment. Akhtar *et al.* (2012) reported increased caspase-3 activity when HepG2 cells were treated with ZnO NPs. In the current study, cell death by hybrid NPs and with UV-A irradiation was concentration dependent (Figure 3.6 & 3.9) and closely related to caspase-3 activation.

A



B

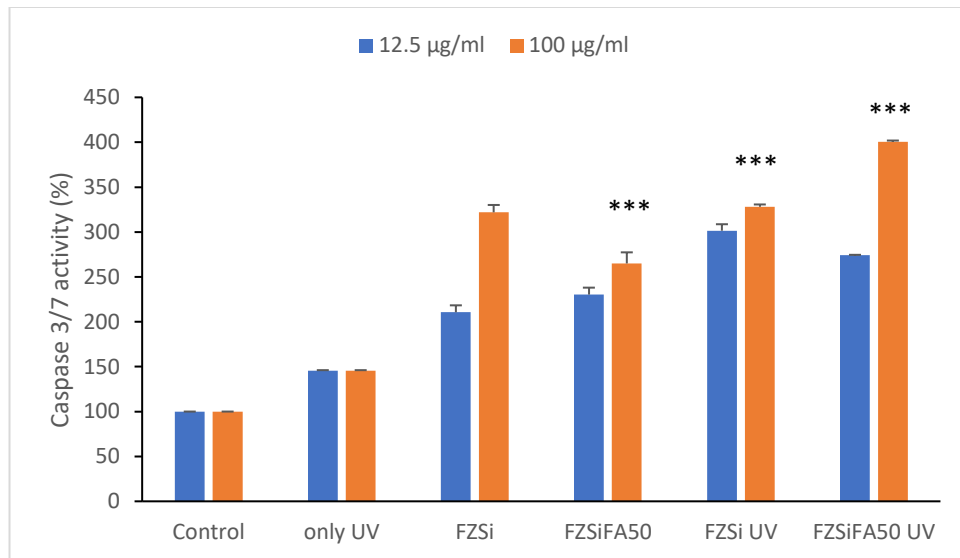


Figure 3.33 Caspase 3/7 activity in B16-F10 cells treated with FZSi and FZSiFA50 NPs (12.5 and 100 µg/mL) for (A) 1h and (B) 2 h (dark and UV irradiated, 10 J/cm²). Data are represented as mean ±SD (n=3). Compared to untreated control and only UV groups, both FZSi & FZSiFA50 NPs were statistically significant at both the concentrations (12.5 & 100 µg/mL). *** indicates p<0.001 when FZSi & FZSiFA50 NPs dark at both the concentrations were compared to FZSi and FZSiFA50 NPs UV.

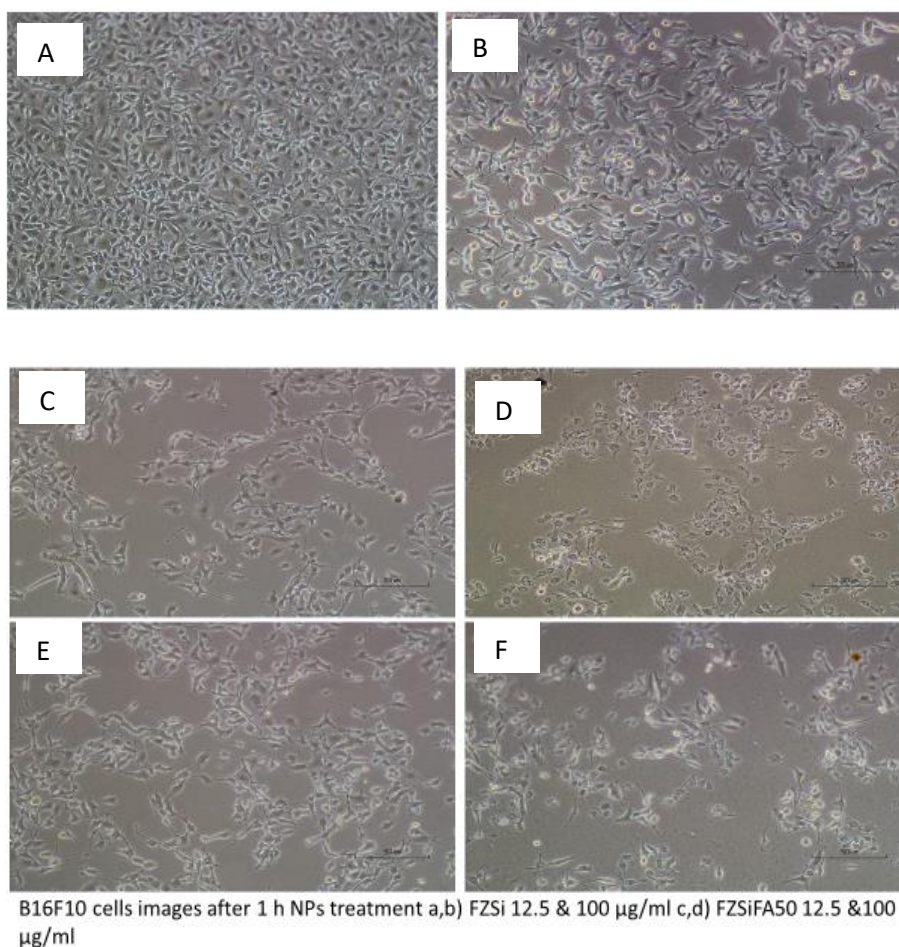


Figure 3.34 Cell morphology changes in B16-F10 cells after FZSi, FZSiFA50 NPs treatment (12.5 and 100 µg/mL) for 1h (dark). A: Control, B: only UV exposed, C&D: FZSi NPs treated with 12.5 & 100 µg/mL. E&F FZSiFA50 NPs treated with 12.5 & 100 µg/mL.

3.16 Selection of melanoma animal model for *in-vivo* studies

The anticancer effect of each formulation was initially assessed using cell culture studies in Chapter 2. However, to fully evaluate the potential of the formulation on live tumour tissues, *in vivo* studies are necessary as cell cultures cannot mimic the biological system and the nature of a tumour in a live body. *In vitro* anticancer cell studies cannot be extrapolated into *in vivo*.

Mouse melanoma cell B16-F10 was originally derived from C57BL/6 mice, and it is one of the most malignant forms of cancer in mice. Researchers considered this melanoma mice model as a good representation of human melanoma, and it has been used by other groups for assessing the effect of PDT (Zhang *et al.*, 2017, Oh *et al.*, 2017, Woodburn *et al.*, 1998, Beack *et al.*, 2015). On this basis, we chose this model for evaluation of hybrid NPs in PDT in our animal studies.

3.17 UV LED SMART optimization

The key features and advantages of UV LED SMART are summarised below:

- It can function without a computer using a breakout box during irradiation
- The UV LED SMART can also be triggered using an external foot switch or an ON/OFF button in the instrument
- Weightless instrument, ~130 g
- Maximum irradiance can be achieved within a brief time

To determine the optimum conditions for UV LED SMART and to deliver 10J/cm² we examined the following parameters:

- 1) Effects of hair on the skin
- 2) Temperature change
- 3) Impact of distance on delivery time for the UV dose

It was found that the hair of mice had a major impact on light penetration through the tumour tissue. It took nearly 10-fold time for the skin with hair to reach 10 J/cm² compared to the tumour skin without hair (Table 3.10). Accordingly, the hair of mice was shaved before tumour inoculation, before treatment of NPs and UV-A to assist in injection and the light penetration during irradiation step. To ensure accurate measurement of tumour volume, the mice were shaved before determination of tumour size using a digital calliper.

An inversely proportional relationship existed between the distance (distance between light source and skin) and the skin temperature. With the increase in distance between the UV light source and skin, the rise in temperature decreased (Table 3.10).

The pilot study showed that the shaved tumour skin delayed the UV-A dose delivery by 3 seconds (at 5 cm distance) compared to UV light directly exposed to the sensor (Table 3.10). This confirmed the penetrating power of the UV-A irradiation and the suitability of the instrument for this study. Also, with an increase in distance (between light source and skin), the time to reach 10 J/cm² dose increased. For these reasons the selected radiation parameters for *in vivo* study were 10 J/cm² and UV light source maintained at 1 cm distance from the mice.

Table 3.10. UV LED SMART optimization

Condition followed	Distance (cm)	Dose (J/cm ²)	Time ^a (min)	Initial Temp ^b (°C)	Final Temp ^b (°C)
Tumour skin shaved	1	10	3.42 ± 0.03	37.3 ± 0.3	38.3 ± 0.2
	2	10	3.47 ± 0.02	37.4 ± 0.1	38.0 ± 0.0
	5	10	3.52 ± 0.01	37.0 ± 0.1	37.2 ± 0.2
Tumour skin with hair	1	10	35.67 ± 1.26	36.7 ± 0.2	38.8 ± 0.2
	1	10	3.37 ± 0.01	36.6 ± 0.1	38.8 ± 0.0
	2	10	3.41 ± 0.02	36.5 ± 0.3	38.8 ± 0.1
No skin	5	10	3.49 ± 0.01	36.3 ± 0.2	38.5 ± 0.2

a Time taken to generate the dose 10J/cm² on the base of the mice skin; **b** Temperature at skin surface before and after UV-A dose delivery

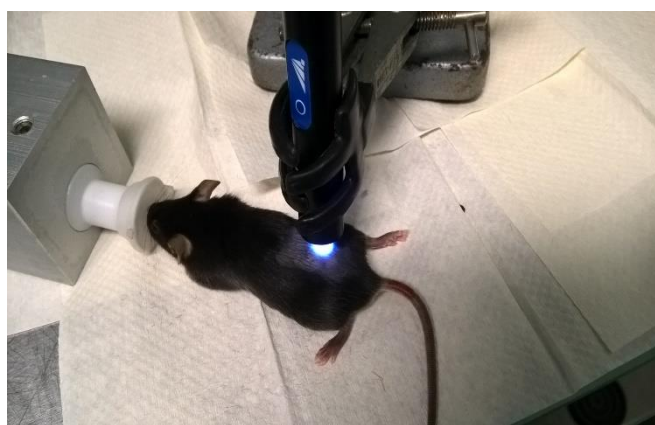


Figure 3.35 Image showing the UV LED SMART and a mouse irradiated with the UV LED SMART.

3.18 Antitumour activity of hybrid NPs alone and in combination with UV-A

Melanoma shows characteristics of high-level proliferation; and strong survival, the potential to metastasize, chemoresistance and ability to resist apoptosis (Davids *et al.*, 2011). The presence of melanin is associated with the higher death rate of cutaneous melanoma. Melanocytes can progress to metastatic malignant melanoma which invades dermis (Davids *et al.*, 2011). Two growth phases, radial and vertical, are commonly seen with skin melanoma but does not appear in other tumours (Urso, 2004). Because of such unique growth pattern melanoma, individual mouse's melanoma cell growth pattern can be variable, and their response to the treatment could be diverse, especially in male mice of C57 BL/6 (Oliveira *et al.*, 2011). We did observe the aberrant growth of melanoma tumour after day 14, which is consistent to reported studies in the literature, indicating the metastatic nature of growth of melanoma (Simeos *et al.*, 2015). As a result, the mice in the same and separate groups had to be sacrificed on different days due to the different tumour growth pattern observed after

treatment. The animal had to be sacrificed according to the animal ethics protocol as stated in Figure 2.4. This presented a challenge in generating data for comparison. Therefore, we had attempted to use different approaches to compare the treatments from different angles to reveal the full picture of treatment effects.

(i) Tumour growth pattern during the whole study

Tumour growth patterns of treated groups up to the end point are plotted individually below (Figure 3.36). The dots represent the size of tumour measured in the study. Animals were culled at different time point due to the different tumour growth pattern observed in different treatment groups. Therefore, the number of animals culled at the endpoint was different too among the groups to be useful for producing meaningful comparison data. Therefore, TVI rate up to day 16 (post tumour inoculation) was calculated first and used for comparison to determine the impact of each treatment on tumour growth in the first 16 days when almost all animals were alive.

Some general trend could be seen during the whole study. 1) NPs and UV treatment groups had more mice survival up to or beyond day 22 compared to the control group. 2) Treatment with PDT of FZSiFA50 NPs delayed the tumour growth and resulted in tighter growth pattern. For comparison purpose, the average survival time of animals in each treated group, life prolongation rate and average tumour weight of mice in each treated group are summarised in Table 3.11. The life enhancement by 25% or more in comparison to control was considered an effective antitumour response (Geran *et al.*, 1972).

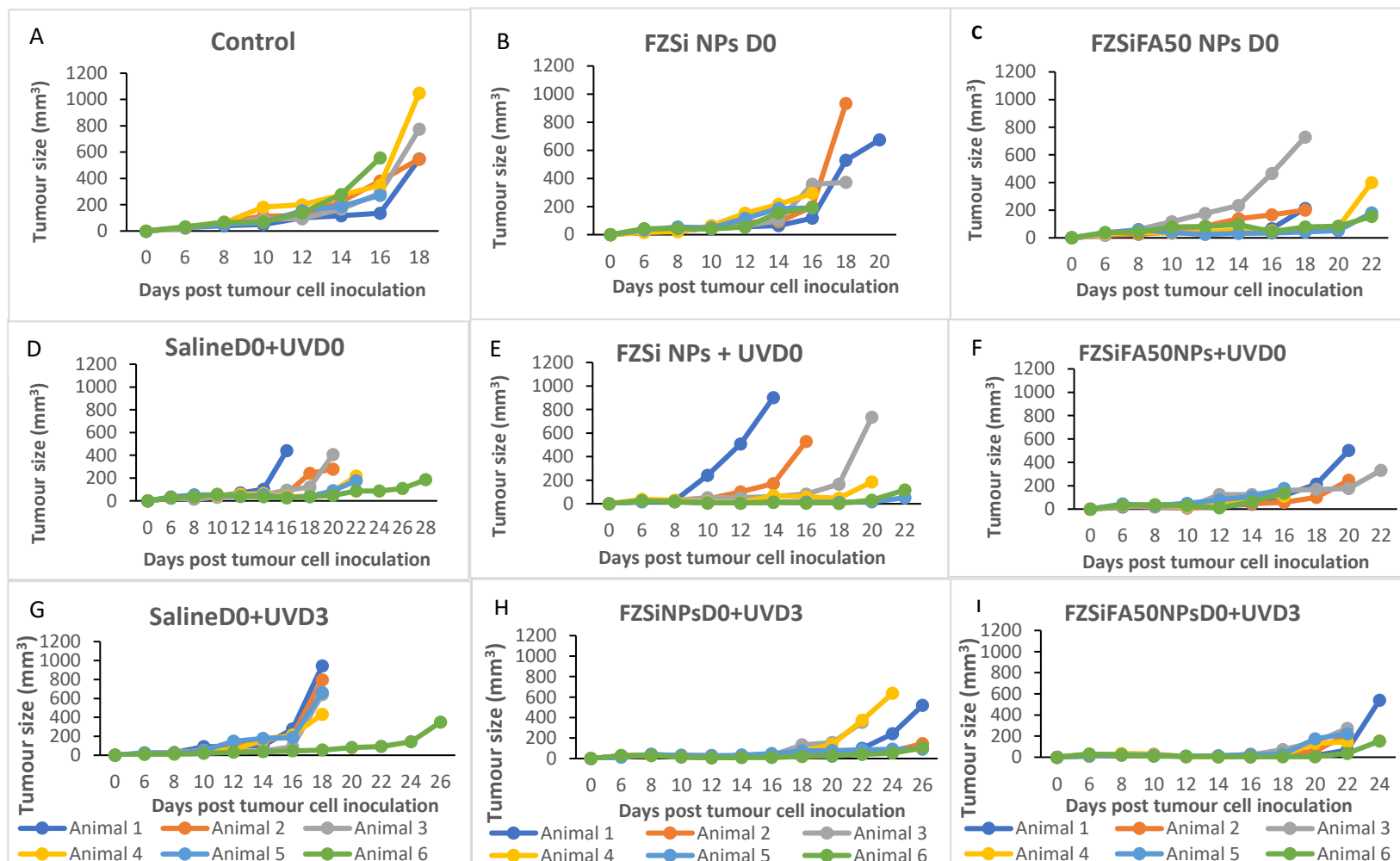


Figure 3.36 The tumour growth pattern of individual treatment groups over the whole study period. Each colour represents an animal in the group. All treatments were administered via intra tumour and hybrid NPs dose was 2 mg/kg in 10 μL . UV-A irradiation was given on sixth day (D0) and ninth day (D3) tumour inoculation, which is equivalent to 0 day and 3 days post NP treatment at a dose of 10 J/cm^2 .

(ii) Tumour growth pattern up to day 16 post-treatment

Tumour growth pattern of treated groups up to day 16 are plotted individually in Appendix 23. The average growth of six animals in each group, except FZSiNPs+UVD0 in which five animals survived on day 16 is presented in Figure 3.37. The dots represent tumour size measured on the day stated in the study.

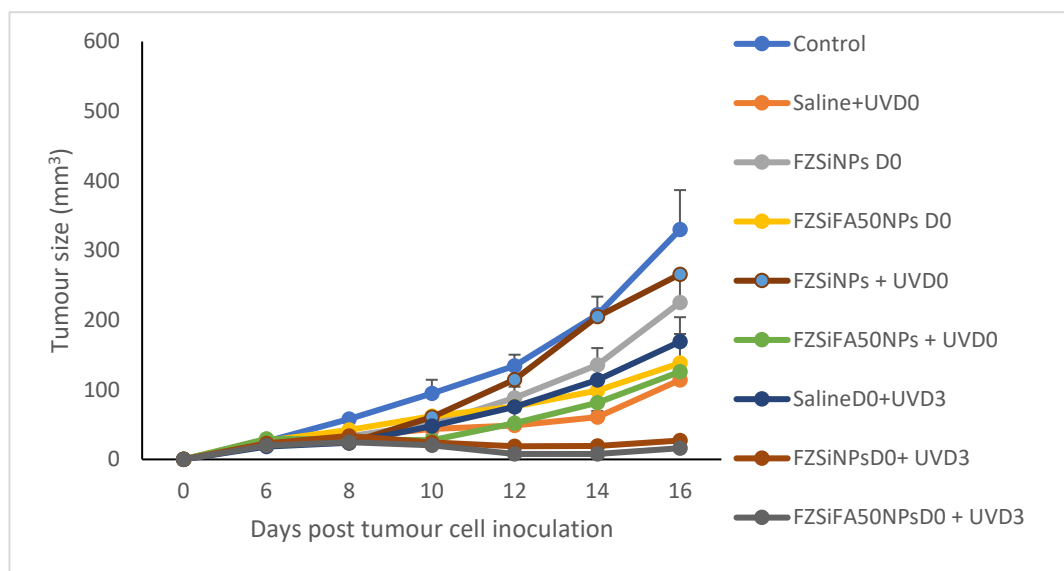


Figure 3.37 The compilation of tumour growth of different treatment groups up to day 16 post tumour cell inoculation. The treatment started when a tumour reached an average size of 20 mm³ (day six after tumour cell inoculation). D0 represented the 6th day after tumour inoculation when NPs and UV-A treatment started. D3 represented the 9th day after tumour inoculation when UV-A treatment was provided. Error bars represent standard error (n=6).

Compared to the initial tumour volume (20 mm³), on day 16 the tumour volume was 330 mm³ in control group, a 15.5-fold increase in tumour size (Table 3.11, Appendix 23). The tumour growth inhibition (expressed as TVI) was promising with FZSiFA50NPs (58.2%) compared to FZSiNPs (31.7%) (Table 3.11). The significant antitumour effect of FZSiFA50 NPs may be attributed to the folate presence, which can target the folate receptors highly expressed in melanoma cells, resulting in better cellular uptake and cytotoxicity. In combination with UV-A irradiation, an even stronger tumour growth inhibition was shown with hybrid NPs. The FZSiFA50 NPs with UV-A given on day 3 produced the strongest antitumour effect (95.2% TVI rate), compared to its NPs alone (58.2% TVI rate), and UV-A day 3 alone (48.8% TVI rate).

In comparison to the control, UV-A irradiated groups (UV-D0 and UV-D3) had 65.5% and 48.8% tumour inhibitory effect respectively (Table 3.11). The TVI rate for FZSiNPs+UVD0 was 58.1%, whereas, FZSiNPs+UVD3 group had TVI of 91.8%,

almost comparable to FZSiFA50 NPs+UVD3. This suggests that the hybrid NPs may not have reached inside the tumour cells at the adequate level when the UV dose was given immediately after NP treatment and an interval time is necessary for the hybrid NPs to accumulate in the tumour cells even administered locally (intra tumour). UVD0 not only appeared to be potent to a tumour but also showed stronger tumour inhibitory effect than that of NPs alone up to day 16. Scar formation was observed in the mice treated with UV-A irradiation (Appendix:24). The UVD0 which had stronger tumour reduction compared to UVD3 indicates the timing of UV-A irradiation is important in inhibiting the tumour growth. Probably, at the UVD3 treatment the tumour had already well established and started metastasis, whereas, during UVD0 the tumour was at the development stage.

The treatment groups with a 3-day interval between NPs and UV-A dose provided the most potent tumour inhibition among all, in both TVI rate and percentage tumour volume to control on day 16 (Table.3.11). The difference in tumour volume between the treatment groups also increased with time, which can be seen when the tumour size of all the groups was compared up to day 16 (Figure 3.37). This confirmed that developed hybrid NPs are effective nano-PSs for PDT with UV-A. Up to day 16, it is evident that FZSiFA50 NPs is more effective than FZSi NPs, either alone or with UV-A (Table 3.11). This could be attributed to the effect of FA which enhanced cellular uptake of hybrid NPs seen in *in vitro* study. The trend seen in the animal study up to day 16 is consistent with results obtained in phototoxicity study, singlet oxygen quantum yield, ROS generation, cellular uptake and apoptosis/necrosis study *in vitro*, where FZSiFA50 NPs showed the superior effect to FZSi NPs.

The analysis of data up to day 16 showed that synergistic effect existed between FZSi NPs and UV-A only. Whether this is the case for the full study is to be confirmed by other methods. This leads us to use other approaches such as the study of average survival time and life prolongation for evaluation and comparison of different treatment over the full treatment period.

Table 3.11 Summary of tumour volume and TVI effect on day 16 of the study

Groups	Tumour volume on day 16 (mm ³)	TVI rate (%) on day 16	Tumour volume to the control on day 16 (%)
Control	329.9±56.9		100
Saline+UVD0	114.0±66.3	65.5±9.4	34.6±9.5
FZSiNPs D0	225.4±35.2	31.7±22.1	68.3±21.8
FZSiFA50NPs D0	138.2±68.6	58.2±17.6	41.9±17.4
FZSiNPs + UVD0	138.5±90.6	58.1±12.0	42.0±11.9
FZSiFA50NPs + UVD0	125.8±17.2	61.9±15.1	38.1±15.2
SalineD0+UVD3	169.1±35.2	48.8±28.5	51.2±28.4
FZSiNPsD0+ UVD3	27.1±5.2***	91.8±6.3***	8.2±6.3***
FZSiFA50NPsD0+ UVD3	16.1±4.3***	95.2±4.2***	4.9±4.3***

Each group contains six animals. The data are represented as mean ± SE. Tumour volume was significant in all the treatment groups compared to the control group. *** indicates means are significantly different ($P < 0.001$) compared to the salineD0+UVD3 group. There was no significant difference between the FZSi and FZSiFA50 NPs treated with UVD3 groups. The FZSi and FZSiFA50 NPs treated with UVD3 were significant compared to saline+UVD0 ($P < 0.05$).

(iii) Tumour weight reduction by hybrid NPs

Tumour mass reduction either at a specific time point or end point of study often indicates the level of antitumour effect. The tumour weights were obtained at endpoint after the mice reached culling criteria. The criteria for which the mice had to be culled has been described already in Figure 2.4. This posed, a limitation on data collection as lateral culled tumour tends to growth erratically with bigger variation even in the same group as shown in Figure 3.38. As the tumour weight at endpoint was determined by direct weighing, it would be more directly reflecting the true size of tumour than those determined using a digital calliper. Therefore, we pooled all tumour weight data of endpoint together and presented in a scatter plot (Figure 3.38) to show the distribution of tumour weights. Caution must be taken when interpreting this data as the tumours were not from the mice culled at the same time.

Figure 3.36 showed the tumour weight distribution pattern of each animal in the treated groups. Tumour weight in the control group was spread in a wide range compared to that with the NPs only treated group, where the data points were together. The group treated with saline and UVD3 also exhibited a spread pattern relative to the unison pattern with that of NPs+UVD3. The spread pattern showed the variation in tumour weight, between animals in the same group, and the unison pattern showed the effect of NPs similar to a group even though it contained 6 different animals. The spread

pattern existed in the NPs+UVD0 groups, which was like control and UVD0 treated groups. The results suggest both hybrid NPs alone produced significant antitumour activity with narrow end tumour weights, which was comparable to or even better than that of UVA irradiation alone. The PDT effect was stronger also with narrow end tumour weight when nano-PS was irradiated on day 3 than on day 0. The high levels of apoptotic (94.9% in FZSi NPs) and necrotic cells (65.4% in FZSiFA50 NPs) after 24 h NPs+ UV-A treatment generated *in vitro* may have attributed to this reduction in tumour weight (Figure 3.32). The comparison must be made with caution as the endpoints were different. Those endpoints (e.g. day 18) labelled on Figure 3.38 were indications of the average day when mice were culled.

Figure 3.39 shows the tumour images of the treated groups against control after the animals were sacrificed. The tumours in the control group were massive compared to the treatment groups. It was noticed when the tumour burden increased the tumour extruded from the surface of the skin and started to spread all over the body of the mice. The literature states this stage of melanoma as the last step of its progression termed metastatic melanoma. It is featured with the spread of melanoma from the primary site to distant site (Damsky *et al.*, 2011). Thus, the massive weight of melanoma along with the spreading growth of melanoma away from the primary site serves as an indicator that it has progressed to a metastatic stage. Our observation of a metastatic tumour in control group (day 14) exactly matched Yoshiura and his group, (2009) who reported, metastatic appearance in the B16-F10 melanoma tumour on 14th day.

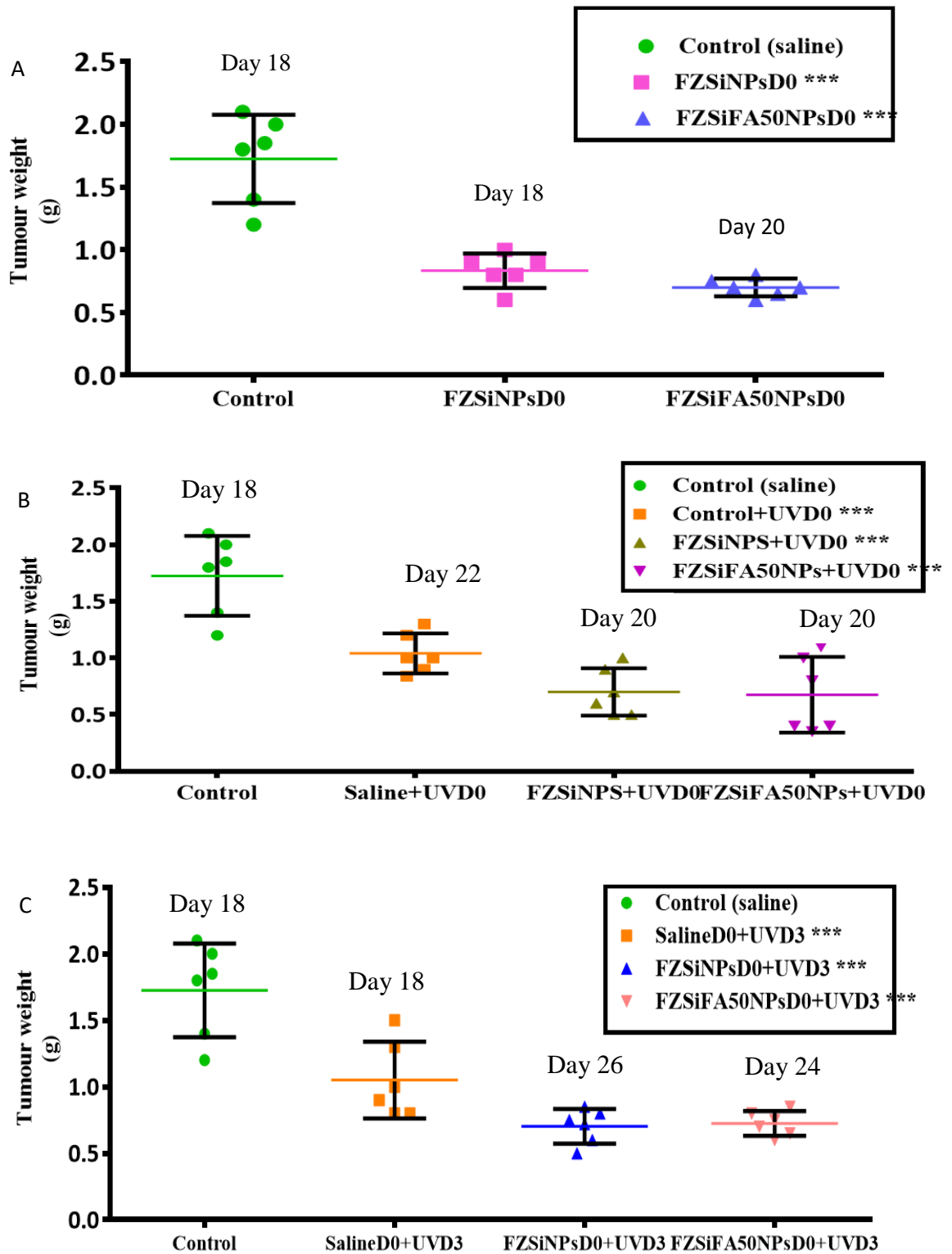


Figure 3.38 The compiled tumour weight in each treated group at the endpoint (an average value of 6 animals). The animals were sacrificed (day of sacrifice provided on top of each group) and tumour collected when the size of a tumour crossed an average 100 mm³ size. Six animals were present in each group, and each dot represents an animal within the group, and their tumour weight which varied as the animals were sacrificed on a different day according to their tumour growth. Error bar represents SEM, *** indicate means are significantly different (P< 0.001) compared to control. A) NPs alone were compared to the control (no treatment) B) Control Vs saline+UVD0, FZSiNPs+UVD0 and FZSiFA50NPs+UVD0 groups C) Control Vs salineD0+UVD3, FZSiNPsD0+UVD3 and FZSiFA50NPsD0+UVD3 groups.

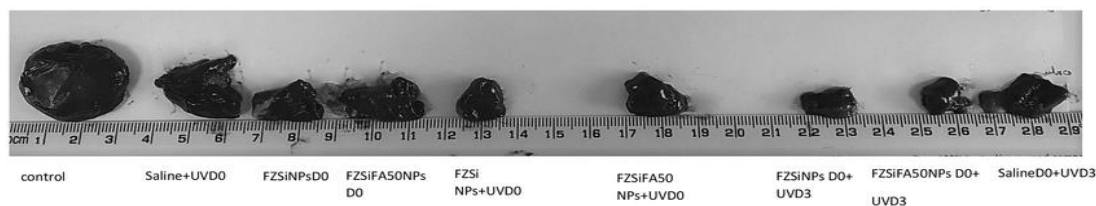


Figure 3.39 The image shows examples of the tumour size of different treated groups after sacrifice. Control and Saline D0+UVD3 groups were culled on the 18th day. FZSiNPsD0 treated group was culled on the 20th day. Saline+UVD0, FZSiNPsD0 and FZSiFA50NPs/FZSiNPs + UVD0 groups were culled on the 22nd day. The FZSiNPsD0+ UVD3 and FZSiFA50NPsD0+ UVD3 groups were culled on the 24th day following tumour cell inoculation.

(iv) The impact of treatments on animal survival and life prolongation rate

The therapeutic effects of the photodynamic effect of the NPs on tumour-bearing mouse models would be reflected in survival time and life prolongation rate. In fact, that animal survival time and life prolongation rate were calculated using data from all mice, therefore more reflective of the overall impact of treatments. We took notice of any changes with treatments. Black scar layer was visible on the site of UV-A treatment two days post PDT (in all the groups irradiated with UV-A), which indicated a vascular PDT (PSs accumulate in the endothelial cells of vascular tissue allowing vascular targeted PDT) regimen (Lepor, 2008) (Appendix 24). The black scar layer was present in the animals until the end point, probably that black scar was a necrotic scab. A pronounced swelling was visible on the tumour site immediately after PDT due to the acute inflammation reaction in mice, which disappeared the following day after PDT.

In our study (Table 3.12) FZSi NPs alone had a survival time of 17 days which is almost identical to that of control, UVD0 and UVD3, whereas, FZSiNPs+ UVD0 and FZSiNPs +UVD3 showed 20 and 25 days respectively (8 days better), which was significant ($P < 0.001$). FZSiFA50NPs+UVD0 and FZSiFA50NPs+UVD3 group had an average survival time of 18 and 23 days. Administering UV-A dose on day 0 instead of day 3, increased the survival time by 25% (additional 5 days), which is a significant enhancement ($P < 0.01$).

The hybrid NPs themselves had certain anti-tumour effect, which further enhanced when irradiated with UV-A light source. Possibly due to $^1\text{O}_2$ and ROS generated inside cells due to NPs uptake by cells and impact of time (confirmed from our *in vitro* studies), and finally, apoptosis was induced by NPs in PDT.

Table 3.12 Survival time and life prolongation over the whole period

Groups	Average survival time (days)	Life prolongation rate (%)
Control (Saline)	17.3± 1.0	
Saline+UVD0	21.0±3.3	21.3± 3.3
FZSiNPs D0	17.3± 1.6	0.0
FZSiFA50NPs D0	20.0± 2.2	15.6± 2.2
FZSiNPs + UVD0	20.0± 2.4	15.6± 2.4
FZSiFA50NPs + UVD0	18.3± 2.7	5.8± 2.7
SalineD0+UVD3	18.0± 0.0	4.0± 0.0
FZSiNPsD0+ UVD3	25.0± 1.7 ***	44.5± 1.7***
FZSiFA50NPsD0+ UVD3	22.7± 1.0 **	31.2± 1.0***

Each group contains six animals. The data are represented as mean ± SE. Life prolongation rate was calculated using the Equation 2.7 in section 2.20. It is the survival time of treatment groups with respect to that of the control. Life prolongation rate of FZSiNPsD0+UVD3 was significantly different compared to the FZSiFA50NPsD0+UVD3 group. *** indicates (life prolongation rate) means are significantly different at (P< 0.001) when FZSiNPsD0+UVD3 and FZSiFA50NPsD0+UVD3 were compared to the FZSiNPsD0, FZSiFA50NPsD0 and salineD0+UVD3 groups. The average survival time was calculated from each mouse within the group with consideration of their time of culling and then averaged. The FZSiNPsD0+UVD3 (P<0.001) and FZSiFA50NPsD0+UVD3 (P<0.01) groups were significantly different compared to salineD0+UVD3. FZSiNPsD0+UVD3 (P<0.05) was also significantly different compared to saline+UVD0 group.

The tumour growth of control (only saline) group was rapid, while tumours of mice treated with hybrid NPs+UV-A irradiation grew slowly with occasional tumour necrosis. The necrotic appearance in melanoma tumours suggested the possibility of vascular damage (Yoshiura *et al.*, 2009).

The life prolongation rate was almost similar for NPs and NPs+UVD0 (15.6%), whereas, the FZSiNPs+UVD3 group had a 3-fold and FZSiFA50NPs+UVD3 had 2-fold better life prolongation rate in comparison with NPs and NPs+UVD0. Such a trend is consistent with our *in vitro* results which showed that hybrid NPs, when used in combination with UV-A irradiation, was stronger than NPs alone and UV-A alone in phototoxicity in B16-F10 cells. The significant extension of survival time and life prolongation rate by FZSi NPs and FZSiFA50 NPs with UV-A irradiation on day 3 demonstrated the synergistic effect of hybrid NPs as PS with UV-A in PDT.

When comparing the tumour inhibition data of TVI (up to day 16) with the life prolongation rate (of whole study), we see a direct correlation in treatment groups of NPs without UV. For instance, the FZSiFA50 NPs alone produced tumour inhibition 58.2% and life prolongation 15.6%, while, FZSi NPs offered only 31.7% tumour

inhibition with 0% life prolongation. However, the trend is different with NPs in PDT. The FZSiNPs +UVD0 produced 58.1% in TVI and 15.6% in life prolongation, while, FZSiFA50 NPs+UVD0 produced 61.9% in TVI but only 5.8% in life prolongation respectively. The TVI rates were 91.8 and 95.2 respectively for FZSi NPs+UVD3 and FZSiFA50 NPs+UVD3, corresponding to the life prolongation of 44.5% by FZSi NPs+UVD3 and 31.2% by FZSiFA50 NPs+UVD3 (Table 3.12). Because the life prolongation rate was calculated by survival days of mice which was very much influenced by conditions set for the end point (in our case it is 100 mm³ and necrotic appearance of tumour). It was noticed in fact some of the necrotic tumour was peeling off and mice could recover from the cancer if kept longer. Closely inspect the raw data in Figure 3.33, both FZSiFA50 NPs group (+UVD0 and +UVD3) showed relatively small tumour growth variation than that of FZSi NPs (+UVD0 and +UVD3) but being culled earlier therefore resulting in lower life prolongation rate. Therefore, TVI (up to day 16) was considered as a better parameter for assessing the efficacy of the treatment as it included all mice.

Based on TVI, we concluded that FZSiFA50 NPs, alone and with UV, is more effective in inhibiting tumour growth than that of FZSi NPs. In addition, hybrid NPs in combination with UV-A irradiation can inhibit tumour growth *in vivo* significantly better when UV-A was given 3 days post NPs treatment, instead of given at the same time with NPs. These results proved that hybrid NPs in combination with UV-A radiation can be used as a potential effective antitumour treatment regimen in PDT.

(v) Impact of treatments on the health of the animal

In assessing the effectiveness of treatment, it is important to evaluate the overall health of animals to investigate potential side effects a treatment may bring. For assessing treatment of subcutaneous tumours, in addition to the tumour volume, tumour ulceration, mobility of an animal and body weight were constantly monitored during the study. The body weight of animal has always been considered as an indicator of the overall health status of the animal (Paster *et al.*, 2009). The body weight of mice was measured from the day of arrival in the facility and groups categorised accordingly. Henceforth, after tumour inoculation, the body weight was monitored every alternate day using a digital weighing balance. The drop-in body weight by more

than 10% on any day of study was considered an endpoint for the animal in our study design.

Body weight data alone cannot be used to study the toxicity of the hybrid NPs. However, it is certain that any significant drop in body weight of mice could be related to the toxicity of NPs. As indicated in Figure 3.40, during the whole study, there was no significant difference between treatment groups on any particular day of the study compared to control group. However, there was a small drop in body weight of mice (but insignificant) in FZSiNPsD0 group towards endpoint (day 18) and FZSiNPs+UVD0 from day 22 towards endpoint (day 26). The results suggested that the hybrid NPs were well tolerated by the mice when given via intra tumour administration. We speculate the non-significant changes in body weight for two reasons: 1) the hybrid NPs and UV-A treatment were given intra tumour (localised treatment) and not systemically. 2) with tumour burden increasing the body weight would plateau or increase, which could compensate for any smaller drop in body weight. However, none of the animals showed any distress, difficulty in mobility or discomfort during the entire study.

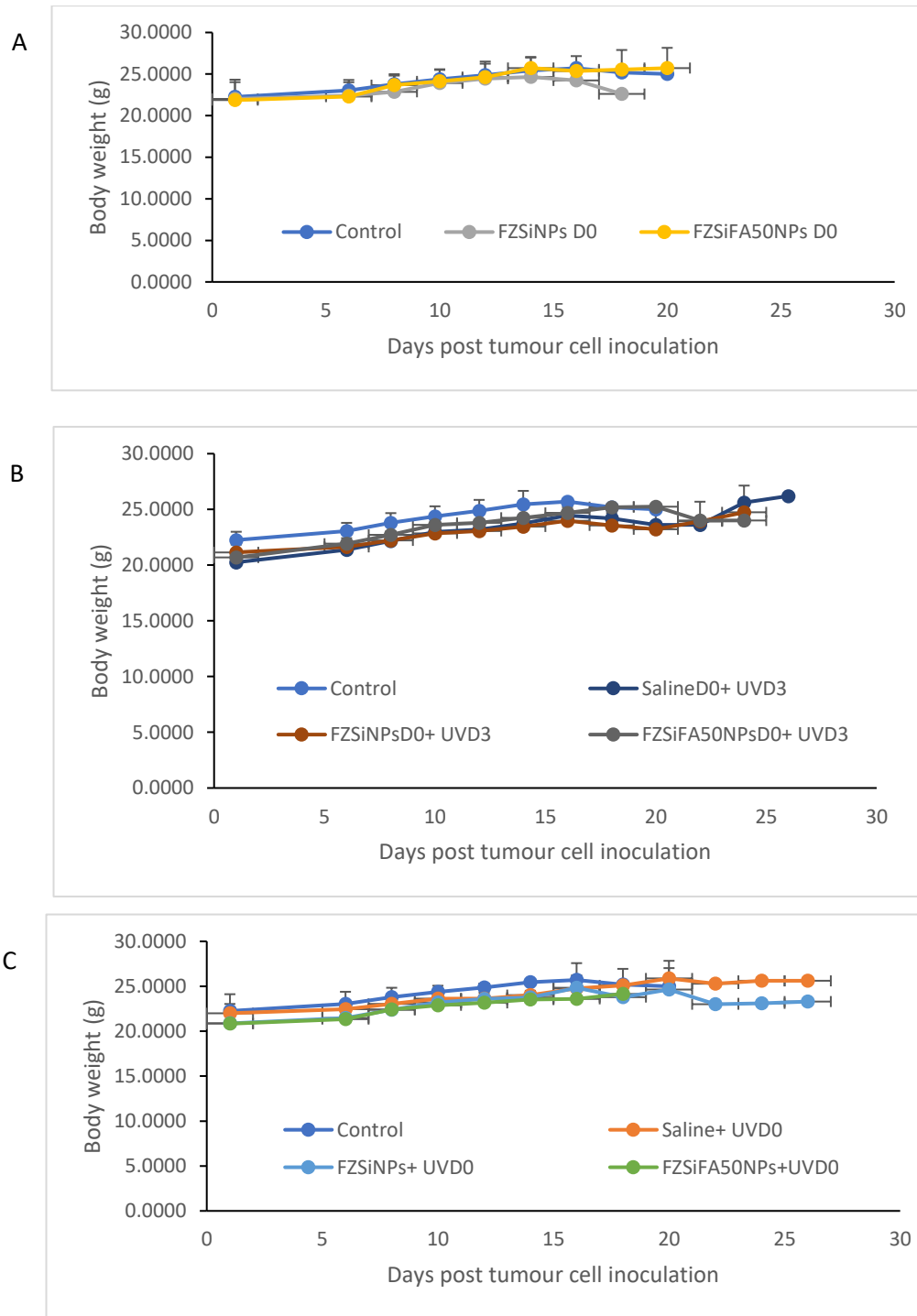


Figure 3.40 Change in body weight of mice bearing B16-F10 melanoma tumour after cell inoculation. The body weight of mice was measured every alternate day starting from the day of tumour cell inoculation using digital weight balance. n=6 and all data are presented as mean \pm SD. A) Control Vs FZSiNPsD0 and FZSiFA50NPsD0 groups B) Control Vs saline+UVD0, FZSiNPs+UVD0 and FZSiFA50NPs+UVD0 groups C) Control Vs salineD0+UVD3, FZSiNPsD0+UVD3 and FZSiFA50NPsD0+UVD3 groups.

It is too early to speculate the hybrid NPs are completely safe considering they were only given intra tumorally. Further studies involving i.v administration of different high doses of hybrid NPs should provide more information on their toxicity.

We assessed the impact of treatments on the weight of major organs such as liver, lungs, kidney and spleen whose weights were collected from each animal at the endpoint. The weight of organs (liver, lungs, kidney and spleen) is summarised in Table 3.13. The lungs and kidney did not show any statistical significance compared to control group.

The liver weight in the FZSiNPsD0+UVD3 group showed the most significant difference compared to the control. The liver has a physiological function to capture small particles of 10-20 nm size for clearance (Ajdari & Ghahnavieh, 2014). The chemical composition and size range of each NP may affect its distribution and properties *in vivo* (Longmire *et al.*, 2008). The chemical nature and size of FZSi NPs and their exposure to UVA on day 3 may have led to decomposition of NPs and solubilisation of components of NPs and consequently caused undesirable effect on liver compared to other groups. Interestingly, the coating composition of NPs and iron particles have different clearance mechanisms in the body (Longmire *et al.*, 2008). Both our hybrid NPs have iron oxide and silica coating and only one conjugated with FA. Conjugation of FA involves chemical bond which may make NPs less susceptible to the degradation by UV-A. This could be a reason behind hepatic effect seen with FZSi NPs in combination with UVD3. There is also a possibility of antitumour effect related mechanism occurring due to PDT, affecting the liver as well. Spleen weight was statistically significant only in the group treated with FZSiNPs D0 when compared to control ($P < 0.01$).

Based on body weight change, organ weight variation among the mice, it appears FZSiNPs may have relatively higher toxicity than FZSiFA50 NPs especially after exposure to UVA. The surface modification of FZSiNPs with targeting ligand FA may have rendered the FZSiFA50 NPs lesser toxic than FZSiNPs. Smaller size, larger surface area, therefore, quicker decomposition under UVA and may be easier uptake by macrophages. NPs trigger ROS production which can lead to oxidative stress, which can cause injuries to organs (Ajdari & Ghahnavieh, 2014). From our *in vitro*

study, we know that the hybrid NPs produce ROS in combination with UV-A irradiation. We speculate these factors are potential reasons behind the impact of FZSi NPs in liver and spleen weight reduction. The images of different organs of individual treatment groups after the sacrifice is shown in Figure 3.41.

Table 3.13 Body weight and organs weight of different treatment groups

Groups	Body weight (g)		Liver weight (g)	Spleen weight (g)	Lungs weight (g)	Kidney weight (g)	Tumour weight (g)
	Start	End					
Control	22.25± 1.72	25.00± 2.15	1.27±0.11	0.10±0.02	0.18±0.01	0.30±0.03	1.73± 0.35
Saline+UVD0	22.00± 2.11	25.60± 1.10	1.00±0.21*	0.10±0.02	0.20±0.02	0.28± 0.03	1.04± 0.18****
FZSiNPs D0	22.01± 2.31	22.60± 0.70	1.14±0.16	0.13± 0.03****	0.16±0.05	0.30± 0.05	0.83± 0.14****
FZSiFA50NPs D0	21.87± 2.16	25.72± 2.43	1.18±0.19	0.11± 0.03	0.18±0.03	0.30±0.02	0.70± 0.07****
FZSiNPs + UVD0	20.86± 2.16	23.30± 3.18	1.23±0.06	0.10±0.02	0.18±0.03	0.31± 0.03	0.70± 0.20****
FZSiFA50NPs + UVD0	20.83± 1.55	24.15± 0.63	1.03±0.13*	0.11± 0.03	0.16±0.03	0.26± 0.06	0.67± 0.33****
SalineD0+UVD3	20.25± 0.91	26.20± 1.64	1.13±0.11*	0.10±0.01	0.16±0.03	0.30±0.02	1.05± 0.29****
FZSiNPsD0+ UVD3	21.15± 0.69	24.73± 2.40	0.82±0.16****	0.10±0.01	0.20±0.01	0.30±0.01	0.70± 0.13****
FZSiFA50NPsD0+ UVD3	20.68± 1.02	24.00± 1.69	1.04±0.13*	0.10±0.01	0.20±0.01	0.30±0.01	0.72±0.09****

Each group contains six animals. The body weight (start) indicates the weight of the animal at the commencement of the study and (end) indicates the weight of the animal at the endpoint of the study. The tumour weight indicated is the average tumour weight of the animals in each group but sacrificed on different days according to tumour growth. Accordingly, the other organs (lungs, spleen, kidney, liver) were also collected the same day tumour was collected. The tumour weight data are represented as mean ± SEM. * indicate means are significantly different at P < 0.05 and **** indicate means are significantly different at P < 0.001 compared to control.

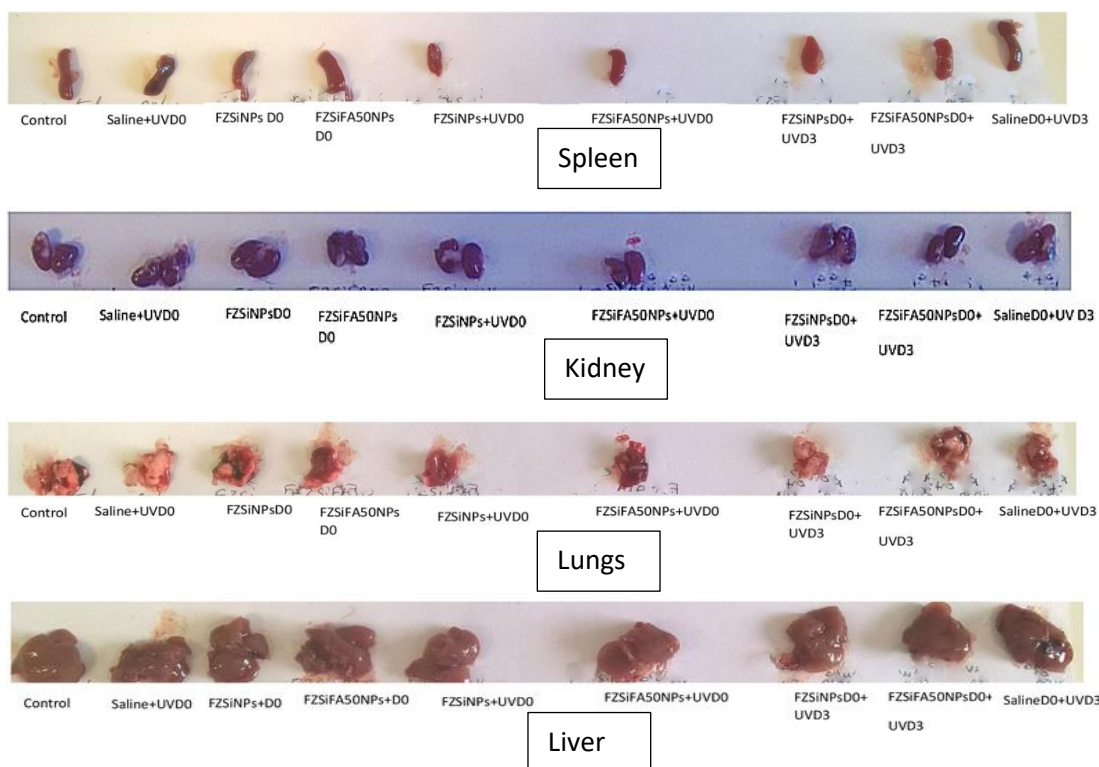


Figure 3.41 Images are showing the organ profile (spleen, kidney, lungs, liver) (top-bottom) of different treatment groups after sacrifice. The culling day represents the average day of culling of animals from each group. Control and Saline D0+UVD3 groups were culled on the 18th day. FZSiNPsD0 treated group was culled on the 20th day. Saline+UVD0, FZSiNPsD0 and FZSiFA50NPs/FZSiNPs + UVD0 groups were culled on the 22nd day. The FZSiNPsD0+ UVD3 and FZSiFA50NPsD0+ UVD3 groups were culled on the 24th day following tumour cell inoculation.

None of the animals showed signs of trouble with posture, movement, eating/drinking, breathing, alertness and dehydration during the entire study period. So, we conclude, the hybrid NPs and its dose (2 mg/kg) were well tolerated administered through the intra tumour route, and they demonstrated the significant photodynamic effect on the tumour cells UV-A radiation (365 nm, 10 J/cm² given on day 3). The benefit of using these nano-sized PS through the intra tumour route in PDT also demonstrated by the minimum toxic effect seen on the weight of body and organ including lung, liver, kidney and spleen.



Figure 3.42 The image is showing the growth of B16-F10 melanoma tumour in C57BL/6 mice.

3.19 General Discussion

The hybrid NPs were highly cytotoxic against B16-F10 and Caco-2 cancer cells. Cytotoxicity was also observed in 3T3 cells as well, highlighting the need for optimizing the dose of hybrid NPs towards each type of cell line. The UV-A light source used was sufficient enough for activation of hybrid NPs to generate phototoxicity in cancer cells. Significant reduction in cell viability was observed even at the lowest dose (12.5 $\mu\text{g/mL}$) of hybrid NPs when they were irradiated with UV-A light. Silica modification of FZ NPs reduced, insignificantly, phototoxicity against melanoma and colon cancer cells when compared to FZ NPs which is consistent with the fact that the surface modification had affected the photocatalytic property of the hybrid NPs. When compared to FZ NPs the FA modified hybrid NPs, at 12.5 $\mu\text{g/mL}$ dose, exhibited strongest phototoxicity against melanoma cells, but not in Caco-2 cells.

The cellular uptake assay indicated the enhanced cellular uptake of FZSiFA50 NPs compared to FZSi-FITC NPs was associated with FA attachment to the surface of NPs. Confocal microscopy images generated after 6 h treatment of B16-F10 cells with hybrid NPs confirmed the cellular uptake and proved a significant amount of the NPs were present inside the cells, many closely associated with nucleus. We speculate that FA might have contributed to the better cellular uptake via targeting the folate receptors which expressed at high levels in these cancer cell lines. The total cell associated metal levels correlated well with the cellular uptake of hybrid NPs as indicated by the significant higher levels of Zn and Fe detected with cells treated with hybrid NPs. The data also suggests that cellular uptake process occurred up to 6 h post NPs treatment and UV irradiation may have facilitated the photo degradation of NPs, releasing soluble metal. Soluble free metal might be a significant contributing factor

towards the cellular toxicity and systemic toxicity in animals. Ng *et al.* (2017) reported earlier that the free Zn were more cytotoxic than ZnO NPs.

The surface modification of hybrid NPs had affected their production of singlet oxygen quantum yield, with FZ NPs generating the maximum quantum yield of singlet oxygen compared to the FA and silica modified FZ NPs. This was not totally unexpected as Chadwick *et al.* (2016) also reported a similar observation in their work with Au NPs.

ROS generation is considered as an up-stream event for apoptotic signalling in cells (Wang *et al.*, 2014). The ROS could attack cancer cells, resulting in anti-cancer effect in a caspase-dependent manner (Alarifi *et al.*, 2017). In this study, significant ROS production induced by the hybrid NPs under UV-A irradiation was confirmed by pre-NAC treatment and found to be highest post 6 h treatment with NPs in both B16-F10 and Caco-2 cells. Silica and FA modified NPs showed even greater level of ROS production, particularly in B16-F10 cells. The cytotoxicity study of hybrid NPs after ROS quenching by NAC supports the hypothesis that cell proliferation inhibition by hybrid NPs was via the production and effect of ROS.

The repeated photo killing ability of NPs through PDT was confirmed when hybrid NPs were treated with double and triple radiation. Double radiation exhibited more drastic cell killing compared to single radiation. Silica and FA coated FZ NPs exhibited the similar trend of phototoxicity during multiple irradiations. When compared to FZ NPs the surface modified silica and FA attached FZ NPs exhibited significantly better reduction in cell viability. This supports the use of a single dose of NPs with multiple irradiations to provide continuous treatment in a clinical setting. In addition to the surface modification of hybrid NPs, the final destination of the NPs and their immediate proximity and interaction with UV-A may well provide the difference in the pattern of cell death and the difference in cytotoxicity and phototoxicity.

Drastic changes in cellular morphology was observed, especially when the NPs were irradiated with UV-A light. These morphology changes were well supported by the higher percentage of apoptotic cells noted during apoptosis assay, when melanoma cells were treated with NPs and irradiated with UV-A radiation. After treatment with high dose (100 µg/mL) of NPs and UV-A for 24 h, the FZSi NPs recorded more

apoptotic cells and FZSiFA50 NPs recorded more necrotic cells, indicating the NPs may have undergone different cell death pathways. Enhanced caspase 3/7 activity levels were detected after NPs were irradiated with UV-A light, suggesting a possible caspase activated apoptosis.

All *in vitro* studies suggested that FZSiFA50 NPs are good potential PSs for PDT. We then examined FZSiFA50 and FZSi NPs with and without UV-A irradiation in a melanoma animal model to assess the PDT effects of hybrid NPs. Melanoma tumour model was selected for its ease access to UV-A irradiation. However, its cells are associated with rapid growth and diversified growth pattern, and they tend to develop resistance to treatment over time (Perrotta *et al.*, 2016). Despite of these, under the currently applied PDT conditions, the FZSiFA50NPs+UVD3 showed the highest tumour inhibition (TVI rate) up to day 16 (95%), compared to FZSiNPs+UVD3 (92%), UV-A alone (UVD0 65.6%; UVD3 48.8%) and NPs alone (FZSiFA50NPs 58.2%; FZSiNPs 31.7%), which was correlated well with *in vitro* phototoxicity study, cellular uptake, singlet oxygen quantum yield, ROS generation, apoptosis and caspase3/7 activity. In terms of life prolongation, FZSiNPsD0+UVD3 was the best with 44.5% while FZSiFA50NPs+UVD3 provided 31%, UVD0 21.3%, UVD3 4%, FZSiNPs 0% and FZSiFA50NPs 15.6%. However, because other factors such as the end point parameters were influencing the value of life prolongation, TVI rate is considered to be the most reliable and unbiased value for the comparison as it was calculated with inclusion of all animals. Systemic toxicity study, which was conducted by examining the weight change of the mice and its various organs, revealed that FZSiFA50NPsD0+UVD3 had less impact on liver compared to FZSiNPsD0+UVD3 and both showed no significant effect on body weight.

Animal study results also suggest that the time of treatment with UV-A irradiation is vital to produce maximum impact on tumour growth inhibition. Having a 3 days interval seems more efficient than giving NPs and UV-A at the same time.

Overall the extensive *in vitro* and *in vivo* studies proved our hypothesis that the hybrid NPs can be used as an effective nano-PS in PDT with UV-A. Such treatment regime provides an advantage over UV-A or NPs alone. It allows more targeted and flexible delivery of PDT. In comparison to those reported in the literature which studied NPs-

PDT effect (Table 3.14), with multiple dose irradiations in combination with a high dose of NPs, our hybrid NPs in PDT has produced a promising antitumour effect even with single irradiation and a low dose of NPs. However, factors such as different nanomaterials, light source, irradiation dose and NPs dose need to be taken into account.

Table 3.14 Comparison of our hybrid NPs with the other reported NPs in melanoma tumour model

NPs	Light source and dose	Antitumour effect	Significance	Data source
C60-IONP-PEG-HMME (4mg/kg, i.v every 2 days for 10 days)	532 nm Laser, 300 J/cm ² (every 2 days for 10 days)	After 10 days: control group:1127 mm ³ NPs group:272 mm ³	Treatment started after reaching 100 mm ³ . The four-fold decrease in tumour volume in NPs treated group compared to control in a B16F10 tumour model.	Shi <i>et al.</i> , 2013
Rose Bengal as photosensitizer (100 µM) (treated 2nd and 4th day)	68.4 J/cm ² , Red light BL1000A lamp, 630 nm	After 6 days: 400 % larger tumours	Treatment started after reaching 246 mm ³ sizes. A four-fold increase in tumour size after PDT in a B16F10 tumour model.	Mc Ewan <i>et al.</i> , 2016
FZSi NPs (2 mg/kg day 0)	UV LED SMART, 365 nm (10J/cm ² , single dose day 3)	After 16 days control: 329.96 mm ³ NPs group: 27.06 mm ³	Twelve-fold decrease in tumour volume compared to control in NPs group	Current study
FZSiFA50 NPs (2 mg/kg day 0)	Same as above	After 16 days control: 329.96 mm ³ NPs group: 16.12 mm ³	Twenty-fold decrease in tumour volume compared to control in NPs group	Current study

C60 = Fullerene, IONP = Iron oxide, HMME = Hematoporphyrin monomethyl ether; All the compared data were performed on C57BL6 strain mice only.

CHAPTER 4

SUMMARY, FUTURE RESEARCH SCOPE AND CONCLUSION

4.1. General Summary

In this PhD research, semiconducting hybrid NPs containing Fe₃O₄-ZnO were investigated, both *in vitro* and *in vivo*, for the potential applications as a new class PSs for PDT. Particle size distribution was determined by DLS and confirmed to be between 13 - 19 nm in size. The hybrid NPs were stable over 24 h period at 37 °C in the DMEM medium containing FBS.

Three cell lines B16-F10, Caco-2 and 3T3 were used for assessing the cytotoxicity. The former two were also used in studies including phototoxicity, cellular uptake and ROS generation. Further, B16-F10 cells were also used for apoptosis and caspase activity studies of the hybrid NPs. The MTT assay confirmed the cellular toxicity of the hybrid NPs in the three cell lines, which was time and concentration-dependent. Although the hybrid NPs exerted cell killing ability against melanoma and colon cancer cells, they were also highly toxic to 3T3 cells, which is a concern that needs to be addressed.

The phototoxicity experiments were successfully conducted with 10 J/cm² UV-A dose (365 nm) in the BS02 UV IRRADIATION CHAMBER. The study showed that there was a synergistic effect between the hybrid NPs and UV-A radiation. The cytotoxicity and phototoxicity of the hybrid NPs confirmed they are an effective new class of nano-PS which can function as an anticancer drug, further attenuated by UV-A radiation at low dose.

Our study demonstrated that FA attached NPs in combination with UV-A radiation produced stronger cancer cell killing effect than that by UV-A radiation alone or those NPs without FA modification. Furthermore, ROS was detected and correlated to the cancer cell killing ability of the NPs. Singlet oxygen quantum yield study confirmed the production of singlet oxygen by hybrid NPs in PDT although the surface modification with silica and FA reduced its level. The ROS effect was quenched using antioxidant NAC. The NAC pre-treated cells reduced ROS and enhanced cell viability, which upheld the ROS generation by hybrid NPs and its role in cellular toxicity.

The cellular uptake study revealed that the FA significantly enhanced the hybrid NPs uptake, possibly via receptor mediated endocytosis process. Confocal microscopy

further confirmed the results of cellular uptake study and proved that most NPs were, internalised instead of attached on the cell surface. This was further supported by the data from total cell associated zinc and iron analysis with and without UV-A irradiation. The latter study also showed that the uptake of hybrid NPs may continue for up to 6 h but significant zinc dissolution occurred in Caco-2 cells, not B16-F10, after 2 h treatment of NPs. Photo degradation of hybrid NPs appeared to be occurring potentially producing soluble metals. This could contribute to the toxicity of hybrid NPs *in vitro* and *in vivo*.

With increased time and concentration, the NPs induced remarkable variations in the cellular morphology. The cells were swollen, broken and showed a reduction in cell number and finally lifted from the cell surface. The morphology changes featured the apoptotic events of cells treated with NPs. The caspase dependent apoptosis pattern of cell death was evident in B16-F10 cells following treatment with the hybrid NPs and UV-A irradiation confirmed by Annexin-V/FITC and caspase 3/7 assays. The pattern of cell death differed between FZSi and FZSiFA50 NPs at the high dose of NPs (100 µg/mL, 24 h) and in combination with UV-A irradiation. The FZSiFA50NPs exerted necrotic pattern cell death, and the FZSi NPs exerted apoptotic mode of cell death. These *in vitro* findings warranted the selection of FZSi and FZSiFA50 NPs for the further *in vivo* study.

B16-F10 melanoma animal model in C57BL/6 male mice was used for the *in vivo* study of the hybrid NPs. This is the first *in vivo* study reporting anti-cancer effects of hybrid NPs with and without UV-A. A clinically applicable UV LED SMART device was used as the UV-A light source in PDT animal study. Because of the diverse growth pattern of the melanoma tumour, the animals had to be sacrificed on different days. Therefore, the TVI rate up to day 16 was found to be the most reliable data for evaluating the therapeutic efficacy of hybrid NPs alone and in PDT as it included the data from all mice.

Data from animal study showed that FZSiFA50 NPs had stronger antitumour activity than FZSiNPs, exhibiting TVI rate of 58.2% over 31.7%. When these two NPs were activated by UV-A, therapeutic efficiency was further improved with FZSiFA50NPs+UVD3 and FZSiNPs+UVD3 reaching TVI rate of 95% and 91%

respectively. In comparison, UV-A alone only had 65.6% (UVD0) and 48.8% (UVD3). These results showed correlation with various *in vitro* studies, suggesting hybrid NPs are indeed effective nano-PSs for PDT of cancer treatment. Their strong antitumour activity could be attributed to the ability of producing ROS in the tumour tissues/cells.

In the animal study, we also examined the time interval between UV irradiation and administration of a single dose of hybrid NPs on the antitumour activity of the hybrid NPs. UV-A irradiation of NPs with the 3-day interval proved to be more effective in tumour inhibition than no interval. Separating UV-A irradiation dosing from NPs treatment allowed the spread of treatment and probably served as two doses of treatment. Further, it provides time for the hybrid NPs to accumulate inside the tumour cells. During the entire study, there was no significant change in the body weight of the treatment groups compared to the control group, which proved the hybrid NPs were well tolerated by the mice when administered intra-tumourally. In terms of liver toxicity, the FZSiNPs+UVD3 group exhibited the most significant reduction in liver weight. This could be due to the toxicity arising from soluble zinc and iron as FZSi appeared to be decomposed faster than FZSi FA50, under the UV-A irradiation, in B16-F10 cells according to metal content study.

The objectives of the study were accomplished as the hybrid NPs have proved to be strong nano-PSs candidates for PDT, exhibiting effective antitumour activity against melanoma cells (both *in vitro* and *in vivo*) when activated by UV-A. This study confirmed the important role targeting ligand FA played in cellular uptake, cell apoptosis, necrosis and consequent impact on phototoxicity and antitumour activity. These hybrid NPs provide us better understanding in designing the semiconductor metal oxides-based nano-PS for PDT.

4.2 Limitations of the study and future work

This research project has successfully explored some of the unique features of using hybrid NPs as PSs in PDT and opens new research leads which could be investigated in the future. During this project, a few challenges were encountered and resolved. However, there are still some that remained. For instance, though we collected the vital organs during the animal study, we could not analyse the distribution of NPs in organs due to the time constrain. As the study involved PDT, multiple irradiation conditions should have been carried out *in vivo*. However, due to the limited resources towards the end of the project, we could not complete those tasks. Therefore, we propose the future studies to include:

- Anticancer effect of hybrid NPs with multiple radiation conditions with a designated time interval in animals.
- Quantitative assessment of the effect and oxidative stress caused by each free radical in ROS.
- Singlet oxygen generation in cells and the mechanisms behind cytotoxicity in 3T3 cells.
- Effect of nano PSs *in vivo* when administered by different routes of administration like i.v or i.p alone and in combination with PDT.
- Biodistribution of hybrid NPs in different organs and blood. Hematoxylin & Eosin (HE) staining of cellular and sub-cellular components in the organ tissues to study histological changes.
- Determination of the soluble metal ion concentrations in the tissues and tumours using ICP-MS.
- The influence of FA photodegradation on cytotoxicity and ROS.
- The antitumour effect of hybrid NPs being used as drug carrier as well as PSs in PDT in a combination therapy.

Although, this Ph.D has made a significant contribution to the knowledge base pertaining to the development of hybrid NPs as PSs in PDT against cancer. We expect that above-suggested research leads would further expand the knowledge and information that could guide the development of the next generation nano-PS in PDT. With the possibility of entrapping chemotherapeutic drugs inside the hybrid NPs, the

dual therapy (chemotherapy + PDT) will further extend the potential of the hybrid NPs used in this study.

4.3 Conclusion

To our best knowledge, to date, this is the first report on Fe₃O₄-ZnO hybrid NPs in combination with UV-A radiation against melanoma cells and melanoma tumours in an animal model. This study highlights the potential of silica and FA modified hybrid NPs as effective nano-PSs in PDT and important role the targeting ligand FA may play. The research in this thesis demonstrated phototoxicity of the nano-PSs and their synergistic effect with UV-A radiation which effectively inhibit the growth of melanoma cancer cells. This work also emphasized the importance of the time interval between NPs and UV-A irradiation *in vivo*. However, further in-depth *in vivo* studies are still required to explore the full potential of hybrid NPs as PSs in PDT, especially under multiple irradiation conditions with different route of administration and various tumours.

Overall this study has demonstrated that silica and FA modified hybrid NPs has fulfilled the criteria to be an effective nano-PS for PDT and its potential to be developed into a clinically relevant nano-PS in PDT.

References

- Abels, C. (2004). Targeting of the vascular system of solid tumours by photodynamic therapy (PDT). *Photochemical and Photobiological Sciences*, 3, 765-671.
- Abu Lila, A.S., & Ishida, T. (2017). Metronomic chemotherapy and nanocarrier platforms. *Cancer Letters*, 1, 400, 232-242.
- Abrahamse, H., & Hamblin, M.R. (2016). New photosensitizers for photodynamic therapy. *Biochemical Journal*, 15, 473 (4), 347-364.
- Agostinis, P., Berg, K., Cengel, K.A., Foster, T.H., Girotti, A.W., Gollnick, S.O.,... Golab, J. (2011). Photodynamic therapy of cancer: An update. *CA Cancer Journal for Clinicians*, 61(4), 250–281.
- Ahmad, J., Ahamed, M., Akhtar, M.J., Alrokayan, S.A., Siddiqui, M.A., Musarrat, J., & Al-Khedhairy, A.A. (2012). Apoptosis induction by silica nanoparticles mediated through reactive oxygen species in human liver cell line HepG2. *Toxicology and Applied Pharmacology*, 259(2), 160-168.
- Ai, J., Liu, B., & Liu, W. (2017). Folic acid-tagged titanium dioxide nanoparticles for enhanced anticancer effect in osteosarcoma cells. *Materials Science and Engineering*, C76, 1181-1187.
- Ajdari, M., & Ghahnavieh, M.Z. (2014). Histopathology effects of nickel nanoparticles on lungs, liver and spleen tissues in male mice. *International Nano Letters*, 4, 113
- Akhtar, M.J., Ahamed, M., Alhadlaq, H.A., Alrokayan, S.A., & Kumar, S. (2014). Targeted anticancer therapy: Overexpressed receptors and nanotechnology. *Clinica Chimica Acta*, 436C, 78-92.
- Akhtar, M.J., Ahamed, M., Kumar, S., Khan, M.M., Ahmad, J., & Alrokayan, S.A. (2012). Zinc oxide nanoparticles selectively induce apoptosis in human cancer cells through reactive oxygen species. *International Journal of Nanomedicine*, 7, 845-57.
- Alarifi, S., Ali, D., Alkahtani, S., Verma, A., Ahamed, M., Ahmed, M., & Alhadlaq, H.A. (2013). Induction of oxidative stress, DNA damage, and apoptosis in a malignant human skin melanoma cell line after exposure to zinc oxide nanoparticles. *International Journal of Nanomedicine*, 8, 983-93.
- Alarifi, S., Ali, D., Alkahtani, S., & Almeer, R.S. (2017). ROS mediated apoptosis and genotoxicity induced by palladium nanoparticles in human skin malignant melanoma cells. *Oxidative Medicine and Cellular Longevity*, 8439098.
- Alam, M.F., Rahim, S., Atif, M., & Majid, A. (2014). ZnO nanoparticles as drug delivery agent for photodynamic therapy. *Laser Physics Letters*, 11, 2.
- Allison, R.R., Mota, H.C., Bagnato, V.S., & Sibata, C.H. (2008). Bio-nanotechnology and photodynamic therapy--state of the art review. *Photodiagnosis and Photodynamic Therapy*, 5(1), 19-28.

Allison, R.R., & Moghissi, K. (2013). Photodynamic Therapy (PDT): PDT Mechanisms. *Clinical Endoscopy*, 46(1), 24–29.

American cancer society [Accessed on 18/Sep/2017] Retrieved from <https://www.cancer.org/research/cancer-facts-statistics/all-cancer-facts-figures/cancer-facts-figures-2017.html>

Anand, K., & Siby, V. (2017). Role of surfactants on the stability of nano-zinc oxide dispersions. *Particulate Science and Technology*, 35, 67-70.

Anbu, S., Velmurugan, P., Lee, J.H., Oh, B.T., & Venkatachalam, P. (2016). Biomolecule-loaded chitosan nanoparticles induce apoptosis and molecular changes in cancer cell line (SiHa). *International Journal of Biological Macromolecules*, 88, 18-26.

Anderle, P., Niederer, E., Rubas, W., Hilgendorf, C., Spahn-Langguth, H., Wunderli-Allenspach, H.,... Langguth, P. (1998). P-Glycoprotein (P-gp) mediated efflux in Caco-2 cell monolayers: the influence of culturing conditions and drug exposure on P-gp expression levels. *Journal of Pharmaceutical Sciences*, 87(6), 757-62.

Anders, C.B., Chess, J.J., Wingett, D.G., & Punnoose, A. (2015). Serum Proteins Enhance Dispersion Stability and Influence the Cytotoxicity and Dosimetry of ZnO Nanoparticles in Suspension and Adherent Cancer Cell Models. *Nanoscale Research Letters*, 10, 448.

Aranda, A., Sequedo, L., Tolosa, L., Quintas, G., Burello, E., Castell, J.V., & Gombau, L. (2013). Dichloro-dihydro-fluorescein diacetate (DCFH-DA) assay: A quantitative method for oxidative stress assessment of nanoparticle-treated cells. *Toxicology In vitro*, 27, 954-963.

Arruebo, M., Vilaboa, N., Saez-Gutierrez, B., Lambea, J., Tres, A., Valladares, M., & Gonzalez-Fernandez, A. (2011). Assessment of the Evolution of Cancer Treatment Therapies. *Cancers*, 3, 3279-3330.

Australian Government, Cancer Australia [Accessed on 18/Sep/2017] Retrieved from <https://canceraustralia.gov.au/affected-cancer/what-cancer/cancer-australia-statistics>

Baek, M., Chung, H.E., Yu, J., Lee, J.A., Kim, T.H., Oh, J.M.,...Choi, S.J. (2012). Pharmacokinetics, tissue distribution, and excretion of zinc oxide nanoparticles. *International Journal of Nanomedicine*, 7, 3081-97.

Baird, F.J., Wadsworth, M.P., & Hill, J.E. (2012). Evaluation and optimization of multiple fluorophore analysis of a *Pseudomonas aeruginosa* biofilm. *Journal of microbiological methods*, 90, 3, 192-196.

Beack, S., Kong, W.H., Jung, H.S., Do, I.H., Han, S., Kim, H.,...Hahn, S.K. (2015). Photodynamic therapy of melanoma skin cancer using carbon dot - chlorin e6 - hyaluronate conjugate. *Acta Biomaterialia*, 26, 295-305.

- Bahrami, B., Hojjat-Farsangi, M., Mohammadi, H., Anvari, E., Ghalamfarsa, G., Yousefi, M., & Jadidi-Niaragh, F. (2017). Nanoparticles and targeted drug delivery in cancer therapy. *Immunology Letters*, 29, 190, 64-83.
- Baskar, R., Lee, K.A., Yeo, R., & Yeoh, K. (2012). Cancer and Radiation therapy: current advances and future directions. *International Journal of Medical Sciences*, 9(3), 193-199.
- Berardis, B., Civitelli, G., Condello, M., Lista, P., Pozzi, R., Arancia, G., & Meschini, S. (2010). Exposure to ZnO nanoparticles induces oxidative stress and cytotoxicity in human colon carcinoma cells. *Toxicology and Applied Pharmacology*, 246, 116-127.
- Berroeta, L., Clark, C., Dawe, R.S., Ibbotson, S.H., & Fleming, C.J. (2007). A randomized study of minimal curettage followed by topical photodynamic therapy compared with surgical excision for low-risk nodular basal cell carcinoma. *British Journal of Dermatology*, 157, 401-403.
- Bhat, S.S., Qurashi, A., & Khanday, F.A. (2017). ZnO nanostructures based biosensors for cancer and infectious disease applications: Perspectives, prospects and promises. *TrAC Trends in Analytical Chemistry*, 86, 1-13.
- Bottero, F., Tomassetti, A., Canevari, S., Miotti, S., Ménard, S., & Colnaghi, M.I. (1993). Gene transfection and expression of the ovarian carcinoma marker folate binding protein on NIH/3T3 cells increases cell growth in vitro and in vivo. *Cancer Research*, 1, 53(23), 5791-5796.
- Brown, S.B., Brown, E.A., & Walker, I. (2004). The present and future role of photodynamic therapy in cancer treatment. *The Lancet Oncology*, 5(8), 497-508.
- Cadenas, E., & Davies, K.J. (2000). Mitochondrial free radical generation, oxidative stress, and aging. *Free Radical Biology & Medicine*, 29(3-4), 222-30.
- Castano, A.P., Mroz, P., & Hamblin, M.R. (2006). Photodynamic therapy and anti-tumour immunity. *Nature Reviews of Cancer*, 6, 535-545.
- Chadwick, S.J., Salah, D., Livesey, P.M., Brust, M., & Volk, M. (2016). Singlet oxygen generation by laser irradiation of gold nanoparticles. *The Journal of Physical Chemistry. C, Nanomaterials and Interfaces*, 120(19), 10647-10657.
- Chandrasekaran, M & Pandurangan, M. (2016). In Vitro Selective Anti-Proliferative Effect of Zinc Oxide Nanoparticles Against Co-Cultured C2C12 Myoblastoma Cancer and 3T3-L1 Normal Cells. *Biological Trace Element Research*, 172(1), 148-54.
- Chang, J., Yoon, I., Sung, P., Yi, E., Jheon, S., & Shim, S. (2014). Anticancer efficacy of photodynamic therapy with hematoporphyrin-modified, doxorubicin-loaded nanoparticles in liver cancer. *Journal of Photochemistry and Photobiology B: Biology*, 140, 49-56.

- Chatterjee, D.K., Fong, L.S., & Zhang, Y. (2008). Nanoparticles in photodynamic therapy: an emerging paradigm. *Advanced Drug Delivery Reviews*, 14, 60(15), 1627-37.
- Chatterjee, K., Sarkar, S., Jagajjanani Rao, K., & Paria, S. (2014). Core/shell nanoparticles in biomedical applications. *Advances in Colloid and Interface Science*, 209, 8-39.
- Chen, B., Pogue, B.W., Goodwin, I.A., O'Hara, J.A., Wilmot, C.M., Hutchins, J.E.,... Hasan, T. (2003). Blood flow dynamics after photodynamic therapy with verteporfin in the RIF-1 tumour. *Radiation Research*, 160, 452-459.
- Chen, Y.L., Chang, M.C., & Cheng, W.F. (2017). Metronomic chemotherapy and immunotherapy in cancer treatment. *Cancer Letters*, 1, 400, 282-292.
- Chen, W., & Zhang, J. (2006). Using nanoparticles to enable simultaneous radiation and photodynamic therapies for cancer treatment. *Journal of Nanoscience and Nanotechnology*, 6, 4, 1159-1166.
- Chen, J., Li, S., Shen, Q., He, H., & Zhang, Y. (2011). Enhanced cellular uptake of folic acid-conjugated PLGA-PEG nanoparticles loaded with vincristine sulfate in human breast cancer. *Drug Development and Industrial Pharmacy*, 37, 11, 1339-46.
- Chen, Z., Xu, P., Chen, J., Chen, H., Xu, P., Chen, X.,... Huang, M. (2014). Zinc phthalocyanine conjugated with the amino-terminal fragment of urokinase for tumour-targeting photodynamic therapy. *Acta Biomaterialia*, 10, 4257-4268.
- Chen, Y., Tezcan, O., Li, D., Beztsinna, N., Lou, B., Etrych, T.,... Hennink, W.E. (2017). Overcoming multidrug resistance using folate receptor-targeted and pH-responsive polymeric nanogels containing covalently entrapped doxorubicin. *Nanoscale*, 9, 10404-10419.
- Chia, S.L., Tay, C.Y., Setyawati, M.I., & Leong, D.T. (2016a). Decoupling the Direct and Indirect Biological Effects of ZnO Nanoparticles Using a Communicative Dual Cell-Type Tissue Construct. *Small*, 3, 12, 647-57.
- Chia, S.L., & Leong, D.T. (2016b). Reducing ZnO nanoparticles toxicity through silica coating. *Heliyon*, 2, 10, 177.
- Choi, B.M., Pae, H.O., Jang, S.I., Kim, Y.M., & Chung, H.T. (2002). Nitric oxide as a pro-apoptotic as well as anti-apoptotic modulator. *Journal of Biochemistry and Molecular Biology*, 35, 116-126.
- Chummun, S., & Mc Lean, N.R. (2017). The management of malignant skin cancers. *Surgery (Oxford)*, 32, 9, 485-490.
- Craythome, E., & Al-Niami, F. (2017). Skin cancer. *Medicine*, 45, 7, 431-434.
- Csogor, Z.S., Nacken, M., Sameti, M., Lehr, C.M., & Schmidt, H. (2003). Modified silica particles for gene delivery. *Materials Science and Engineering: C*, 23, 93-97.

- Dąbrowski, J.M., Pucelik, B., Regiel-Futyra, A., Brindell, M., Mazuryk, O., Kyzioł, A.,... Arnaut, L.G. (2016). Engineering of relevant photodynamic processes through structural modifications of metallotetrapyrrolic photosensitizers. *Coordination Chemistry Reviews*, 325, 67-101.
- Dai, T., Fuchs, B.B., Coleman, J.J., Prates, R.A., Astrakas, C., St. Denis, T.G.,...Tegos, G.P. (2012). Concepts and Principles of Photodynamic Therapy as an Alternative Antifungal Discovery Platform. *Frontiers in Microbiology*, 3, 120.
- Dahle, J., Kaalhus, O., Moan, J., & Steen, H.B. (1997). Cooperative effects of photodynamic treatment of cells in microcolonies. *Proceedings of the National Academy of Sciences of the United States of America*, 94, 1773-1778.
- Daiana, D., & Koiti, A. (2015). Nanotechnology, Light and Chemical Action: an Effective Combination to Kill Cancer Cells. *Journal of Brazilian Chemical Society*, 26, 12, 2448-2470.
- Damsky, Jr, W.E., Rosenbaum, L.E., & Bosenberg, M. (2011). Decoding melanoma metastasis. *Cancers*, 3, 126-163.
- Davids, L.M., & Kleemann, B. (2011). Combating melanoma: the use of photodynamic therapy as a novel, adjuvant therapeutic tool. *Cancer Treat Reviews*, 37(6), 465-75.
- DeRosa, M.C., & Crutchley, R.J. (2002). Photosensitized singlet oxygen and its applications. *Coordination Chemistry Reviews*, 233-234, 351-371.
- De Gruijl, F.R.(1999). Skin Cancer and Solar UV Radiation. *European Journal of Cancer*, 35, 14, 2003-2009.
- De Berardis, B., Civitelli, G., Condello, M., Lista, P., Pozzi, R., Arancia, G., & Meschini, S. (2010). Exposure to ZnO nanoparticles induces oxidative stress and cytotoxicity in human colon carcinoma cells. *Toxicology and Applied Pharmacology*, 246(3), 116-27.
- Deng, X., Xiong, L., Lin, L., Xiong, G., & Miao, X. (2013). Photosan-II loaded hollow silica nanoparticles: preparation and its effect in killing for QBC939 cells. *Photodiagnosis and Photodynamic Therapy*, 10(4), 460-9.
- Dolmans, D.E., Fukumura, D., & Jain, R.K. (2003). Photodynamic therapy for cancer. *Nature Reviews Cancer*, 3, 380-387.
- Dominguez-Medina, S., Blankenburg, J., Olson, J., Landes, C.F., & Link, S. (2013). Adsorption of a Protein Monolayer via Hydrophobic Interactions Prevents Nanoparticle Aggregation under Harsh Environmental Conditions. *ACS Sustain Chemical Engineering*, 1, 1(7), 833-842.
- Dougherty, T.J., Gomer, C.J., Henderson, B.W, Jori, G., Kessel, D., Korblick, M.,...Peng, Q. (1998). Photodynamic therapy. *Journal of the National Cancer Institute*, 90, 889-905.

- Dougherty, T.J. (1993). Photodynamic Therapy. *Journal of Photochemistry and Photobiology*, 58, 895-900.
- Dougherty, T.J. (1989). Photodynamic therapy-new approaches. *Seminars in Surgical Oncology*, 5, 6-16.
- Dougherty, T.J., Kaufman, J.E., Goldfarb, A., Weishaupt, K.R., Boyle, D., & Mittleman, A. (1978). Photoradiation therapy for the treatment of malignant tumours. *Cancer Research*, 38, 2628-2635.
- Eide, D.J. (2006). Zinc transporters and the cellular trafficking of zinc. *Biochimica et Biophysica Acta*, 1763(7), 711-22.
- Eigenmann, D.E., Xue, G., Kim, K.S., Moses, A.V., Hamburger, M., & Oufir, M. (2013). Comparative study of four immortalized human brain capillary endothelial cell lines, hcMEC/D3, HBMEC, TY10, and BB19, and optimization of culture conditions, for an in vitro blood-brain barrier model for drug permeability studies. *Fluids and Barriers of the CNS*, 10 (1), 1-17.
- Fahmy, R.G., Dass, C.R., Sun, L.Q., Chesterman, C.N., & Khacigian, L.M. (2003). Transcription factor Egr-1 supports FGF-dependent angiogenesis during neovascularization and tumour growth. *Nature Medicine*, 9(8), 1026-1032.
- Feng, X., Zhang, S., Wu, H., & Lou, X. (2015a). A novel folic acid-conjugated TiO₂-SiO₂ photosensitizer for cancer targeting in photodynamic therapy. *Colloids and Surfaces B: Bio interfaces*, 125, 197-205.
- Feng, X., & Lou, X. (2015b). The effect of surfactants-bound magnetite (Fe₃O₄) on the photocatalytic properties of the heterogeneous magnetic zinc oxides nanoparticles. *Separation and Purification Technology*, 147, 266-275.
- Feng, X., Guo, H., Patel, K., Zhou, H., & Lou, X. (2014). High performance, recoverable Fe₃O₄ZnO nanoparticles for enhanced photocatalytic degradation of phenol. *Chemical Engineering Journal*, 244, 327-334.
- Feng, X., Zhang, S., & Lou, X. (2013). Controlling silica coating thickness on TiO₂ nanoparticles for effective photodynamic therapy. *Colloids and Surfaces B: Biointerfaces*, 107, 220-226.
- FITC, Sigma-Aldrich [Accessed on 30/Jan/2018] Retrieved from <https://www.sigmaaldrich.com/catalog/product/sigma/f7250?lang=en®ion=AU>
- Fokas, E., & Rödel, C. (2016). Targeted agents in GI radiotherapy: Clinical efficacy and side effects. *Best Practice and Research Clinical Gastroenterology*, 30, 4, 537-549.
- Fukui, H., Horie, M., Endoh, S., Kato, H., Fujita, K., Nishio, K.,... Iwahashi, H. (2012). Association of zinc ion release and oxidative stress induced by intratracheal instillation of ZnO nanoparticles to rat lung. *Chemico-Biological Interactions*, 198(1-3), 29-37.

- Friedrich, J., Eder, W., Castaneda, J., Doss, M., Huber, E., Ebner, R., & Kunz-Schughart, L.A. (2007). A reliable tool to determine cell viability in complex 3-d culture: the acid phosphatase assay. *Journal of Biomolecular Screening*, 12(7), 925-37.
- Gao, S., Wang, G., Qin, Z., Wang, X., Zhao, G., Ma, Q., & Zhu, L. (2017). Oxygen-generating hybrid nanoparticles to enhance fluorescent/photoacoustic/ultrasound imaging guided tumour photodynamic therapy. *Biomaterials*, 112, 324-335.
- Gary-Bobo, M., Hocine, O., Brevet, D., Maynadier, M., Raehm, L., Richeter, S.,... Durand, J.O. (2012). Cancer therapy improvement with mesoporous silica nanoparticles combining targeting, drug delivery and PDT. *International Journal of Pharmaceutics*, 28, 423(2), 509-15.
- Gatoo, M.A., Naseem, S., Arfat, A.Y., Dar, A.M., Qasim, K., & Zubair, S. (2014). Physicochemical properties of nanomaetrial: Implication in associated toxic manifestattions. *Biomed Research International*, 498420, 1-8.
- Geran, R.I., Greenberg, N.H., Macdonald, M.M., Schumacher, A.M., & Abbott, B.J. (1972). Protocols for screening chemical agents and natural products against animal tumours and other biological systems (3rd edition). *Cancer Chemotherapy Reports*, 3: 1-88.
- Gilissen, M.J., van de Merbel-de Wit, L.E., Star, W.M., Koster, J.F., & Sluiter, W. (1993). Effect of photodynamic therapy on the endothelium-dependent relaxation of isolated rat aortas. *Cancer Research*, 53, 2548-2552.
- Gomer, C.J., Rucker, N., Ferrario, A., & Wong, S. (1989). Properties and applications of photodynamic therapy. *Radiation Research*, 120, 1-18.
- Gomes, A., Fernandes, E., & Lima, J.L.F.C. (2005). Fluorescence probes used for detection of reactive oxygen species. *Journal of Biochemical and Biophysical Methods*, 65, 45-80.
- Guo, D., Wu, C., Jiang, H., Li, Q., Wang, X., & Chen, B. (2008). Synergistic cytotoxic effect of different sized ZnO nanoparticles and daunorubicin against leukemia cancer cells under UV irradiation. *Journal of Photochemistry and Photobiology B*, 93(3), 119-26.
- Gupta, A., Avci, P., Sadasivam, M., Chandran, R., Parizotto, N., Vecchio, D.,...Hamblin, M.R. (2013). Shining light on nanotechnology to help repair and regeneration. *Biotechnology Advances*, 31(5), 607-631.
- Hackenberg, S., Scherzed, A., Harnisch, W., Froelich, K., Ginzkey, C., Koehler, C.,...Kleinsasser, N. (2012). Antitumour activity of photo-stimulated zinc oxide nanoparticles combined with paclitaxel or cisplatin in HNSCC cell lines. *Journal of Photochemistry and Photobiology B*, 114, 87-93.
- Hanley, C., Layne, J., Punnoose, A., Reddy, K.M., Coombs, I., Coombs, A.,...Wingett, D. (2008). Preferential killing of cancer cells and activated human T cells using ZnO nanoparticles. *Nanotechnology*, 19, 29.

- Han, Y., Kiat-amnuay, S., Powers, J. M., & Zhao, Y (2008). Effect of nano-oxide concentration on the mechanical properties of a maxillofacial silicone elastomer. *The Journal of Prosthetic Dentistry*, 100(6), 465–473.
- Hariharan, R., Senthil Kumar, S., & Suganthi, A. (2013). Synthesis and characterization of daunorubicin modified ZnO/PVP nanorods and its photodynamic action. *Journal of Photochemistry and Photobiology A: Chemistry*, 252,107-115.
- Hassanpour, S.H., & Dehghani, M. (2017). Review of cancer from perspective of molecular. *Journal of Cancer Research and Practice*, 4, 127-129.
- Haylett, A.K., Ross, S., Truscott, T.G., & Moore, J.V. (1995). Pharmacokinetic and therapeutic outcome in melanoma cells of the administration of symmetric and asymmetric cationic photosensitizers. *Cancer Letters*, 88, 191-199.
- He, C., Lu, J., & Lin, W. (2015). Hybrid nanoparticles for combination therapy of cancer. *Journal of Controlled Release*, 219, 224-236.
- Heim, J., Felder, E., Tahir, M.N., Kaltbeitzel, A., Heinrich, U.R., Brochhausen, C.,...Breiger, J. (2015). Genotoxic effects of zinc oxide nanoparticles. *Nanoscale*, 7, 8931.
- Henderson, B.W., & Fingar, V.H. (1987). Relationship of tumour hypoxia and response to photodynamic treatment in an experimental mouse tumour. *Cancer Research*, 47, 3110- 3114.
- Henderson, B.W., Busch, T.M., & Snyder, J.W. (2006). Fluence rate as a modulator of PDT mechanisms. *Lasers in Surgery and Medicine*, 38, 489-493.
- Hoet, P.H.M., Brueske-Hohlfeld, I., & Salata, O. (2004). Nanoparticles—known and unknown health risks. *Journal of Nanotoxicology*, 2, 1–2.
- Hoffman, S.J., Yohn, J.J., Norris, D.A., Smith, C.M., & Robinson, W.A. (1993). Cutaneous malignant melanoma. *Current Problems in Dermatology*, 7-41.
- Hong, T.K., Tripathy, N., Son, H., Ha, K., Jeong, H., & Hahn, Y. (2013). A comprehensive in vitro and in vivo study of ZnO nanoparticles toxicity. *Journal of Materials Chemistry B*, 1(23), 2985.
- Hu, Z., Li, J., Li, C., Zhao, S., Li, N., Wang, Y.,...Huang, Y. (2013). Folic acid-conjugated graphene–ZnO nanohybrid for targeting photodynamic therapy under visible light irradiation. *Journal of Materials Chemistry B*, 38, 1, 5003-5013.
- Huarac, J.C.B., Tomar, M.S., Singh, S.P., Perales-Perez, O., Rivera, L., & Pena, S. (2010). Multifunctional Fe₃O₄/ZnO core-shell nanoparticles for photodynamic therapy. *Nanotech*, 3, 405-408.
- Huang, Y., Vecchio, D., Avci, P., Yin, R., Garcia-Diaz, M., & Hamblin, M.R. (2013). Melanoma resistance to photodynamic therapy: new insights. *Biological Chemistry*, 394 (2), 239-250.

- Indran, I.R., Tufo, G., Pervaiz, S., & Brenner, C. (2011). Recent advances in apoptosis, mitochondria and drug resistance in cancer cells. *Biochimica et Biophysica Acta*, 1807, 735-745.
- Ismail, A.F.M., Ali, M.M., & Ismail, L.F.M. (2014). Photodynamic therapy mediated antiproliferative activity of some metal-doped ZnO nanoparticles in human liver adenocarcinoma HepG2 cells under UV irradiation. *Journal of Photochemistry and Photobiology B: Biology*, 5, 138, 99-108.
- Ismail, L.F.M., Emara, M.M., El-Moselhy, M.M., Maziad, N.A., & Hussein, O.K. (2014). Silica coating and photocatalytic activities of ZnO nanoparticles: Effect of operational parameters and kinetic study. *Spectrochimica Acta Part A: Molecular and Biomolecular Spectroscopy*, 131, 158-168.
- Ivankovic, S., Music, S., Gotic, M., & Ljubescic, N. (2006). Cytotoxicity of nanosize V2O5 particles to selected fibroblast and tumour cells. *Toxicology In vitro*, 20, 286-294.
- Kalluru, P., Vankalaya, R., Chiang, C., & Hwang, K.C. (2016). Nano-graphene oxide-mediated In vivo fluorescence imaging and bimodal photodynamic and photothermal destruction of tumours. *Biomaterials*, 95, 1-10.
- Kang, T., Guan, R., Chen, X., Song, Y., Jiang, H., & Zhao, J. (2013). In vitro toxicity of different-sized ZnO nanoparticles in Caco-2 cells. *Nanoscale Research Letters*, 21, 8(1), 496.
- Kang, Z., Yan, X., Zhao, L., Liao, Q., Zhao, K., Du, H.,...Zhang, Y. (2015). Gold nanoparticle/ZnO nanorod hybrids for enhanced reactive oxygen species generation and photodynamic therapy. *Nanoresearch*, 8, 6, 2004-2014.
- Karbalaei, A., Mohammadalipour, Z., Rahmati, M., Khataee, A., & Moosavi, M.A. (2016). GO/TiO₂ Hybrid Nanoparticles as a New Photosensitizer in photodynamic Therapy of A375 Melanoma cancer cells. *Skin and Stem Cell Journal*, 3(2), 1-5.
- Karrer, S., Szeimies, R.M., Hohenleutner, U., & Landthaler, M. (2001). Role of lasers and photodynamic therapy in the treatment of cutaneous malignancy. *American Journal of Clininical Dermatology*, 2(4), 229-37.
- Kessler, D & Oleinick, N.L. (2018). Cell death pathways associated with photodynamic therapy: An update. *Photochemistry and Photobiology*, doi: 10.1111/php.12857.
- Kim, I., Joachim, E., Choi, H., & Kim, K. (2015). Toxicity of silica nanoparticles depends on size, dose, and cell type. *Nanomedicine: Nanotechnology, Biology and Medicine*, 11, 6, 1407-1416.
- Kim, K.M., Kim, T.H., Kim, H.M., Kim, H.J., Gwak, G.H., Paek, S.M., & Oh, J.M. (2012). Colloidal behaviors of ZnO nanoparticles in various aqueous media. *Toxicology and Environmental Health Sciences*, 4, 2, 121-131.

- Khaing Oo, M.K., Yang, Y., Hu, Y., Gomez, M., Du, H., & Wang, H. (2012). Gold Nanoparticle-Enhanced and Size-Dependent Generation of Reactive Oxygen Species from Protoporphyrin IX. *ACS Nano*, 6 (3), 1939–1947.
- Kooijmans, S.A.A., Senyschyn, D., Mazhiselvam, M.M., Morizzi, J., Charman, S.A., Weksler, B.,...Nicolazzo, J.A. (2012). The involvement of a Na⁺ and Cl⁻ Dependent transporter in the brain uptake of Amantadine and Rimantadine. *Molecular Pharmaceutics*, 9 (4), 883-893.
- Krukiewicz, K., & Zak, J.K. (2016). Biomaterial-based regional chemotherapy: Local anticancer drug delivery to enhance chemotherapy and minimize its side-effects. *Materials Science and Engineering: C*, 62, 927-942.
- Krutmann, J., & Morita, A. (1999). Mechanisms of ultraviolet (UV) B and UVA phototherapy. *The Journal of Investigative Dermatology Symposium Proceedings*, 4(1), 70-2.
- Lambert, C.A., Garbacki, N., & Colige, A.C. (2017). Chemotherapy induces alternative transcription and splicing: Facts and hopes for cancer treatment. *The International Journal of Biochemistry and Cell Biology*, 91, 84-97.
- Lammers, T., Peschke, P., Kuhnlein, R., Subr, V., Ulbrich, K., Huber, P.,...Storm, G. (2006). Effect of Intratumoural Injection on the Biodistribution and the Therapeutic Potential of HPMA Copolymer-Based Drug Delivery Systems. *Neoplasia*, 8(10), 788-795.
- Lee, C.H., Lai, P.S., Lu, Y.P., Chen, H.Y., Chai, C.Y., Tsai, R.K.,...Tsai, D.P. (2015). Real-time vascular imaging and photodynamic therapy efficacy with micelle-nanocarrier delivery of chlorin e6 to the microenvironment of melanoma. *Journal of Dermatological Science*, 80(2), 124-32.
- Lepor, H. (2008). Vascular targeted photodynamic therapy for localized prostate cancer. *Reviews in Urology*, 10, 4.
- Lesniak, A., Salvati, A., Santos-Martinez, M.J., Radomski, M.W., Dawson, K.A., & Aberg, C. (2013). Nanoparticle adhesion to the cell membrane and its effect on nanoparticle uptake efficiency. *Journal of the American Chemical Society*, 135(4), 1438-44.
- Li, J., Wang, Y., Liang, R., An, X., Wang, K., Shen, G.,...Tao, J. (2015). Recent advances in targeted nanoparticles drug delivery to melanoma. *Nanomedicine*, 11(3), 769-94.
- Li, J., Wang, S., Han, J., Xu, H., Xu, X., & Xue, J. (2017). Inhibition of Yuyihe Powder on Tumour Growth in Mice Models of Sarcoma 180. *Chinese Herbal Medicines*, 9(2), 183-187.
- Li, J., Guo, D., Wang, X., Wang, H., Jiang, H., & Chen, B. (2010). The photodynamic effect of different size ZnO Nanoparticles on cancer cell proliferation In vitro. *Nanoscale Research Letters*, 5, 1063-1071.

- Li, D., & Haneda, H. (2003). Morphologies of zinc oxide particles and their effects on photocatalysis. *Chemosphere*, 51 (2), 129-137.
- Li, W.T. (2013). Nanoparticles for photodynamic therapy. Handbook of Biophotonics. Volume 2, US, John Wiley & Sons, P321-336.
- Liberman, A., Mendez, N., Trogler, W.C., & Kummel, A.C. (2014). Synthesis and surface functionalization of silica nanoparticles for nanomedicine. *Surface Science Reports*, 69, (2-3), 132-158.
- Lim, C., Heo, J., Shin, S., Jeong, K., Seo, Y.H., Jang, W.,...Won, I.C.K. (2013). Nanophotosensitizers toward advanced photodynamic therapy of cancer. *Cancer Letters*, 334 (2),176-187.
- Liou, G., & Storz, P. (2010). Reactive oxygen species in Cancer. *Free Radical Research*, 44 (5).
- Liu, F., Garcia, A.M.G., & Meyskens, F.L. (2012). *Journal of Investigative Dermatology*, 132, 8, 2033-2041.
- Longmire, M., Choyke, P.L., & Kobayashi, H. (2008). Clearance properties of Nano-sized particles and molecules as imaging agents: considerations and caveats. *Nanomedicine (Lond)*, 3(5), 703-717.
- Lu, J., Li, Z., Zink, J.I., & Tamanoi, F. (2012). In vivo tumour suppression efficacy of mesoporous silica nanoparticles-based drug-delivery system: enhanced efficacy by folate modification. *Nanomedicine*, 8(2), 212-20.
- Lu, S., Zhang, W., Zhang, R., Liu, P., Wang, Q., Shang, Y.,...Wang, Q. (2015). Comparison of cellular toxicity caused by ambient ultrafine particles and engineered metal oxide nanoparticles. *Particle and Fibre Toxicology*, 12, 5.
- Lucky, S.S., Soo, K.C., & Zhang, Y. (2015). Nanoparticles in photodynamic therapy. *Chemical Reviews*, 25, 115 (4), 1990-2042.
- Luengas, S.L., Marin, G.H., Aviles, K., Acuna, R.C., Roque, G., Nieto, F.R.,... Mansilla, E. (2014). Enhanced Singlet Oxygen Production by Photodynamic Therapy and a Novel Method for Its Intracellular Measurement. *Cancer Biotherapy and Radiopharmaceuticals*, 1, 29(10), 435-443.
- Luo, M., Shen, C., Feltis, B.N., Martin L.L., Hughes, A.E., & Wright, P.F. (2014). Reducing ZnO nanoparticles cytotoxicity by surface modification. *Nanoscale*, 7, 6 (11), 5791-8.
- Luo, y., Chang, C.K., & Kessel, D. (1996). Rapid initiation of apoptosis by photodynamic therapy. *Photochemistry and Photobiology*, 63, 528-534.
- Ma, X., Qu, Q., & Zhao, Y. (2015). Targeted delivery of 5-aminolevulinic acid by multifunctional hollow mesoporous silica nanoparticles for photodynamic skin cancer therapy. *ACS Applied Materials and Interfaces*, 27, 7(20), 10671-6.

- Ma, Y., Ding, H., & Xiong, H. (2015). Folic acid functionalized ZnO quantum dots for targeted cancer cell imaging. *Nanotechnology*, 26, 30.
- Maddodi, N., Jayanthi, A., & Setaluri, V. (2012). Shining light on skin pigmentation: The darker and the brighter side of effects of UV radiation. *Photochemistry and Photobiology*, 88(5), 1075-1082.
- Majno, G., & Joris, I. (1995). Apoptosis, oncosis, and necrosis. An overview of cell death. *American Journal of Pathology*, 146, 3-15.
- Malvindi, M.A., Matteis, V.D., Galeone, A., Brunetti, V., Anyfantis, G.C., Athanassiou, A.,...Pompa, P.P. (2014). Toxicity assessment of silica coated Iron oxide nanoparticles and biocompatibility improvement by surface engineering. *Plos One*, 9 (1), e85835.
- Mang, T.S. (2004). Lasers and light sources for PDT: Past, present and future. *Photodiagnosis and Photodynamic Therapy*, 1, 43-48.
- Manke, A., Wang, L., & Rojanasakul, Y. (2013). Mechanisms of nanoparticle-induced oxidative stress and toxicity. *Biomed Research International*, 942916, 1-15.
- Mazonakis, M., & Damilakis, J. (2017). Cancer risk after radiotherapy for benign diseases. *Physica Medica*, 8, S1120-1797, (17), 30015-7.
- McEwan, C., Nesbitt, H., Nicholas, D., Kavanagh, O.N., McKenna, K., Loan, P.,...Callan, J.F. (2016). Comparing the efficacy of photodynamic and sonodynamic therapy in non-melanoma and melanoma skin cancer. *Bioorganic and Medicinal Chemistry*, 1, 24(13), 3023-3028.
- Melanoma Institute, Australia [Accessed on: 13/Aug/2017] Retrieved from <https://www.melanoma.org.au/>
- Mellier, G., & Pervaiz, S. (2012). The three Rs along the TRAIL: Resistance, re-sensitization and reactive oxygen species (ROS). *Free Radical Research*, 46(8), 996-1003.
- Mion, G., Gianferrara, T., Bergamo, A., Gasser, G., Pierroz, V., Rubbiani, R.,... Alessio, E. (2015). Phototoxic Activity and DNA Interactions of Water-Soluble Porphyrins and Their Rhenium(I) Conjugates. *ChemMedChem*, 10(11), 1901-14.
- Mirzaei, H., & Darroudi, M. (2017). Zinc oxide nanoparticles: biological synthesis and biomedical applications. *Ceramics International*, 43, 907- 914.
- Moan, J., & Peng, Q. (2003). An outline of the hundred-year history of PDT. *Anticancer Research*, 23, (5A), 3591-600.
- Mohammadi, Z., Sazgarnia, A., Rajabi, O., Soudmand, S., Esmaily, H., & Sadeghi, H.R. (2013). An in vitro study on the photosensitivity of 5-aminolevulinic acid conjugated gold nanoparticles. *Photodiagnosis and Photodynamic Therapy*, 10(4), 382-388.

- Morton, C.A., McKenna, K.E., & Rhodes, L.E. (2008). Guidelines for topical photodynamic therapy: update. *British Journal of Dermatology*, 159, 1245-1266.
- Morton, C.A., Szeimies, R.M., Sidoroff, A., & Braathen, L.R. (2013). European guidelines for topical photodynamic therapy part 1: Treatment delivery and current indications - actinic keratosis, Bowen's disease, basal cell carcinoma. *Journal of the European Academy of Dermatology and Venerology*, 27, 536-544.
- Mosmann, T. (1983). Rapid colorimetric assay for cellular growth and survival: Application to proliferation and cytotoxicity assays. *Journal of Immunological Methods*, 65, 55-63.
- Mroz, P., Yaroslavsky, A., Kharkwal, G.B., & Hamblin, M.R. (2011). Cell death pathways in photodynamic therapy of cancer. *Cancers*, 3, 2516-2539.
- Mudshinge, S.R., Deore, A.B., Patil, S., & Bhalgat, C.M. (2011). Nanoparticles: Emerging carriers for drug delivery. *Saudi Pharmaceutical Journal*, 19, 3, 129-141.
- Nadhman, A., Nazir, S., Khan, M.I., Arooj, S., Bakhtiar, M., Shahnaz, G., & Yasinzai, M. (2014). PEGylated silver doped zinc oxide nanoparticles as novel photosensitizers for photodynamic therapy against Leishmania. *Free Radical Biology and Medicine*, 77, 230-238.
- Nazir, S., Hussain, T., Ayub, A., Rashid, U., & macRobert, A.J. (2014). Nanomaterials in combating cancer: Therapeutic applications and developments. *Nanomedicine: Nanotechnology, Biology and Medicine*, 10, 19-34.
- Nedyalkova, M., Donkova, B., Romanova, J., Tzvetkov, G., Madurga, S., & Simeonov, V. (2017). Iron oxide nanoparticles- in vivo/ in vitro biomedical applications and in silico studies. *Advances in Colloid and Interface Science*, 249, 192-212.
- Ng, J., & Shuryak, I. (2015). Minimizing second cancer risk following radiotherapy: current perspectives. *Cancer Management and Research*, 7, 1-11.
- Ng, C.T., Yong, L.Q., Hande, M.P., Ong, C.N., Yu, L.E., Bay, B.H., & Baeg, G.H. (2017). Zinc oxide nanoparticles exhibit cytotoxicity and genotoxicity through oxidative stress responses in human lung fibroblasts and *Drosophila melanogaster*. *International Journal of Nanomedicine*, 28, 12, 1621-1637.
- Nonell, S., & Flors, C. (2016). Singlet Oxygen: Applications in Biosciences and Nanosciences (Volume 1). p1-21, Britain, Royal Society of Chemistry.
- Off, M.K., Steindal, A.E., Porojnicu, A.C., Juzeniene, A., Vorobey, A., Johnsson, A., & Moan, J. (2005). Ultraviolet photodegradation of folic acid. *Journal of Photochemistry and Photobiology B: Biology*, 80 (1), 47-55.
- Oh, W., Kim, S., Choi, M., Kim, C., Jeong, Y., Cho, B.,...Jang, J. (2010). Cellular uptake, Cytotoxicity, and Innate Immune response of silica -Titania Hollow Nanoparticles based on size and surface functionality. *ACS Nano*, 4 (9), 5301-5313.

- Oh, D.S., Kim, H., Oh, J.E., Jung, H.E., Lee, Y.S., Park, J.H., & Lee, H.K. (2017). Intratumoural depletion of regulatory T cells using CD25-targeted photodynamic therapy in a mouse melanoma model induces antitumoural immune responses. *Oncotarget*, 18, 8(29), 47440-47453.
- Okada, Y., & Okajima, H. (1998). Scavenging activity of furan derivatives against hydroxyl radical generated by fenton system. *Yakugaku Zasshi*, 118, 6, 226-230.
- Oliveira, J., Magliarelli, H.F., Pereira, F.V., Gianotti, A., Soares-Costa, A., Henrique-Silva, F.,...Paschoalin, T. (2011). Sugarcane cystatin CaneCPI-4 inhibits melanoma growth by angiogenesis disruption. *Journal of Cancer Science and Therapy*, 3, 161-167.
- Oniszczyk, A., Wojtunik-Kulesza, K.A., Oniszczyk, T., & Kasprzak, K. (2016). The potential of photodynamic therapy (PDT)-Experimental investigations and clinical use. *Biomedicine & Pharmacotherapy*, 83, 912-929.
- Orrenius, S., Nicotera, P., & Zhivotovsky, B. (2011). Cell death mechanisms and their implications in toxicology. *Toxicological Sciences*, 119, 3-19.
- Ostrovsky, S., Kazimirsky, G., Gedanken, A., & Brodie, C. (2009). Selective cytotoxic effect of ZnO nanoparticles on glioma cells. *Nano Research*, 2 (11), 882-890.
- Overwijk, W.W., & Restifo, N.P. (2001). B16 as a Mouse Model for Human Melanoma. *Current Protocols in Immunology*, (Chapter 20), US, John Wiley & Sons.
- Paek, H.J., Lee, Y.J., Chung, H.E., Yoo, N.H., Lee, J.A., Kim, M.K.,...Choi, S.J. (2013). Modulation of the pharmacokinetics of zinc oxide nanoparticles and their fates in vivo. *Nanoscale*, 5 (23), 11416-27.
- Pal, A., Alam, S., Mittal, S., Arjaria, N., Shankar, J., Kumar, M.,...Ansari, K.M. (2016). UVB irradiation-enhanced zinc oxide nanoparticles-induced DNA damage and cell death in mouse skin. *Mutation Research/Genetic Toxicology and Environmental Mutagenesis*, 807, 15-24.
- Pandurangan, M., & Kim, D.H. (2015). *In vitro* toxicity of zinc oxide nanoparticles: a review. *Journal of Nanoparticle Research*, 17, 158.
- Pandurangan, M., Veerappan, M., & Kim, D.H. (2015). Cytotoxicity of zinc oxide nanoparticles on antioxidant enzyme activities and mRNA expression in the cocultured C2C12 and 3T3-L1 cells. *Applied Biochemistry and Biotechnology*, 75(3), 1270-80.
- Pandey, C.M., Dewan, S., Chawla, S., Yadav, B.K., Sumana, G., & Malhotra, B.D. (2016). Controlled deposition of functionalized silica coated zinc oxide nano-assemblies at the air/water interface for blood cancer detection. *Analytica Chimica Acta*, 937, 29-38.

- Parvanian, S., Mostafavi, S.M., & Aghasiri, M. (2017). Multifunctional nanoparticle developments in cancer diagnosis and treatment. *Sensing and Bio-Sensing Research*, 13, 81-87.
- Paster, E.V., Villines, K.A., & Hickman, D.L. (2009). Endpoints for mouse abdominal tumour models: Refinement of current scenario. *Comparative Medicine*, 59(3), 234-241.
- Paszko, E., Ehrhardt, C., Senge, M.O., Kelleher, D.P., & Reynolds, J.V. (2011). Nanodrug applications in photodynamic therapy. *Photodiagnosis and Photodynamic Therapy*, 8 (1), 14-29.
- Patel, K., Sundara Raj, B., Chen, Y., & Lou, X. (2016). Cytotoxicity of folic acid conjugated hollow silica nanoparticles toward Caco2 and 3T3 cells, with and without encapsulated DOX. *Colloids and Surfaces B: Biointerfaces*, 140, 213-222.
- Patel, K., Sundara Raj, B., Chen, Y., & Lou, X. (2017). Novel folic acid conjugated Fe₃O₄-ZnO hybrid nanoparticles for targeted photodynamic therapy. *Colloids and Surfaces B: Biointerfaces*, 150, 1, 317-325.
- Patel, R.P., McAndrew, J., Sellak, H., White, C.R., Jo, H., Freeman, B.A., & Darley-Usmar, V.M. (1999). Biological aspects of reactive nitrogen species. *Biochimica et Biophys Acta*, 1411(2-3), 385-400.
- Perrotta, C., Buonanno, F., Zecchini, S., Giavazzi, A., Proietti Serafini, F., Catalani, E.,...Cervia, D. (2016). Climacostol reduces tumour progression in a mouse model of melanoma via the p53-dependent intrinsic apoptotic programme. *Scientific Reports*, 7, 6, 27281.
- Petersen, L.F., Brockton, N.T., Bakkar, A., Liu, S., Wen, J., Weljie, A.M., & Bismar, T.A. (2012). Elevated physiological levels of folic acid can increase in vitro growth and invasiveness of prostate cancer cells. *BJU International*, 109(5), 788-95.
- Punnoose, A., Dodge, K., Rasmussen, J.W., Chess, J., Wingett, D., & Anders, C. (2014). Cytotoxicity of ZnO Nanoparticles Can Be Tailored by Modifying Their Surface Structure: A Green Chemistry Approach for Safer Nanomaterials. *ACS Sustainable Chemistry & Engineering*, 2 (7), 1666-1673.
- Purdem, S., & Chen, Q.M. (2005). Epidermal growth factor receptor-dependent and independent pathways in hydrogen peroxide- induced mitogen activated protein kinase activation in cardiomyocytes and heart fibroblasts. *Journal of Pharmacology and Experimental Therapeutics*, 312, 1179-1186.
- Quirk, B.J., Brandal G., Donlon, S., Vera, J.C., Mang, T.S., Foy, A.B.,...Whelan, H .T. (2015). Photodynamic therapy (PDT) for malignant brain tumours – Where do we stand? *Photodiagnosis and Photodynamic Therapy*, 12, 3, 530-544.
- Radzimska, A., & Jesionowski, T. (2014). Zinc Oxide—From Synthesis to Application: A Review. *Materials*, 7(4), 2833-2881.

- Ramírez-García, G., Martínez-Alfaro, M., d'Orlyé, F., Bedioui, F., Mignet, N., Varenne, A.,...Richard, C. (2017). Photo-stimulation of persistent luminescence nanoparticles enhances cancer cells death. *International Journal of Pharmaceutics*, 13, pii: S0378-5173(17), 30608-7.
- Rasmussen, J.W., Martinez, E., Louka, P., & Wingett, D.G. (2010). Zinc oxide nanoparticles for selective destruction of tumour cells and potential for drug delivery applications. *Expert Opinion on Drug Delivery*, 7(9), 1063-77.
- Research facility manual, Curtin University [Accessed on: 31/Aug/2017] Retrieved from <http://research.curtin.edu.au/ethics-integrity/animal/>
- Rhee, S.G., Yang, K.S., Kang, S.W., Woo, H.A., & Chang, T.S. (2005). Controlled elimination of intracellular H₂O₂: regulation of peroxiredoxin, catalase, and glutathione peroxidase via post-translational modification. *Antioxidant Redox Signal*, 7, 619-626.
- Roger, E., Kalscheuer, S., Kirtane, A., Guru, B.R., Grill, A.E., Whittum-Hudson, J., & Panyam, J. (2012). Folic acid functionalized nanoparticles for enhanced oral drug delivery. *Molecular Pharmaceutics*, 2, 9(7), 2103-10.
- Roy, R., Singh, S.K., Chauhan, L.K.S., Das, M., Tripathi, A., & Dwivedi, P.D. (2014). Zinc oxide nanoparticles induce apoptosis by enhancement of autophagy via PI3K/Akt/mTOR inhibition. *Toxicology Letters*, 227(1), 29-40.
- Romanovsky, A.A. (2014). Skin temperature: its role in thermoregulation. *Acta Physiologica*, 210, 498–507.
- Roy, I., Ohulchanskyy, T.Y., Pudavar, H.E., Bergey, E.J., Oseroff, A.R., Morgan, J.,...Prasad, P.N. (2003). Ceramic based nanoparticles entrapping water-insoluble photosensitizing anticancer drugs: a novel drug-carrier system for photodynamic therapy. *Journal of the American Chemical Society*, 125, 7860-7865.
- Ruhlmann, C.H., Iversen, T.Z., Okera, M., Muhic, A., Kristensen, G., Feyer, P.,... Herrstedt, J. (2015). Multinational study exploring patients' perceptions of side-effects induced by chemo-radiotherapy. *Radiotherapy and Oncology*, 117, 2, 333-337.
- Sailor, M.J., & Park, J.H. (2012). Hybrid Nanoparticles for detection and treatment of cancer. *Advanced Materials*, 24, 3779-3802.
- Saladi, R.N., & Persaud, A.N. (2005). The causes of skin cancer: A comprehensive review. *Drugs of Today*, 41(1), 37.
- Salim, A., Leman, J.A., McColl, J.H., Chapman, R., & Morton, C.A. (2003). Randomized comparison of photodynamic therapy with topical 5-fluorouracil in Bowen's disease. *British Journal of Dermatology*, 148, 539-543.
- See, J-A., Shumack, S., Murrell, D.F., Rubel, D.M, Fernandez-Penas, P., Salmon, R.,...Spelman, L. (2016). Consensus recommendations on the use of daylight photodynamic therapy with methyl aminolevulinic acid cream for actinic keratosis in Australia. *Australasian Journal of Dermatology*, 57, 167-174.

- Sebaugh, J.L. (2011). Guidelines for accurate EC50/IC50 estimation. *Pharmaceutical Statistics*, 10(2), 128-34.
- Sharman, W. (2004). Targeted photodynamic therapy via receptor mediated delivery systems. *Advanced Drug Delivery Reviews*, 56(1), 53-76.
- Shen, C., James, S.A., De Jonge, M.D., Turney, T.W., Wright, P.F., & Feltis, B.N. (2013). Relating cytotoxicity, zinc ions, and reactive oxygen in ZnO nanoparticle-exposed human immune cells. *Toxicological Sciences*, 136 (1), 120-30.
- Shen, H.M., & Liu, Z.G. (2006). JNK signaling pathway is a key modulator in cell death mediated by reactive oxygen and nitrogen species. *Free Radical Biology and Medicine*, 40, 928-939.
- Shi, J., Yu, X., Wang, L., Liu, Y., Gao, J., Zhang, J.,...Zhang, Z. (2013). PEGylated fullerene/iron oxide nanocomposites for photodynamic therapy, targeted drug delivery and MR imaging. *Biomaterials*, 34(37), 9666-77.
- Shibhu, E.S., Hamada, M., Murase, N., & Biju, V. (2013). Nanomaterials formulations for photothermal and photodynamic therapy of cancer. *Journal of Photochemistry and Photobiology C: Photochemistry Reviews*, 15, 53-72.
- Shrikandhe, S.S., Jain, D.S., Athawale, R.B., Bajaj, A.N., Goel, P., Kamran, Z.,...Gude, R. (2015). Evaluation of anti-metastatic potential of cisplatin polymeric nanocarriers on B16F10 melanoma cells. *Saudi Pharmaceutical Journal*, 23, 341-351.
- Silva, Z.S.Jr., Bussadori, S.K., Fernandes, K.P., Huang, Y.Y., & Hamblin, M.R. (2015). Animal models for photodynamic therapy (PDT). *Bioscience Reports*, 35, 6.
- Simões, M.C.F., Sousa, J.J.S., & Pais, A.A.C.C. (2015). Skin cancer and new treatment perspectives: A review. *Cancer Letters*, 357, 1, 8-42.
- Simon, V., Devaux, C., Darmon, A., Donnet, T., Thienot, E., Germain, M.,...Marill, J. (2010). PP IX Silica nanoparticles demonstrate differential interactions with in vitro tumour cell lines and in vivo mouse models of human cancers. *Photochemistry and Photobiology*, 86, 213-222.
- Sivalingappa, P.C., Jin, H., Anantharam, V., Kanthasamy, A., & Kanthasamy, A. (2012). N-Acetyl Cysteine Protects against Methamphetamine-Induced Dopaminergic Neurodegeneration via Modulation of Redox Status and Autophagy in Dopaminergic Cells. *Parkinsons Disease*, 2012, 424285.
- Skin and Cancer Foundation, Australia [Accessed on: 31/Aug/2017] Retrieved from <https://www.skincancer.asn.au/page/59/learn-about-skin-cancer>
- Smith, S., & Prewett, S. (2017). Principles of chemotherapy and radiotherapy. *Obstetrics, Gynaecology & Reproductive Medicine*, 27, 7, 206-12.
- Smith, L., Kuncic, Z., Ostrikov, K., & Kumar, S. (2012). Nanoparticles in cancer imaging and therapy. *Journal of Nanomaterials*, 891318, 1-7.

- Song, Y., Guan, R., Lyu, F., Kang, T., Wu, Y., & Chen, X. (2014). In vitro cytotoxicity of silver nanoparticles and zinc oxide nanoparticles to human epithelial colorectal adenocarcinoma (Caco-2) cells. *Mutation Research*, 769, 113-8.
- Song, G., Cheng, L., Chao, Y., Yang, K., & Liu, Z. (2017). Emerging nanotechnology and advanced materials for cancer radiation therapy. *Advanced Materials*, 29 (32), 1-26.
- Souris, J.S., Lee, C.H., Cheng, S.H., Chen, C.T., Yang, C.S., Ho, J.A.,...Lo, L.W. (2010). Surface charge-mediated rapid hepatobiliary excretion of mesoporous silica nanoparticles. *Biomaterials*, 31(21), 5564-74.
- Stępnik, M., Arkusz, J., Smok-Pieniżek, A., Bratek-Skicki, A., Salvati, A., Lynch, I.,...Rydzynski, K. (2012). Cytotoxic effects in 3T3-L1 mouse and WI-38 human fibroblasts following 72 hour and 7 day exposures to commercial silica nanoparticles. *Toxicology and Applied Pharmacology*, 15, 263(1), 89-101.
- Tan, G., Li, W., Cheng, J., Wang, Z., Wei, S., Jin, Y., Guo, C., & Qu, F. (2016). Magnetic iron oxide modified pyropheophorbide-a fluorescence nanoparticles as photosensitizers for photodynamic therapy against ovarian cancer (SKOV-3) cells. *Photochemical and Photobiological Sciences*, 30, 15(12), 1567-1578.
- Tang, L., & Cheng, J. (2013). Nonporous Silica Nanoparticles for Nanomedicine Application. *Nano Today*, 8(3), 290-312.
- Tetz, L.M., Kamau, P.W., Cheng, A.A., Meeker, J.D., & Loch-Carusio, R. (2013). Troubleshooting the dichlorofluorescein assay to avoid artifacts in measurement of toxicant-stimulated cellular production of reactive oxidant species. *Journal of Pharmacological and Toxicological Methods*, 67(2), 56-60.
- Thakor, A.S., & Gambhir, S.S. (2013). Nanooncology: the future of cancer diagnosis and therapy. *CA: A Cancer Journal for Clinicians*, 63(6), 395-418.
- Tobias, M., Kathrin, O., & Annegret, P. (2014). Implications of the stability behavior of zinc oxide nanoparticles for toxicological studies. *International Nano Letters*, 4, 116.
- Trevizan, L.C., & Nobrega, J.A. (2007). Inductively coupled plasma optical emission spectrometry with axially viewed configuration: an overview of applications. *Journal of the Brazilian Chemical Society*, 18, 4.
- Triesscheijn, M., Baas, P., Schellens, J.H.M., & Stewart, F.A. (2006). Photodynamic Therapy in Oncology. *The Oncologist*, 11,1034-1044.
- Tso, C.P., Zhung, C.M., Shih, Y.H., Tseng, Y.M., Wu, S.C., & Doong, R.A. (2010). Stability of metal oxide nanoparticles in aqueous solutions. *Water Science and Technology*, 61(1), 127-33.
- Tu, J., Wang, T., Shi, W., Wu, G., Tian, X., Wang, Y.,...Ren, L. (2012). Multifunctional ZnPc-loaded mesoporous silica nanoparticles for enhancement of

photodynamic therapy efficacy by endolysosomal escape. *Biomaterials*, 33(31), 7903-14.

Urso, C. (2004). Are growth phases exclusive to cutaneous melanoma? *Journal of Clinical Pathology*, 57(5), 560.

UV irradiation chamber. [Accessed on: 13/Aug/2017] Retrieved from <http://www.opsytec.com/products/irradiation-chamber/bs-02/>

UV LED SMART. [Accessed on: 13/Aug/2017] Retrieved from <http://www.opsytec.com/products/uv-led-light-sources/uv-led-smart/>

Vijayaraghavan, P., Vankayala, R., Chiang, C.S., Sung, H.W., & Hwang, K.C. (2015). Complete destruction of deep-tissue buried tumours via combination of gene silencing and gold nanoechinus-mediated photodynamic therapy. *Biomaterials*, 62, 13-23.

Vinardell, M.A., & Mitjans, M. (2015). Antitumor activities of metal oxide nanoparticles. *Nanomaterials*, 5, 1004-1021.

Vitali, M., Ripamonti, C.I., Roila, F., Proto, C., Signorelli, D., Imbimbo, M.,...Russo, G.L. (2017). *Critical Reviews in Oncology/Hematology*, 118, 7-14.

Vorobei, A.V., & Vorobei, P.A. (2011). Photosensitized degradation of folic acid. *Journal of Applied Spectroscopy*, 78, 614.

Wahab, R., Dwivedi, S., Umar, A., Singh, S., Hwang, I.H., Shin, H.S., A.A.,... Kim, Y.S. (2013). ZnO nanoparticles induce oxidative stress in Cloudman S91 melanoma cancer cells. *Journal of Biomedical Nanotechnology*, 9(3), 441-9.

Wang, B., Feng, W., Wang, M., Wang, T., Gu, Y., Zhu, M.,...Wang, J. (2007). Acute toxicological impact of nano- and submicro-scaled zinc oxide powder on healthy adult mice. *Journal of Nanoparticle Research*, 10(2), 263-276.

Wang, D., Fei, B., Halig, L.V., Qin, X., Hu, Z., Xu, H.,...Chen, Z. (2014). Targeted iron oxide nanoparticle for photodynamic therapy and imaging of head and neck cancer. *ACS Nano*, 22, 8(7), 6620-6632.

Wang, L., Yang, W., Read, P., Larner, J., & Sheng, K. (2010). Tumour cell apoptosis induced by nanoparticle conjugate in combination with radiation therapy. *Nanotechnology*, 26, 21(47), 475103.

Wang, L., Zhao, W., & Tan, W. (2008). Bio-conjugated silica nano-particles: development and applications. *Nano Research*, 1, 99-115.

Wang, J., Deng, X., Zhang, F., Chen, D., & Ding, W. (2014). ZnO nanoparticle-induced oxidative stress triggers apoptosis by activating JNK signaling pathway in cultured primary astrocytes. *Nanoscale Research Letters*, 13(9).

Wang, K., Kievit, F.M., & Zhang, M. (2016). Nanoparticles for cancer gene therapy: Recent advances, challenges, and strategies. *Pharmacological Research*, 114, 56-66.

- Wan, M.T., & Lin, J.Y. (2014). Current evidence and applications of photodynamic therapy in dermatology. *Clinical, Cosmetic and Investigational Dermatology*, 7, 145-163.
- Weitman, S.D., Lark, R.H., Coney, L.R., Fort, D.W., Frasca, V., Zurawski, V.R Jr., & Kamen, B.A. (1992). Distribution of the folate receptor GP38 in normal and malignant cell lines and tissues. *Cancer Research*, 15, 52(12), 3396-401.
- Weyden, V. L., & Adams, D.J. (2012). Using mice to unveil the genetics of cancer resistance. *Biochimica et Biophysica Acta*, 1826(2), 312-30.
- Wilson, M.R., Lightbody, J.H., Donaldson, K., Sales, J., & Stone, V. (2002). Interactions between ultrafine particles and transition metals in vivo and in vitro. *Toxicology and Applied Pharmacology*, 184(3), 172-9.
- Wink, D.A., & Mitchell, J.B (1998). Chemical biology of nitric oxide: insights into regulatory, cytotoxic and cryoprotective mechanisms of nitric oxide. *Free Radical Biology and Medicine*, 25, 434-456.
- World Health organisation, Cancer fact sheet [Accessed on 18/Sep/2017] Retrieved from <http://www.who.int/mediacentre/factsheets/fs297/en/>
- Woodburn, K.W., Fan, Q., Kessel, D., Luo, Y., & Young, S.W. (1998). Photodynamic Therapy of B16F10 Murine Melanoma with Lutetium Texaphyrin. *Journal of Investigative Dermatology*, 110, 5, 746-51.
- Wu, D., An, T., Li, G., Wang, W., Cai, Y., Yip, H.Y.,...Wong, P.K. (2015). Mechanistic study of the visible-light-driven photocatalytic inactivation of bacteria by graphene oxide–zinc oxide composite. *Applied Surface Science*, 358, 15, 137-145.
- Wu, G., Wilson, G., George, J., Liddle, C., Hebbard, L., & Qiao, L. (2017). Overcoming treatment resistance in cancer: Current understanding and tactics. *Cancer Letters*, 28, 387, 69-76.
- Xiao, L., Gu, L., Howell, S.B., & Sailor, M.J. (2011). Porous silicon nanoparticle photosensitizers for singlet oxygen and their phototoxicity against cancer cells. *ACS Nano*, 24, 5(5), 3651-3659.
- Yamaura, M., Mitsushita, J., Furuta, S, Kiniwa, Y., Ashida, A., Goto, Y.,...Kamata, T. (2009). NADPH oxidase 4 contributes to transformation phenotype of melanoma cells by regulating G2-M cell cycle progression. *Cancer Research*, 15, 69 (6), 2647-54.
- Yang, Q., & Ma, Y. (2014). Irradiation-Enhanced Cytotoxicity of Zinc Oxide Nanoparticles. *International Journal of Toxicology*, 33(3), 187-203.
- Yang, Y., Jiang, G., Zhang, P., & Fan, J. (2015). Programmed cell death and its role in inflammation. *Military Medical Research*, 2, 12.

- Yang, L., Zhang, S., Ling, X., Shao, P., Jia, N., & Bai, M. (2017). Multilayer photodynamic therapy for highly effective and safe cancer treatment. *Acta Biomaterialia*, 54, 271-280.
- Yee, N.S., Ignatenko, N., Finnberg, N., Lee, N., & Stairs, D. (2015). Animal models of cancer biology. *Cancer Growth Metastasis*, 8, (Suppl 1), 115–118.
- Yoon, I., Li, J.Z., & Shim, Y.K. (2013). Advance in photosensitizers and light delivery for photodynamic therapy. *Clinical Endoscopy*, 46, 7-23.
- Yoshiura, K., Nishishita, T., Nakaoka, T., Yamashita, N., & Yamashita, N. (2009). Inhibition of B16 melanoma growth and metastasis in C57BL mice by vaccination with a syngeneic endothelial cell line. *Journal of Experimental and Clinical Cancer Research*, 31, 28:13.
- Yu, J., Baek, M., Chung, H.E., & Choi, S.J. (2011). Effects of physicochemical properties of zinc oxide nanoparticles on cellular uptake. *Journal of Physics: Conference Series*, 304, 012007.
- Yu, Y., Duan, J., Li, Y., Yu, Y., Jin, M., Li, C.,...Sun, Z. (2015). Combined toxicity of amorphous silica nanoparticles and methylmercury to human lung epithelial cells. *Ecotoxicology and Environmental Safety*, 112, 144-52.
- Yu, T., Malugin, A., & Ghandehari, H. (2011). Impact of silica nanoparticle design on cellular toxicity and haemolytic activity. *ACS Nano*, 5(7), 5717-5728.
- Yu, X., Yang, L., Cairns, M.J., Dass, C., Saravolac, E., Li, X., & Sun, L.Q. (2014). Chemosensitization of Solid Tumours by Inhibition of Bcl-xL Expression Using DNazyme. *Oncotarget*, 5(19), 9039-9048.
- Yuan, J.H., Chen, Y., Zha, H.X., Song, L.J., Li, C.Y., Li, J.Q., & Xia, X.H. (2010). Determination, characterization and cytotoxicity on HELF cells of ZnO nanoparticles. *Colloids and Surfaces B: Biointerfaces*, 76(1), 145-50.
- Yuan, Q., Hein, S., & Misra, R.D.K. (2010). New generation of chitosan-encapsulated ZnO quantum dots loaded with drug: Synthesis, characterization and in vitro drug delivery response. *Acta Biomaterialia*, 6(7), 2732-2739.
- Zhang, H., Shan, Y., & Dong, L. (2014). A comparison of TiO₂ and ZnO Nanoparticles as photosensitizers in photodynamic therapy for cancer. *Journal of Biomedical Nanotechnology*, 10, 1450-1457.
- Zhang, J., Jianga, C., Longo, J.P.F., Azevedo, R.B., Zhang, H., & Muehlmann, L.A. (2017). An updated overview on the development of new photosensitizers for anticancer photodynamic therapy. *Acta Pharmaceutica Sinica B*, <https://doi.org/10.1016/j.apsb.2017.09.003>
- Zhang, L., Wang, S., Liu, Z., Zhang, L., Wang, S., & Wang, B. (2017). Procyanidin, a kind of biological flavonoid, induces protective anti-tumour immunity and protects mice from lethal B16F10 challenge. *International Immunopharmacology*, 47, 251-258.

Zhang, H., Guo, L., Ding, S., Xiong, J., & Chen, B. (2016). Targeted photo-chemo therapy of malignancy on the chest wall while cardio pulmonary avoidance based on Fe₃O₄@ZnO nanocomposites. *Oncotarget*, 7, 24, 36602-36613.

Zhang, Z., & Xiong, H. (2015). Photoluminescent ZnO Nanoparticles and their biological applications. *Materials*, 8, 3101-3127.

Zhao, L., Zhang, R., Zhang, J., & Sun, S. (2012). Synthesis and characterization of biocompatible ZnO nanoparticles. *CrystEngComm*, 14, 945-950.

Zhao, B., & He, y. (2010). Recent advances in the prevention and treatment of skin cancer using photodynamic therapy. *Expert Reviews in Anticancer Therapy*, 10 (11), 1797–1809.

Zheng, X., Feng, X., & Lou, X. (2016). Zinc oxide based nano-semiconductors as a new generation of photosensitizers for photodynamic therapy. *Chemeca*, 3384750, 155-166.

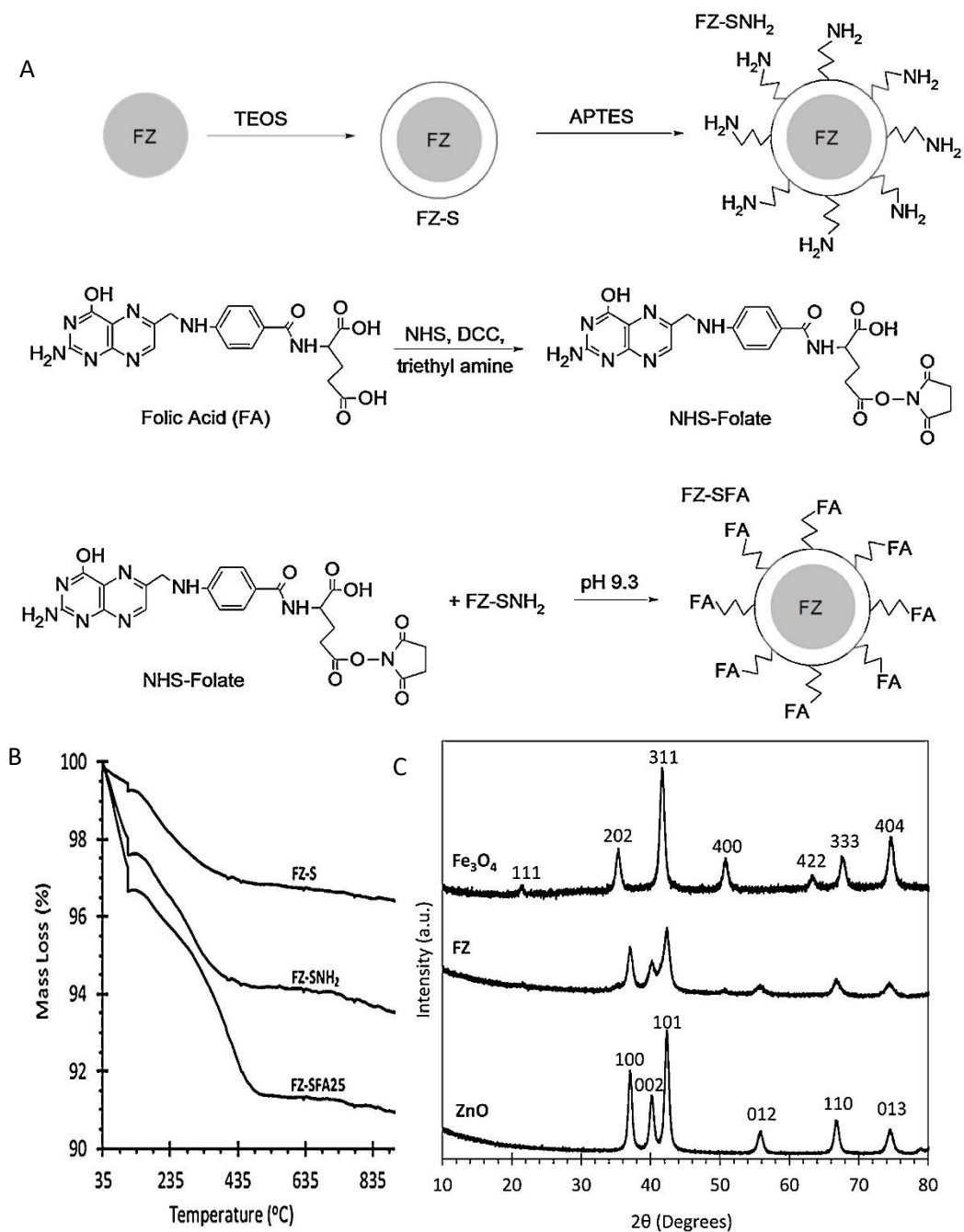
Zhu, T.C., Finlay, J.C., Zhou, X., & Li, J. (2007). Macroscopic modeling of the singlet oxygen production during PDT. *Proceedings of SPIE-the International Society for Optical Engineering*, 6, 6427, 642708.

Zwicke, G.L., Mansoori, G.A., & Jeffery, C.J. (2012). Utilizing the folate receptor for active targeting of cancer nanotherapeutics. *Nano Reviews*, 3, 10.3402.

APPENDICES

Appendix 1: Structure, TGA curve and XRD analysis of the hybrid NPs

(Data from Patel et al., 2017)



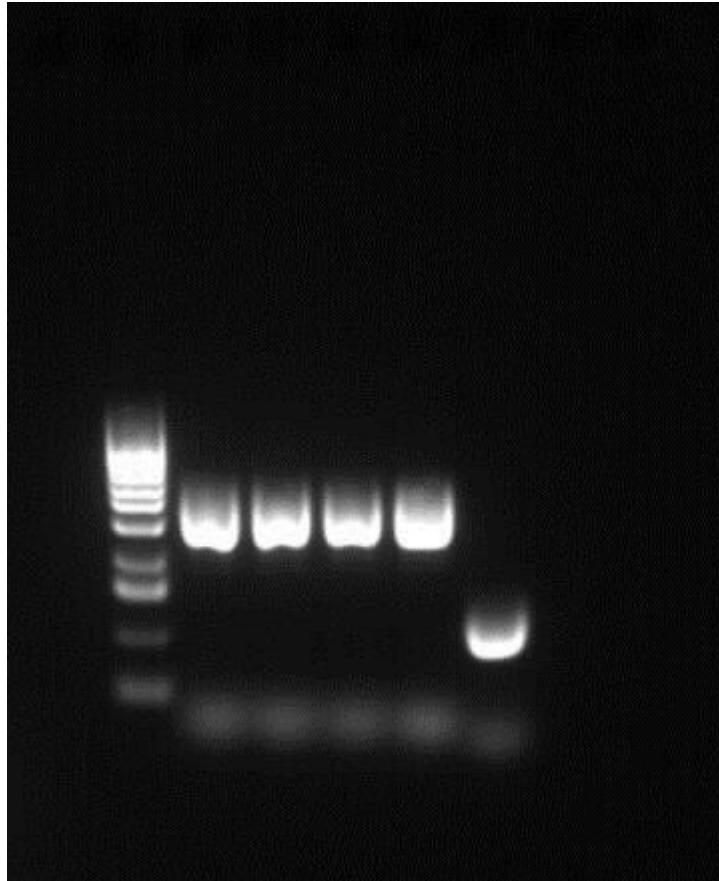
A) Synthetic scheme outlining preparation of FZ-S and FZ-SFA NPs, B) TGA curves & C) XRD diffraction patterns for Fe₃O₄, FZ and Zn NPs.

Appendix 2: Sample Preparation for Mycoplasma Testing

Mycoplasmas can drastically alter DNA, RNA and protein synthesis as well as can compete with host cells for biosynthetic precursors, nutrients, amino acid and ATP. As a result, research results can be skewed and become non-reproducible. Although the proper aseptic technique was always employed in the laboratory work and antibiotic was always present in the medium to prevent bacterial infection, regular (three monthly) testing of all cell cultures was performed to ensure the absence of mycoplasma. The procedure followed was as below:

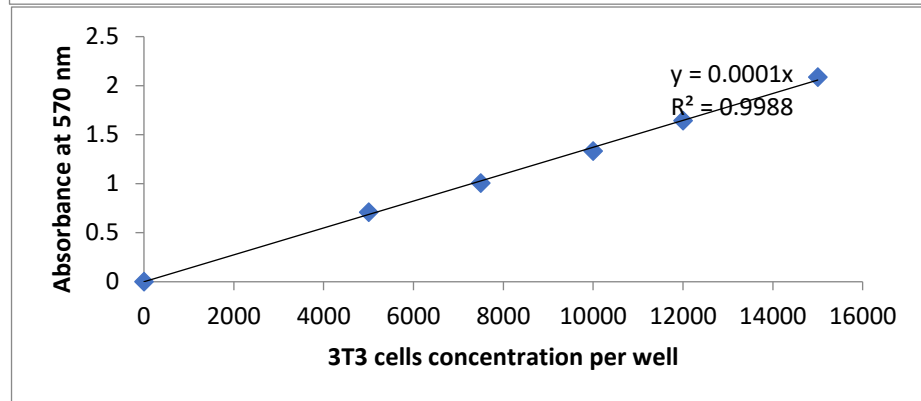
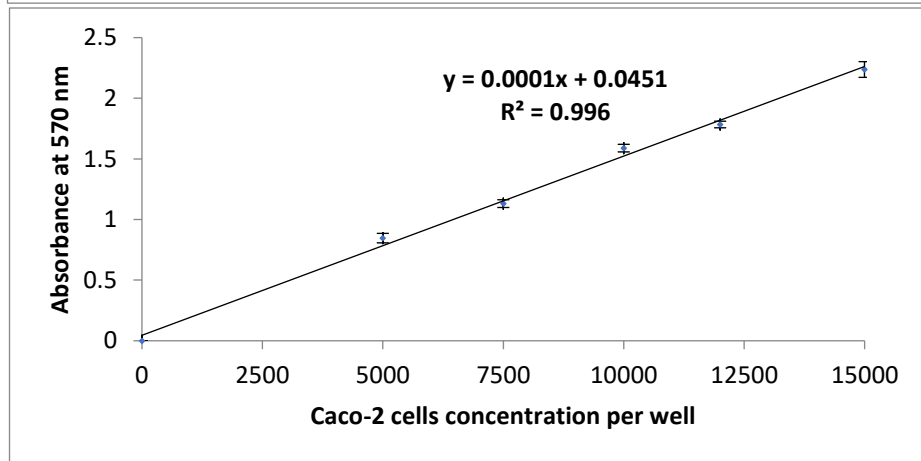
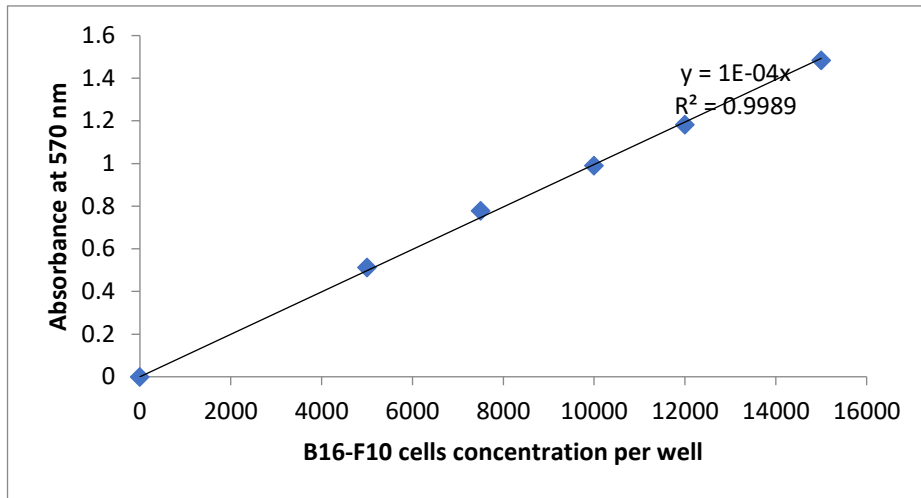
- Cells were cultured for two weeks without any antibiotics. The B16-F10 and 3T3 cells grew fast so they were split as usual and continued growing in the medium without antibiotics.
- Samples were prepared when cells were 70-80% confluent.
- 100 μ L of cell conditioned medium was collected into 1.5 mL Eppendorf tube and boiled for 5 min at 95°C using bench heat block. The sample was stored at 4°C and tested within one week.
- Cells were washed with PBS and removed by cell scraper into PBS. An aliquot was used for cell counting and the rest was centrifuged at 2000 rpm for 5 minutes at 4°C.
- Cells were resuspended in PBS and approximately 1×10^6 cells were placed into a 1.5 ml Eppendorf tube.
- The tube was centrifuged at 3750 g for 1 min at 4°C, the supernatant was removed, the cell pellet was resuspended in 1 mL PBS and centrifuged again.
- Finally, the supernatant was removed, and the cell pellet was stored at 4°C for mycoplasma testing was carried out within one week.
- Optimised PCR-based technique was used for mycoplasma detection, which was performed by CHIRI facility researcher, Curtin University.

The results presented in this chapter were generated from mycoplasma negative cell lines which were regularly checked by the facility, figure below shows an example of the mycoplasma negative results of cell lines used in this study.



PCR gel image of B16-F10 and Caco-2 mycoplasma negative result. 1st lane (left): 100 base pair (bp) ladder, 2nd lane: B16-F10 cells, 3rd lane: Caco-2, 4th lane: only medium, 5th lane: negative control, 6th lane: positive control. The upper band of 500 bp is an internal positive control showing that PCR reaction has worked; the lower band (second from the bottom) of 250 bp is a mycoplasma positive band.

Appendix 3: Calibration curve of B16-F10, Caco-2 and 3T3 cells



Appendix 4: Cryopreservation and thawing of cells

Cryopreservation of cells

A sterile freezing medium containing 95% FBS and 5% filter-sterilised DMSO as cryopreservant was prepared. For cryopreservation, cells at the last step during culturing procedure were resuspended in the freezing medium instead of a regular medium. The cell suspension was then transferred into 1.8 mL cryopreservation vials and placed in a -80°C freezer to allow controlled cooling of the vials down to -80°C. Cells were stored at -80°C if needed to be revived within next 1-4 months. For long term preservation, after -80°C overnight storage, the vials were then transferred into a liquid nitrogen tank.

Thawing of cells

The cryovials were removed from the -80°C freezer or liquid nitrogen tank and placed at the room temperature (inside biosafety hood) to thaw the cell suspension. The melted cell suspension was immediately diluted into pre-warmed cell medium in a 15-mL falcon tube and was centrifuged at 3270 g for 5 minutes to get rid of the toxic DMSO. The cell pellet was then resuspended in pre-warmed cell medium (3.5 mL) and transferred into a T25 flask. Following addition of 5-6 mL of culture medium, the flask was incubated at 37°C temperature with 5% CO₂ in the humidified atmosphere in a cell culture incubator. Culture medium was replaced twice a week.

Appendix 5: UV CHAMBER BS02 Radiation officer approval

Hi Behin

Thanks for the information. We don't need to register this equipment.

We do need to confirm that there is no possibility of exposure to UV. I understand there is a safety interlock feature that automatically switches off the UV lights if the door is opened. Can you confirm this is operational. I'm happy to come over and have a look if you are not sure.

We will have to write up some working rules if there is the possibility of UV exposure – I can help with this if required. Otherwise I'll just advise you to use the device in accordance with the manufacturer's instructions and to refrain from using the instrument if there are any suspected or known faults.

Kind regards

Matt

Dr Matt Carroll

Radiation Safety Advisor | Office of Research and Development

Curtin University

Tel | +61 8 9266 1708

Mobile | 0424 537 431

Email | matthew.carroll@curtin.edu.au

Web | <http://curtin.edu.au>

Curtin University is a trademark of Curtin University of Technology.
CRICOS Provider Code 00301J (WA), 02637B (NSW)

Appendix 6: MTT solution preparation and storage

According to the manufacturer website- “Reconstituted MTT solution is stable for at least 6 months when stored frozen (-20°C). Storage of reconstituted MTT solution at 2-8°C for more than 2 weeks may cause decomposition and yield erroneous results”. So, the following procedure was carried out in a biosafety cabinet (where applicable) always protecting the reagent from light:

100 mg of MTT was weighed out in a 50-ml glass beaker and dissolved in 100 ml PBS (pH 7.4) on a magnetic stirrer to obtain a stock concentration of 1 mg/mL.

The MTT solution was filter-sterilized using 0.2 µm syringe tip filter directly into 4 mL sterile containers and wrapped with aluminium foil for light protection.

The stock solution was stored, at 4°C for frequent usage within 7 days or at -20°C for long term storage (up to 3 months), in a light protected container.

Appendix 7: 10X binding buffer preparation for apoptosis assay

1.4 M sodium chloride, 25 mM calcium chloride dihydrate and 0.1 M HEPES was weighed and made up to 100 mL using deionised water and stored in 4°C for further use.

For the apoptosis assay 1X binding buffer was prepared and used by dilution with deionised water as per requirement.

Appendix 8: Animal ethics approval



Curtin University

29 November 2016

Yan Chen
Curtin University

Dear Yan

Animal Ethics

Approval Number: AEC_2016_41

Project Title: *An in vivo study of Nano Photosensitizers for Cancer therapy (Application Number 34-2016)*

Thank you for providing additional information for the project titled "*An in vivo study of Nano Photosensitizers for Cancer therapy*". The information you have provided has satisfactorily addressed the queries raised by the Committee.

Your application has been **approved** and the relevant approval number is **AEC_2016_41** and the period of the project approval is from **29/11/2016** to **29/11/2017**.

Species Approved	Strain	No
Mouse	C57BL/6	159

OTHER REQUIREMENTS/NOTES

An Annual Progress Report must be submitted to the Ethics Office annually, on the anniversary of approval.

An Annual Animal Use Report that captures the relevant details regarding the number of animals used in the preceding year i.e. 1 January to 31 December must be submitted before 31 January of the following year.

Any amendments to the approved protocol must be submitted to the Ethics Office.

A Completion Report must be submitted to the Ethics Office on completion of the project.

You are reminded that it is your responsibility to maintain your own animal records and to report annually to the Committee.

Should any animal(s) experience an adverse or unexpected outcome resulting from the experimentation, the AEC is to be notified in writing immediately.

Please ensure that you quote the Animal Ethics Committee approval number whenever you order animals for this project. Note also that an AEC approval number must be displayed on the cage(s)/aquaria etc used to house/maintain animals during an approved activity.

If the results of this research will be published, citations should state: "All experiments were performed according to the Australian Code of Practice for the care and use of animals for scientific purposes".

Regards

Mr Charlie Thorn
Chairperson, Animal Ethics Committee

Office of Research and Development

Building 100 Level 1 West
Dumas Road
Bentley Western Australia 6102

GPO Box U1987
Perth Western Australia 6845

Telephone +61 8 9266 7863
Facsimile +61 8 9266 3793
Web research.curtin.edu.au

Animal Ethics Committee

Telephone +61 8 9266 2784
Facsimile +61 8 9266 3793
Email aec@curtin.edu.au

Appendix 9: Animal health monitoring score card

AEC APPROVAL #: _____

<i>Investigator:</i>	<i>Phone:</i>							
	<i>Email:</i>							
<i>Cage#/Box#/Animal ID</i>	<i>Species/Strain/Sex/Age</i>							
<i>Procedure: Pre-procedure</i>	<i>Date performed:</i>							
Clinical Observation	Day	Day	Day	Day	Day	Day	Dayx	Day
	x	x	x	x	x	x		x
Date								
UNDISTURBED								
Activity (<i>Normal=0,; isolated=1; huddled/inactive=2; moribund/fitting/=3</i>)								
Posture (<i>Normal = 0; hunched = 2; trembling=3</i>)								
Movement/Gait (<i>Normal=0; slight incoordination=1; tiptoe walking or reluctance to move=2; staggering/limb dragging/paralysis=3</i>)								
Coat condition (<i>Normal/groomed=0; rough=1; ruffled/unkept=2; bleeding or infected wounds or self mutilation=3</i>)								
Eating/drinking (<i>normal=0; decreased intake during the 1st 24 hrs day=1; decreased intake more than 1 day=2; decreased intake over 48hrs=3</i>)								
Breathing (<i>normal=0; rapid,shallow=1; rapid,abdominal breathing=2; laboured, irregular,skin blue=3</i>)								
ON HANDLING								
Alertness (<i>normal=0; dull or depressed=1; little response to handling=2; unconscious=3</i>)								
Body weight (gm or kg / Score) (<i>normal weight & growth rate=0; reduced growth weight=1; chronic weight loss>5% =2;weight loss = or >10%=3</i>)								
Dehydration (<i>none=0; skin less elastic=1; skin tenting=2; skin tenting & sunken eyes=3</i>)								
Eyes, Nose (<i>normal=0; wetness or dull eyes=1; discharge/squinty eyes=2; coagulated nasal discharge/matted eyes=3</i>)								
Faeces (<i>normal=0; moist but formed=1; loose, soiled peri-anal area or mucoid=2; watery or no faeces for 48hrs or blood=3</i>)								
Urine (<i>normal = 0; Increased/decreased = 3</i>)								
Treatment/support (<i>e.g. fluids, antibiotics, mushy food, hydrating gels,etc.</i>)								
Monitored by:								
Other Comments								

Criteria for euthanasia: Assessment score of 3 for any of the following clinical observations: **Movement/Gait, Breathing, Alertness, Body weight loss is equal to or greater than 10% .**

Immediate veterinary treatment required: A score of 2-3 for clinical observations listed above.

References:

- <https://research.unsw.edu.au/unsw-acec-examples-animal-monitoring-sheets>
- <http://www.dpi.vic.gov.au/agriculture/about-agriculture/legislation-regulation/animal-welfare-legislation/codes-of-practice-animal-welfare/care-of-laboratory-mice-rats-guinea-pigs-rabbits>
- Morton D.B. 2000. A systematic approach for establishing humane endpoints. *ILAR Journal* 41(2): 80-86.
- Morton D.B., and P.H.M. Griffiths. 1985. Guidelines on the recognition of pain, distress, and discomfort in experimental animals and a hypothesis for assessment. *Veterinary Record* 116:431-36.

Appendix 10: Radiation safety approval for UV LED SMART

Hi Behin

There are no registration or licencing requirements with this instrument. At 365 nm the recommended occupational exposure limit is 27 J/cm². As you will be operating at 10 J/cm² there are no other special safety requirements.

For equipment such as this our advice is that if it is used in accordance with the manufacturer's instructions then it is sufficient to ensure users have read the safe working procedures and risk assessments for the apparatus and undergo training on its use.

Kind regards

Matt

Dr Matt Carroll

Radiation Safety Advisor | Office of Research and Development

Curtin University

Tel | +61 8 9266 1708

Email | matthew.carroll@curtin.edu.au

Web | <http://curtin.edu.au>

Curtin University is a trademark of Curtin University of Technology.
CRICOS Provider Code 00301J (WA)

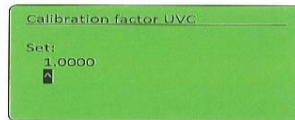
Appendix 11: BS02 UV CHAMBER-SENSOR, UV-MAT and UV LED SMART company manuals

6.5.1 Sensor factors

In this submenu the sensor specific adjustments are placed. It is possible to do the sensor calibration and set the upper and lower limits. In all three submenu points you have to decide first for which sensor port you want to do the adjustment, if Your UV-Mat version is capable of more than one sensor.

6.5.2 Calibration / Calibration each spectral range*

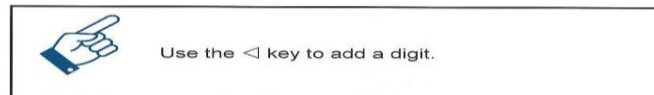
The calibration factor is used to calculate the irradiance for another place then the sensor place. For example:



The standard value for this is 1.000 (one). Therefore the irradiance is the irradiance at the sensor place.

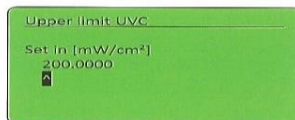
If you want to convert the reading for another position you have to measure the irradiance in the target position and in the sensor position. The result of the division from the target value and the sensor value is the necessary calibration factor.

Navigate with \leftarrow , \rightarrow and set value with Δ , ∇ . Confirm with \checkmark to go back to setup menu.



6.5.3 Upper and lower limit / Calibration each spectral range*

The upper and lower limits have the function of monitoring the sensors. For example:



For the determination of the limit values you have to set the upper limit on 200 mW/cm² and the lower limit on 0 mW/cm². No error can occur with this setup (if the calibration

factor is set to 1.0). After an adequate warm up time you have to read the values and can now adjust the upper and lower limit e.g. $\pm 25\%$ of the sensor value. Strong fluctuations during the warming up should be faded out with the delay time.

6.5.4 Safty time

Timing values can be adjusted in menu "safty time". See delay time, max. time and waiting time.

6.5.4.1 Delay time

The delay time is the time, which the UV-AB-Mat waits until it starts to monitor the sensor signal. It should be as long as the lamps need to get on a constant irradiancy delivery.

6.5.4.2 Max. time

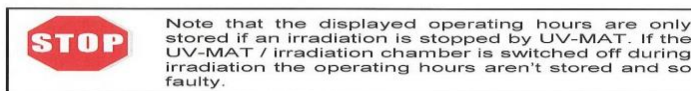
Max. time is a safety function. After reaching this time the irradiation is stopped. This value should be programmed carefully, because it can be very important e.g. sunburn through a wrong input of the dose can be prevented.

6.5.4.3 Waiting time

The waiting time is the time after the irradiation which must be waited to start a new irradiation. This time should be so long, that double irradiation is to be excluded. Maybe some lamps also need a cool-down phase, so "waiting time" may prevent hot-reignition. It should be set at least to **3 seconds** to prevent immediate user restart of the lamps.

6.6 Operating hours

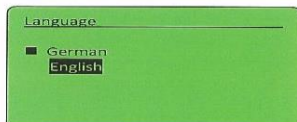
The user may reset the lamps operating hours using the menu item. Reset must be confirmed by pressing \leftarrow for at least 2 seconds.



6.7 Chamber settings

6.7.1 Language

The UVMAT comes with a menu in the German and English language.



Select the desired language with the keys ∇ and \triangle and confirm with \checkmark .

6.7.2 Channel control

Use channel control to select mode

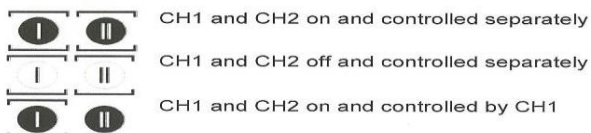


CH1 controls: all lamps controlled by CH1 by reached dose or time

CH2 controls: all lamps controlled by CH2 by reached dose or time

CH1-CH1; CH2-CH2: odd-numbered lamps controlled by CH1, even-numbered lamps controlled by CH2. The lamps are controlled by each sensor using this mode. This setting makes sense, while other setting may be for special applications.

Note, that the channel control is displayed during irradiation in the upper right corner. Here the icons have e.g. the following meaning:



7 Technical Data

7.1 Radiometer UV-MAT

Size (L x W x H)	250 x 185 x 100 mm ³
Weight	2,6 kg
Power	85-264V /47-440Hz / 12VA
Operational temperature	0 - 30°C
Storage temperature	0 - 60°C
Humidity	< 80%, non-condensing
Display	graphical, 128 x 64 px
Dose calculation	for all irradiance readings > 0,1 mW/cm ² to avoid offset failure

7.2 Sensor

Weight	150g
Operational temperature	0 - 40 °C
Storage temperature	-10 - 40 °C
Humidity	< 80%, non-condensing
Spectral range, UVC	200 – 280 nm
radiometric measurement range	0 – 19,9 mW/cm ²
Cosine correction	yes
Calibration	yes, traceable to PTB / NIST
frequency of checks (Recalibration)	12 months

7.3 Code number

CODE NUMBER	7243
-------------	------

BS02 CHAMBER-UV MAT



Dosimeter system UV-Mat



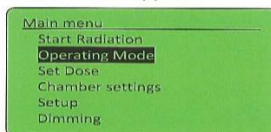
manual

Version: 1.0.4

Opsytec Dr. Gröbel GmbH
Goethestraße 17
76275 Ettlingen
Tel.: 07243 94 783 50
Fax: 07243 94 783 65
info@uv-groebel.de

6 Operation

Two seconds after startup the main menu appears:



Use the four cursor keys \leftarrow , \rightarrow , \triangle , ∇ and the center ok key (\checkmark) to navigate through the menu. Inverted text highlights the selected menu item.

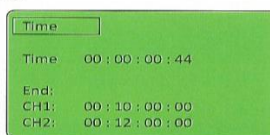
To confirm the selected function press the \checkmark key.

Press the \leftarrow key to return to previous menu.

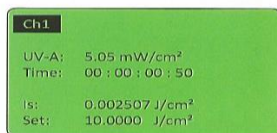
6.1 Start / Stop Radiation

Start an irradiation by selecting "Start Radiation" and press \checkmark .

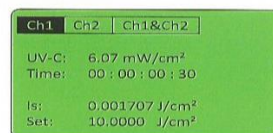
In time controlled operation mode the current irradiation time and end time are displayed in the form DD:HH:MM:SS.



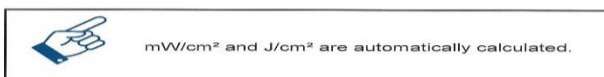
In dose controlled operation mode the current irradiance in mW/cm^2 , the actual irradiation time, the current dose (Is:) and the target dose (Set:) are displayed:



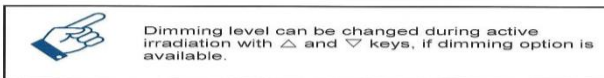
1 channel version



2 channel version*



Stop an irradiation by pressing \checkmark for at least 2 seconds.



6.2 Operation mode


Select operating mode the select dose controlled or time controlled irradiation.


6.2.1 Controlling Mode

Select operating mode the select dose controlled or time controlled irradiation.



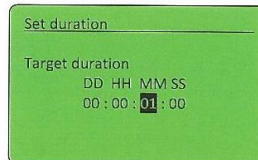
Confirm by with \checkmark or \rightarrow . With \leftarrow you can cancel your input and go back to main menu.

 In dose controlled mode the irradiation time is automatically controlled and stops if the desired dose is reached. Note a sensor must be connected therefore.


 In time controlled mode the irradiation time controlled by a timer only. On the display only the irradiation time is displayed. A sensor is not necessary.
For 2-channel version: set irradiation time is selectable for both channels individually.

6.3 Set time

Depending on the operation mode you can set the duration of irradiation:

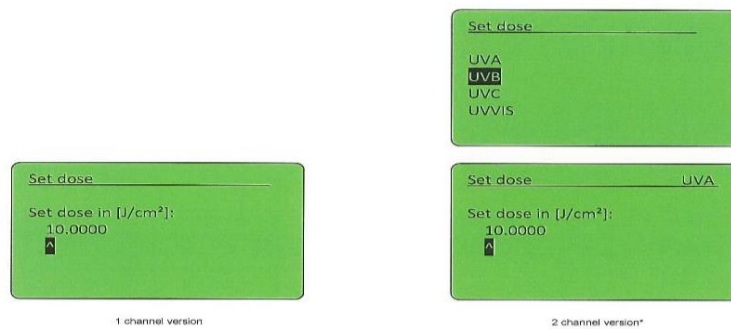



Use ◀ and ▶ keys to select day (DD), hours (HH), minutes (MM) or seconds (SS). Use ▲ and ▼ to enter value and confirm with ✓.

 The maximum duration is 99 days, 23 hours, 59 minutes and 59 seconds.
For 2-channel version: set irradiation time is equal for all channels.

6.4 Set Dose

Set the target dose for an irradiation (or channel*):

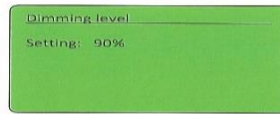


 Use the ◀ key to add a digit.

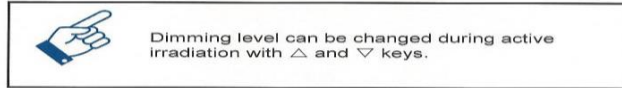
Use ◀ and ▶ keys to select day (DD), hours (HH), minutes (MM) or seconds (SS). Use ▲ and ▼ to enter value and confirm with ✓.

6.4.1 Dimming*

Select dimming to adjust lamp output. Therefore got to menu "Dimming", select channel to be dimmed:

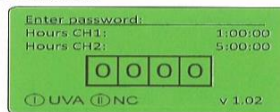


Use Δ and ∇ keys to set desired value. Confirm with \checkmark .

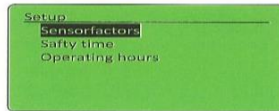


6.5 Setup

Using this menu you can set the system settings. Therefore enter the PIN code, see chapter technical data, must be entered.



Even without PIN the operational hours, connected sensors and firmware version are displayed. After entering PIN and confirmation with OK you can change system settings:

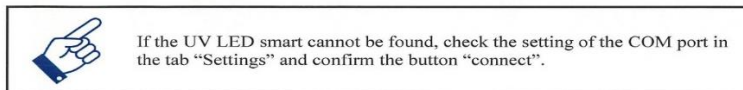
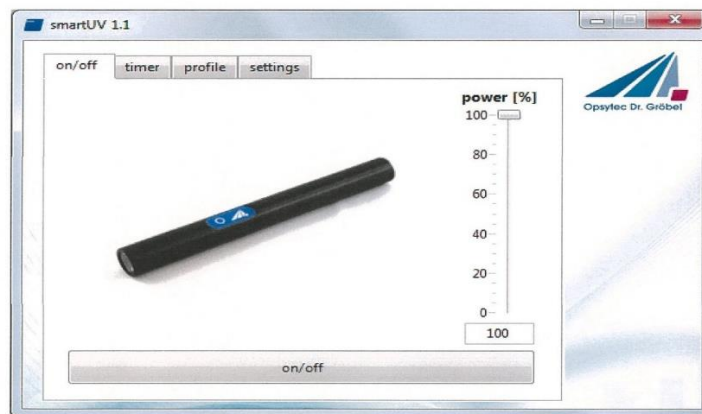


UV LED SMART

5 Operating the Software

5.1 Starting the Software

When starting the software, the UV LED is connected.

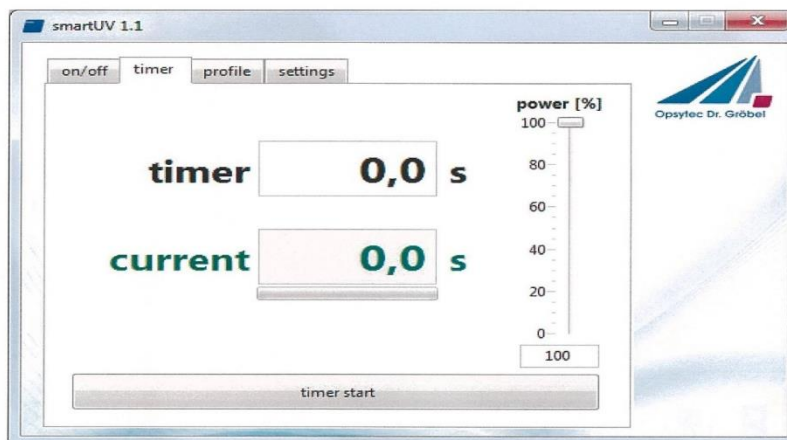


5.2 Permanent Operation

The UV LED can easily be switched on and off at the PC with the button "LED on / off". The performance can be set between 0% and 100% via the slide control.

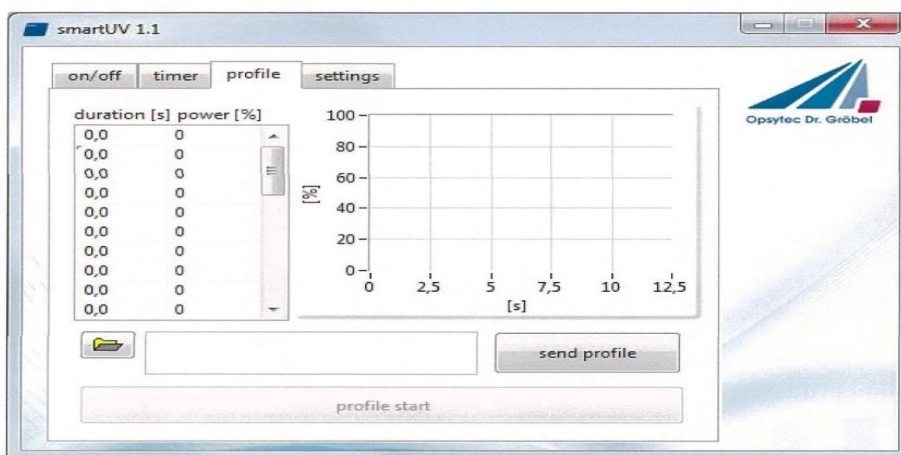
5.3 Timer

The UV LED can be controlled by PC in permanent operation mode. Therefore a useful timer is available. Set timer duration and performance and press timer start to start irradiation. Press button again to stop irradiation.



5.4 Profiles

The UV LED smart offers a profile mode for an adjustable, reproducible exposure of the samples. In the profile mode, dynamic exposures, i.e. exposures with temporally variable irradiance, and exposures with constant irradiances are possible. The user interface, with the function groups, is illustrated below.



Activate the profile mode by button “send profile”.



The exposure is taken out in the profile mode by pressing once the button or creating the trigger signal, as long as the button is pressed / the trigger is active. In that case, the profile is continuously repeated. The exposure is taken out on the PC only once and is not repeated.

5.5 Setting the irradiation profile

The irradiation profile is shown in the table and the graph. Changes are editable directly in the table.

Furthermore, profiles can be imported via text files. To select a text file, click on the folder icon at the bottom. The text file must be two-columned and tab-separated, and must have **exactly 29 time and irradiance values**.

The first column contains the exposure time; the second column contains the irradiance. Note: The text files can be generated in Microsoft Excel via any text editor or via the function “Save as” as a “text (tab-separated) (*.txt)”.

Example:

```
1.0 100
1.0 0
1.0 100
```

```
0 0
0 0
...
```

The first step is 100% performance for 1 second, followed by 1 second with 0% and 1 second with 100% performance. Please note that the duration must be > 0. Otherwise all the consecutive steps will be ignored.

Transfer the profile into the UV LED smart with the button “send profile”. This process takes a few seconds. Now the profile is permanently saved.

Start irradiation by button “profile start”.



The maximum step length is 25s. Split a longer irradiation in several single steps.

5.6 Settings

Once the UV LED smart is successfully connected, this COM port is automatically saved. If the module is not identified, please check the COM port on the page “Settings” and press the button “Connect”.

The software saves the settings in a text file under C: \ OpSyTec-Daten \ UVLED Smart\COM.INI. This can be edited with any text editor. When using Microsoft, please use the setting “Text Only” (*.txt).

This ini-file defines the COM port Default. Example (when using COM port 2):

```
COM2
```

If no COM port is displayed or the UV LED smart is not listed, check the installation and / or the device manager (Windows Control Panel).



If the COM port is listed, but the UV LED smart cannot be identified, you can reset it via „RESET Communication“.

6 Operation without any PC

The UV LED smart can be operated without any PC at the breakout box or at the optional power adaptor. Here, the operating mode that was last set at the PC will be executed.

In permanent operation, the UV LED is active, when the pushbutton/footswitch (optional) is pressed or a trigger signal is present.

In the profile operation, the profile is repeated until the pushbutton is pressed. The same applies for the trigger signal.

Pre-set the desired operating mode at the PC. This mode will be permanently saved in the UV LED smart.

Calibration certificate from UV GROBEL



Werks-Kalibrierschein

Factory Calibration Certificate

Auftraggeber: <i>Customer:</i>	Curtin University
Durchführende Person: <i>Executing person:</i>	Klaus Fritz
Kalibrierdatum: <i>Calibration date:</i>	05.05.2015
Gegenstand: <i>Item:</i>	UV-Mat und UVA-Sensor
Hersteller: <i>Manufacturer:</i>	Opsytec Dr. Gröbel GmbH
Radiometer-SN: <i>Radiometer serial number:</i>	820 220 0089
Sensor-SN: <i>Sensor serial number:</i>	811 030 0652
Prüfmittel-ID: <i>Device ID:</i>	
Vorgangsnummer: <i>Process Number:</i>	000127
Empfohlene Gültigkeit der Kalibrierung: <i>Recommended validity of the calibration:</i>	4.5.2016
Anzahl der Seiten: <i>Number of Pages:</i>	2

Klaus Fritz

we apply photonics.

Opsytec Dr. Gröbel GmbH
Goethestraße 17
D-76275 Ettlingen
HRB 361394 Mannheim

Tel. +49(0)7243/9 47 83-50
Fax +49(0)7243/9 47 83-65
info@opsytec.de
www.opsytec.de

Geschäftsführer:
Dr.-Ing. Mark Paravia
Dr.-Ing. Stefan Pieke

Volksbank Ettlingen
IBAN DE67 6609 1200 0000 6461 13
BIC GENODE61ETT
USt. Id.-Nr. DE 811 443 274



Durchführung / Execution

Das vorliegende Radiometer wurde auf Bestrahlungsstärke im angegebenen Wellenlängenbereich kalibriert. Die Kalibrierung erfolgte unter Verwendung der angegebenen Lampe. Die Strahlung der Lampe wird mit einem kalibrierten Spektralradiometer, Typ PC-Spektrometer, SN 840320 0052, der Fa. Dr. Gröbel UV-Elektronik GmbH spektral gemessen und hieraus die Bestrahlungsstärke im angegebenen Spektralbereich als Sollwert bestimmt. Das Spektralradiometer war zum Zeitpunkt der Messung rückführbar auf die PTB kalibriert. Die Kalibrierung erfolgte am 04.02.2015 mit dem Halogenleuchtampenstandard FEL 1000 W (#860 300 101) gemäß Kalibrierschein S108-4.11-PTB98 und ist gültig bis 03.02.2016. Die Umgebungstemperatur lag bei $23\text{ °C} \pm 2\text{ °C}$. Die Luftfeuchtigkeit betrug 69%.

This radiometer has been calibrated to irradiance in the specified wavelength range. The calibration was carried out using the given lamp.

The radiation from the lamp is spectrally measured with a calibrated spectroradiometer, Type PC spectrometer, SN 840320 0052, from Dr. Gröbel UV-Elektronik GmbH, and this determines the irradiance in the given spectral range as the target value. The spectral radiometer was calibrated traceable at the time of measurement against the PTB. Calibration was carried out on 02/04/2015 with the FEL 1000 W (# 860 300 101) halogen bulb standard in accordance with S108-4.11 PTB98 calibration certificate and is valid until 02/03/2016. The ambient temperature was $23\text{ °C} \pm 2\text{ °C}$. The humidity was 69%.

Die resultierende Unsicherheit der Kalibrierung wird aus der erweiterten Messunsicherheit des Halogenleuchtampenstandard (3%) unter Berücksichtigung der Positionier- und Wiederholgenauigkeit der Sensors und des Spektrometers berechnet. Die Messunsicherheit entspricht bei einer Normalverteilung der Abweichung vom Kalibrierwert einer Überdeckungswahrscheinlichkeit von 95% ($k=2$).

The resulting uncertainty of the calibration is calculated from the expanded uncertainty of the halogen bulb standard (3%) based on the positioning accuracy and repeatability of the sensors and the spectrometer. The uncertainty of measurement corresponds to a normal distribution of the deviation from the calibration value of a coverage probability of 95% ($k=2$).

Kalibrierdaten / Calibration data

Verwendete Strahlenquelle <i>Calibration Source</i>	:	Osram L100W/79
Spektralbereich <i>Spectral range</i>	:	315 - 400 nm
Sollwert <i>Target value</i>	:	5,00 mW/cm²
Wert vor Kalibrierung <i>Display value before calibration</i>	:	5,00 mW/cm² +0%
Wert nach Kalibrierung <i>Display value after calibration</i>	:	5,00 mW/cm²
Messunsicherheit <i>Measurement uncertainty</i>	:	±7%

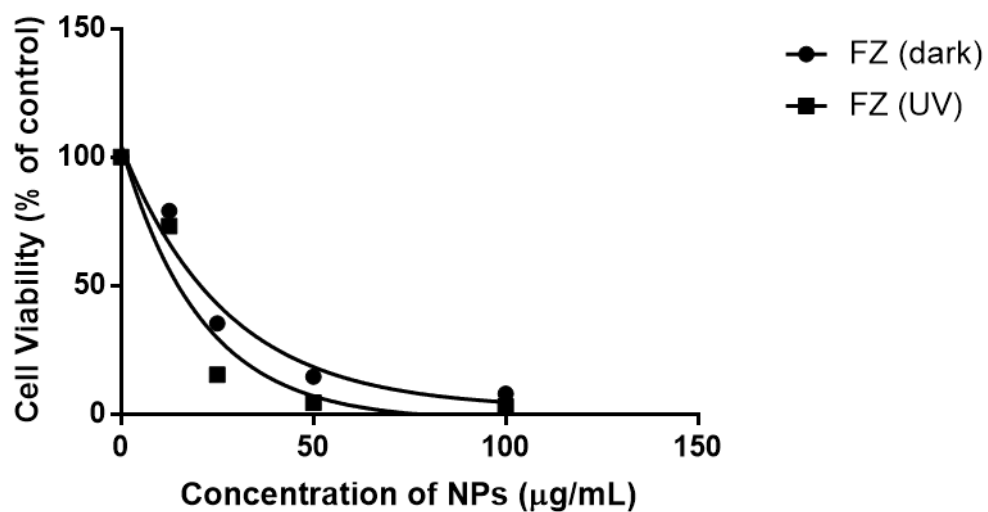
Die Kalibrierung erfolgte mit Justage des Anzeigewertes auf den Sollwert.

The calibration was performed with adjustment of display value to the target value.

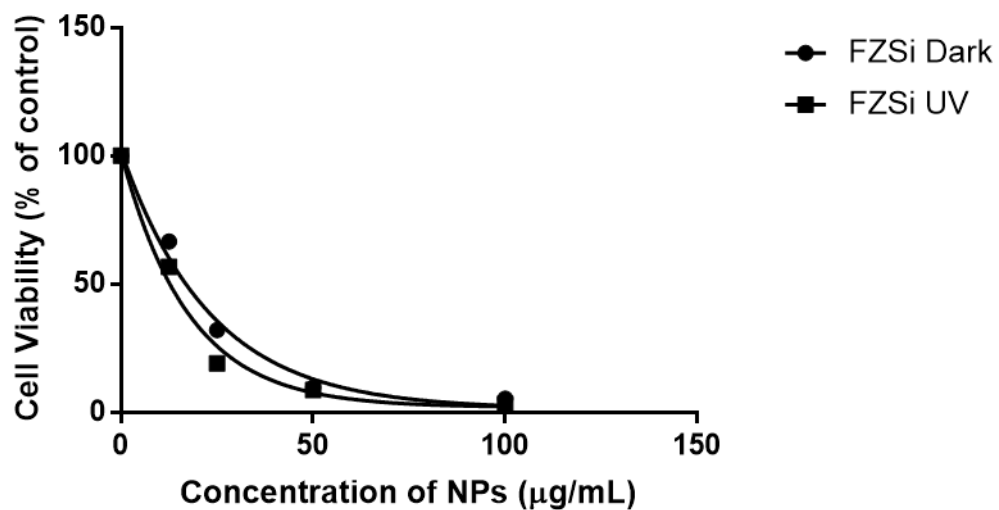
Appendix 12:

Dose response curves of hybrid NPs at 24 h dark and 24 h UV-A treated in B16-F10 cells

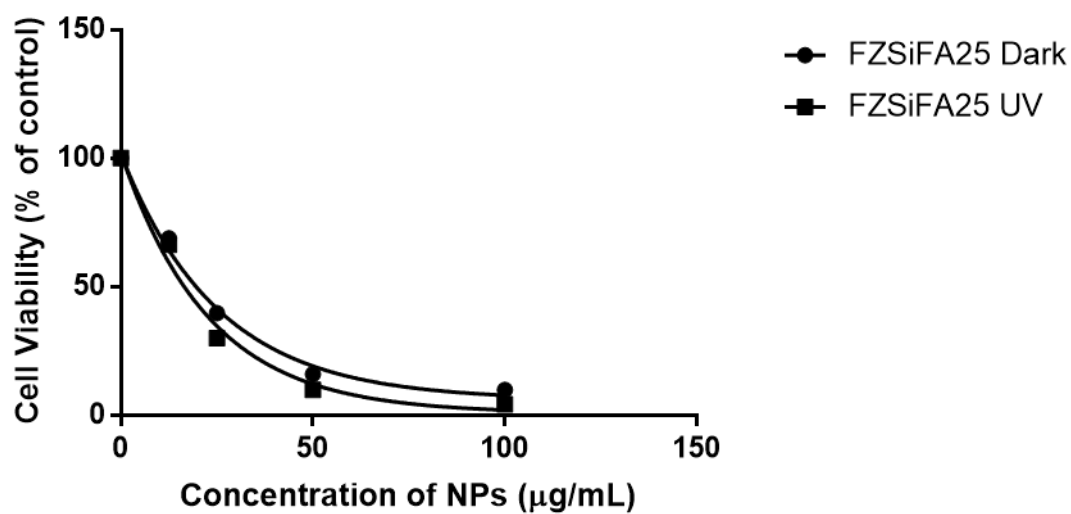
FZ Dose response curve



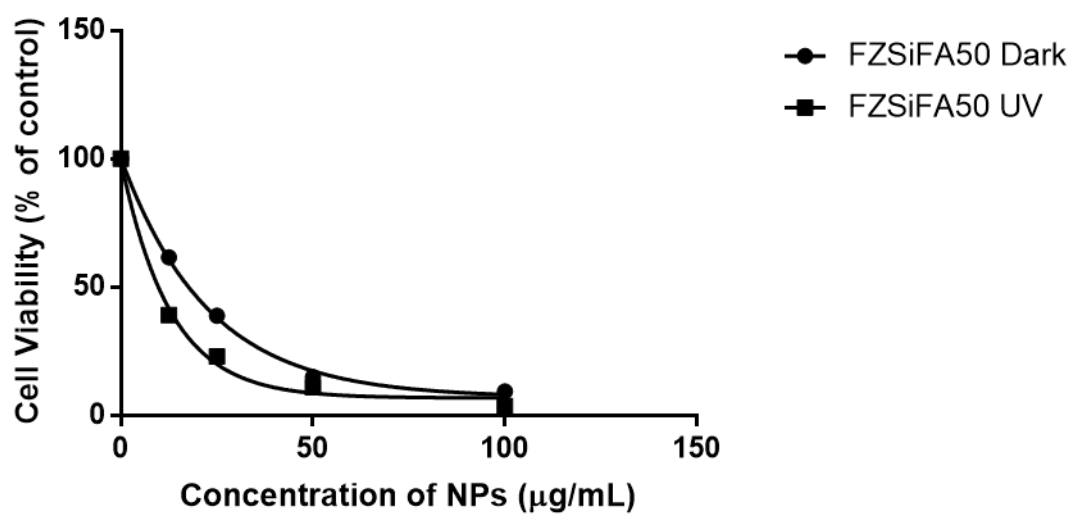
FZSi Dose response curve



FZSiFA25 Dose response curve



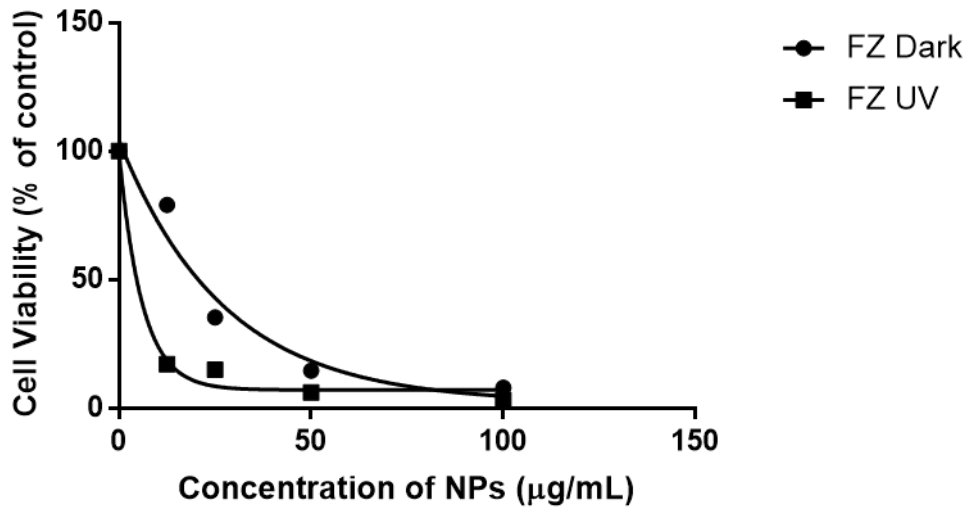
FZSiFA50 Dose response curve



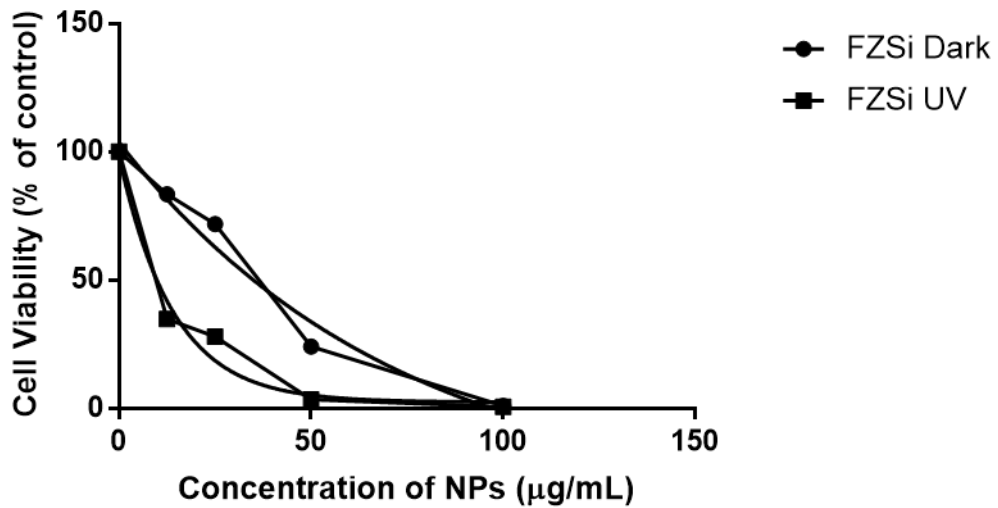
Appendix 13

Dose response curves of hybrid NPs at 24 h dark and 24 h UV-A treated in Caco-2 cells

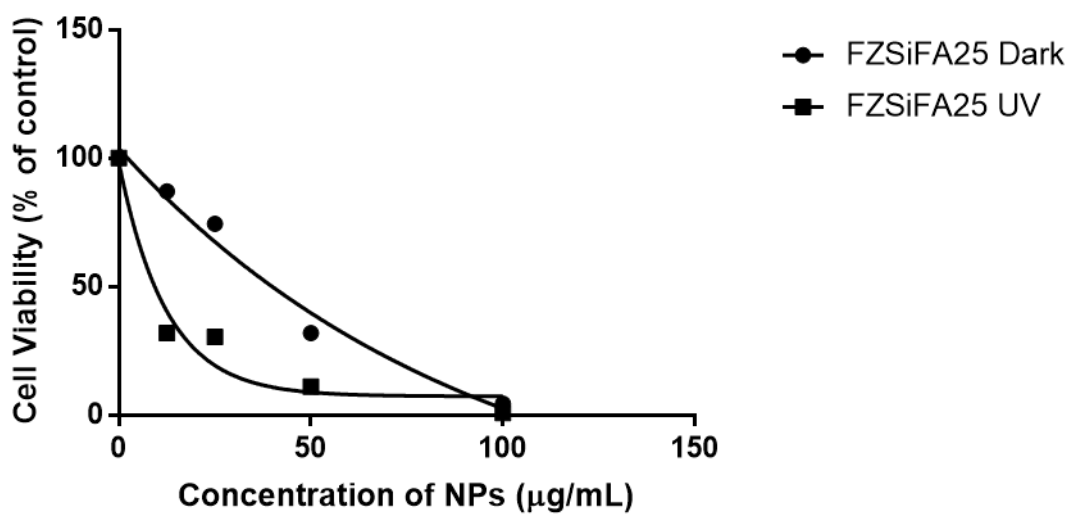
FZ Dose response curve



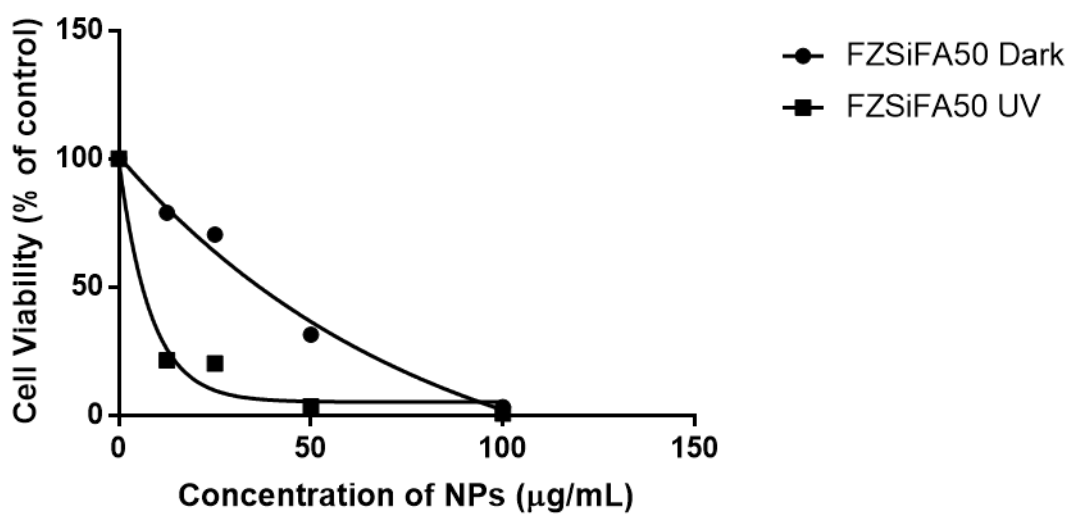
FZSi Dose response curve



FZSiFA25 Dose response curve



FZSiFA50 Dose response curve



Appendix 14: ROS generation in B16-F10 cells by hybrid NPs alone and in combination with UV-A irradiation

Nanoparticle	Dark ^a					UV-A irradiated ^b			
	Control (%)	0 h (%)	2 h (%)	6 h (%)	24 h (%)	0 h (%)	2 h (%)	6 h (%)	24 h (%)
FZ 12.5 µg/mL	100	101.94±8.37	104.05±4.19	104.12±5.30	5.73±1.25	107.15±3.87	113.34±1.33	120.18±5.34	89.59±1.51
FZ 25 µg/mL		107.34±9.25	109.41±3.52	111.82±11.10	10.75±1.46	118.81±1.73	121.82±4.54	124.36±2.80	92.18±4.38
FZ 50 µg/mL		108.51±5.87	111.40±5.36	135.86±7.05	11.01±0.48	136.55±2.16	146.66±3.21	152.33±3.40	107.56±1.26
FZSi 12.5 µg/mL		102.80±2.33	107.24±2.09	104.67±4.46	9.31±1.84	109.13±9.38	110.76±1.79	112.36±3.01	74.09±4.08
FZSi 25 µg/mL		104.89±3.14	114.99±2.62	113.87±6.67	9.75±3.10	112.59±2.49	113.37±6.58	129.83±1.64	79.92±3.54
FZSi 50 µg/mL		110.60±3.51	118.97±10.64	130.61±11.01	10.17±1.88	128.78±4.47	134.74±11.02	156.08±2.61	99.95±7.54
FZSiFA25 12.5 µg/mL		103.03±7.04	109.27±4.58	104.09±4.74	4.95±1.48	127.62±2.90	138.50±2.53	143.76±3.64	104.70±5.93
FZSiFA25 25 µg/mL		110.42±9.37	111.22±7.12	115.74±5.00	10.96±2.59	136.13±2.44	155.92±3.52	190.51±1.45	109.89±6.57
FZSiFA25 50 µg/mL		113.72±2.61	119.92±10.42	121.18±7.87	11.09±0.74	143.02±5.83	218.40±5.58	237.29±7.40	124.16±2.68
FZSiFA50 12.5 µg/mL		100.81±6.07	101.99±5.33	103.74±5.24	6.22±0.95	132.51±6.51	159.41±7.85	188.73±2.51	87.00±1.97
FZSiFA50 25 µg/mL		100.95±3.57	107.46±4.54	111.46±4.50	8.25±1.32	143.83±2.64	178.27±9.08	196.30±4.71	102.99±4.08
FZSiFA50 50 µg/mL		108.01±2.46	118.07±6.38	123.01±5.33	10.39±0.37	149.53±9.39	211.21±13.54	245.65±19.96	113.19±7.99
Only UV						101.44±1.33	108.21±2.85	109.11±3.44	99.31±2.87

^aDark represents the ROS generated in B16-F10 cells upon treatment with hybrid NPs.

^bUV-A irradiated represents the ROS generated in B16-F10 cells upon treatment with hybrid NPs and UV-A irradiation at the dose of (10 J/cm²).

Control represents B16-F10 cells in culture growth medium without NPs treatment.

UV-A irradiated groups contain only UV-A exposed B16-F10 cells as the control.

Data are represented as mean ±SD (n=4). The ROS yield from only NPs in DMEM medium (no cells) and ROS yield from only NPs in DMEM medium exposed to UV-A radiation (10 J/cm²) (no cells) have been deducted from ROS generated by samples in dark (in cells), and in UV-A irradiated (in cells) respectively.

Appendix 15:

ROS generation in DMEM medium treated with NPs (no cells)

Nanoparticle	Dark					UV-A irradiated			
	Control	0 h (%)	2 h (%)	6 h (%)	24 h (%)	0 h (%)	2 h (%)	6 h (%)	24 h (%)
FZ 12.5 µg/mL	100	29.66±4.37	27.04±4.47	22.20±7.52	19.27±0.95	41.27±0.65	48.77±2.69	45.83±2.55	15.89±1.75
FZ 25 µg/mL		33.38±0.56	30.82±3.34	27.37±3.92	19.45±2.33	54.40±3.40	69.95±1.69	62.62±1.66	9.05±2.26
FZ 50 µg/mL		22.92±1.31	16.85±1.87	18.76±8.17	14.32±1.32	46.91±1.37	42.54±2.55	48.35±2.10	5.52±2.71
FZSi 12.5 µg/mL		27.54±1.29	25.85±9.08	26.52±6.81	21.96±1.25	58.82±2.45	42.58±2.95	46.10±2.24	17.12±1.81
FZSi 25 µg/mL		27.56±0.59	28.02±1.77	27.66±5.27	23.58±1.36	55.42±1.67	52.46±3.12	27.13±0.91	7.31±0.88
FZSi 50 µg/mL		25.72±1.81	21.13±3.07	18.77±4.47	15.98±0.89	48.47±1.64	47.01±2.20	52.82±1.61	6.39±1.30
FZSiFA25 12.5 µg/mL		24.76±2.16	23.45±3.62	21.66±14.30	19.31±0.81	53.89±0.11	56.40±0.14	37.20±2.55	11.52±1.92
FZSiFA25 25 µg/mL		18.43±5.38	19.73±3.25	18.49±3.51	15.99±1.02	52.51±2.58	53.10±2.29	61.98±2.35	7.54±1.97
FZSiFA25 50 µg/mL		6.76±8.88	11.56±1.07	11.82±5.65	11.87±1.05	52.16±1.59	50.71±2.46	53.83±1.83	6.23±2.13
FZSiFA50 12.5 µg/mL		22.11±4.31	21.09±9.09	21.87±2.21	17.71±1.61	47.91±0.36	62.20±1.87	60.07±2.29	9.72±0.59
FZSiFA50 25 µg/mL		18.35±1.35	17.95±6.11	16.97±4.31	14.69±1.39	57.93±1.41	50.32±1.28	58.30±0.36	10.56±0.52
FZSiFA50 50 µg/mL		17.25±2.74	17.41±1.68	16.08±2.83	13.93±0.61	54.51±0.40	52.98±0.64	39.93±1.60	12.65±1.63

Dark represents the ROS generated in DMEM medium with hybrid NPs alone. UV-A irradiated represents the ROS generated in DMEM medium with hybrid NPs + UV-A irradiation (10 J/cm²). Data are represented as mean ±SD (n=4). B16-F10 cells not treated with NPs served as the control for the dark and B16-F10 cells treated with UV-A radiation served as the control for the UV-A irradiated group.

Appendix 16: ROS generation in Caco-2 cells by hybrid nanoparticles and UV-A irradiation

Nanoparticle	Dark ^a					UV-A irradiated ^b			
	Control	0 h (%)	2 h (%)	6 h (%)	24 h (%)	0 h (%)	2 h (%)	6 h (%)	24 h (%)
FZ 12.5 µg/mL	100	102.56±7.69	102.83±10.20	106.38±4.01	31.75±13.15	115.70±11.03	103.74±7.15	115.26±4.62	11.55±1.65
FZ 25 µg/mL		107.69±7.69	120.75±5.66	129.78±12.04	78.83±7.12	115.92±7.42	120.97±2.48	122.79±4.71	12.83±1.41
FZ 50 µg/mL		123.07±13.86	137.73±4.32	143.61±6.95	84.30±13.27	124.78±4.20	154.15±3.67	147.09±3.11	14.32±5.30
FZSi 12.5 µg/mL		106.41±15.54	117.92±7.12	120.74±6.95	36.49±9.93	114.86±6.62	113.46±3.81	115.04±3.86	11.85±0.86
FZSi 25 µg/mL		116.66±18.17	122.64±9.93	130.31±8.18	51.45±4.77	131.08±2.71	130.44±4.06	118.65±6.90	31.35±2.00
FZSi 50 µg/mL		132.05±17.76	132.07±4.32	135.63±2.43	83.21±3.28	147.33±7.99	147.65±10.93	127.01±10.06	30.46±1.04
FZSiFA25 12.5 µg/mL		102.56±5.87	114.15±9.09	115.95±4.87	33.21±11.70	104.18±7.99	108.79±3.18	110.63±5.90	16.56±6.23
FZSiFA25 25 µg/mL		106.41±3.84	116.03±4.32	117.55±10.46	43.79±9.93	106.84±8.72	115.04±5.27	120.53±4.35	41.22±1.10
FZSiFA25 50 µg/mL		111.53±14.56	134.90±9.39	137.76±12.08	85.03±4.42	112.58±11.99	112.33±6.89	125.26±6.98	38.98±1.67
FZSiFA50 12.5 µg/mL		107.69±8.88	108.49±13.96	112.76±8.18	37.59±9.81	123.81±8.16	125.16±3.49	121.99±3.67	67.08±2.02
FZSiFA50 25 µg/mL		117.94±14.56	126.41±14.15	131.38±4.60	43.79±7.29	132.39±6.01	141.01±3.77	147.73±3.37	31.70±7.32
FZSiFA50 50 µg/mL		120.51±8.00	133.96±10.71	143.08±6.38	78.10±6.41	129.26±11.40	142.90±4.08	149.75±2.90	24.20±4.25

^aDark represents the ROS generated in Caco-2 cells upon treatment with hybrid NPs.

^bUV-A irradiated represents the ROS generated in Caco-2 cells upon treatment with hybrid NPs and UV-A irradiation at the dose of (10 J/cm²).

Control represents Caco-2 cells in culture growth medium without NPs treatment.

UV-A irradiated groups contain only UV-A exposed Caco-2 cells as the control.

Data are represented as mean ±SD (n=4). The ROS yield from only NPs in DMEM medium (no cells) and ROS yield from only NPs in DMEM medium exposed to UV-A radiation (10 J/cm²) (no cells) have been deducted from ROS generated by samples in dark (in cells), and in UV-A irradiated (in cells) respectively.

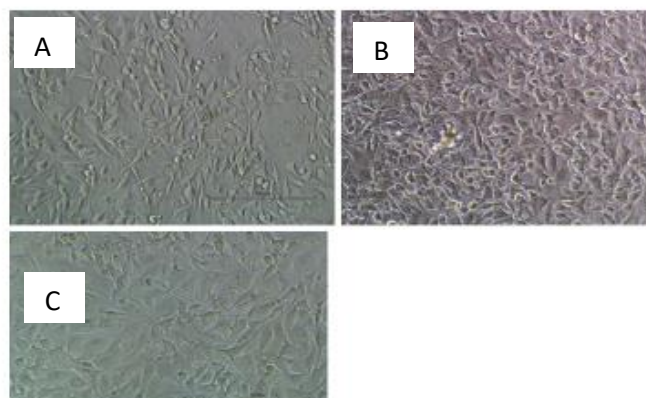
Appendix 17:

ROS generation in DMEM medium treated with NPs (no cells)

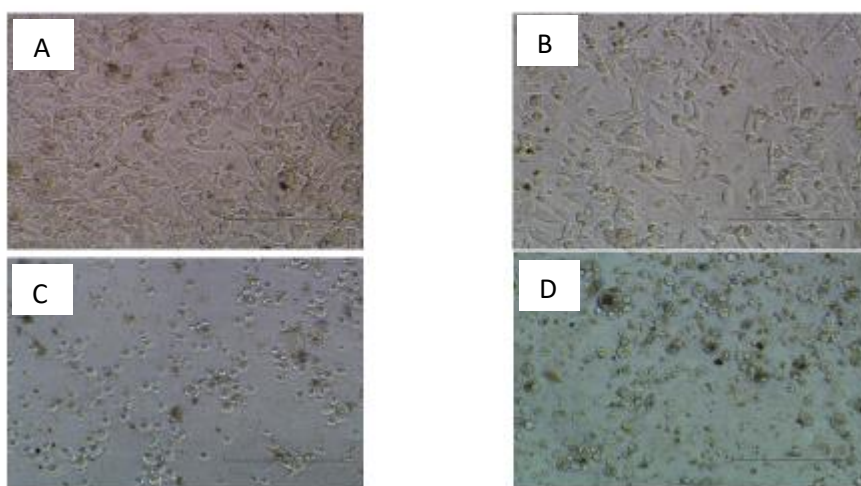
Nanoparticle	Dark					UV-A irradiated			
	Control	0 h (%)	2 h (%)	6 h (%)	24 h (%)	0 h (%)	2 h (%)	6 h (%)	24 h (%)
FZ 12.5 µg/mL	100	31.86±0.64	24.89±1.66	53.03±19.58	21.83±3.19	43.53±4.79	46.52±2.03	31.11±12.47	27.36±6.70
FZ 25 µg/mL		26.14±2.83	17.56±3.77	20.71±6.74	13.05±2.03	41.94±3.73	44.44±6.95	45.40±1.86	24.66±5.93
FZ 50 µg/mL		22.53±2.33	26.30±0.65	16.88±14.55	9.71±1.05	41.16±6.63	43.11±5.22	45.00±0.85	22.69±9.13
FZSi 12.5 µg/mL		23.20±1.96	34.53±2.22	33.94±10.06	19.62±3.19	36.31±1.87	44.20±10.51	27.01±2.80	30.93±12.01
FZSi 25 µg/mL		17.33±1.87	23.44±7.25	24.99±18.01	8.20±1.01	48.00±3.52	66.40±3.22	31.11±4.18	33.39±3.21
FZSi 50 µg/mL		31.75±2.14	25.26±2.10	31.72±13.93	25.41±1.93	40.89±2.23	42.43±8.27	44.74±4.83	31.18±9.22
FZSiFA25 12.5 µg/mL		30.00±1.67	17.72±3.88	28.77±11.02	13.73±1.84	44.52±4.96	40.96±9.23	38.17±3.71	28.35±5.64
FZSiFA25 25 µg/mL		35.89±1.75	18.51±0.43	28.45±12.45	11.05±2.60	45.02±3.36	49.26±3.72	43.26±1.50	34.99±6.30
FZSiFA25 50 µg/mL		21.89±3.89	8.29±2.56	13.38±8.69	5.66±0.69	49.95±12.71	43.35±1.15	46.71±0.56	24.90±12.78
FZSiFA50 12.5 µg/mL		20.54±3.15	29.52±1.92	35.82±28.64	11.63±0.22	45.57±7.90	48.45±5.04	40.14±2.14	26.50±1.85
FZSiFA50 25 µg/mL		21.10±1.35	11.71±15.97	28.68±11.54	16.23±4.51	44.22±8.22	46.02±0.88	47.20±3.16	38.06±9.72
FZSiFA50 50 µg/mL		23.29±1.05	11.89±1.76	31.17±32.31	12.09±1.65	41.94±16.36	47.45±4.49	42.62±0.75	32.04±15.90

Dark represents the ROS generated on treatment with hybrid NPs alone. UV-A irradiated represents the ROS generated on treatment with hybrid NPs + UV-A irradiation (10 J/cm²). Data are represented as mean ±SD (n=4). Caco-2 cells not treated with NPs served as the control for the dark and Caco-2 cells treated with UV-A radiation served as the control for the UV-A irradiated group.

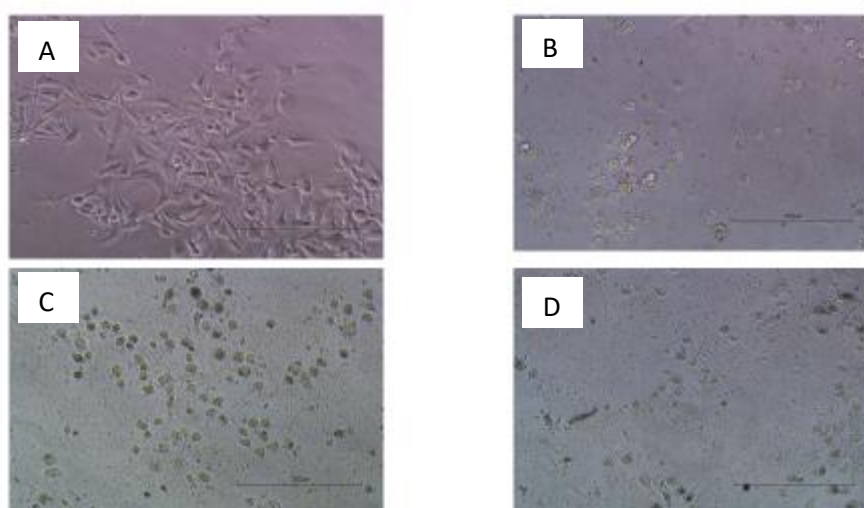
Appendix 18: Morphology of B16-F10 cells after hybrid NPs treatment



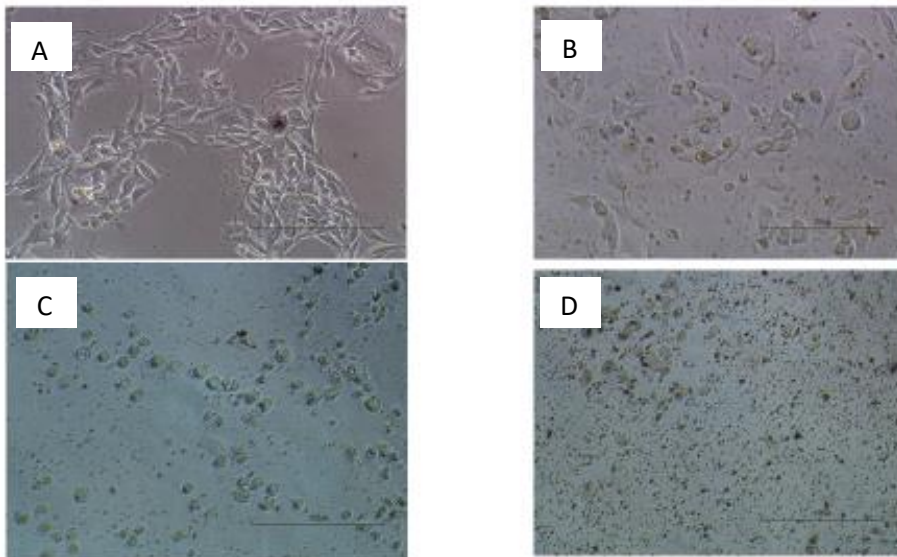
B16-F10 cells A) Control after 6h B) control after 24h C) control after 24h UV-A exposure



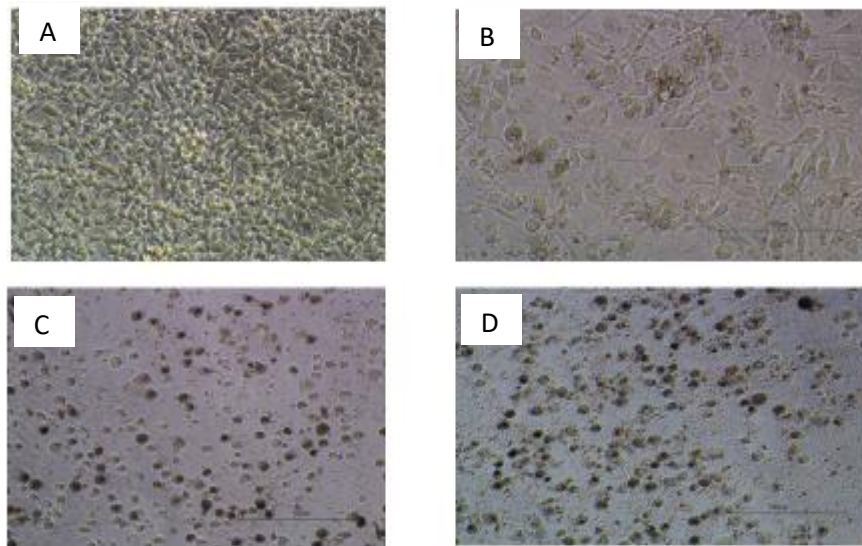
B16-F10 cells after 6 h FZSi NPs treatment A) 12.5 B) 25 C) 50 D)100 µg/mL



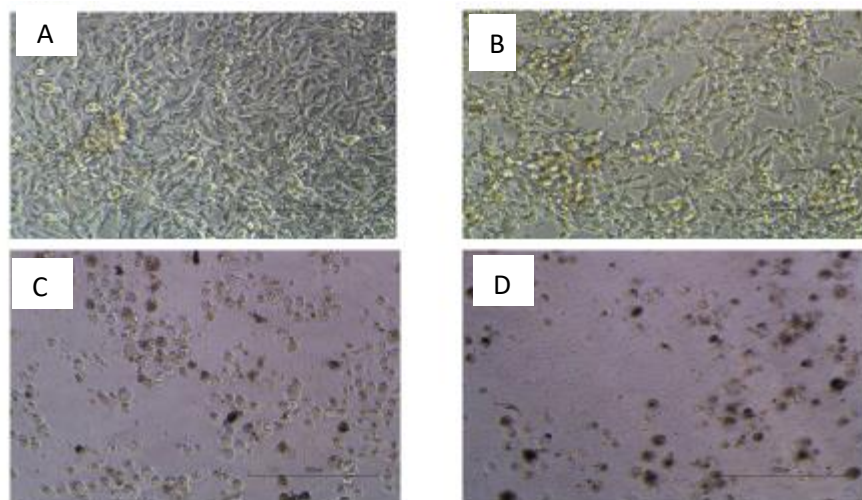
B16-F10 cells after 6 h FZSiFA25 NPs treatment A) 12.5 B) 25 C) 50 D)100 µg/mL



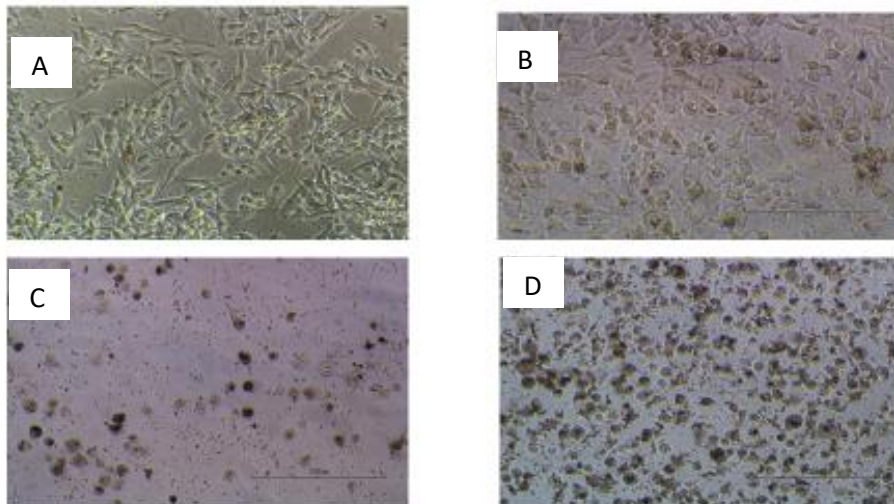
B16-F10 cells after 6 h FZSiFA50 NPs treatment A) 12.5 B) 25 C) 50 D)100 µg/mL



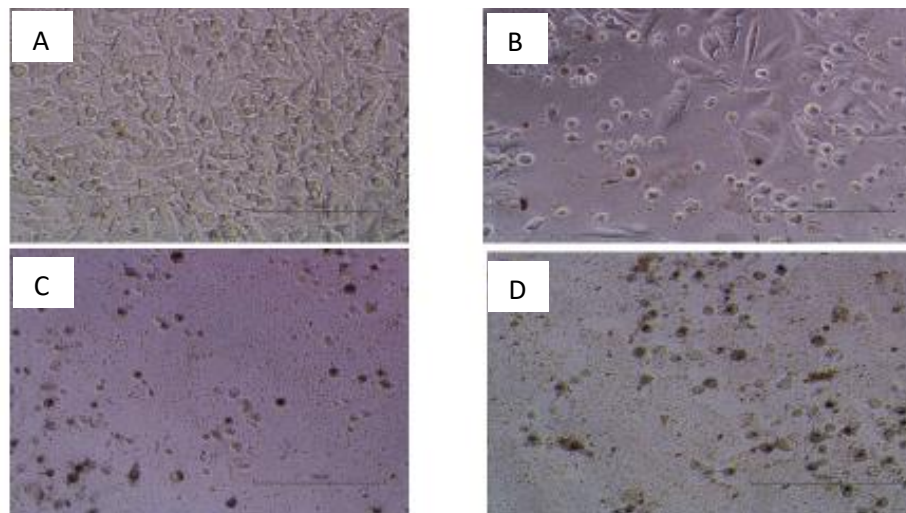
B16-F10 cells after 24 h FZSi NPs treatment A) 12.5 B) 25 C) 50 D)100 µg/mL



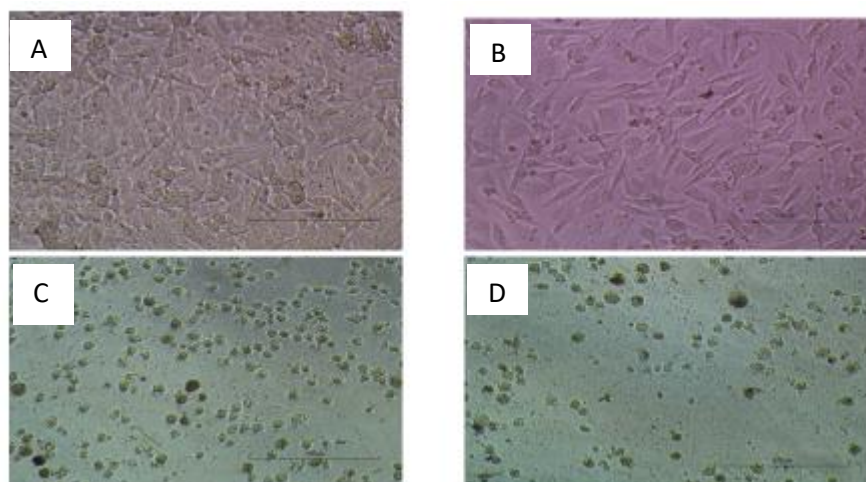
B16-F10 cells after 24 h FZSiFA25 NPs treatment A) 12.5 B) 25 C) 50 D)100 µg/mL



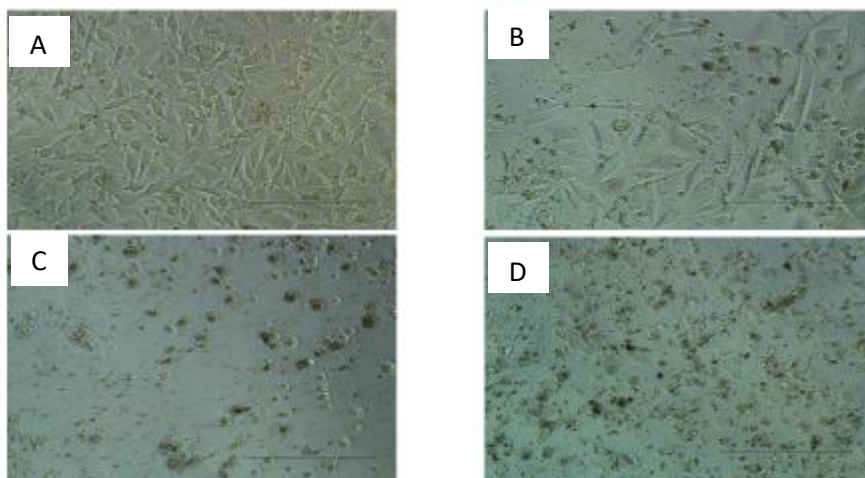
B16-F10 cells after 24 h FZSiFA50 NPs treatment A) 12.5 B) 25 C) 50 D)100 µg/mL



B16-F10 cells after 24 h FZSi NPs & UV-A treatment A) 12.5 B) 25 C) 50 D)100 µg/mL

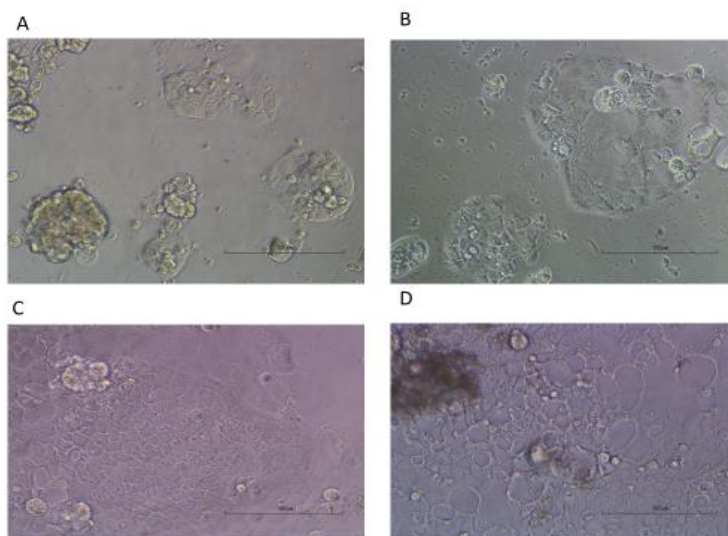


B16-F10 cells after 24 h FZSiFA25 NPs & UV-A treatment A) 12.5 B) 25 C) 50 D)100 µg/mL

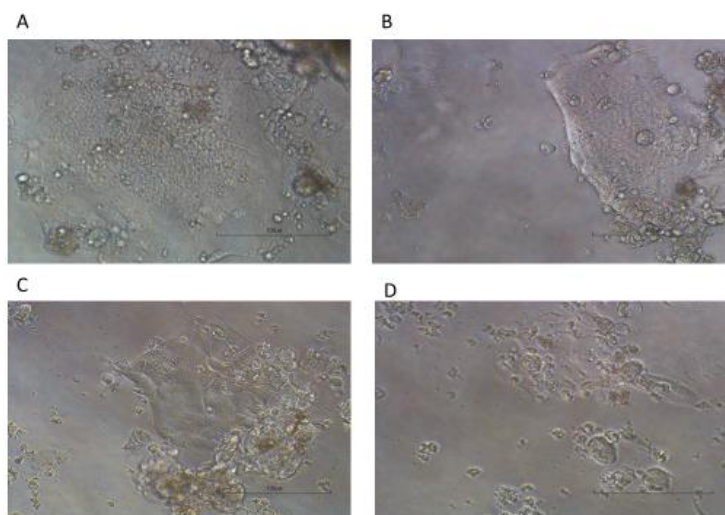


B16-F10 cells after 24 h FZSiFA50 NPs & UV-A treatment A) 12.5 B) 25 C) 50 D)100 $\mu\text{g}/\text{mL}$

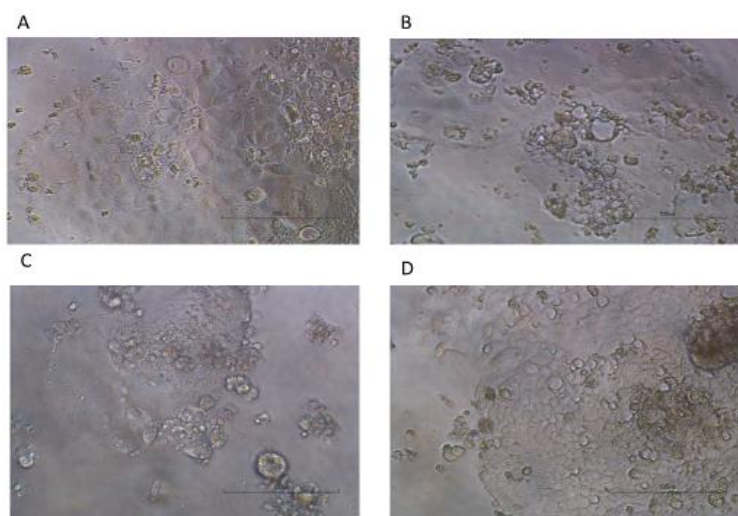
Appendix 19: Morphology of Caco-2 cells after hybrid NPs treatment



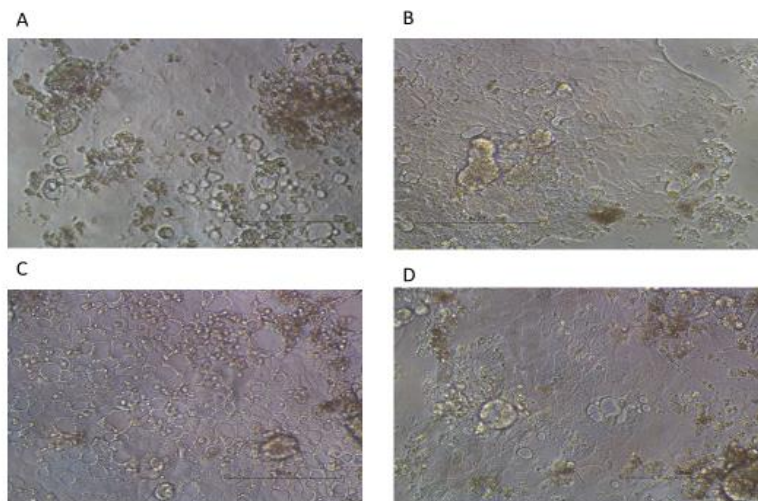
A & B: Caco-2 cells growth after 24h & 48h seeding C&D: control from NPs treated & UV exposed plate



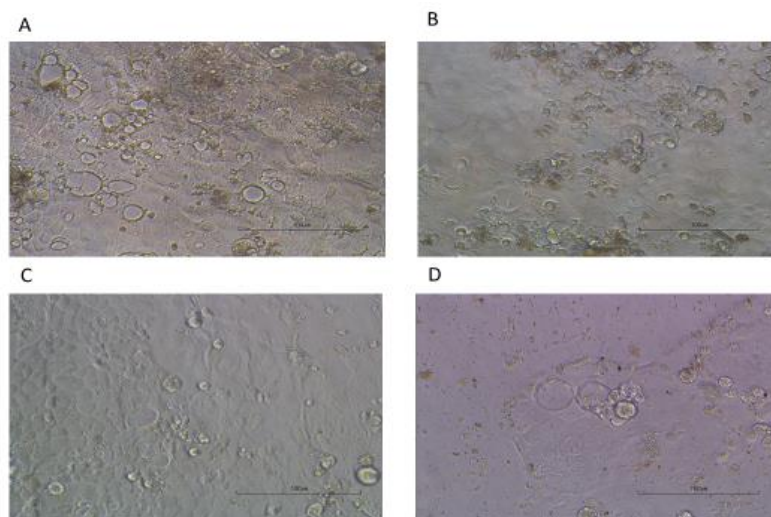
Caco-2 cells after 6h FZ NPs treatment (A:12.5, B:25, C:50, D:100 µg/ml)



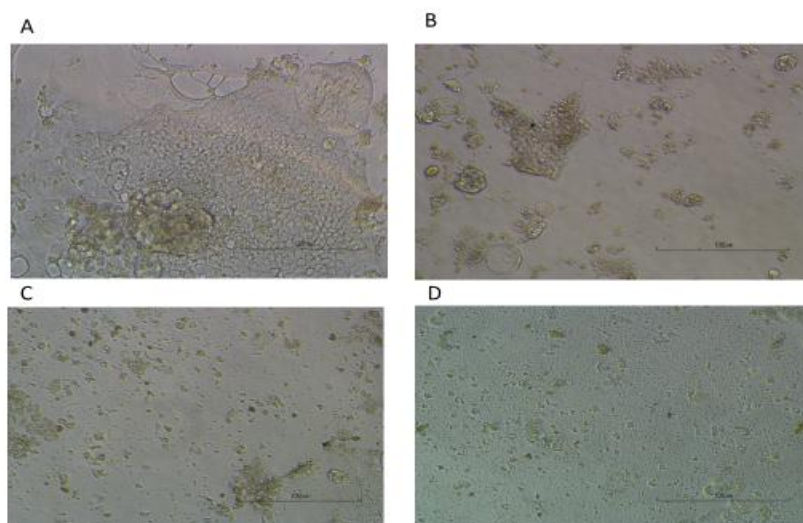
Caco-2 cells after 6h FZSi NPs treatment (A:12.5, B:25, C:50, D:100 µg/ml)



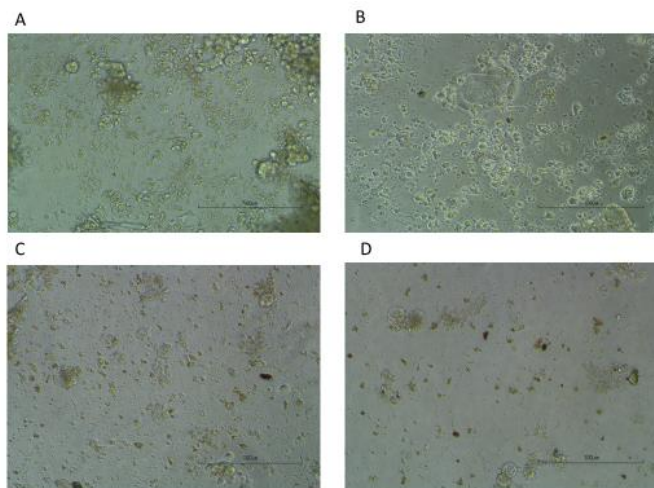
Caco-2 cells after 6h FZSiFA25 NPs treatment (A:12.5, B:25, C:50, D:100 µg/ml)



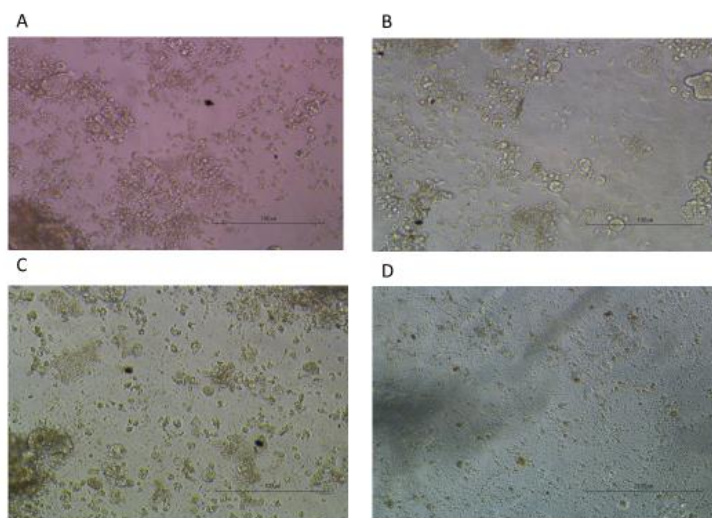
Caco-2 cells after 6h FZSiFA50 NPs treatment (A:12.5, B:25, C:50, D:100 µg/ml)



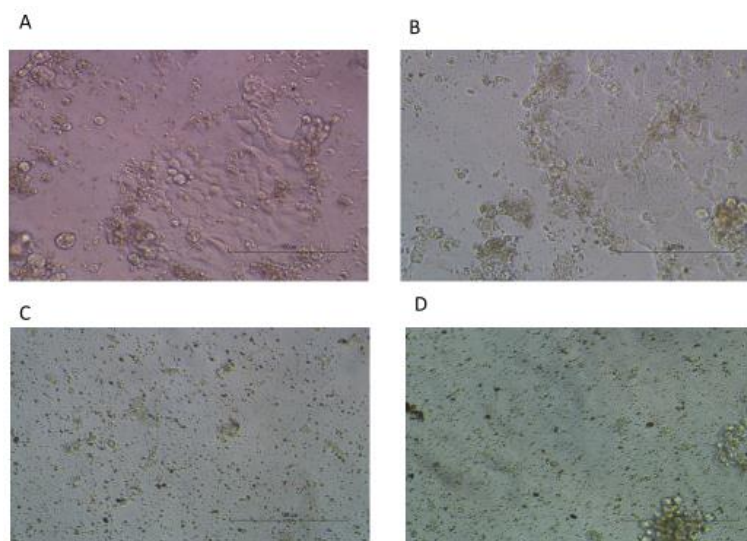
Caco-2 cells after 24h FZNPs treatment (A:12.5, B:25, C:50, D:100 µg/ml)



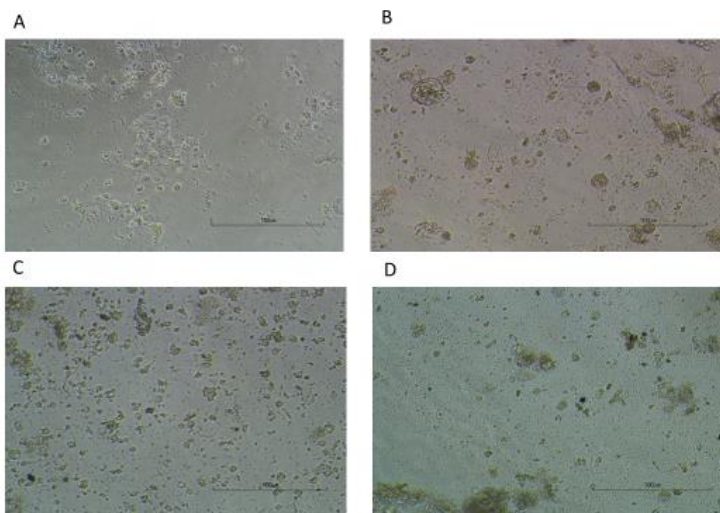
Caco-2 cells after 24h FZSiNPs treatment (A:12.5, B:25, C:50, D:100 µg/ml)



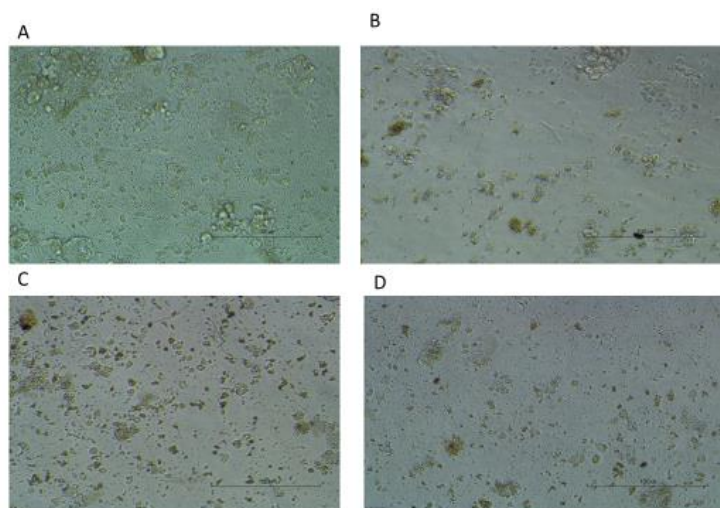
Caco-2 cells after 24h FZSiFA25 NPs treatment (A:12.5, B:25, C:50, D:100 µg/ml)



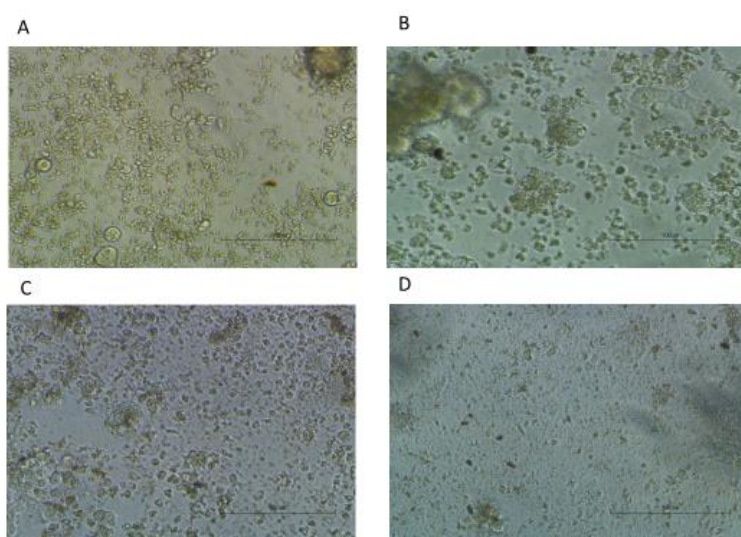
Caco-2 cells after 24h FZSiFA50 NPs treatment (A:12.5, B:25, C:50, D:100 µg/ml)



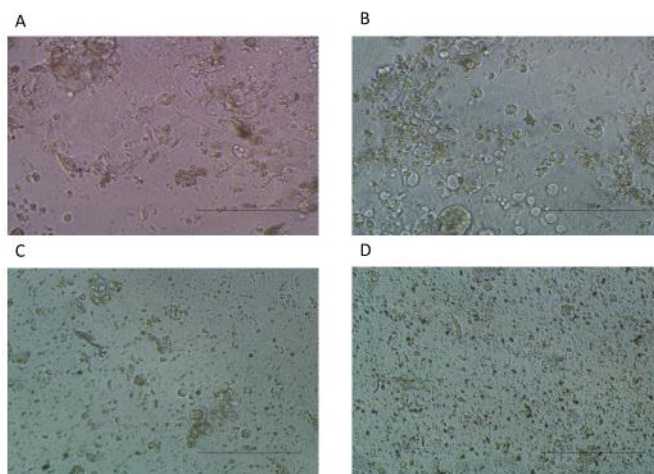
Caco-2 cells after 24h FZNP & UV treatment (A:12.5, B:25, C:50, D:100 $\mu\text{g/ml}$)



Caco-2 cells after 24h FZSiNP & UV treatment (A:12.5, B:25, C:50, D:100 $\mu\text{g/ml}$)

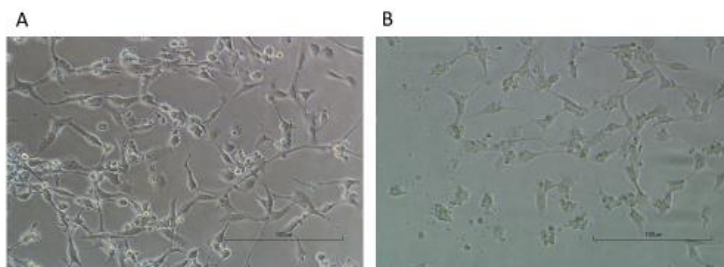


Caco-2 cells after 24h FZSiFA25NP & UV treatment (A:12.5, B:25, C:50, D:100 $\mu\text{g/ml}$)

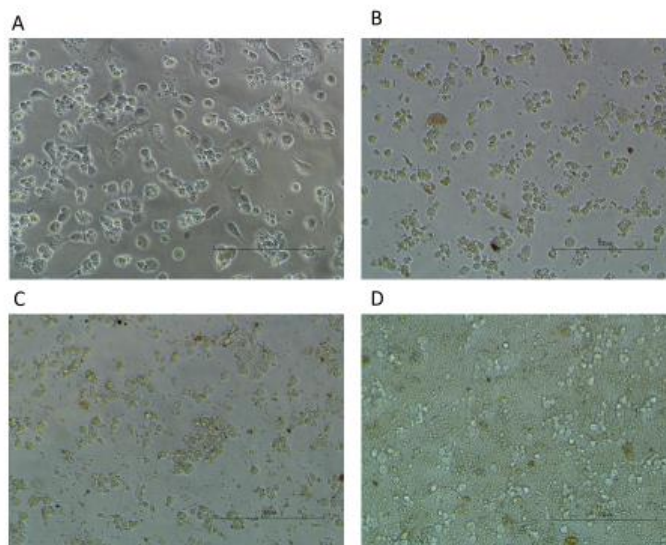


Caco-2 cells after 24h FZSiFA50NPs & UV treatment (A:12.5, B:25, C:50, D:100 $\mu\text{g/ml}$)

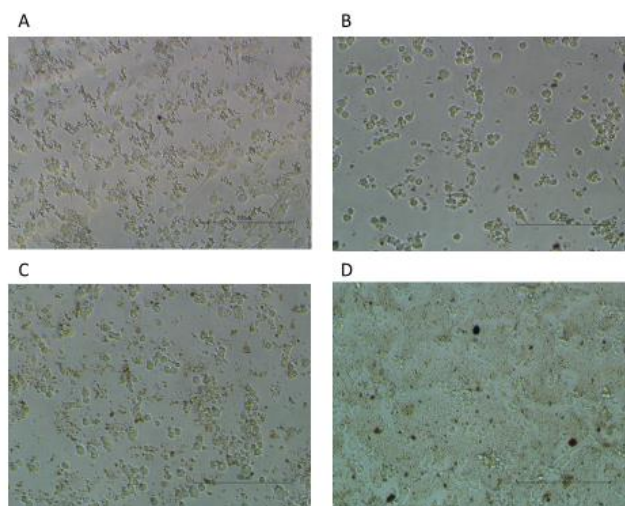
Appendix 20: Morphology of 3T3 cells after hybrid NPs treatment



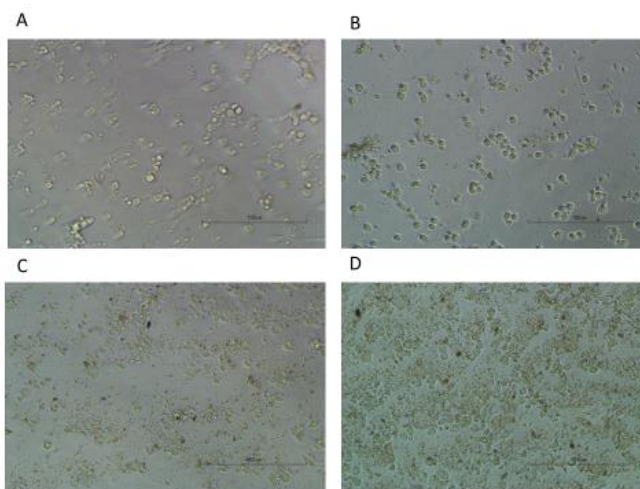
3T3 cells untreated after A: 6 h & B: 24h



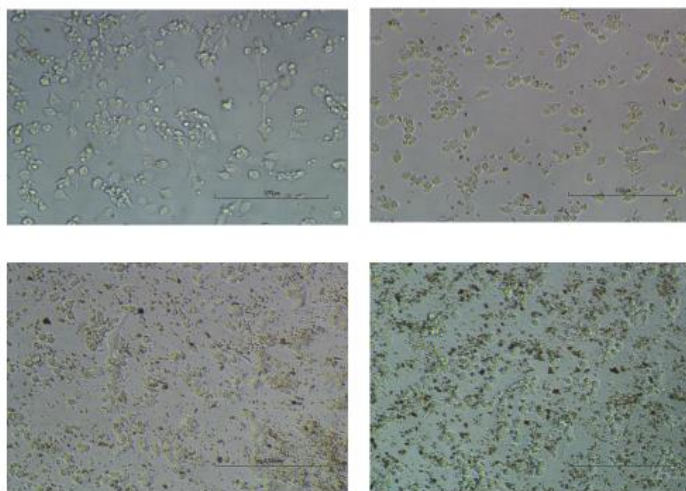
3T3 cells after 6 h FZ NPs treatment (A:12.5,B:25,C:50,D:100 µg/ml)



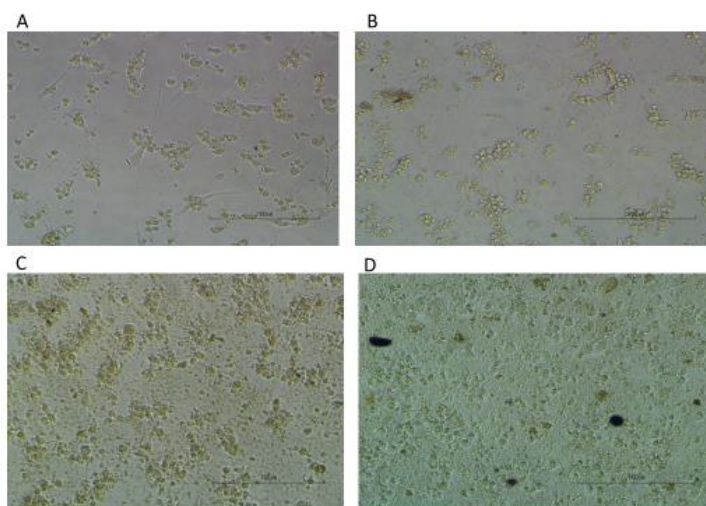
3T3 cells after 6 h FZSi NPs treatment (A:12.5,B:25,C:50,D:100 µg/ml)



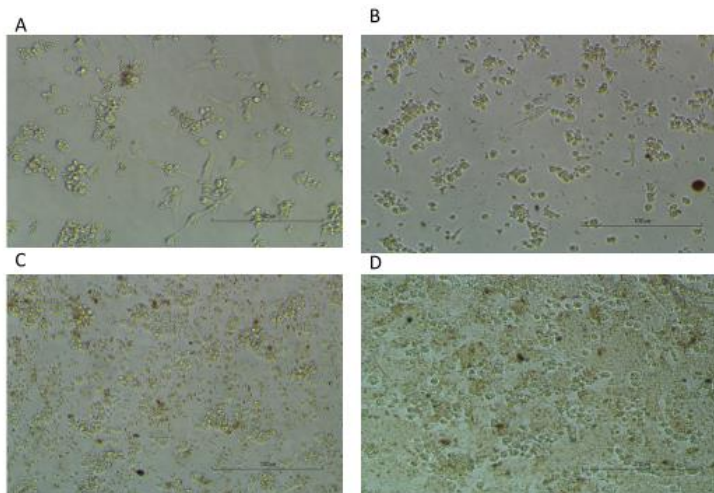
3T3 cells after 6 h FZSiFA25 NPs treatment (A:12.5,B:25,C:50,D:100 µg/ml)



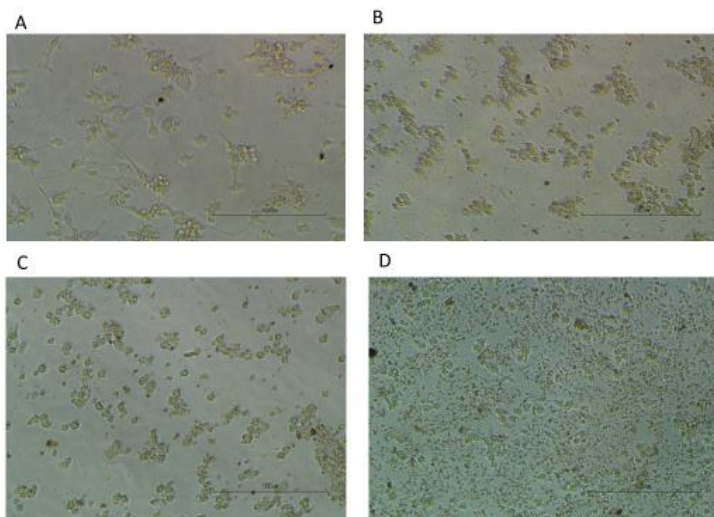
3T3 cells after 6 h FZSiFA50 NPs treatment (A:12.5,B:25,C:50,D:100 µg/ml)



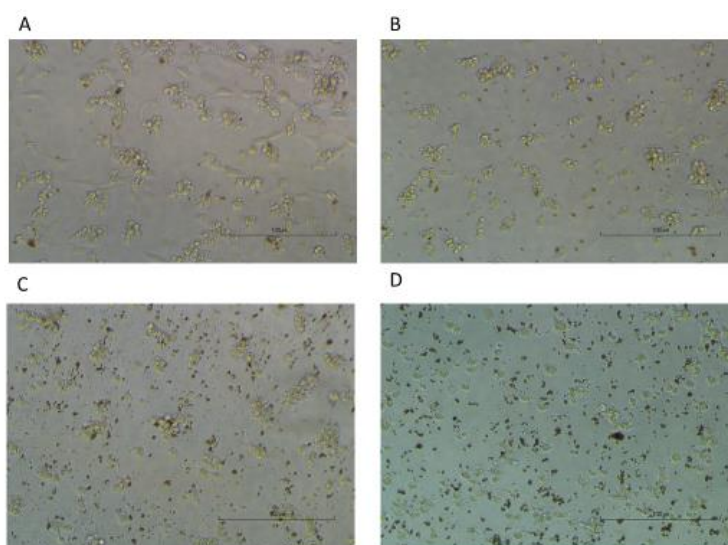
3T3 cells after 24 h FZ NPs treatment (A:12.5,B:25,C:50,D:100 µg/ml)



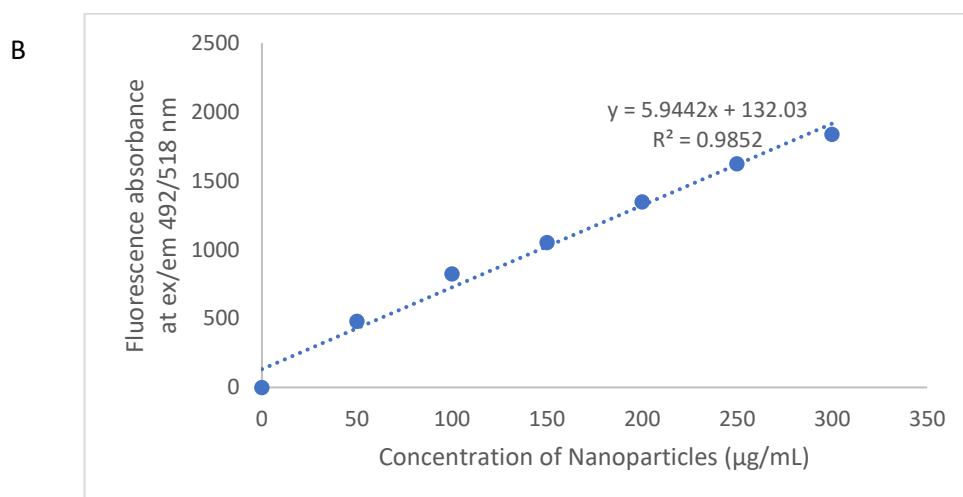
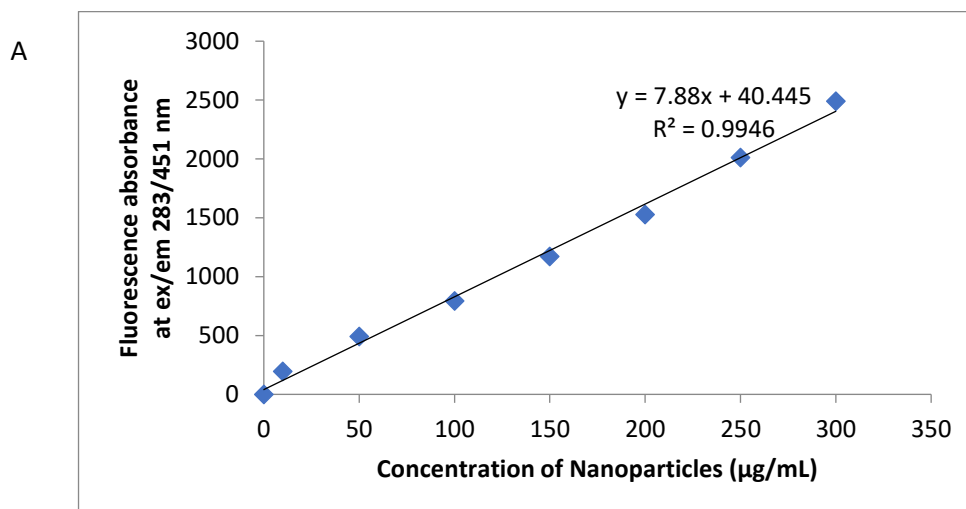
3T3 cells after 24 h FZSi NPs treatment (A:12.5,B:25,C:50,D:100 µg/ml)



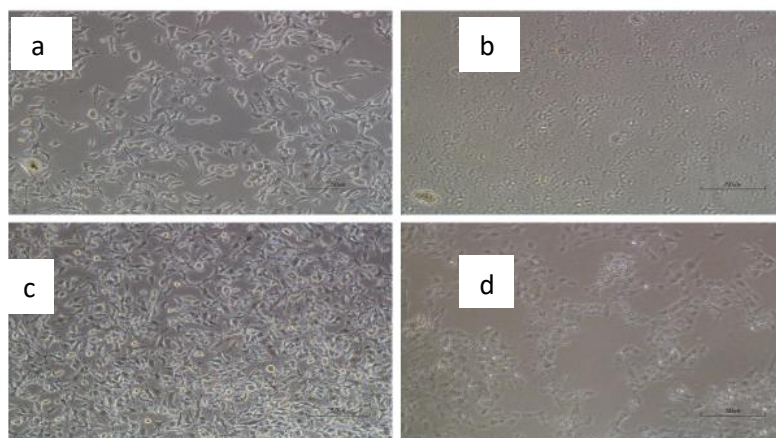
3T3 cells after 24 h FZSiFA25 NPs treatment (A:12.5,B:25,C:50,D:100 µg/ml)



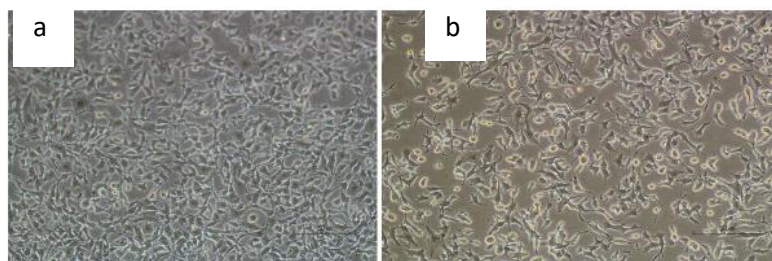
3T3 cells after 24 h FZSiFA50 NPs treatment (A:12.5,B:25,C:50,D:100 µg/ml)

Appendix 21: Calibration curve of (A) FZSiFA50 and (B) FZSi-FITC NPs in RIPA buffer

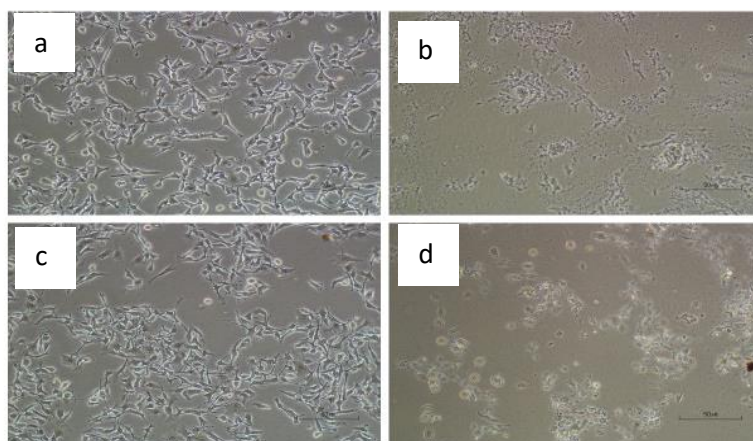
Appendix 22: Morphology of B16-F10 cells after NPs treatment (caspase)



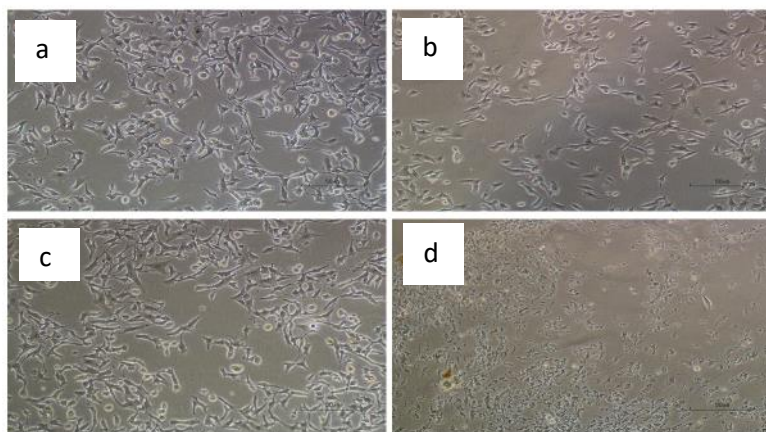
B16F10 cells images after 1 h NPs & UV treatment a,b) FZSi 12.5 & 100 µg/ml c,d) FZSiFA50 12.5 & 100 µg/ml



B16F10 control images at 2 h a) No treatment b) only UV exposed



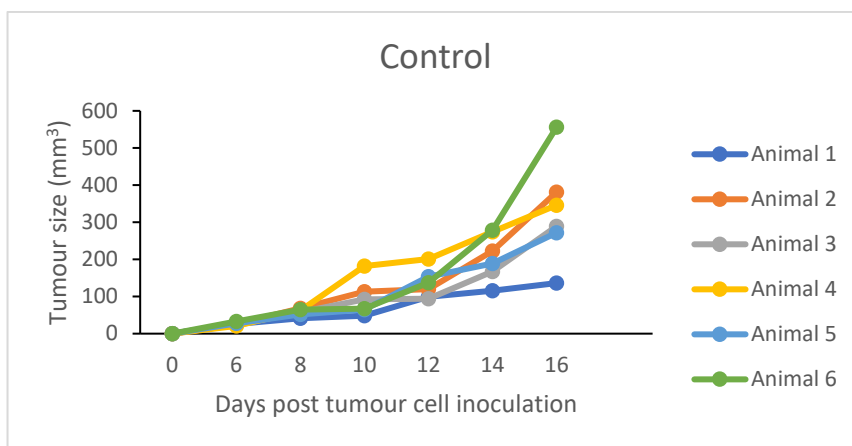
B16F10 cells images after 2 h NPs treatment a,b) FZSi 12.5 & 100 µg/ml c,d) FZSiFA50 12.5 & 100 µg/ml



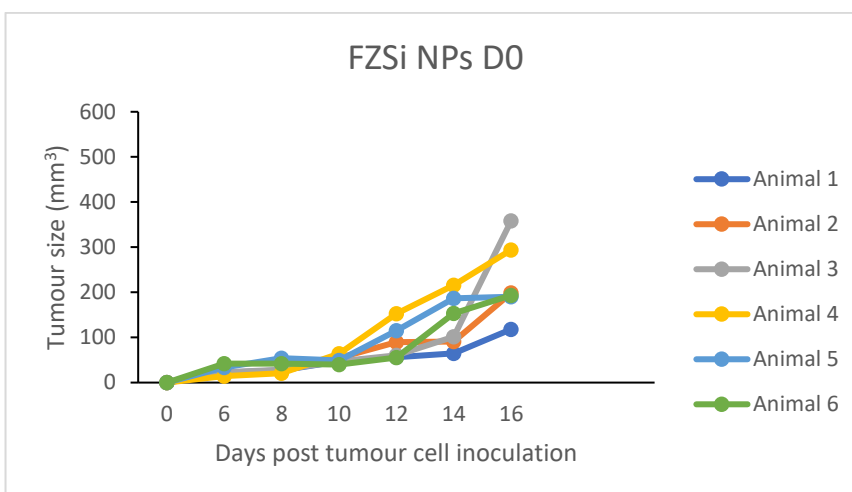
B16F10 cells images after 2 h NPs & UV treatment a,b) FZSi 12.5 & 100 $\mu\text{g/ml}$ c,d) FZSiFA50 12.5 & 100 $\mu\text{g/ml}$

Appendix 23: Tumour growth pattern of individual treatment groups up to day 16 post treatment

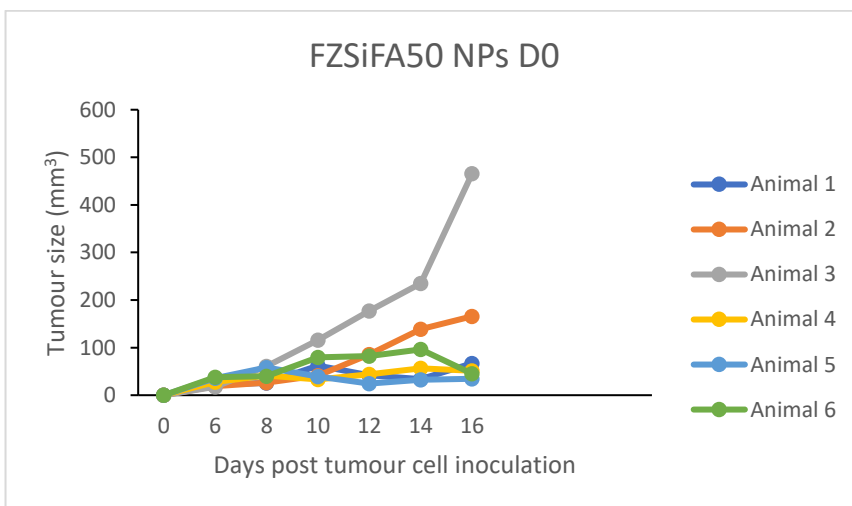
A

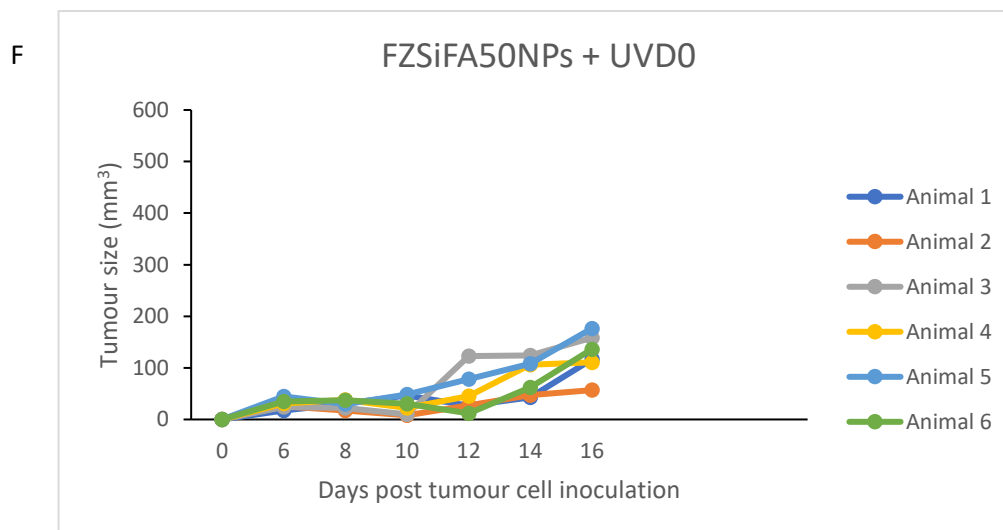
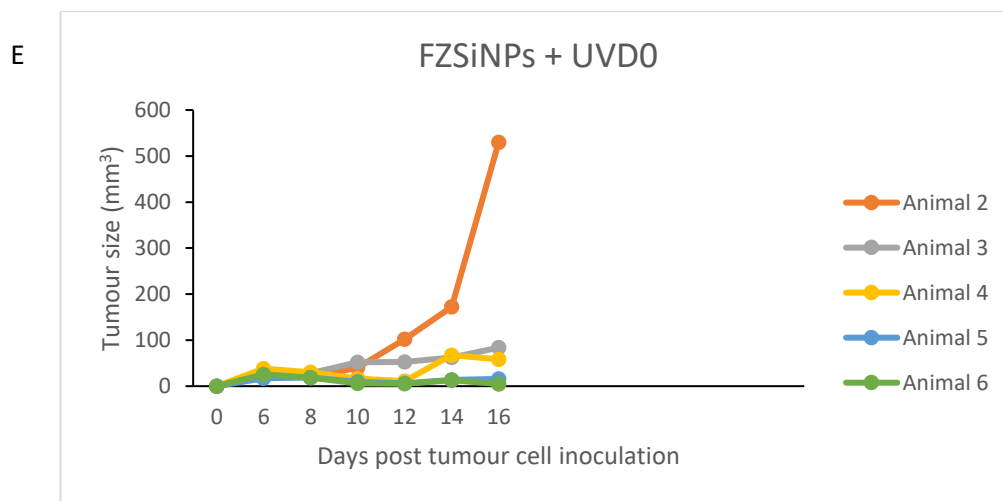
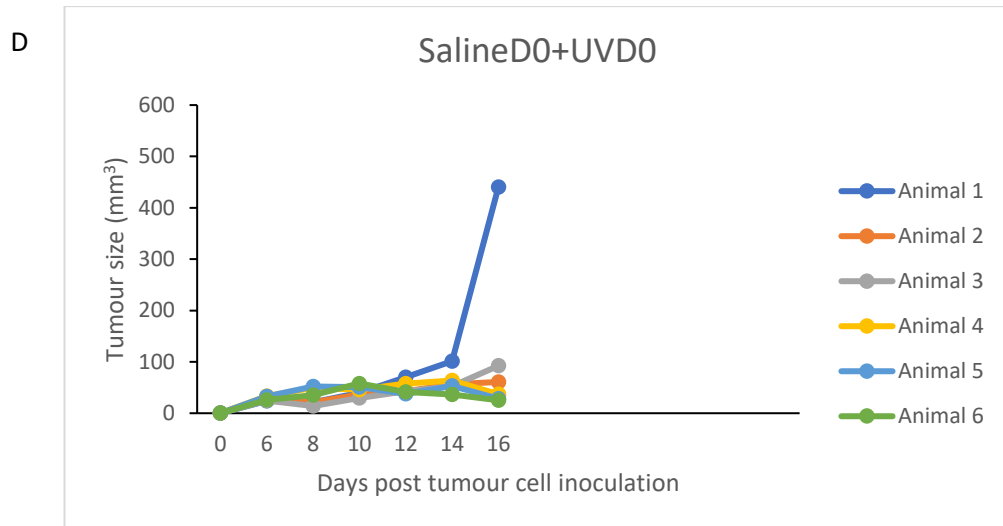


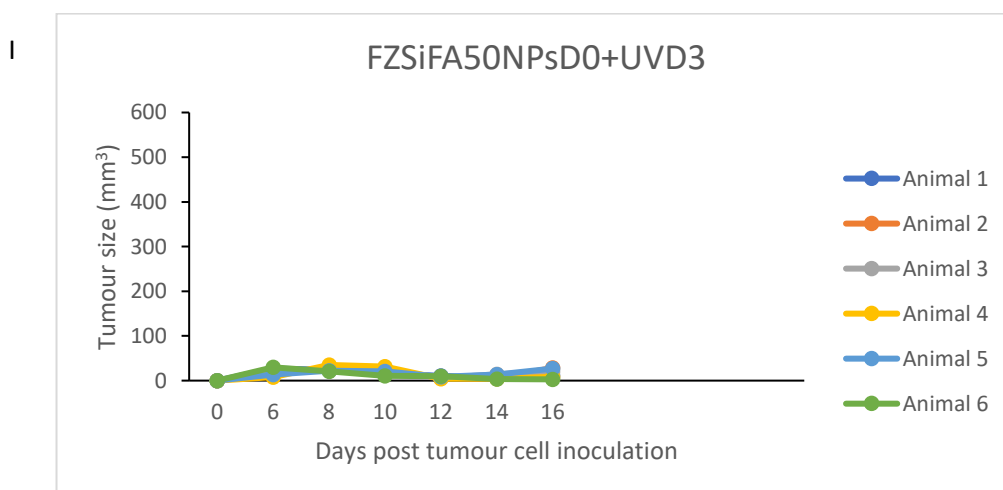
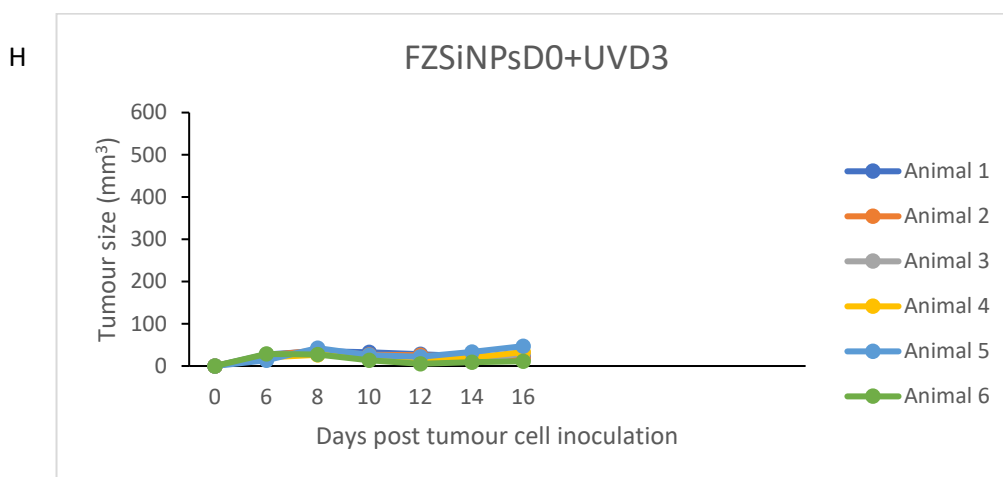
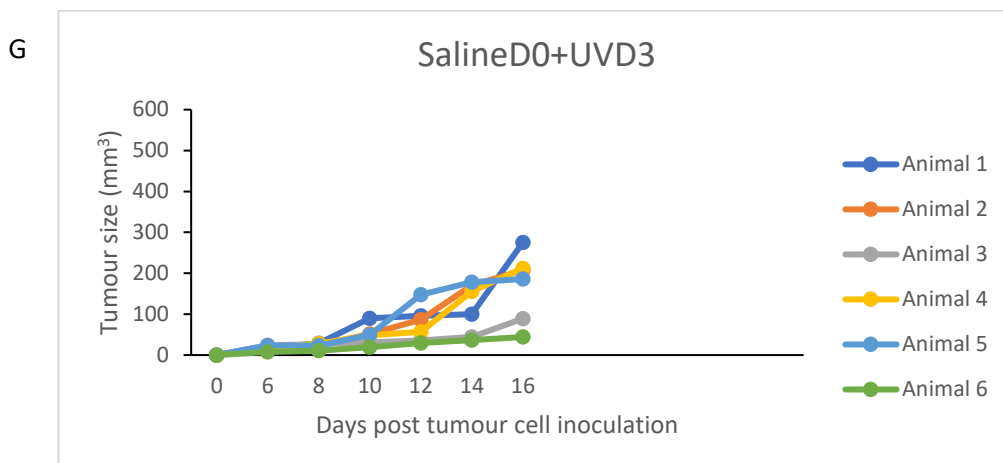
B



C

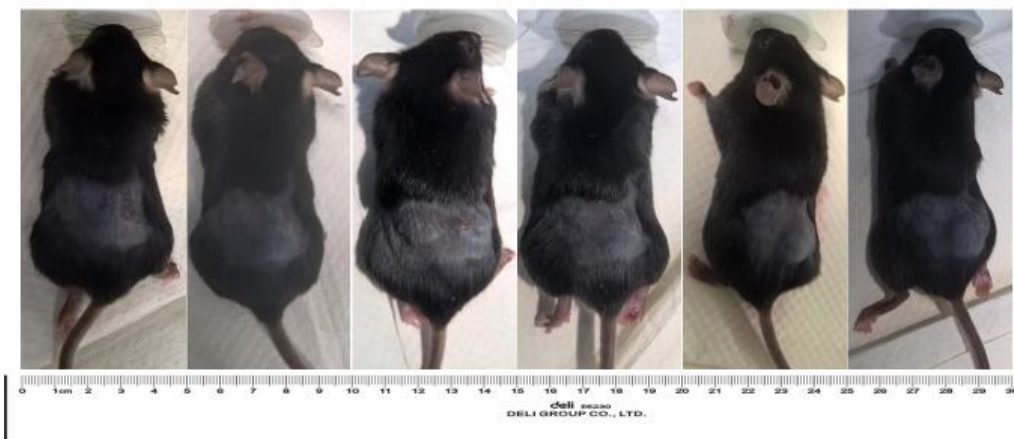




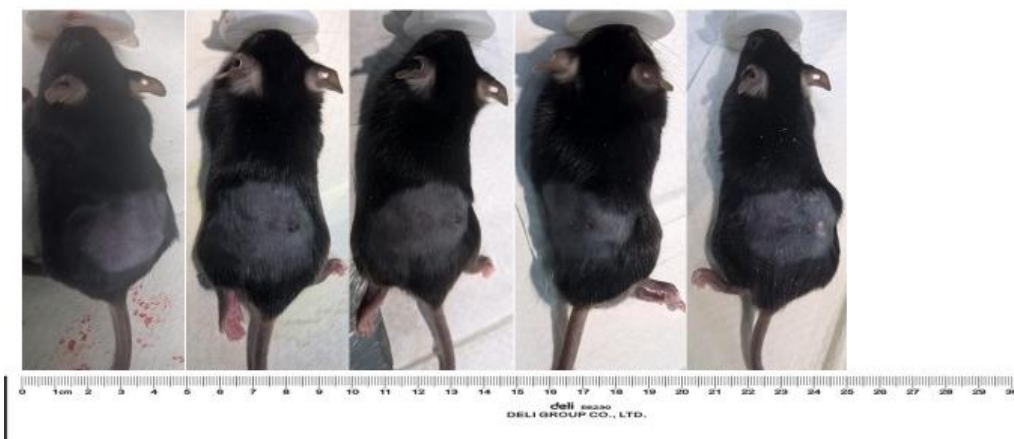


All treatments were administered via intra tumour and hybrid NPs dose were 2 mg/kg in 10 μ L. UV-A irradiation was given on sixth (D0) and ninth day (D3) post nanoparticles treatment at a dose of 10 J/cm². A: Saline, B: FZSiNPsD0, C: FZSiFA50NPsD0, D: Saline+UVD0, E: FZSiNPs+UVD0, F: FZSiFA50NPs+UVD0, G: SalineD0+UVD3, H: FZSiNPsD0+UVD3 and I: FZSiFA50NPsD0+UVD3.

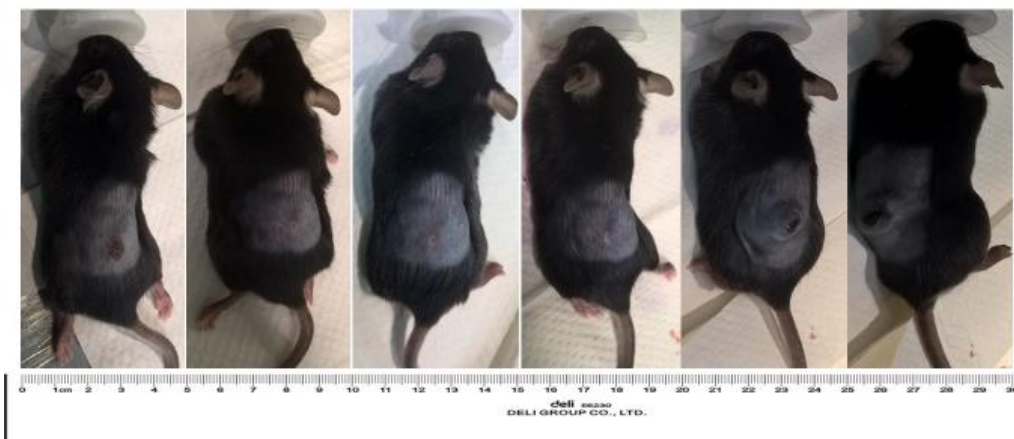
Appendix 24: Images of melanoma tumour in different treatment groups



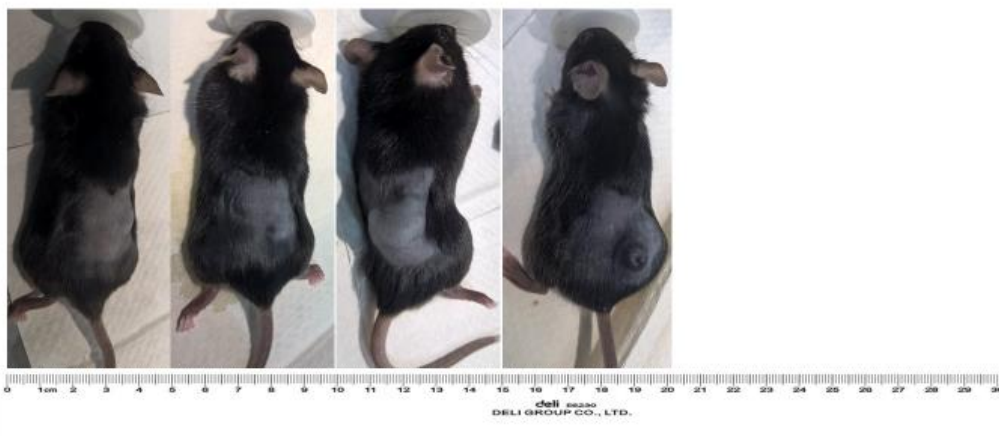
Images showing exposure of mice to FZSiFA50NPsD0+UVD3 on 10th, 12th, 16th, 20th, 22nd and 24th day (left to right). The scar formation occurred only after UV exposure and followed by tumour reduction later tumour recurrence and growth was visible away from the initial tumour site of treatment.



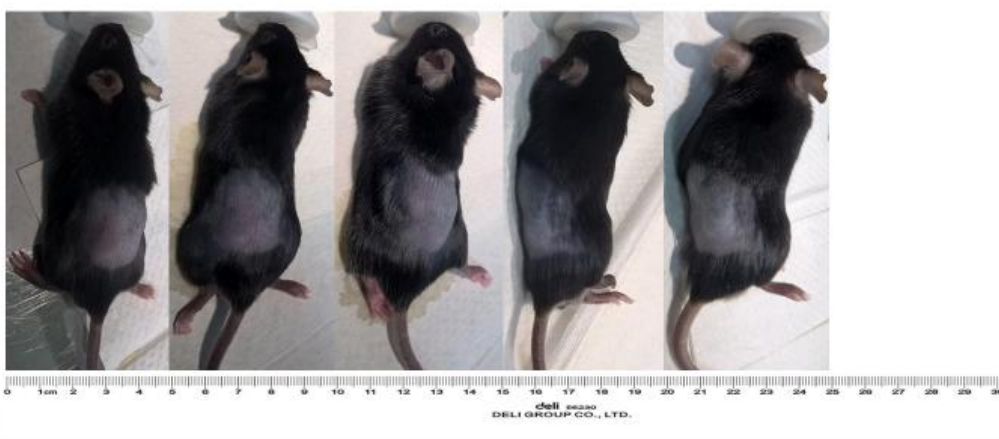
Images showing exposure of mice to FZSiNPs+UVD0 on 10th, 12th, 16th, 20th and 22nd day (left to right). The scar formation occurred only after UV exposure and followed by tumour reduction later tumour recurrence and growth was visible away from the initial tumour site of treatment.



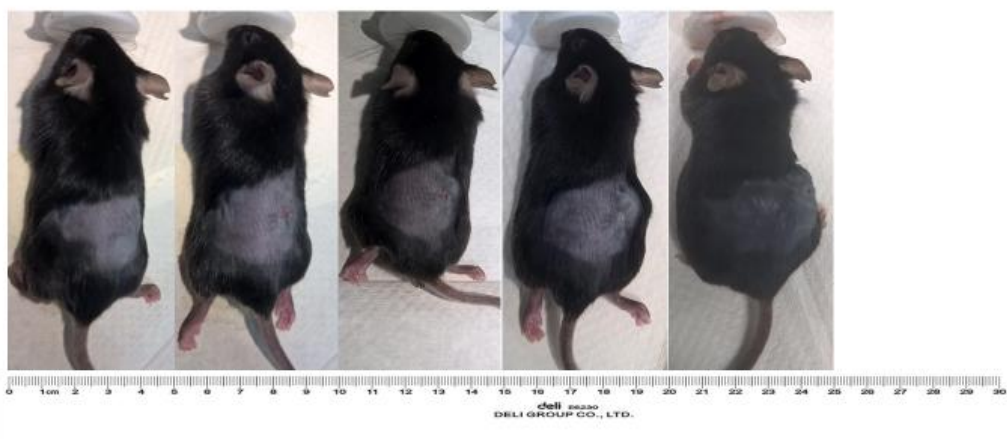
Images showing exposure of mice to FZSiNPsD0+UVD3 on 10th, 12th, 16th, 20th, 22nd and 24th day (left to right). The scar formation occurred only after UV exposure and followed by tumour reduction later tumour recurrence and growth was visible away from the initial tumour site of treatment.



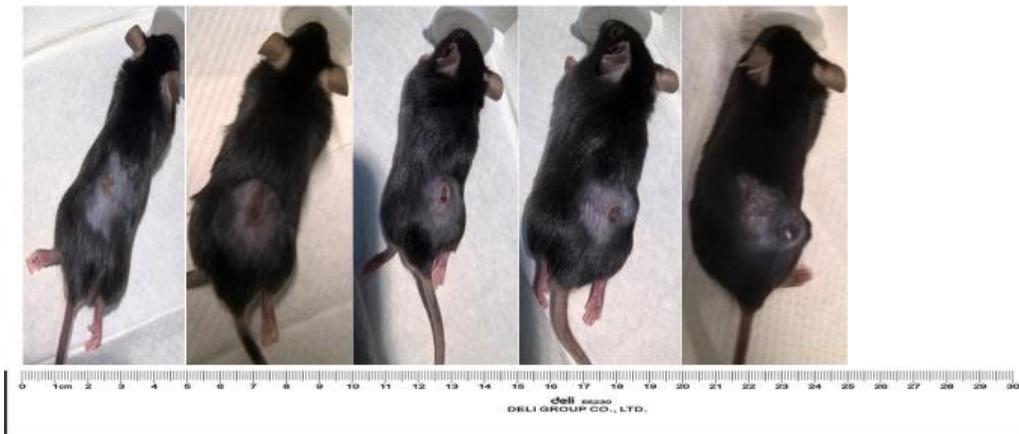
Images showing exposure of mice to FZSiNPsD0 on 10th, 12th, 16th and 20th day (left to right). The tumour was necrotic on 20th day.



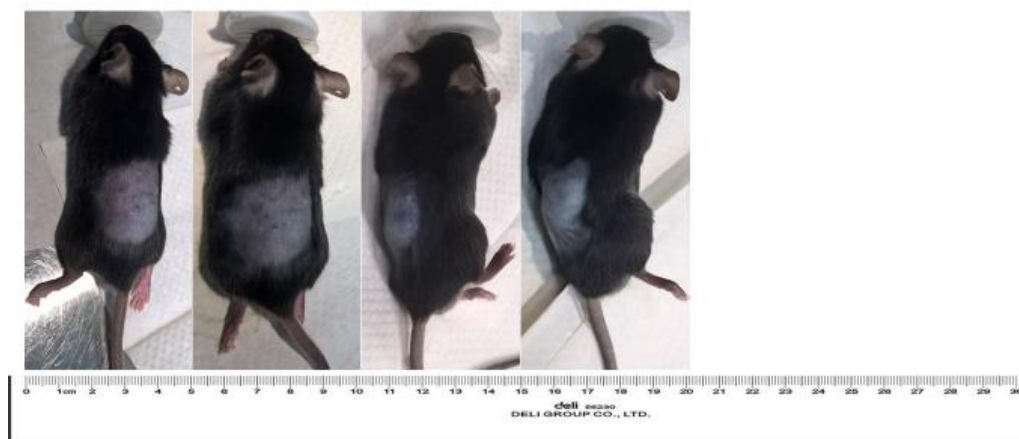
Images showing exposure of mice to FZSiFA50NPsD0 on 10th, 12th, 16th, 20th and 22nd day (left to right).



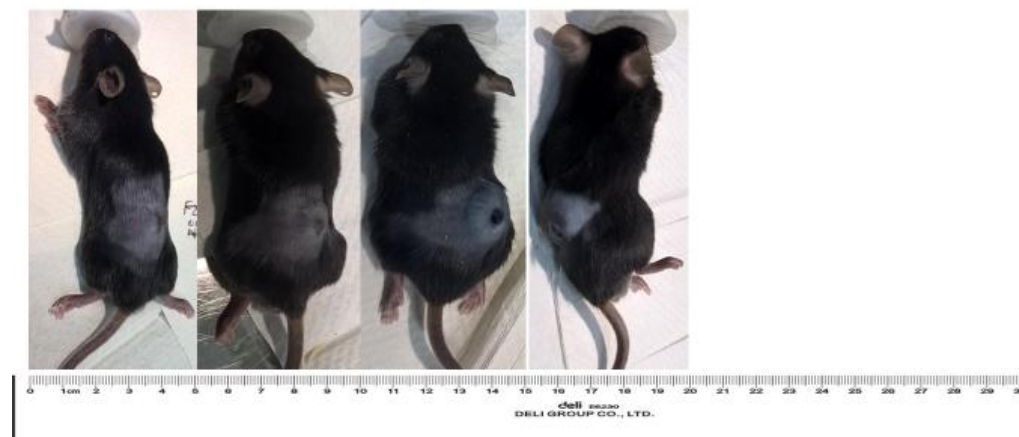
Images showing exposure of mice to FZSiFA50NPs+UVD0 on 10th, 12th, 16th, 20th and 22nd day (left to right). The scar formation occurred only after UV exposure and followed by tumour reduction later tumour recurrence and growth was visible away from the initial tumour site of treatment.



Images showing exposure of mice to Saline+UVD0 on 10th, 12th, 16th, 20th and 22nd day (left to right). The scar formation occurred only after UV exposure followed by tumour growth around and along the scar.



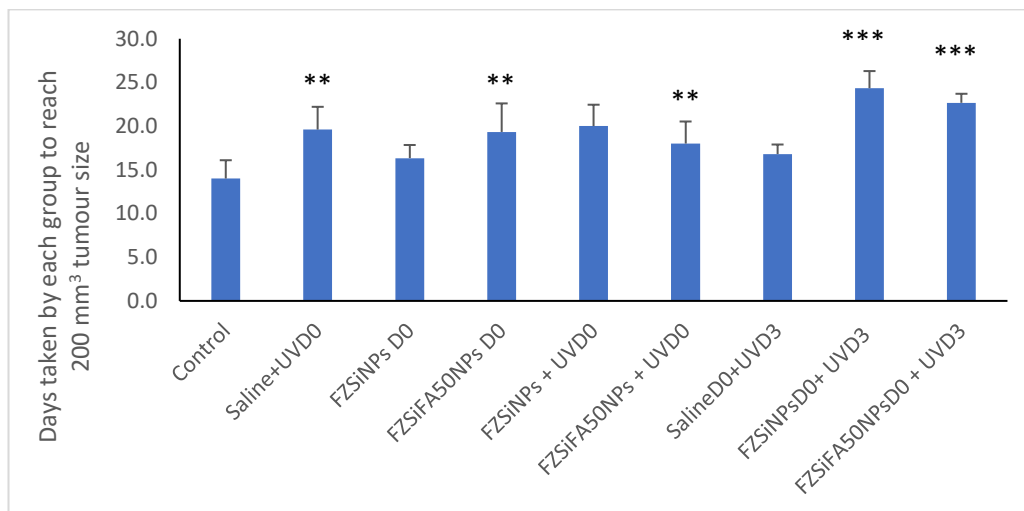
Images showing exposure of mice to SalineD0 on 10th, 12th, 16th, and 18th day (left to right).



Images showing exposure of mice to SalineD0+UVD3 on 10th, 12th, 16th, and 18th day (left to right). The scar formation occurred only after UV exposure followed by tumour growth around and along the scar.

Appendix 25

Tumour growth delay and average tumour weight at the end of the study



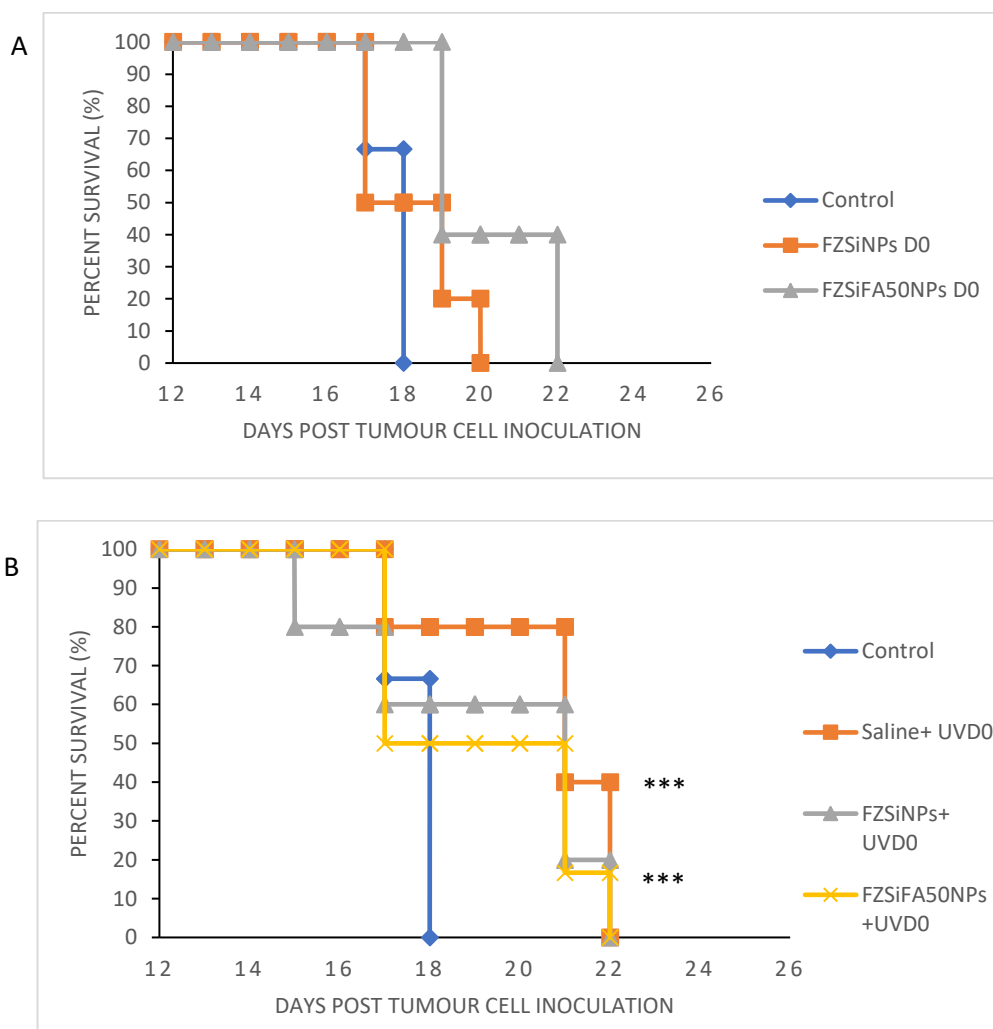
Tumour growth delay. Tumour maximum size was set as 200 mm³ and the time taken by each treated group to reach the maximum size is calculated as tumour growth delay. A) shows the fixed tumour size (200 mm³) reached by each treated group B) illustrates the number of days taken by each treated group to arrive at the maximum size. All data are presented as mean ± SEM. ** indicate means are significantly different (P < 0.01), *** indicate means are significantly different (P < 0.001) compared to the control.

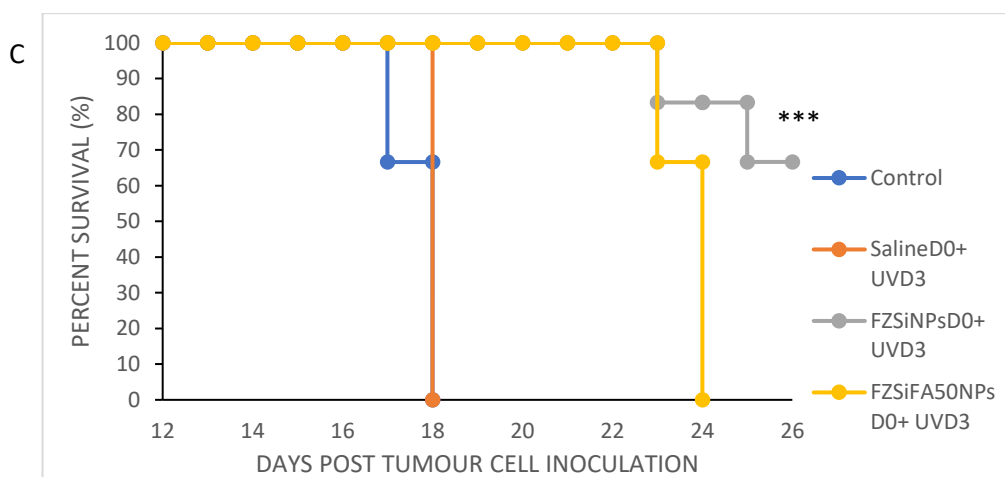
Different treatment groups and their average tumour weight

Groups	Average tumour weight (g)
Control (Saline)	1.73± 0.35
Saline+UVD0	1.04± 0.176***
FZSiNPs D0	0.83± 0.136***
FZSiFA50NPs D0	0.70± 0.070***
FZSiNPs + UVD0	0.70± 0.209***
FZSiFA50NPs + UVD0	0.67± 0.334***
SalineD0+UVD3	1.05± 0.288***
FZSiNPsD0+ UVD3	0.70± 0.130***
FZSiFA50NPsD0+ UVD3	0.72± 0.093***

Tumour weight was noted at the end of culling each animal and the average was calculated for each group. *** indicates p<0.001 compared to control group.

In the control group, the animals had tumour volume exceeded 100 mm³ by day 18 and were sacrificed, whereas in the FZSiFA50NPs treated group 40% animals survived up to day 22, and in FZSi NPs group 20% animals survived up to day 20 (Figure 3.38A). In NPs+UVD0 groups, 20% animals survived up to day 22, whereas 40% animals survived during the same period in saline+UVD0 group, which is significant (P<0.001) (Figure 3.38B). The animals which received NPs were treated with UV on day 3, 66% animals survived up to day 24 in the FZSiFA50 group, and 66% survived up to day 26 in FZSi group (Figure 3.38C), which was a significant extension of survival time (P< 0.001). The better survival rate of mice treated with hybrid NPs and UVD3 confirmed that the tumour burden was significantly reduced compared to control group.





The survival rate of animals following tumour cell inoculation. A) Control Vs FZSiNPsD0 and FZSiFA50NPsD0 groups B) Control Vs saline+UVD0, FZSiNPs+UVD0 and FZSiFA50NPs+UVD0 groups C) Control Vs salineD0+UVD3, FZSiNPsD0+UVD3 and FZSiFA50NPsD0+UVD3 groups. *** indicate means are significantly different ($P < 0.001$) compared to the control.

Appendix 26: Copyright Clearance

2/6/2018 Rightslink® by Copyright Clearance Center



Copyright Clearance Center

RightsLink®

[Home](#)
[Create Account](#)
[Help](#)




Title: Cytotoxicity of folic acid conjugated hollow silica nanoparticles toward Caco2 and 3T3 cells, with and without encapsulated DOX

Author: Kunal Patel, Behin Sundara Raj, Yan Chen, Xia Lou

Publication: Colloids and Surfaces B: Biointerfaces

Publisher: Elsevier

Date: 1 April 2016

Copyright © 2016 Elsevier B.V. All rights reserved.

LOGIN

If you're a [copyright.com](#) user, you can login to RightsLink using your [copyright.com](#) credentials. Already a [RightsLink](#) user or want to [learn more?](#)

Please note that, as the author of this Elsevier article, you retain the right to include it in a thesis or dissertation, provided it is not published commercially. Permission is not required, but please ensure that you reference the journal as the original source. For more information on this and on your other retained rights, please visit: <https://www.elsevier.com/about/our-business/policies/copyright#Author-rights>

[BACK](#)
[CLOSE WINDOW](#)

Copyright © 2018 [Copyright Clearance Center, Inc.](#) All Rights Reserved. [Privacy statement](#). [Terms and Conditions](#). Comments? We would like to hear from you. E-mail us at customercare@copyright.com

<https://s100.copyright.com/AppDispatchServlet#formTop>
1/1

1/30/2018 RightsLink Printable License

**ELSEVIER LICENSE
TERMS AND CONDITIONS**

Jan 29, 2018

This Agreement between Mr. BEHIN RAJ ("You") and Elsevier ("Elsevier") consists of your license details and the terms and conditions provided by Elsevier and Copyright Clearance Center.

License Number	4278550688800
License date	Jan 29, 2018
Licensed Content Publisher	Elsevier
Licensed Content Publication	Advances in Colloid and Interface Science
Licensed Content Title	Core/shell nanoparticles in biomedical applications
Licensed Content Author	Krishnendu Chatterjee,Sreerupa Sarkar,K. Jagajjanani Rao,Santanu Paria
Licensed Content Date	Jul 1, 2014
Licensed Content Volume	209
Licensed Content Issue	n/a
Licensed Content Pages	32
Start Page	8
End Page	39
Type of Use	reuse in a thesis/dissertation
Intended publisher of new work	other
Portion	figures/tables/illustrations
Number of figures/tables/illustrations	1
Format	both print and electronic
Are you the author of this Elsevier article?	No
Will you be translating?	No
Original figure numbers	Figure 1
Title of your thesis/dissertation	Pharmaceutical and Biological Evaluation of Nano Photosensitizers for Cancer Therapy
Expected completion date	Feb 2018
Estimated size (number of pages)	275
Requestor Location	Mr. BEHIN RAJ Unit 13, 79 South Terrace, Como PERTH, WA 6152 Australia Attn: Mr. BEHIN RAJ
Total	0.00 USD
Terms and Conditions	

INTRODUCTION

1. The publisher for this copyrighted material is Elsevier. By clicking "accept" in connection with completing this licensing transaction, you agree that the following terms and conditions

<https://s100.copyright.com/AppDispatchServlet> 1/5

1/30/2018

RightsLink Printable License

**ELSEVIER LICENSE
TERMS AND CONDITIONS**

Jan 29, 2018

This Agreement between Mr. BEHIN RAJ ("You") and Elsevier ("Elsevier") consists of your license details and the terms and conditions provided by Elsevier and Copyright Clearance Center.

License Number	4278541478362
License date	Jan 29, 2018
Licensed Content Publisher	Elsevier
Licensed Content Publication	TRAC Trends in Analytical Chemistry
Licensed Content Title	ZnO nanostructures based biosensors for cancer and infectious disease applications: Perspectives, prospects and promises
Licensed Content Author	Sahar Saleem Bhat,Ahsanulhaq Qurashi,Firdous Ahmad Khanday
Licensed Content Date	Jan 1, 2017
Licensed Content Volume	86
Licensed Content Issue	n/a
Licensed Content Pages	13
Start Page	1
End Page	13
Type of Use	reuse in a thesis/dissertation
Portion	figures/tables/illustrations
Number of figures/tables/illustrations	1
Format	both print and electronic
Are you the author of this Elsevier article?	No
Will you be translating?	No
Original figure numbers	Figure 12
Title of your thesis/dissertation	Pharmaceutical and Biological Evaluation of Nano Photosensitizers for Cancer Therapy
Expected completion date	Feb 2018
Estimated size (number of pages)	275
Requestor Location	Mr. BEHIN RAJ Unit 13, 79 South Terrace, Como PERTH, WA 6152 Australia Attn: Mr. BEHIN RAJ
Total	0.00 AUD
Terms and Conditions	

INTRODUCTION

1. The publisher for this copyrighted material is Elsevier. By clicking "accept" in connection with completing this licensing transaction, you agree that the following terms and conditions apply to this transaction (along with the Billing and Payment terms and conditions

<https://s100.copyright.com/AppDispatchServlet>

1/5

established by Copyright Clearance Center, Inc. ("CCC"), at the time that you opened your Rightslink account and that are available at any time at <http://myaccount.copyright.com>).

GENERAL TERMS

2. Elsevier hereby grants you permission to reproduce the aforementioned material subject to the terms and conditions indicated.

3. Acknowledgement: If any part of the material to be used (for example, figures) has appeared in our publication with credit or acknowledgement to another source, permission must also be sought from that source. If such permission is not obtained then that material may not be included in your publication/copies. Suitable acknowledgement to the source must be made, either as a footnote or in a reference list at the end of your publication, as follows:

"Reprinted from Publication title, Vol /edition number, Author(s), Title of article / title of chapter, Pages No., Copyright (Year), with permission from Elsevier [OR APPLICABLE SOCIETY COPYRIGHT OWNER]." Also Lancet special credit - "Reprinted from The Lancet, Vol. number, Author(s), Title of article, Pages No., Copyright (Year), with permission from Elsevier."

4. Reproduction of this material is confined to the purpose and/or media for which permission is hereby given.

5. Altering/Modifying Material: Not Permitted. However figures and illustrations may be altered/adapted minimally to serve your work. Any other abbreviations, additions, deletions and/or any other alterations shall be made only with prior written authorization of Elsevier Ltd. (Please contact Elsevier at permissions@elsevier.com). No modifications can be made to any Lancet figures/tables and they must be reproduced in full.

6. If the permission fee for the requested use of our material is waived in this instance, please be advised that your future requests for Elsevier materials may attract a fee.

7. Reservation of Rights: Publisher reserves all rights not specifically granted in the combination of (i) the license details provided by you and accepted in the course of this licensing transaction, (ii) these terms and conditions and (iii) CCC's Billing and Payment terms and conditions.

8. License Contingent Upon Payment: While you may exercise the rights licensed immediately upon issuance of the license at the end of the licensing process for the transaction, provided that you have disclosed complete and accurate details of your proposed use, no license is finally effective unless and until full payment is received from you (either by publisher or by CCC) as provided in CCC's Billing and Payment terms and conditions. If full payment is not received on a timely basis, then any license preliminarily granted shall be deemed automatically revoked and shall be void as if never granted. Further, in the event that you breach any of these terms and conditions or any of CCC's Billing and Payment terms and conditions, the license is automatically revoked and shall be void as if never granted. Use of materials as described in a revoked license, as well as any use of the materials beyond the scope of an unrevoked license, may constitute copyright infringement and publisher reserves the right to take any and all action to protect its copyright in the materials.

9. Warranties: Publisher makes no representations or warranties with respect to the licensed material.

10. Indemnity: You hereby indemnify and agree to hold harmless publisher and CCC, and their respective officers, directors, employees and agents, from and against any and all claims arising out of your use of the licensed material other than as specifically authorized pursuant to this license.

11. No Transfer of License: This license is personal to you and may not be sublicensed, assigned, or transferred by you to any other person without publisher's written permission.

12. No Amendment Except in Writing: This license may not be amended except in a writing signed by both parties (or, in the case of publisher, by CCC on publisher's behalf).

13. Objection to Contrary Terms: Publisher hereby objects to any terms contained in any purchase order, acknowledgment, check endorsement or other writing prepared by you, which terms are inconsistent with these terms and conditions or CCC's Billing and Payment terms and conditions. These terms and conditions, together with CCC's Billing and Payment terms and conditions (which are incorporated herein), comprise the entire agreement between you and publisher (and CCC) concerning this licensing transaction. In the event of

between you and publisher (and CCC) concerning this licensing transaction. In the event of any conflict between your obligations established by these terms and conditions and those established by CCC's Billing and Payment terms and conditions, these terms and conditions shall control.

14. Revocation: Elsevier or Copyright Clearance Center may deny the permissions described in this License at their sole discretion, for any reason or no reason, with a full refund payable to you. Notice of such denial will be made using the contact information provided by you. Failure to receive such notice will not alter or invalidate the denial. In no event will Elsevier or Copyright Clearance Center be responsible or liable for any costs, expenses or damage incurred by you as a result of a denial of your permission request, other than a refund of the amount(s) paid by you to Elsevier and/or Copyright Clearance Center for denied permissions.

LIMITED LICENSE

The following terms and conditions apply only to specific license types:

15. **Translation:** This permission is granted for non-exclusive world **English** rights only unless your license was granted for translation rights. If you licensed translation rights you may only translate this content into the languages you requested. A professional translator must perform all translations and reproduce the content word for word preserving the integrity of the article.

16. **Posting licensed content on any Website:** The following terms and conditions apply as follows: Licensing material from an Elsevier journal: All content posted to the web site must maintain the copyright information line on the bottom of each image; A hyper-text must be included to the Homepage of the journal from which you are licensing at <http://www.sciencedirect.com/science/journal/xxxxx> or the Elsevier homepage for books at <http://www.elsevier.com>; Central Storage: This license does not include permission for a scanned version of the material to be stored in a central repository such as that provided by Heron/XanEdu.

Licensing material from an Elsevier book: A hyper-text link must be included to the Elsevier homepage at <http://www.elsevier.com>. All content posted to the web site must maintain the copyright information line on the bottom of each image.

Posting licensed content on Electronic reserve: In addition to the above the following clauses are applicable: The web site must be password-protected and made available only to bona fide students registered on a relevant course. This permission is granted for 1 year only. You may obtain a new license for future website posting.

17. **For journal authors:** the following clauses are applicable in addition to the above:

Preprints:

A preprint is an author's own write-up of research results and analysis, it has not been peer-reviewed, nor has it had any other value added to it by a publisher (such as formatting, copyright, technical enhancement etc.).

Authors can share their preprints anywhere at any time. Preprints should not be added to or enhanced in any way in order to appear more like, or to substitute for, the final versions of articles however authors can update their preprints on arXiv or RePEc with their Accepted Author Manuscript (see below).

If accepted for publication, we encourage authors to link from the preprint to their formal publication via its DOI. Millions of researchers have access to the formal publications on ScienceDirect, and so links will help users to find, access, cite and use the best available version. Please note that Cell Press, The Lancet and some society-owned have different preprint policies. Information on these policies is available on the journal homepage.

Accepted Author Manuscripts: An accepted author manuscript is the manuscript of an article that has been accepted for publication and which typically includes author-incorporated changes suggested during submission, peer review and editor-author communications.

Authors can share their accepted author manuscript:

- immediately
 - via their non-commercial person homepage or blog
 - by updating a preprint in arXiv or RePEc with the accepted manuscript

1/30/2018

RightsLink Printable License

1/30/2018

- o via their research institute or institutional repository for internal institutional uses or as part of an invitation-only research collaboration work-group
- o directly by providing copies to their students or to research collaborators for their personal use
- o for private scholarly sharing as part of an invitation-only work group on commercial sites with which Elsevier has an agreement
- After the embargo period
 - o via non-commercial hosting platforms such as their institutional repository
 - o via commercial sites with which Elsevier has an agreement

In all cases accepted manuscripts should:

- link to the formal publication via its DOI
- bear a CC-BY-NC-ND license - this is easy to do
- if aggregated with other manuscripts, for example in a repository or other site, be shared in alignment with our hosting policy not be added to or enhanced in any way to appear more like, or to substitute for, the published journal article.

Published journal article (JPA): A published journal article (PJA) is the definitive final record of published research that appears or will appear in the journal and embodies all value-adding publishing activities including peer review co-ordination, copy-editing, formatting, (if relevant) pagination and online enrichment.

Policies for sharing publishing journal articles differ for subscription and gold open access articles:

Subscription Articles: If you are an author, please share a link to your article rather than the full-text. Millions of researchers have access to the formal publications on ScienceDirect, and so links will help your users to find, access, cite, and use the best available version. Theses and dissertations which contain embedded PJAs as part of the formal submission can be posted publicly by the awarding institution with DOI links back to the formal publications on ScienceDirect.

If you are affiliated with a library that subscribes to ScienceDirect you have additional private sharing rights for others' research accessed under that agreement. This includes use for classroom teaching and internal training at the institution (including use in course packs and courseware programs), and inclusion of the article for grant funding purposes.

Gold Open Access Articles: May be shared according to the author-selected end-user license and should contain a [CrossMark logo](#), the end user license, and a DOI link to the formal publication on ScienceDirect.

Please refer to Elsevier's [posting policy](#) for further information.

18. **For book authors** the following clauses are applicable in addition to the above:

Authors are permitted to place a brief summary of their work online only. You are not allowed to download and post the published electronic version of your chapter, nor may you scan the printed edition to create an electronic version. **Posting to a repository:** Authors are permitted to post a summary of their chapter only in their institution's repository.

19. **Thesis/Dissertation:** If your license is for use in a thesis/dissertation your thesis may be submitted to your institution in either print or electronic form. Should your thesis be published commercially, please reapply for permission. These requirements include permission for the Library and Archives of Canada to supply single copies, on demand, of the complete thesis and include permission for Proquest/UMI to supply single copies, on demand, of the complete thesis. Should your thesis be published commercially, please reapply for permission. Theses and dissertations which contain embedded PJAs as part of the formal submission can be posted publicly by the awarding institution with DOI links back to the formal publications on ScienceDirect.

Elsevier Open Access Terms and Conditions

You can publish open access with Elsevier in hundreds of open access journals or in nearly 2000 established subscription journals that support open access publishing. Permitted third party re-use of these open access articles is defined by the author's choice of Creative Commons user license. See our [open access license policy](#) for more information.

https://s100.copyright.com/AppDispatchServlet

https://s100.copyright.com/AppDispatchServlet 4/5

Terms & Conditions applicable to all Open Access articles published with Elsevier:

Any reuse of the article must not represent the author as endorsing the adaptation of the article nor should the article be modified in such a way as to damage the author's honour or reputation. If any changes have been made, such changes must be clearly indicated.

The author(s) must be appropriately credited and we ask that you include the end user license and a DOI link to the formal publication on ScienceDirect.

If any part of the material to be used (for example, figures) has appeared in our publication with credit or acknowledgement to another source it is the responsibility of the user to ensure their reuse complies with the terms and conditions determined by the rights holder.

Additional Terms & Conditions applicable to each Creative Commons user license:

CC BY: The CC-BY license allows users to copy, to create extracts, abstracts and new works from the Article, to alter and revise the Article and to make commercial use of the Article (including reuse and/or resale of the Article by commercial entities), provided the user gives appropriate credit (with a link to the formal publication through the relevant DOI), provides a link to the license, indicates if changes were made and the licensor is not represented as endorsing the use made of the work. The full details of the license are available at <http://creativecommons.org/licenses/by/4.0>.

CC BY NC SA: The CC BY-NC-SA license allows users to copy, to create extracts, abstracts and new works from the Article, to alter and revise the Article, provided this is not done for commercial purposes, and that the user gives appropriate credit (with a link to the formal publication through the relevant DOI), provides a link to the license, indicates if changes were made and the licensor is not represented as endorsing the use made of the work. Further, any new works must be made available on the same conditions. The full details of the license are available at <http://creativecommons.org/licenses/by-nc-sa/4.0>.

CC BY NC ND: The CC BY-NC-ND license allows users to copy and distribute the Article, provided this is not done for commercial purposes and further does not permit distribution of the Article if it is changed or edited in any way, and provided the user gives appropriate credit (with a link to the formal publication through the relevant DOI), provides a link to the license, and that the licensor is not represented as endorsing the use made of the work. The full details of the license are available at <http://creativecommons.org/licenses/by-nc-nd/4.0>. Any commercial reuse of Open Access articles published with a CC BY NC SA or CC BY NC ND license requires permission from Elsevier and will be subject to a fee.

Commercial reuse includes:

- Associating advertising with the full text of the Article
- Charging fees for document delivery or access
- Article aggregation
- Systematic distribution via e-mail lists or share buttons

Posting or linking by commercial companies for use by customers of those companies.

20. Other Conditions:

v1.9

Questions? customercare@copyright.com or +1-855-239-3415 (toll free in the US) or +1-978-646-2777.

Appendix 27**Publications and presentations**

- Patel K, Sundara Raj B, Chen Y, Lou X. Cytotoxicity of folic acid conjugated hollow silica nanoparticles toward Caco2 and 3T3 cells, with and without encapsulated DOX. *Colloids and Surfaces B: Biointerfaces*, 2016, 140, 213-222.
- Patel K, Sundara Raj B, Chen Y, Lou X. Novel, folic acid conjugated, Fe₃O₄-ZnO hybrid nanoparticles for targeted photodynamic therapy. *Colloids and Surfaces B: Biointerfaces*, 2017, 150, 317-325.
- Cellular Responses of Hollow Silica Nanoparticles. Mark Liveris Research Day, Perth, Curtin University, April 2016.
- Cellular Responses of Silica-Coated Hybrid Nanoparticles in Photodynamic therapy, poster presented at Science on the Swan conference, Fremantle, 2-4th May 2017.